# Chromium Free Adhesive Primer Formulations For Aerospace Applications

**Mark Edward Harriman**

A Thesis Submitted For The Qualification Of PhD

**The University Of York**

**Department Of Chemistry**

2006

## Abstract

Hexavalent chromium containing primer systems have been used on aircraft for the last 30-40 years. Primers have several functions but the key ones are to promote adhesion and to increase the corrosion resistance of the metal. Due to the highly toxic nature of hexavalent chromium current legislation has banned its use from many parts of Europe and the USA and there is the need to find a more environmentally benign alternative which can give similar, if not better, properties. Unfortunately, at present there is a lack of understanding of the actual mechanisms by which chromium acts and this has hindered the development of alternatives.

The main objective of this research was to carry out a broad ranging investigation to allow future study to focus on the most promising observations and provisional conclusions. The initial aims were to develop a more thorough understanding of the mechanism by which chromium operates in primer systems and to then use this increased understanding to make progress towards finding successful 'green' alternatives.

The points outlined above were investigated using a series of model systems in conjunction with a variety of analytical techniques such as ESI-MS, DRIFTS and DRUVS and also a range of surface analysis tools such as XPS, SEM and EDX.

From the research carried out several conclusions can be made. Chromium acts as a Lewis acid catalyst in primer systems to cause oligomerisation of the epoxides present; an organochromate species is formed during the priming process; chromium is positioned at the metal-primer interface and not at the surface on a primed aluminium substrate. A successful alternative should be a Lewis acid, possess a strong Al-O-X bond and have some redox capability. Zirconate appears to be a highly promising replacement for chromium. A one step pretreatment and primer process is feasible and a simple fluoride treatment gives similar results to a surface as anodisation.

## Acknowledgements

Firstly, I would like to thank Professor James Clark for his continued encouragement, enthusiasm and suggestions during the three years of the project as without his guidance the project would not have been a success.

I would also like to offer my sincerest thanks to Dr. Steven Ward and Professor Terry McGrail of Cytec Engineered Materials, firstly for suggesting the project, secondly for helping with funding and finally for aiding me with many useful ideas.

For their help with analysis I offer thanks to Dr. Trevor Dransfield, Ian Wright and Paul Elliott, who also offered first class technical support during the three years.

I also offer my appreciation to the EPSRC and the Crystal Faraday Partnership whom provided the funding for this research project.

My thanks must also go to my family and friends who offered me so much support and encouragement during both the experimental and writing up stages of this project. Special mentions must go to my parents (particularly in the writing up year) and brother, current and past members of the Green Chemistry Group at York, my housemates in Ambrose St. and everyone at Cytec in Wilton.

## *List of Abbreviations*

| | |
|---|---|
| ATR | Attenuated Total Internal Reflection Infrared Spectroscopy |
| CAA | Chromic Acid Anodisation |
| DRIFTS | Diffuse Reflectance Infrared Spectroscopy |
| DRUVS | Diffuse Reflectance Ultraviolet-Visible Spectroscopy |
| EDX | Energy Dispersive X-ray Analysis |
| ESI-MS | Electrospray Ionisation Mass Spectrometry |
| FTIR | Fourier Transform Infrared Spectroscopy |
| LC-MS | Liquid Chromatography - Mass Spectrometry |
| $^{13}$C-NMR | Carbon-13 Nuclear Magnetic Resonance Spectroscopy |
| PAA | Phosphoric Acid Anodisation |
| PTC | Phase Transfer Catalyst |
| SEM | Scanning Electron Microscopy |
| TG-IR | Thermogravimetric Infrared Spectroscopy |
| XPS | X-ray Photoelectron Spectroscopy |

# Chapter 1

# Introduction

## 1.1 Aerospace technology

### *1.1.1 History*

Since the first powered flight by the Wright brothers in 1903 the manufacturing of aircraft has always used the most suitable state-of-the-art materials available[1]. The Wright brothers may have only used wood and other simple compounds in their early designs but it did not take long for more advanced materials to become commonplace on aircraft.

Spurred on by the need for tougher, stronger machines in World War One, manufacturers began to use metals in combination with wood. Although these machines were heavy and difficult to manoeuvre, they were much more capable of withstanding the forces exerted on them compared to their wooden counterparts.

World War Two again used mainly metal craft, but at this point, manufacturers were moving away from dense metals. Instead of using iron, materials that could provide both great strength and good manoeuvrability were employed[2].

Today, aircraft use a vast combination of different state-of-the-art materials, each developed with special properties for specific functions (figure 1.01).

| Material | | Usage (Weight %) |
|---|---|---|
| Metallics | | 73 |
| Al | | |
| Ti | | |
| Steel | | |
| Non-Metallics | | |
| Acrylic | | 2 |
| Carbon/Epoxy | | 21 |
| Carbon/BMI | | 3 |
| Fibreglass/Epoxy | | 0.5 |
| Fibreglass/BMI | | 0.5 |

Figure 1.01. Materials usage on a Harrier Jump Jet[3]

Today, composite materials are commonplace on aircraft. Most are employed as they are able to offer great strength coupled with low densities[4]. However, until recently composites have been too expensive to be used in great abundance in commercial aircraft due to their high manufacturing costs. Military craft have been composed of a higher percentage of composites for some time, but for commercial uses, composites are used in conjunction with other materials that have illustrated the ability to survive the extremes required for use in the aerospace industry.

For the last fifty years the most commonly used bulk material on aircraft has been aluminium. Each Boeing 747-400, the most recognisable aircraft in the world, comprises of 66,150kg of aluminium[5].

### *1.1.2 Aluminium*

Aluminium is the most abundant metallic constituent in the crust of the Earth[6]; only the non-metals oxygen and silicon are more plentiful. It is most commonly found as aluminium silicate or as a silicate of aluminium mixed with other metals such as sodium, potassium, iron, and magnesium, but never as a free metal. Bauxite, an impure hydrated aluminium oxide, is the commercial source of the metal because it is difficult, and therefore expensive, to extract aluminium from the silicates[7].

A Danish chemist, Hans Christian Oersted, first isolated aluminium in 1825 using a chemical process involving potassium amalgam. During 1827 and 1845, a German chemist, Friedrich Wöhler improved Oersted's process by using metallic potassium. He was the first to measure the relative density of aluminium and show its lightness.

Aluminium is strongly electropositive and extremely reactive. In contact with air it rapidly becomes covered with a tough, transparent layer of aluminium oxide that resists further corrosive action

Since its discovery, the global production of aluminium has increased greatly. In 1886 the world production was less than 45 kg with a price of more than $11 per kg. In 1989, by contrast, the estimated production of primary aluminium was 18 million tonnes, costing less than $2 per kg. Because of this decrease in price and other attractive properties that the metal exhibits, primarily its low density, aluminium became used extensively for applications in which more expensive, heavier metals are not suitable. More recently the aluminium price has risen once again but due to its attractive properties remains commonly employed in many fields. A given volume of aluminium weighs less than one-third as much as the same volume of steel, the only less dense metals being lithium, beryllium and magnesium. It is used in the construction of railway carriages, aircraft, and motor vehicles, and for other applications in which energy conservation is important. Due to its high heat conductivity, aluminium is used in cooking equipment and the pistons of internal-combustion engines.

Aluminium also has many other applications. The metal is becoming increasingly important architecturally, for both structural[8] and ornamental purposes. Also because of its ease of forming, low weight and compatibility with food and beverages, it is widely used for containers, flexible packages, and bottles and cans. The recycling of such containers is an increasingly important energy-conservation measure[9]. Its excellent corrosion resistance in salt water also makes aluminium useful in boat hulls and various aquatic devices where it is used in conjunction with composite materials and other more dense metals.

### *1.1.3 Alloys*

Alloys are either materials composed of two or more metals or a metal combined with a small quantity of a non-metallic element[10]. Most commonly used metals are not of very high purity: impurity atoms are intentionally added, thus forming an alloy. Alloying is used in metals to improve many characteristics such as their mechanical strength, electrical and magnetic properties and resistance to corrosion[11].

Recent estimates suggest that there may be as many as 40,000 alloys in existence. Commonly employed ones today are; sterling silver, silver alloyed with copper to increase its strength; brass, copper alloyed with zinc; bronze, copper alloyed with tin and all steels.

### *1.1.4 Aerospace aluminium*

Aluminium has been used in the manufacture of aircraft since the middle of the 1930s. Elemental aluminium has a density low enough to be compared with some composite materials, and has excellent corrosion resistance to survive the severe climate changes aircraft work in[2]. However, because of the extreme forces exerted on modern-day planes it has been essential to increase the strength of the metal used. Therefore, different elements have been alloyed with aluminium to provide this change.

As there are so many different alloys, a system for designating wrought aluminium and its alloys was established by the Aluminium Association[12]. It must be noted, however, that this system does not cover cast aluminium alloys. A system of four-digit numerical designation is used to identify wrought aluminium and wrought aluminium alloys.

The first digit indicates the alloy group as follows:

| | |
|---|---|
| 1XXX | Aluminium, 99.00% minimum and greater |

In the 1XXX group for minimum aluminium purities of 99.00 percent and greater, the last two of the four digits in the designation indicate the minimum aluminium percentage. These digits are the same as the last two digits to the right of the decimal point in the minimum aluminium percentage when it is expressed to the nearest 0.01 percent. The second digit in the designation indicates modifications in impurity limits; if it is zero, it indicates unalloyed aluminium having natural impurity limits; if

it is between 1 and 9, it indicates special control of the individual impurities or alloying elements.

Aluminium alloys are grouped by their major alloying elements (figure 1.02).

| | |
|---|---|
| 2XXX | Copper (Cu) |
| 3XXX | Manganese (Mn) |
| 4XXX | Silicon (Si) |
| 5XXX | Magnesium (Mg) |
| 6XXX | Magnesium and Silicon (Mg and Si) |
| 7XXX | Zinc (Zn) |
| 8XXX | Other elements |
| 9XXX | Unused series |

Figure 1.02. Table showing the major alloying elements of different series of aluminium alloys

In the 2XXX to 8XXX alloy groups the final two digits in the designation serve only to identify the different aluminium alloys in the group. The second digit in the alloy designation indicates alloy modifications. If the second digit is zero, it indicates the original alloy. 1-9, which are assigned consecutively, indicate alloy modifications.

The temper designation system is used for all forms of wrought and cast aluminium and aluminium alloys (Chapter 8, appendix 1). It is based on a sequence of basic treatments used to produce various tempers. The temper designation follows the alloy designation separated by a hyphen. Basic designations consist of a letter while subdivisions of those basic tempers, where required, are indicated by one or more digits following those letters (Chapter 8, appendix 2). The system is designed to set down specific sequences of fabrication processes. Should some other variation of the same sequence of basic operations be applied to the same alloy, resulting in different characteristics, additional digits will be added to the numerical designation.

The current aerospace grade of aluminium used in the fuselage and wings of commercial aircraft is referred to as aluminium alloy 2024-T3 (AA2024-T3)[13]. It is therefore heavily based upon copper as well as having several other key alloying components (figure 1.03). This alloy has proven to show a great increase in mechanical properties but, unfortunately, as a result of adding these slightly more corrosion prone elements the likelihood of corrosion also goes up.

| **Alloying Element** | **Composition (%)** |
|---|---|
| Aluminium | 91.4 |
| Copper | 4.5 |
| Magnesium | 2.0 |
| Manganese | 0.8 |
| Silicon | 0.8 |
| Iron | 0.5 |

Figure 1.03. Elemental composition of Aluminium Alloy 2024-T3[14]

### *1.1.5 S-phase intermetallics*

The major reason that alloying causes an increase in corrosion likelihood is through the formation of intermetallic particles on the surface of the metal (figure 1.04).

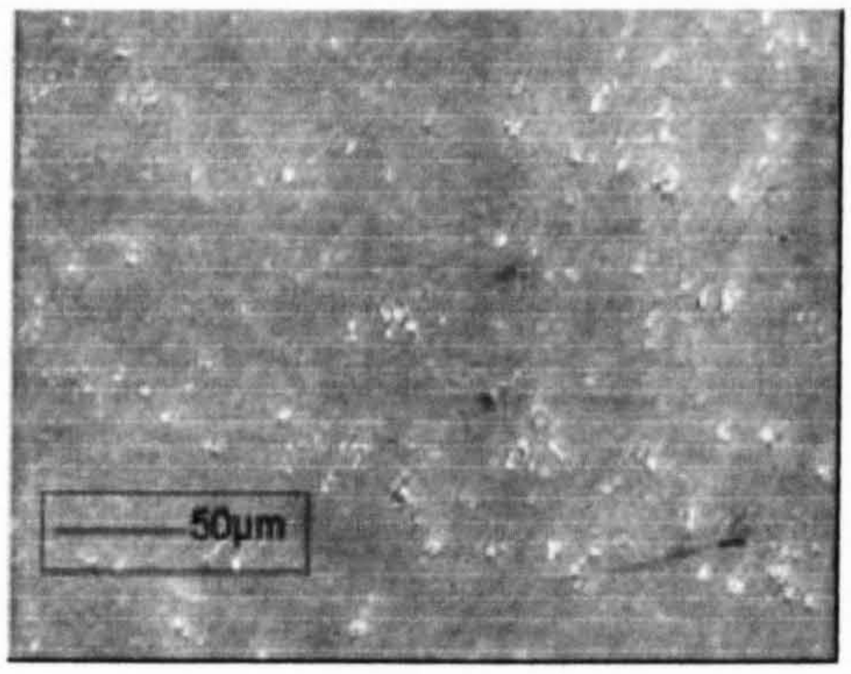


Figure 1.04. SEM image obtained at 10kV and 200x magnification showing an Al 2024-T3 surface with visible intermetallic particles[15]

In AA2024-T3 the most common group of intermetallics are the secondary phase or S-phase particles (figure 1.05).

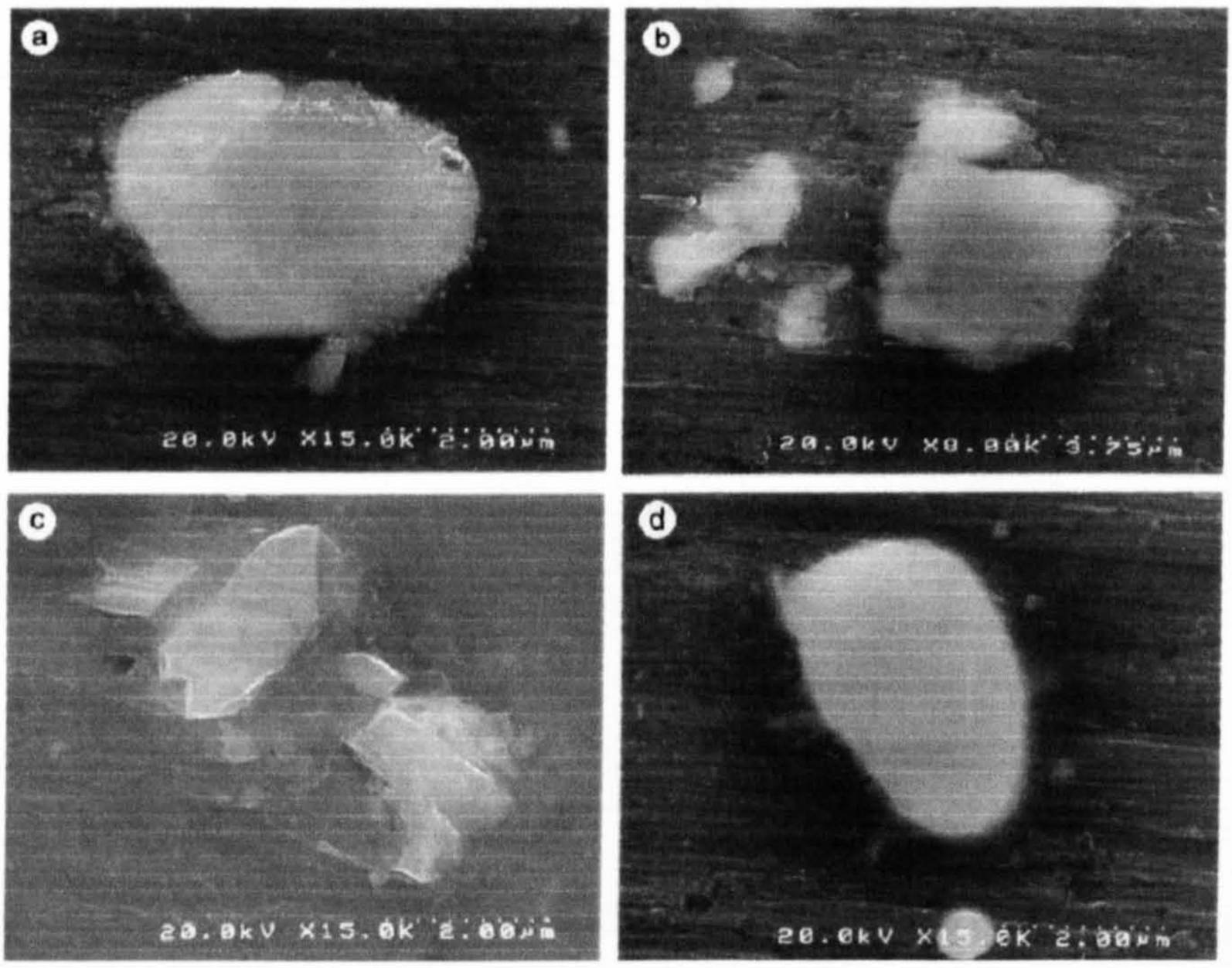


Figure 1.05. SEM images obtained at 20kV and 15000x magnification showing the four different types of S-phase particle in Al2024-T3

a) Al-Cu-Mg. b) Al-Cu-Fe-Mn. c) Al-Si. d) Al-Cu[15]

The two most common types of particle are Al-Cu-Mg and Al-Cu-Fe-Mn, the former acting anodically to the aluminium matrix and the latter cathodically. These and other intermetallics serve as pit initiators for corrosion to spread throughout the metal. Pit initiators are unwanted on the metal as the presence of pits on the surface increases the likelihood of fatigue failure.

### *1.1.6 Future Technologies*

Even though aluminium is currently used in large amounts on today's aircraft, the planes of tomorrow will more likely be built out of other, more specialised materials. The Airbus A380, for example, is currently in production and is primarily manufactured from GLARE, a fibre-metal-laminate compound[16]. GLARE is only

the fifth new material to ever be used on commercial aeroplanes and was initially developed at Delft University in the Netherlands[17]. First used in small amounts on their 777 aircraft, Boeing considered the material too expensive to be used in the quantities required for the body of a plane. This was due in part to the complex manufacturing process which was needed to join the 4 layers of aluminium and 3 layers of fibres together (figure 1.06). However, Airbus continued development of the technology and their new "superjumbo" craft will be composed of between 3-4 wt% of the compound.

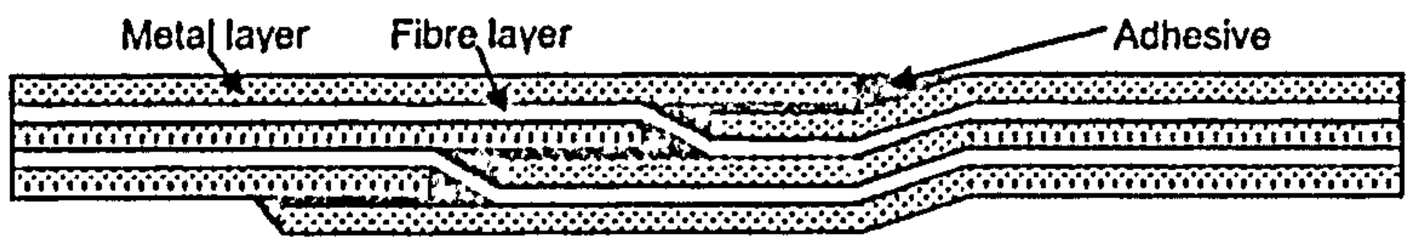


Figure 1.06. Schematic representation of GLARE structure[17]

On the other hand, Boeing's new aircraft, the "787 Dreamliner" will be composed of approximately 50% of standard carbon fibre composite materials. Similarly to aluminium, both these materials have advantages and disadvantages and it will be interesting to see which of these new technologies is more successful.

## 1.2 Corrosion resistance

Corrosion resistance is hugely important to materials used today. It is estimated that corrosion costs the global economy at least $275 billion per annum[18].

The type of corrosion mechanism and its rate of attack differ greatly depending on the exact nature of the atmosphere in which the material is located. For example, in today's industrial setting, waste products materialise in the atmosphere acting as catalysts or inhibitors to corrosion. This differs enormously to rural areas where no catalysis can occur and corrosion likelihood is much lower[19].

Corrosion occurs because of the existence of anodic and cathodic areas on the metal's surface[20]. This difference in electric potential can be attributed to a number of causes, the primary one being a change in oxygen concentration.

The best-known type of corrosion, galvanic corrosion, occurs at the contact point of two metals with different electric potentials[21]. Similar differences in potential can develop between areas of a single metal where small changes in either composition or crystal structure may exist. The area of metal that becomes corroding is the anode, the other being the cathode which does not corrode.

In the aerospace industry, the most common type of corrosion is filiform (or wormtrack) corrosion[22]. This occurs under organic coatings in the form of randomly distributed threadlike filaments. It is most commonly found on aluminium but has also been observed on nickel alloys that possessed a thick oxide layer.

The corrosion filaments grow along the metal / coating interface at typical rates of up to 1mm per day (figure 1.07). The moving end of the filament is called the "head", and the remainder of the track is called the "tail".

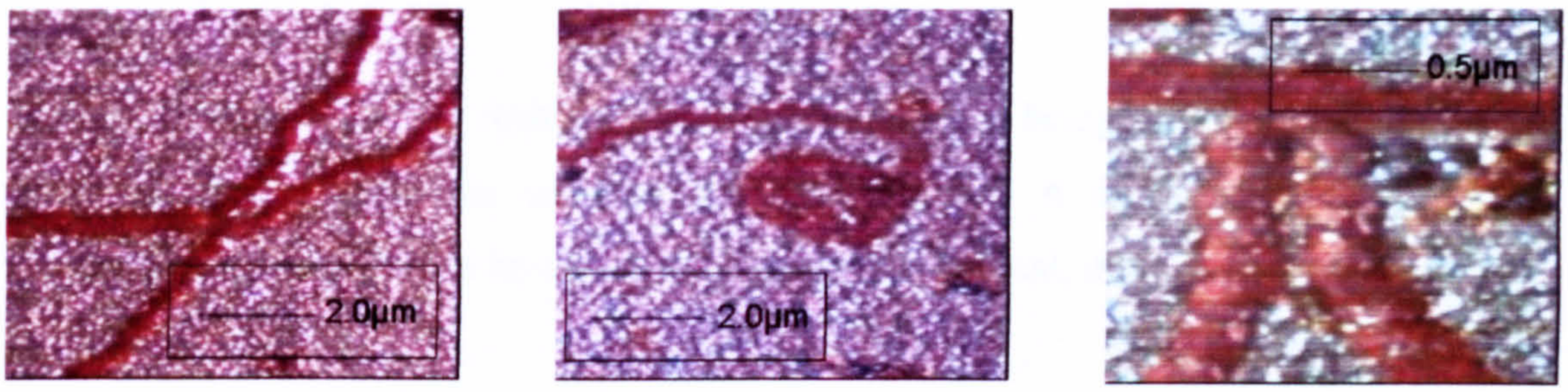


a b c

Figure 1.07. SEM images obtained at a and b 10kV and 4000x magnification and c 10kV and 9000x magnification showing filiform corrosion on low carbon steel[22]

Filiform heads are oxygen concentration cells meaning that the centre of the head acts as an anode and the periphery of the head acts as the. Large potential differences have been measured across the anode-cathode junction, which is where the primary corrosion reaction occurs.

Although the electrochemical aspects of filiform corrosion are well established, it remains unclear why there is thread-like[23]. Filiforms do not cross the inactive tails of other filaments, but can reflect if they collide with other filaments. However, if an active filiform strikes an inactive tail at 90°, it may either become inactive or, split into two new filaments, each being reflected at approximately 45°. Growing filaments cannot cross inactive areas and are often trapped as the available space decreases (figure 1.07b). Although the first report on the interaction of filiform patterns dates back into the 1970s[24], hardly any quantitative data exists on this phenomenon and the underlying mechanisms remain unclear.

## 1.3 Adhesion

A second area of huge importance in the aerospace industry is the successful bonding of component parts in the creation of the aircraft. Obviously, aeroplanes are vast structures and are composed of many sections. Previously, these parts have been either welded, riveted or a combination of the two together but today, modern adhesives are able to give similar effects to these techniques[25].

Welding is carried out by melting pieces of the material being joined and adding a filler material. When the molten material is cooled, it forms a strong joint. Alternatively, pressure can be used in conjunction with heat, or sometimes by itself, to produce the weld.

Rivets are mechanical fasteners made up of smooth cylindrical shafts with heads on either end. The two heads are larger than the diameter of the hole into which the rivet has been inserted. Generally one head is factory formed and the other formed by applying a force to the metal after the rivet has been inserted.

Adhesion science and the corresponding technology behind it has only thoroughly developed in the last 60-70 years[26]. This has been due to the advent of successful

commercial synthetic polymers and the superior structural and load-bearing properties they possess compared to natural derivatives.

An adhesive joint is attained by interfacial contact between an adhesive and substrate. Once this has been established, an intrinsic adhesive force needs to be activated to hold the two components together throughout its service life. This intrinsic force can be caused by any adhesive mechanism. Currently there are six of these which have been investigated since the 1940s[27]:

### *1.3.1 Mechanical interlocking*

This is based on the principle that when an adhesive is applied, it can "lock" into irregularities present on the substrate surface. This mechanism is primarily mechanically based although it can contribute to intrinsic adhesion if the surface has been pretreated to obtain the correct topography.

### *1.3.2 Diffusion theory*

This deals with the transfer of polymer chain ends across an interface to react with another polymer to create autoadhesion. This requires sufficiently mobile polymers meaning that they must be above their glass transition temperatures and mutually soluble. Diffusion of different polymers is a controversial topic as there is uncertainty as to whether the enhancement is actually due to diffusion or simply because of better interfacial contact.

### *1.3.3 Electronic theory*

This theory is involved with the interaction between two substances of differing electronegativities. It is probable that there will be electronic transfer to balance the Fermi levels, resulting in the formation of an electronic double layer at the interface. To separate the materials, the electronic attraction of the double layer has to be overcome; this corresponds to an increase in potential difference, culminating in an electronic discharge.

### *1.3.4 Van der Vaal's forces*

These are sometimes called secondary molecular forces, and are involved in the mechanism of physical absorption. These secondary forces can be separated into three categories involving interactions between dipoles: Dipole-dipole interactions (Keesom forces), dipole-induced dipole interactions (Debye forces) and molecule-molecule interactions (London dispersion forces). The latter occur as a result of a fluctuation in electron density around an atom, temporarily inducing a dipole in another atom thus causing a force of attraction. These forces are small due to an inversely proportional relationship to the sixth power with respect to atomic radius, thus meaning any increase in adhesive force will only be due to the surface layers.

### *1.3.5 Primary interactions*

These involve the formation of covalent, ionic or acid-base chemical bonds. Modern surface analysis techniques such as X-ray photoelectron spectroscopy (XPS) and static secondary ion mass spectrometry (SSIMS) have produced results that clearly prove these chemical interactions are occurring across the interface. This theory originated from the investigation of adhering silanes onto stainless steel surfaces. Kinloch and Gettings discovered that ionic species of $FeOSi^+$ and $CrOSi^+$ were present after SIMS analysis, suggesting the formation of cross-interface ionic bonds[28].

As with chemical bonding, it was suggested that acid-base interactions represented a major type of intrinsic adhesion force across the interface. Both Brønsted and Lewis acidity can occur and materials bonding this way can have one of three types of acid-base capabilities: The first is where the adhesive material acts as the acid eg. partially halogenated polymers. The second is where the surface acts as a base eg. esters, ketones and polystyrene. The third possible type of interaction involves both acid and base capabilities e.g. polyamides.

### *1.3.6 Weak boundary layers*

The final known theory of adhesion involves the concept of weak boundary layers forming either chemically or mechanically at the interface. Proposed by Bikerman in

the 1960s, this does not give information on how substances adhere to one another, it does, however, give information on why adhesives sometimes fail under low stress levels. Mechanically, he proposed that physical damage to the surface could have occurred to leave it cohesively weak. Chemically, he proposed that water or oil could cause surface oxidation to occur.

Obviously, it is common that several of these processes occur simultaneously to form a strong adhesive bond. Figure 1.08 shows the difference in bond energies associated with each different process. From this table it is clear that, for successful bonding, secondary interactions are not really suitable for adhesive joints under high stress, but in combination with a primary interaction they could assist the formation of a secure joint.

| **Type** | **Bond energy (kJ/mol)** |
|---|---|
| Primary Bonds: | |
| Ionic | 600-1100 |
| Covalent | 60-700 |
| Metallic | 110-350 |
| Donor-acceptor bonds: | |
| Bronsted acid-base interactions (i.e. up to a primary ionic bond) | Up to 1000 |
| Lewis acid-base interactions | Up to 80 |
| Secondary bonds: | |
| Hydrogen bonds: | |
| Hydrogen bonds involving fluorine | Up to 40 |
| Hydrogen bonds excluding fluorine | 10-25 |
| Van der Waals bonds: | |
| Permanent dipole-dipole interactions | 4-20 |
| Dipole-induced dipole interactions | Less than 2 |
| Dispersion (London) forces | 0.08-40 |

Figure 1.08. Table showing adhesive bond types and the energies associated with them[27]

Adhesives, however, do have some drawbacks compared to conventional mechanical means of attachment an example being the fact that their upper service temperature is normally lower than a riveted joint[29]. However, their main disadvantage is that for

successful adhesion, especially for use in severe conditions, surface pretreatment is essential.

## 1.4 Pretreatments

To help limit corrosion and provide greater adhesion to the metal surface different chemical and electrochemical pretreatments can be carried out to the aluminium. For many years the most common practice was a chromic acid etch which involved immersing the aluminium into a bath containing a mixture of potassium dichromate and sulphuric acid. The effect of the acid was to create a thin, corrosion resistant oxide film[30]. This film also gave the metal some surface roughness which it was believed aided mechanical-interlocking thus allowing greater adhesion to be achieved.

One way of achieving a more porous network for bonding is via the application of a voltage through the metal whilst it is immersed in the acid. This process is referred to as anodisation. Figure 1.09 shows that this electrochemical technique provides a highly structured oxide layer which is ideal for mechanical-interlocking.

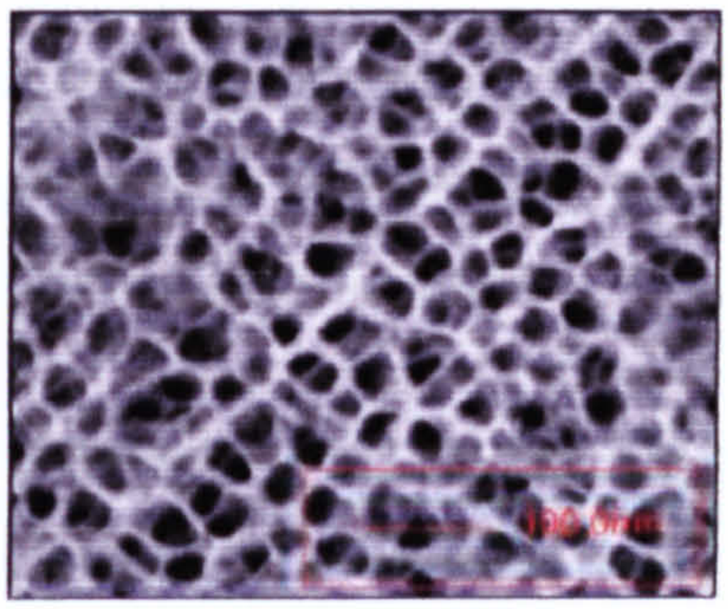

Figure 1.09. SEM image from this study obtained at 10kV and 100000x magnification showing a phosphoric acid anodised AA2024-T3 surface

In the last couple of years, chromic acid has been replaced due to environmental concerns from governments across the world[31]. The most commonly used alternative is phosphoric acid which is more benign but similarly creates a highly ordered surface oxide layer; albeit, a mirror image of that achieved with chromic acid.

However, as the aerospace industry requires such high levels of both adhesion and corrosion resistance, these electrochemical pretreatments are still not sufficient to withstand the harsh environments they are required to work in. Therefore, in the search to increase the working life of planes, scientists came up with the theory of coating the metals used so they could more readily withstand the harsh conditions in which they were expected to work.

## 1.5 Primers

Primer solutions have been used for the protection of aerospace metals for the last 20-30 years. In commercial aircraft primers are used mainly to coat the wings before painting and in the fuselage section between two bonded layers of aluminium alloy (Figure 1.10). Before the epoxy-based, thin film adhesive is bonded the metal surface is spray covered with the primer solution forming a layer of typically 2-4μm.

Primers are used for several different reasons[32]; including protecting the metal surface until bonding is carried out. If the primer consists of the adhesive dissolved in solution, the primer is more readily able to wet the surface providing a greater opportunity for a strong bond. Primers are also able to act as vehicles for corrosion inhibitors, allowing them to be kept near to the surface where they are required. The ability of the primer to form both chemical and physical bonds with the surface and adhesive is also advantageous as this forms a more closely bonded surface meaning that it is more difficult for corrosion to occur.

The choice of primer depends largely on the adhesive being used and also on the specific properties that the surface possesses.

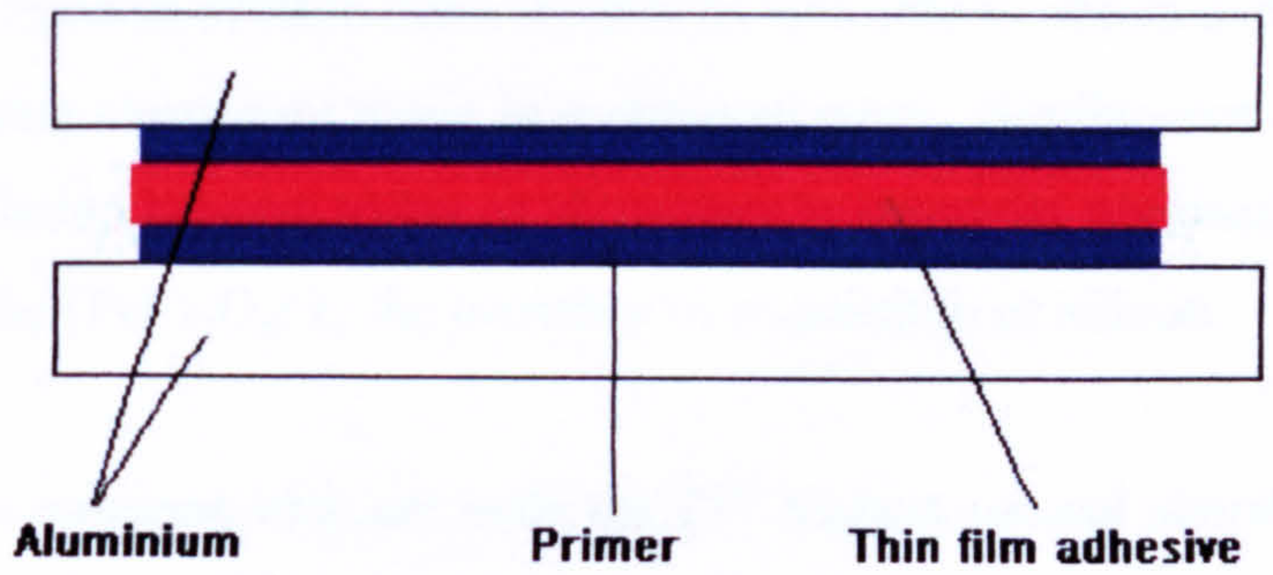


Figure 1.10. Use of primer in aerospace applications

However, there are also several problems with the current generation of primers. Most of these are due to the formulation, which consists of approximately 90wt% volatile organics, 8wt% epoxy-phenolic resins and 2wt% strontium chromate or zinc chromate.

The first two compounds present hazards to the environment by causing damage to the ozone layer and marine life but can be thought of as to possess minor hazards to human health. However, the presence of chromates, which are highly toxic to humans, especially for workers handling the materials, means that these chemicals have been banned from use in some parts of America and Europe[33].

In recent years the European Union adopted, the Restriction of Hazardous Substances Directive (RoHS)[34] in February 2003 by. The RoHS directive took effect on July 1st 2006, but it is not a law, simply a set of guidelines. RoHS restricts the use of six hazardous materials in the manufacture of various types of electronic and electrical equipment, one of which is hexavalent chromium.

### *1.5.1 Chromium*

Chromium was discovered in 1797 by the French chemist Louis Nicolas Vauquelin, who named it after the Greek word chroma (colour) because of the many different colours of its compounds. Vauquelin was experimenting with a material known as Siberian red lead, also known as the mineral crocoite ($PbCrO_4$). He produced chromium oxide ($CrO_3$) by mixing crocoite with hydrochloric acid (HCl). Although he believed a method for isolating chromium did not yet exist, Vauquelin was pleasantly surprised in 1798 to discover that he was able to obtain metallic chromium by simply heating chromium oxide in a charcoal oven. Similar methodology is still used in the isolation process today as chromium is primarily obtained by heating the mineral chromite ($FeCr_2O_4$) in the presence of aluminium or silicon.

Chromium is a common element with the 21$^{st}$ highest natural abundance in crustal rocks[5]. It is a blue-white metal that is hard and brittle with excellent corrosion

resistance. It can be polished to form a very shiny surface and is often plated to other metals to form a protective and attractive covering.

Chromium forms many colourful compounds that have industrial uses. Lead chromate ($PbCrO_4$), also known as chrome yellow, is still used as a yellow pigment in paints, whilst chromic oxide ($Cr_2O_3$) the ninth most abundant compound in the earth's crust is a widely used green pigment. Rubies and emeralds also owe their colours to chromium compounds. Potassium dichromate ($K_2Cr_2O_7$) is used in the tanning of leather while other chromium compounds are used as mordants, materials which permanently fix dyes to fabrics. Chromite, chromium's primary ore, is used to make moulds for the firing of bricks because of its high melting point, moderate thermal expansion and stable crystal structure[35].

### *1.5.2 The chemistry of chromium*

Chromium exists most commonly in the III and VI oxidation states; however, there are examples of the rarer II, IV and V species[36].

The chromium II ion is most easily prepared by dissolving chromium metal in dilute mineral acids. The solutions must be kept under inert conditions as they are liable to decompose, reducing water, giving the liberation of hydrogen gas.

Chromium III complexes are highly abundant, usually appearing as six coordinate species. They are highly studied due to their excellent kinetic stability. Because of this many species have been isolated, the most numerous normally possessing amine ligands. These complexes have provided examples of virtually every kind of isomerism possible for octahedral species.

The most easily accessible species of chromium IV and V are those that are bonded to carbon, oxygen or nitrogen. Chromium IV is often formed by the oxidation of chromium III complexes, for example $Cr(OCMe_3)_4$. Chromium V complexes are

often formed by the reduction of $CrO_3$ with concentrated hydrochloric acid in the presence of alkali ions at 0°C, for example $M_2(CrOCl_5)$.

Chromium VI is the second most common form of chromium after the trivalent species. It is most often found in the chromate ion ($CrO_4^{2-}$) or the dichromate ion ($Cr_2O_7^{2-}$). The former is tetrahedral in structure and the latter similar, incorporating a bridging oxygen (figure 1.11).

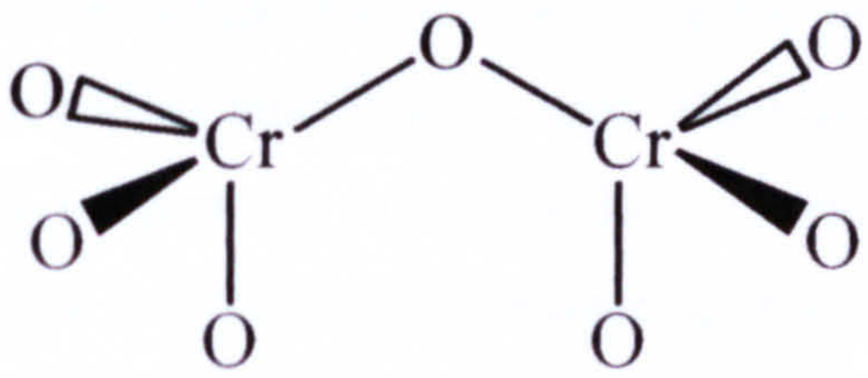


Figure 1.11. Diagram showing the dichromate ion structure

Unlike more acidic oxides such as molybdenum VI and tungsten VI, chromium VI does not show an extensive series of polyacids or polyanions. This is due to the fact that there is much more multiple bonding in chromium VI complexes because of possessing a smaller central ion.

The exact mechanism through which chromium VI operates is not thoroughly understood. From a biological point of view it has been studied extensively with the development of such theories as reducing to the less toxic Cr (III) through an unstable Cr (V) intermediate.

However, it is not known whether the theories suggested for these biological applications will be consistent throughout the materials chemistry sector. Consequently, the aerospace and electronics industries have been conducting large amounts of research in the aim of furthering the understanding of the mechanisms by which chromium operates

### *1.5.3 Other uses of hexavalent chromium*

Chromium VI is a commonly used chemical in may other industries as well as for aerospace technologies; due to its bright colour, it is often employed in the paint and pigments industry for inks and plastics[37]. Additionally, hexavalent chromium is used in the construction industry both in cements and anticorrosive plating[38].

Hexavalent chromium compounds are also widely employed and very powerful oxidation agents for several functional groups. Their most common application is the selective oxidation of primary and secondary alcohols to aldehydes, ketones or carboxylic acids. The mechanism of this reaction is known to proceed via chromyl-esters which are cleaved to their products through base-catalysis[39].

Common reagents for the selective oxidation of alcohols to aldehydes and ketones are pyridinium chlorochromate, known as Corey's reagent, and a mixture of chromium VI oxide and pyridine in dichloromethane, known as Collins reagent.

However, the problems associated with hexavalent chromium have garnered much media attention for the past couple of decades. It has been 80 years since it was first noticed that workers in the German chrome ore industry developed lung cancer more often than the rest of the population. Study after study since the 1920s has shown that people who work around industrial processes using chromium have higher-than-normal rates of lung and nasal cancers. Certain Cr (VI) compounds have been found to be carcinogenic in humans, but the evidence to date indicates that the carcinogenicity is site-specific, limited to the lung and sinonasal cavity, and dependent on high exposures[40].

Ingestion of very high doses of Cr (VI) can cause kidney and liver damage, nausea, irritation of the gastrointestinal tract, stomach ulcers, convulsions, and death. Dermal exposures may cause skin ulcers or allergic reactions (Cr (VI) is one of the most highly allergenic metals, second only to nickel)[41]. Also, studies of mice fed high doses of Cr (VI) have shown reproductive effects including reduced litter size and decreased foetal weight.

Due to the large number of drawbacks associated with hexavalent chromium, suitable 'greener', more environmentally benign alternatives are being sought and much research has been carried out to achieve this. These alternatives have been investigated as both direct replacements for chromium within the primer formulation and also as alternative methods of primer deposition onto the aluminium surface.

However, none of the alternative primers generated have been as successful at corrosion protection and adhesion promotion and it is believed that this is due to an inherent lack of knowledge of the functions of chromate.

## 1.6 Alternatives

Previously investigated alternatives have included a range of materials from rare-earth metals (e.g. Ce (IV)) to organic based compounds. Much of the early research was concentrated in the USA but in the last decade there has also been work conducted in Europe, Australia and the Far East.

### *1.6.1 Lanthanides*

The lanthanides have been studied extensively as chromate alternatives[42], with work focussing on cerium and lanthanum. These are favourable when compared to chromate because they are non-harmful and also relatively abundant in the earth so are not economically restrictive.

Early research concentrated on the chloride derivatives which showed vast increases in corrosion resistance up to metal concentrations of 100ppm. Beyond this level there was a plateau and this saturation is similar to what happens with the addition of some transition metals compounds when used as corrosion inhibitors.

More recent research has looked at the formation of a salicylate derivative $Ce(salicylate)_3$ [43].

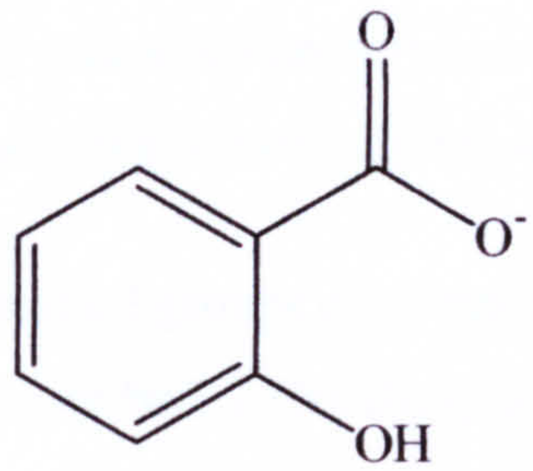


Figure 1.12. Diagram showing the structure of the salicylate ion

Salicylate (figure 1.12) is a known organic corrosion inhibitor and this compound was added to a steel surface. It was found that an inert chemically bonded species containing cerium, iron and salicylate had been formed.

### *1.6.2 Citric acid*

A further natural product that has shown some use in increasing corrosion resistance is citric acid[44]. It is believed that this species forms a chelate along with Al (III) (figure 1.13) to prevent the evolution of hydrogen in the following reaction:

$$2Al + 6H_2O \rightarrow 2Al(OH)_3 + 3H_2$$

The hydrogen evolved lead to pressure build-ups in beverage cans and therefore a form of corrosion inhibition was required.

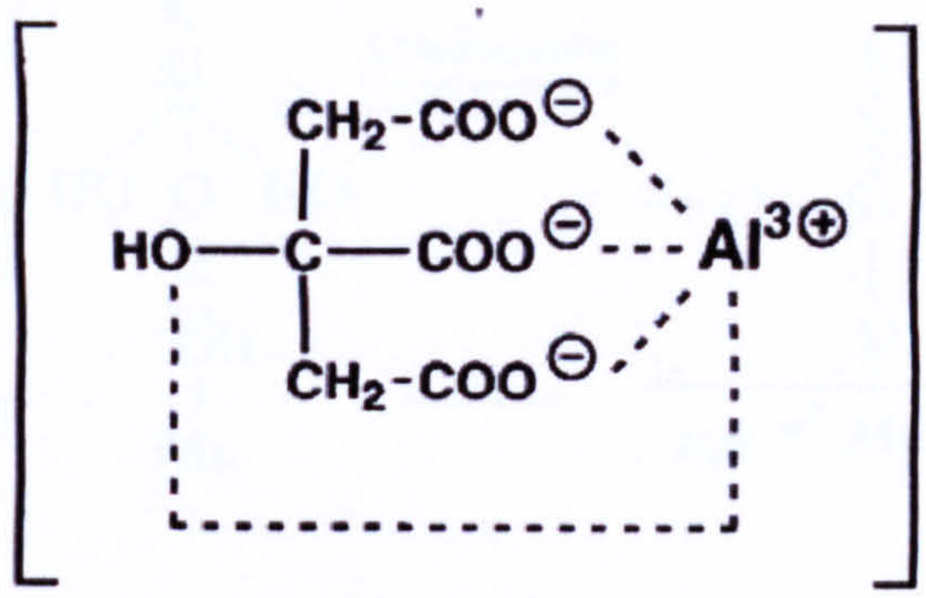


Figure 1.13. Probable structure of citric acid – aluminium (III) chelate species

### *1.6.3 Silicon based alternatives*

However, it is silicon and its related species that have been investigated in greatest detail. For the last thirty years researchers have believed that silanes offer the best opportunity to generate an environmentally benign alternative.

One of the most highly studied groups of compounds are the bis-silanes (figure 1.14), in particular species based on bis1,2-(triethoxy silyl)ethane (BTSE)[45].

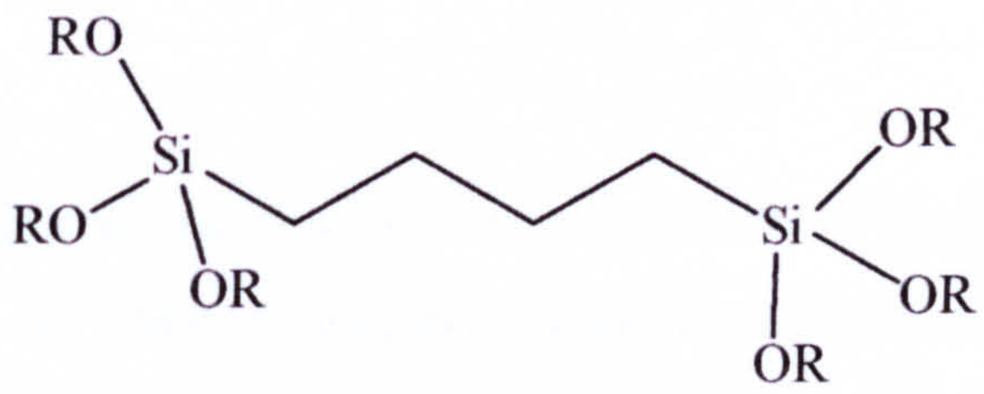


Figure 1.14. Structure of bis-silane molecule

The bis-silanes have proven to be more successful at providing good corrosion resistance than the mono compounds due to the fact that they have twice as many hydrolysable OR groups. This means that they are able to form more covalent bonds at the interface, whilst also building a crosslinked Si-O-Si network, thus providing stronger coverage that is more difficult to corrode (figure 1.15).

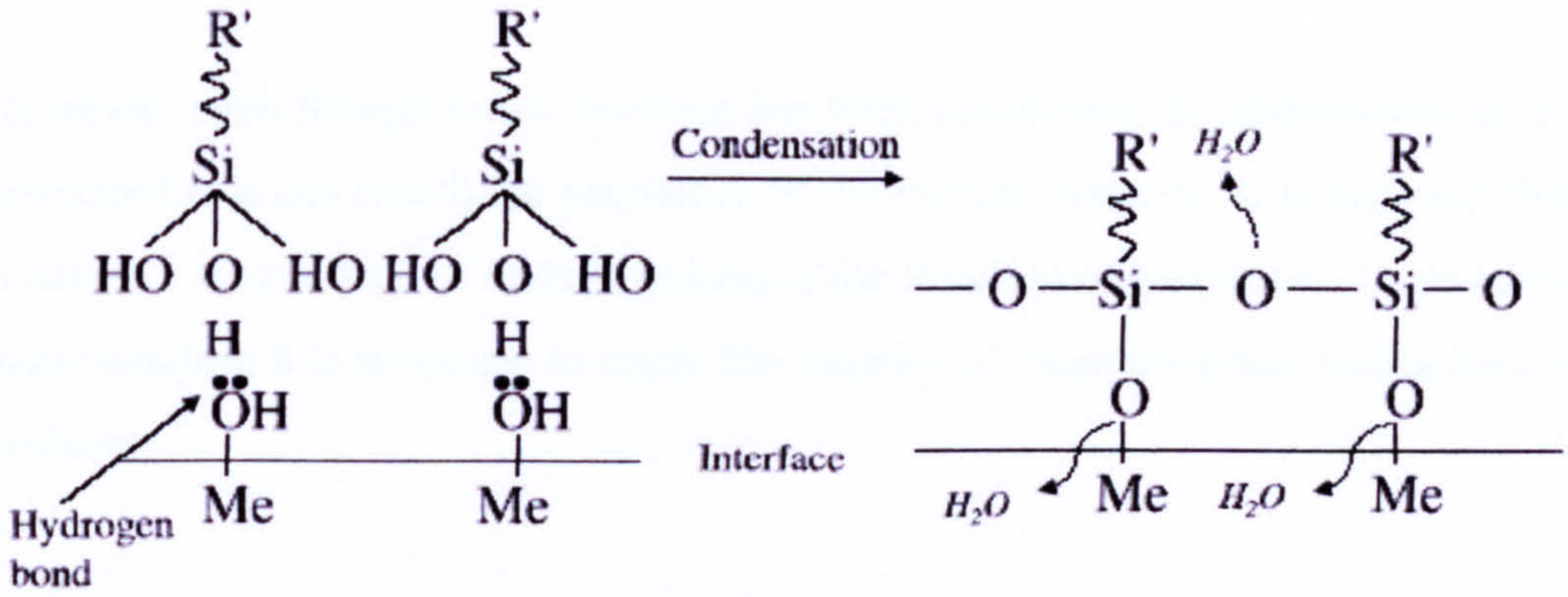


Figure 1.15. Diagram of bonding mechanism and formation of Si-O-Si network[45]

More recent work has been focussed on γ-glycidoxypropyltrimethoxy silane (GPS). These species have again shown the ability to form covalent bonds between a hydrolysed form of the compound and oxidised metals. This gives added stability to the surface providing a solid base for good adhesion[46]. A recent, wide-ranging investigation into the effects of surface treatment with γ-GPS by Shaw et al [30,47,48,49,50,51,52,53,54,55,56] suggests that this compound gives superior adhesive performance to similar phophonate compounds[52] and good corrosion resistance stating that corrosion would not be a determining fact in the joint failure mechanism[54].

An up and coming technology in the area of silicon chemistry is that of sol-gel coatings. These are organic-inorganic hybrid compounds containing approximately 2.5-4.5% solids that have shown both good corrosion resistance and adhesion promotion[57]. They are formed by many hydrolysis and condensation reactions (figure 1.16).

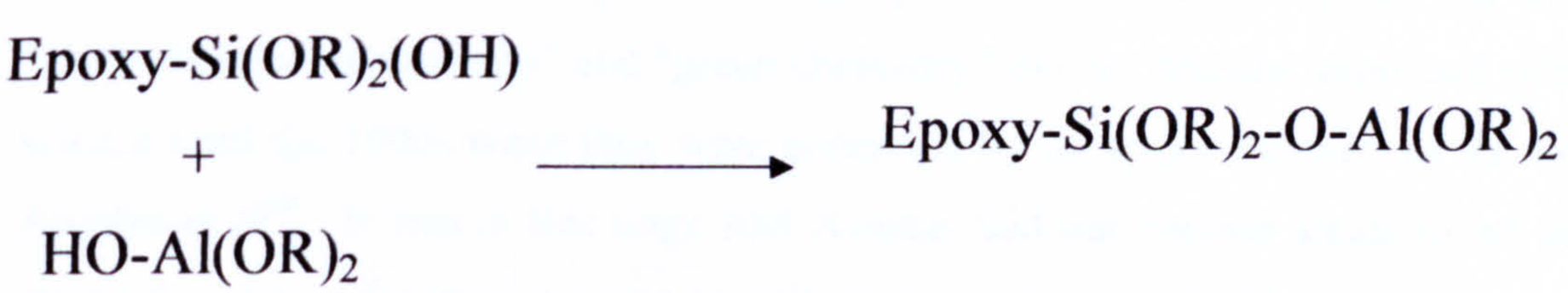


Figure 1.16. Formation of a sol-gel system[57]

However, even though much research has been conducted, no alternatives have been generated that can match the properties of the current primers. It is believed that this is due to a simple lack of understanding of the function of chromate. To increase this understanding it is proposed to apply the theories of clean chemical technology to the problem.

## 1.7 Clean chemical technology

Clean chemical technology or "green chemistry" is most clearly characterised as the design of chemical products and processes that reduce or eliminate the use and generation of hazardous substances. In more specific terms, clean chemical technology concentrates on the design of chemical products and processes that provide greater environmental benignity. For example, if clean chemical technology were to be used in a process, then the inputs and outputs of that process should be safer, with lower energy consumption, less waste and reduced costs. In return, the yields of the desired products would increase and by-product separation become simpler.

Increasingly strong environmental protection laws have meant that the chemical industry has had to focus on greater benignity for some years, however, the terms "clean chemical technology" and "green chemistry" did not become important within science until the 1990s when they were generated by the major pioneers of the field Anastas et al[58]. It was at this stage that Anastas laid out various ideals to act as a strong foundation for more environmentally benign science to build upon.

Anastas' "Twelve Principles of Green Chemistry" are reproduced below.

1. Prevention: It is better to prevent waste than to treat or clean up waste after it has been created.

2. Atom Economy: Synthetic methods should be designed to maximize the incorporation of all materials used in the process into the final product.

3. Less Hazardous Chemical Synthesis: Wherever practical, synthetic methods should be designed to use and generate substances that possess little or no toxicity to human health and the environment.

4. Designing Safer Chemicals: Chemical products should be designed to affect their desired function whilst minimising their toxicity.

5. Safer Solvents and Auxiliaries: The use of auxiliary substances (e.g. solvents, separation agents, etc.) should be made unnecessary wherever possible and innocuous when used.

6. Design for Energy Efficiency: Energy requirements of chemical processes should be noted for their environmental and economic impacts and should be minimised. If possible, synthetic methods should be conducted at ambient temperature and pressure.

7. Use of Renewable Feedstocks: A raw material or feedstock should be renewable rather than depleting whenever technically and economically practical.

8. Reduce Derivatives: Unnecessary derivatisation (e.g. use of blocking groups, protection/deprotection, temporary modification of physical/chemical processes) should be minimised or avoided if possible, because such steps require additional reagents and can generate waste.

9. Catalysis: Catalytic reagents (as selective as possible) are superior to stoichiometric reagents.

10. Design for Degradation: Chemical products should be designed so that at the end of their function they break down into innocuous degradation products and do not persist in the environment.

11. Real-Time Analysis for Pollution Prevention: Analytical methodologies need to be further developed to allow for real-time in-process monitoring and control prior to the formation of hazardous substances.

12. Inherently Safer Chemistry for Accident Prevention: Substances and the form of a substance used in a chemical process should be chosen to minimise the potential for chemical accidents, including releases, explosions and fire.

Since their introduction, these initial principles have been adapted and expanded by others in the hope of generating an ideal, environmentally benign synthesis.

In this project we seek to apply the principles of clean chemical technology to create a new primer system. It is hoped that this alternative system will be more atom efficient, use less solvent and have a more simple formulation than those that are currently used. To do this an initial, in-depth study of the mechanism of chromate and its interaction with various epoxides will be conducted through the use of many different, state-of-the-art analytical techniques.

## 1.8 Analytical Techniques

Analytical techniques will be mostly used to characterise the surface and interfacial properties of the formulations that are synthesised. As a large variety of materials are to be studied, many different techniques will be employed. These will range from commonly used processes such as $^{1}H$ & $^{13}C$ NMR and liquid FT-IR to more specialised equipment, some of which is explained in further detail below.

### *1.8.1 Electrospray Ionisation Mass Spectrometry (ESI-MS)*

Mass spectrometry will be used to investigate the possible formation of polymeric species formed during reactions between the epoxy resins and chromate species in the primer system. As these species may contain some ionic character it is necessary to use the ESI-MS technique, using a quadrupole mass spectrometer.

#### *1.8.1.1 Background*

In a general sense, electrospray is a method of generating a very fine liquid aerosol through electrostatic charging[59], rather than the more familiar gas (pneumatic) methods, commonly used in the fragrance industry.

In an electrospray system, liquid passes through a nozzle, causing a plume of droplets to be generated by electrically charging the liquid to a very high voltage. The charged liquid in the nozzle becomes unstable as it is forced to hold an increasing concentration of charge. Soon the liquid reaches a critical point, at which it can hold no more electrical charge and at the tip of the nozzle it explodes into a cloud of highly charged micro-droplets (figure 1.17).

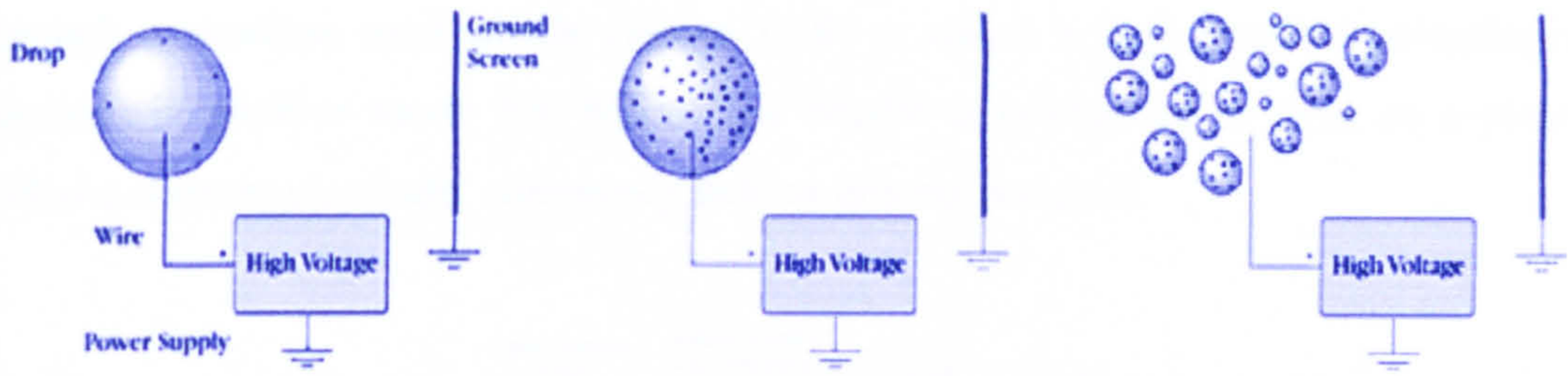


Figure 1.17. Diagram showing the effect of applying a charge on a droplet[60]

These droplets are less than 10μm in diameter and try to locate a potential surface that is opposite in charge to their own. As they move about, they rapidly shrink as solvent molecules evaporate from their surface, causing the distance between electrical charges in the droplet to dramatically decrease. If the droplet can not find a surface on which to dissipate its charge in time, the electrical charge reaches a critical state and the droplet will violently explode again. Originally observed by the physicist John Zeleny in 1914[61], the electrospray process has profoundly affected the field of mass spectrometry by allowing structural analysis of unlimited molecular weight, e.g., large biomolecules, and being directly compatible with liquid chromatography methods.

### *1.8.1.2 Mass Spectrometry*

Pioneering efforts in developing this mass spectrometry method were undertaken as early as 1968 by Dole et al[62] but only since the beginning of the '90s has ESI-MS become more widely used and have chemists begun to understand the great potential of this technique[63].

ESI-MS is one of the so-called 'soft' ionisation methods that are characterised by their ability to analyse large, complex and fragile molecules without incurring significant fragmentation to the parent compound[64]. This makes the process extremely useful in the analysis of polymers or large biomolecules such as DNA.

### *1.8.1.3 Instrumentation*

The most common electrospray apparatus used by mass spectrometrists involves the injection of sample solutions (organic or aqueous) into the electrospray chamber through a stainless steel needle (figure 1.18) at which a high positive potential is applied (in positive mode ESI-MS). The needle is positioned in front of a plate, called a counter-electrode, commonly held at ground potential

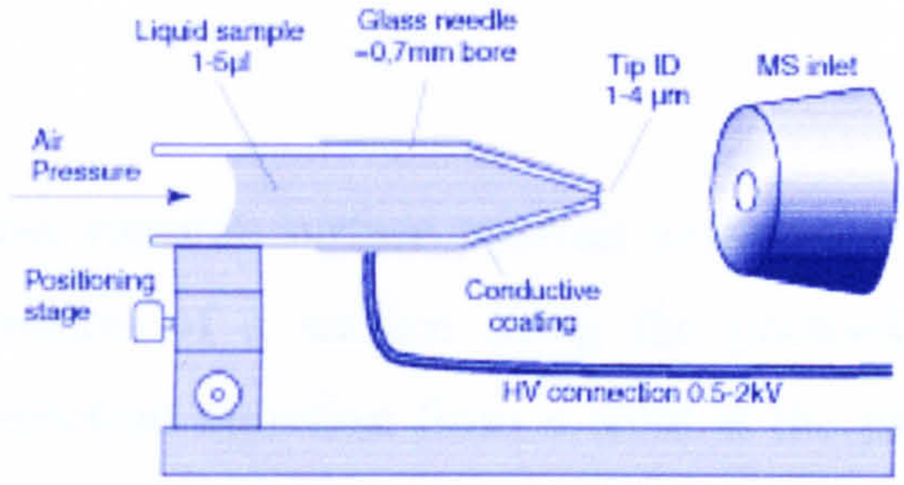


Figure 1.18. Diagram of needle tip and charging equipment used in an ESI-MS system[60]

The field at the needle tip charges the surface of the emerging liquid, dispersing it by Coulomb forces into a fine spray of charged droplets. The electric field causes the droplets to migrate from the sample inlet towards the detector carried by a flow of nitrogen gas. The temperature driving this process is approximately 200°C and the solvent vapour is swept away by the carrier gas flow. As the charged droplets evaporate, their surface charge density increases until a limit is reached at which the forces due to the electrostatic repulsion approach equality with those due to surface tension. This results in extreme instability, sometimes called a 'Coulomb explosion', which produces an array of daughter droplets which also evaporate until they too 'explode'.

This sequence is repeated until the ultimate droplets contain only one solute molecule and as the last solvent evaporates from this droplet a fuse ion is produced which is then detected[63].

### *1.8.2 X-Ray Photoelectron Spectroscopy (XPS)*

XPS will be used to investigate the surface properties of coatings applied to aluminium substrates. Initially, it will be used to monitor the possible reaction between chromium and aluminium alloys.

#### *1.8.2.1 Background*

XPS is one of the most versatile surface analysis techniques. It is able to determine the chemical composition of a surface using the photoelectric effect, whereby, photons can induce electron emission from a solid if the photon energy is greater than the work function of the solid[65].

#### *1.8.2.2 Instrumentation*

This consists of an X-ray source, a series of lenses to focus the photoelectrons and an energy analyser and detector. Samples are irradiated with X-ray photons and electrons are emitted from the sample if the photon is of sufficient energy. The kinetic energy of these photoelectrons is measured by the analyser and the binding energy of the photoelectron is calculated from the equation:-

$$KE = hv - BE - \Phi$$

where KE is the kinetic energy of the emitted photoelectron, hv is the X-ray photon energy and BE is the binding energy of the photoelectron which is the energy required to remove the electron from the atom. A work function Φ, predetermined for each spectrometer, is required for photoemission from solids as extra energy is required to transfer the electron from the surface to the vacuum level (figure 1.20). A spectrum of intensity vs. binding energy is generated from the above equation.

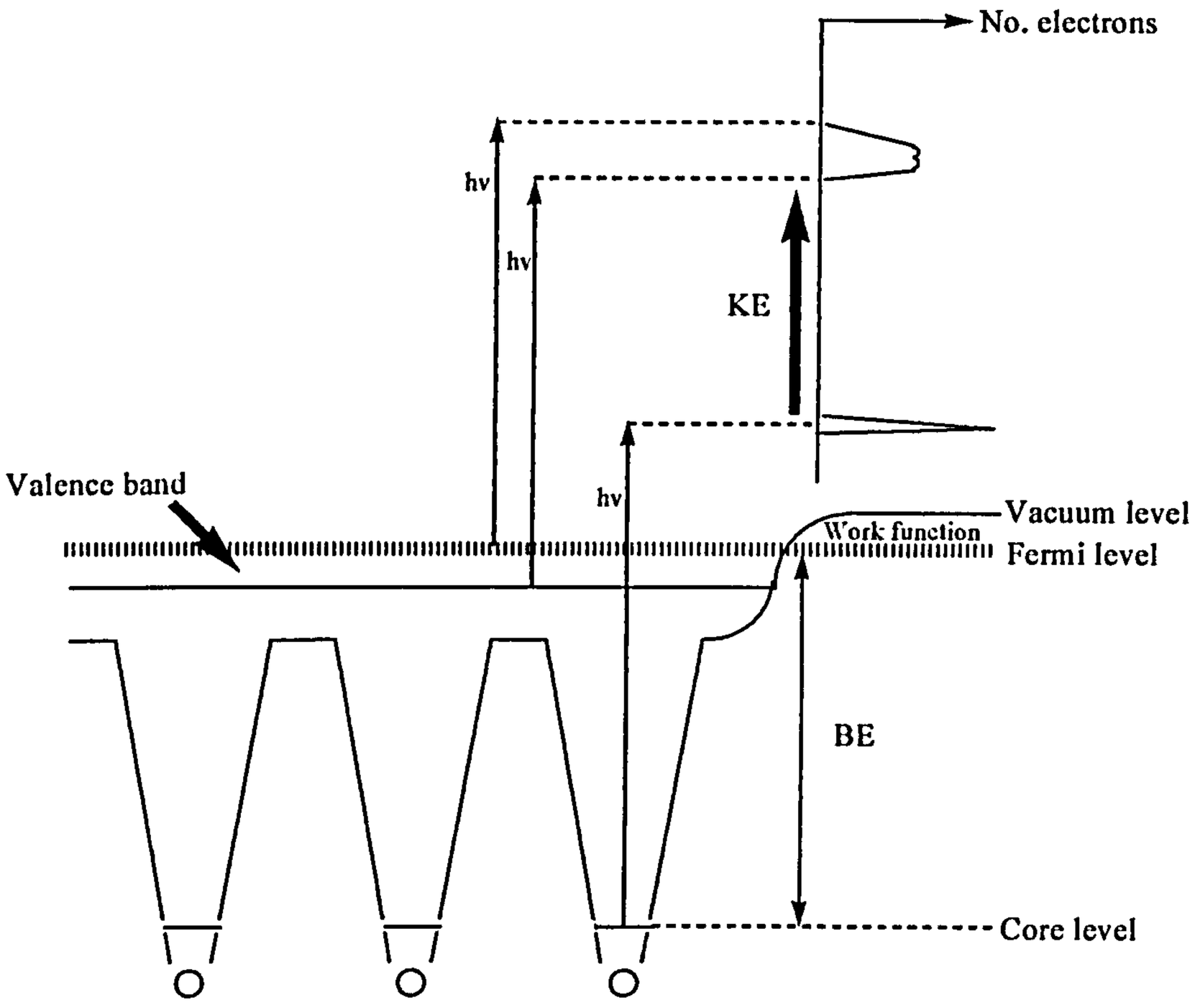


Figure 1.19. Diagram showing the energetics of an X-ray photoemission experiment[66]

The binding energy of an electron is not just characteristic of the element, but is also able to give information on the orbital and chemical environment. Therefore, XPS has the ability to determine the bonding state and oxidation states of materials and surface concentrations.

This is partly due to the monochromatic beam of X-rays used in XPS causing photoemission from both the core and valence levels of surface atoms. Core levels, or inner quantum bands, do not participate in chemical bonding. Valence levels are electrons in partially filled outer quantum shells which are more weakly bound. This

aids in chemical identification as the core electrons are insensitive to their surroundings and have binding energies that are a signature of the atom. The electrons that are involved in chemical bonding are broadened into a valence band and are emitted with a much higher kinetic energy, allowing for easy differentiation between the two bands.

XPS is a surface-sensitive technique as the mean free path of photoelectrons are of the order of a few nanometres in a solid. Electrons originating further below the surface suffer energy loss through collisions and may not even escape the surface. XPS analyses between 2-10 atomic layers, but greater depths can be investigated using a different X-ray source, ion etching and depth profiling. XPS is sensitive to surface concentrations as low as 0.1 atomic percent[67] and detects all elements except H and He. It offers the advantage over other surface-sensitive techniques of low beam damage and capability of analysis of insulating materials.

## 1.8.3 Scanning Electron Microscopy (SEM)

SEM will be used to study the effects of surface pretreatments such as acid anodisation and etching. It is hoped that through this technique, observable surface morphologies will give information on adhesive performance and the presence of corrosion inhibitors.

### *1.8.3.1 Background*

SEM was developed mainly because of the limitations of optical microscopy. Those been the large wavelength of visible light and the poor depth of field[68]. However, using electrons also has limitations. Firstly, electrons are not visible to the human eye; and secondly, electrons will not travel through air. This is because there are enough molecules in air to easily absorb an electron beam. Therefore, the electron source, lenses, and sample must all be under a vacuum. A further problem is that since electrons are electrically charged, the sample needs to be conductive enough to

dissipate this charge, meaning that gold coating of samples (particularly organic ones) is commonly employed.

### *1.8.3.2 Instrumentation*

Most SEMs have a hot cathode source, usually a tungsten filament which is heated by passing current through it. This not only emits light, but an electron cloud forms around the filament. Without further stimulation, the electrons would remain in the cloud and would reabsorb into the filament when the current is removed. A negatively charged cathode plate with a hole in it is placed near the filament (which they are repelled by) and a positively charged anode (which they are attracted to) under this with another hole in it.

The electron cloud is strongly attracted enough to the anode plate that it will travel through the hole in the cathode. In doing so, it gains enough speed that most of them travel through the hole in the anode plate. The speed of the electrons emitted from this system is controlled by the amount of potential (accelerating voltage) applied to the cathode and anode plates.

As in a light microscope, lenses are used to control the flow of electrons; however, the glass lenses of a light microscope are replaced by electromagnetic ones. The condenser lens controls the size of the beam (the amount of electrons travelling down the column). Increasing the beam intensity achieves a better signal to noise ratio, but because the beam diameter is larger, a lower resolution is obtained. The objective lens focuses the beam into a spot on the sample. This is necessary to have an image in proper focus (figure 1.20).

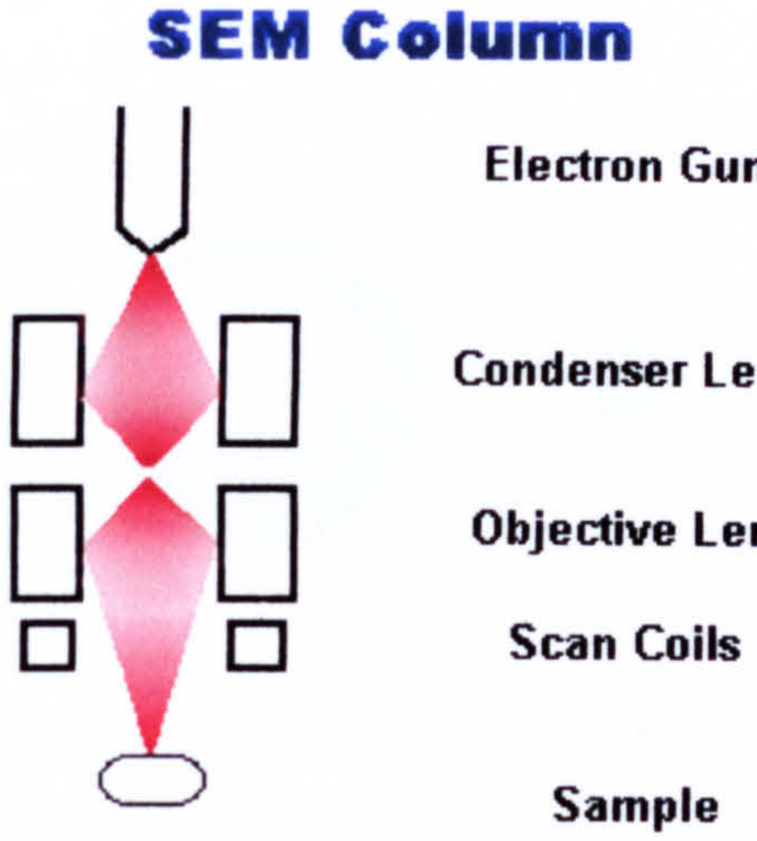


Figure 1.20. Schematic representation of an SEM[69]

By placing plates around the beam and varying the potential between them, the electron beam can be deflected. If attached to a scan generator, the beam can scan lines across the sample; hence, scanning electron microscope.

An electron detector is placed in the sample chamber which has a 10keV positive potential on its face, attracting the electrons emitted from the sample surface. One advantage of this biased detector is that it can attract electrons emitted from sides of the sample which are physically blocked from the detector face, greatly reducing shadowing effects in SEM images.

### *1.8.3.3 Methodology*

A single electron from the beam does not simply reflect off the sample surface. As it travels through the sample it has three possible paths: Firstly, it can pass unhindered through the sample. Secondly, it can collide with electrons belonging to the sample atoms, creating secondary electrons (figure 1.21). Or thirdly, it can collide directly with the nucleus of the sample atom, creating a backscattered electron.

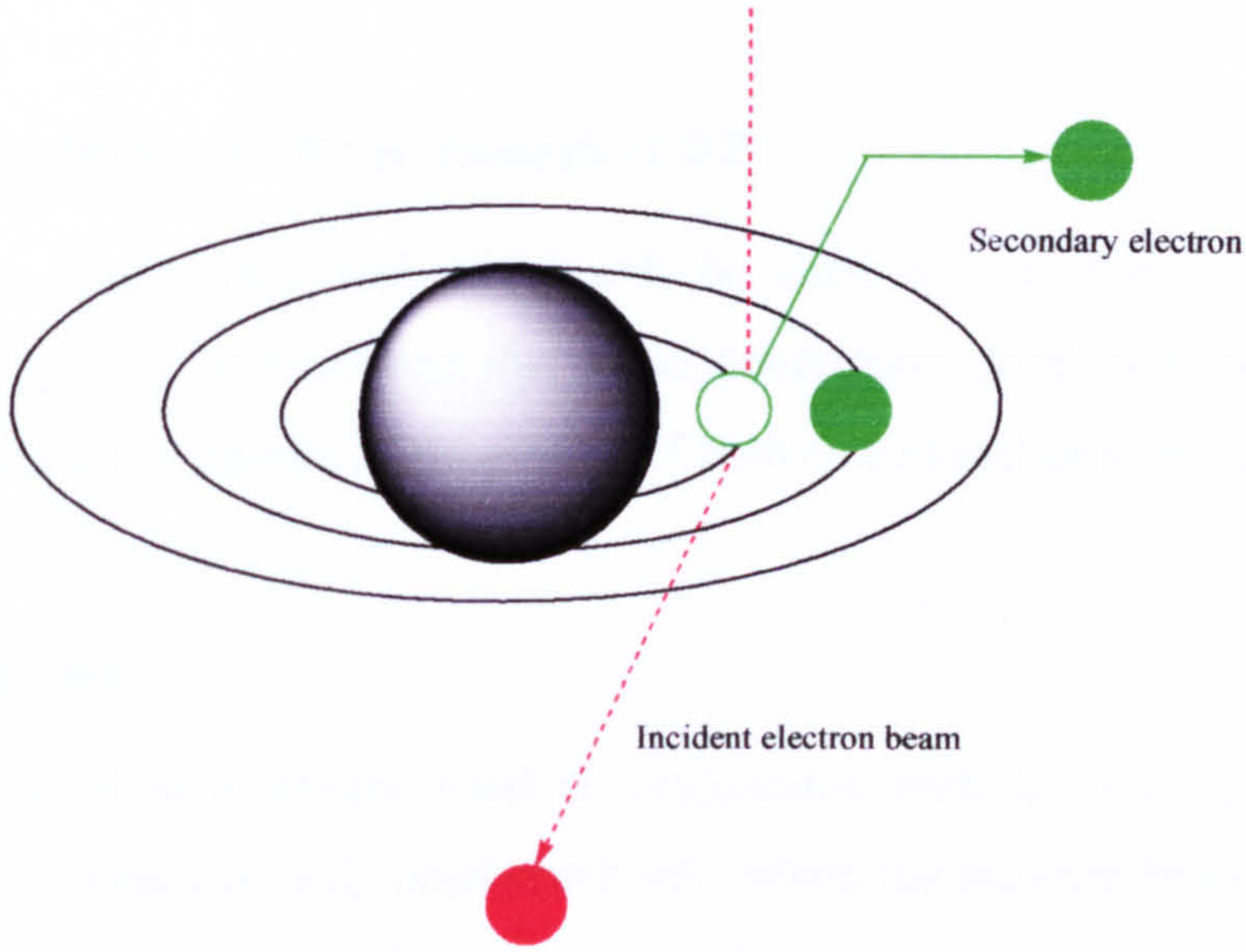


Figure 1.21. Schematic representation of secondary electron formation

The most common occurring possibility is the formation of secondary electrons. As the incident beam electron loses little energy in these collisions, a single beam electron can produce many secondary electrons. If these secondary electrons are close enough to the sample surface they can be collected to form an SEM image. If the beam travels into a depression or hole in the sample, the amount of secondary electrons that can escape the sample surface is reduced and the image processor places a corresponding dark spot on the screen. Conversely, a projection or rise on the sample means more secondary electrons can escape the sample surface, and the image processor places a bright spot on the screen.

Another type of imaging mode is used to observe backscattered electrons, as these electrons have high energies. As a sample with a higher density will create more of them, they are used to form backscattered electron images, which generally can discern the difference in sample densities.

### *1.8.4 Energy Dispersive X-ray Analysis (EDX)*

EDX used in conjunction with SEM will be used to investigate the elemental properties of applied coatings and due to its penetration depth will be particularly useful in studying the interfacial properties of both coated and pretreated samples.

#### *1.8.4.1 Background*

EDX is an analytical technique used in conjunction with SEM to give elemental analysis of the image currently been observed. When the incident beam of electrons creates secondary electrons, it leaves the sample atoms with holes in their electron shells. If the holes are in inner shells, the atoms are unstable. Therefore, to stabilise the atoms, electrons from outer shells drop into the inner shells. However, as the outer shells are at a higher energy state, the atom must lose some energy; it therefore emits energy in the form of X-rays[70].

#### *1.8.4.2 Methodology*

The X-rays emitted are characteristic in energy and wavelength to, not only the element of the parent atom, but which shells lost electrons and which shells replaced them. For example, if the innermost shell (the K shell) electron of an iron atom is replaced by an L shell electron, a 6400eV K alpha X-ray is emitted from the sample (figure 1.22). However, if the L shell electron of an iron atom is replaced by an M shell electron, a 704eV L alpha X-ray is emitted from the sample.

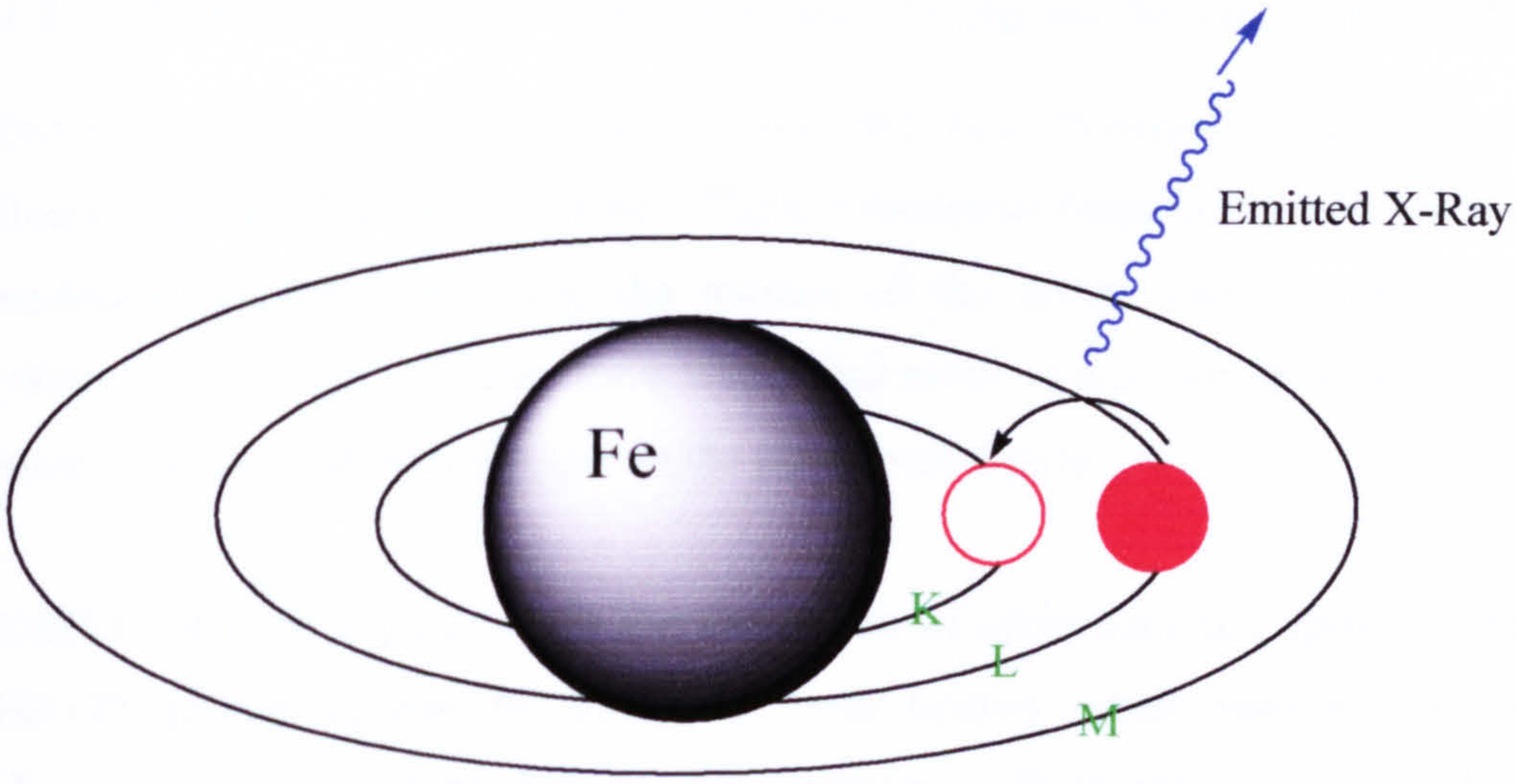


Figure 1.22. Schematic representation of the emission of a K alpha X-ray[72]

Since lower atomic number elements have fewer filled shells, they have fewer X-ray peaks. For example, carbon has only one peak, a K alpha X-ray at 282eV. Conversely, higher atomic numbered elements have a greater number of X-ray peaks. While some of the high atomic numbered X-rays can be over 50KeV, a spectral range of 0-20KeV can detect all the elements from boron to uranium.

As the X-rays are formed by the interaction between the electron beam and the sample surface, analysis is possible over the area being imaged. The X-rays are emitted from a depth equivalent to how deep the secondary electrons are formed. Depending on the sample density and accelerating voltage of the incident beam, this is usually from 0.5-2μm in depth.

Quantification into either atomic or weight percent is possible by calculating the area under the peak of each identified element and after taking account for the accelerating voltage of the beam to produce the spectrum. It is also possible to map the elements by setting windows around the peaks of specific elements. The software is then able to scan the sample and create digital images or maps of each element.

### *1.8.5 Diffuse Reflectance Infrared Fourier Transform Spectroscopy (DRIFTS)*

Infrared spectroscopy works due to the fact that chemical bonds have specific frequencies at which they vibrate. These vibrational frequencies are determined by molecular potential energies, the masses of the atoms and by their associated vibronic couplings. In order for a vibrational mode in a molecule to be IR active, it must be associated with changes in the permanent dipole.

DRIFTS will be used to study the interaction of chromium and epoxies within the BR127 primer system by analysing both treated metal samples and various chromium / epoxide formulations. The technique will be able to monitor changes in the structure of the chromate and also the ability of different chromates to react with epoxides. Further tests will then investigate more environmentally benign alternative systems to gain a comparison between them and chromate.

#### *1.8.5.1 Background*

DRIFTS is a technique that analyses scattered IR energy. It is used primarily for the measurement of fine particles and powders but is also able to analyse rough surfaces[72].

#### *1.8.5.2 Methodology*

When the IR beam comes into contact with the sample, it can either be reflected off the surface (specular reflectance) or be transmitted through a particle (figure 1.23a). The IR energy reflected off the surface is lost. The beam that passes through the particle can then either reflect off the next particle or be transmitted through another particle. This transmission-reflectance process occurs many times in the sample, which causes the path length to increase. Finally, the scattered IR energy is collected by a spherical mirror (figure 1.23b), focussed onto the detector which calculates the sample information due to some of the IR light been partially absorbed by the sample.

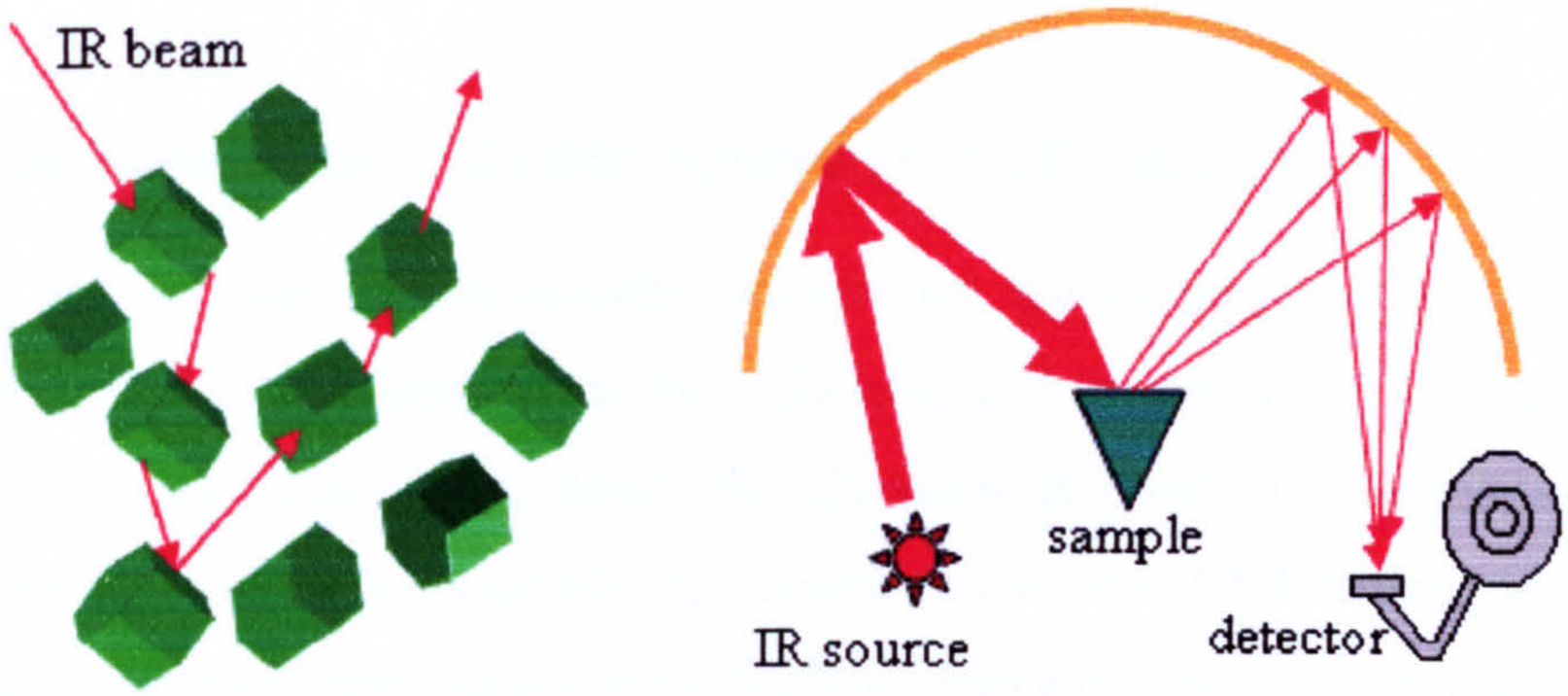


Figure 1.23. Diagram showing a. IR beam passing through fine particles
b. Schematic representation of DRIFT apparatus[73]

There are three common ways to prepare samples for DRIFTS measurement[74]:

1) A micro-cup is filled with a finely ground mixture of the powder under investigation and KBr (used due to its IR insensitivity). The DRIFT accessory uses a mirror to focus the beam onto the sample surface and collect the IR energy.
2) The sample surface is scratched with a piece of abrasive SiC paper and then the particles adhered to the paper are measured.
3) Drops of a colloidal or powder solution can be placed onto a substrate. If they are dissolved or suspended in a volatile solvent, this will readily evaporate and subsequently the remaining particles on the substrate can be analysed.

One important part of sample preparation is the fact that particle sizes analysed must be the equivalent of 5μm or less. This is because, in every IR technique, large particles will result in the scattering of energy, leading to a shift in the spectrum baseline and the broadening of IR bands. The scenario is worse in a diffuse reflectance measurement, because the IR beam travels in the sample for a long period and the optics collects a large portion of the distorted energy.

### *1.8.6 Attenuated Total Reflection Infrared (ATR-IR) Spectroscopy*

ATR-IR will be used to chemically characterise the surface of both treated and pretreated samples. It is hoped that the technique will be able to observe changes in chromate structure and hence, where the chromate is positioned in relation to the aluminium substrate. Additionally, the sensitivity of the ATR technique makes it useful for some interfacial studies as well when observing thin film treatments.

#### *1.8.6.1 Background*

ATR is used primarily as a surface and interfacial analysis technique[75]. It is also suitable for characterisation of materials which are either too thick or too highly absorbing to be analysed by standard transmission spectroscopy. For the bulk material or thick film, no sample preparation is required for ATR analysis.

#### *1.8.6.2 Methodology*

For ATR-IR spectroscopy, infrared radiation is passed through an infrared transmitting crystal with a high refractive index, allowing the radiation to reflect within the ATR element several times (figure 1.24).

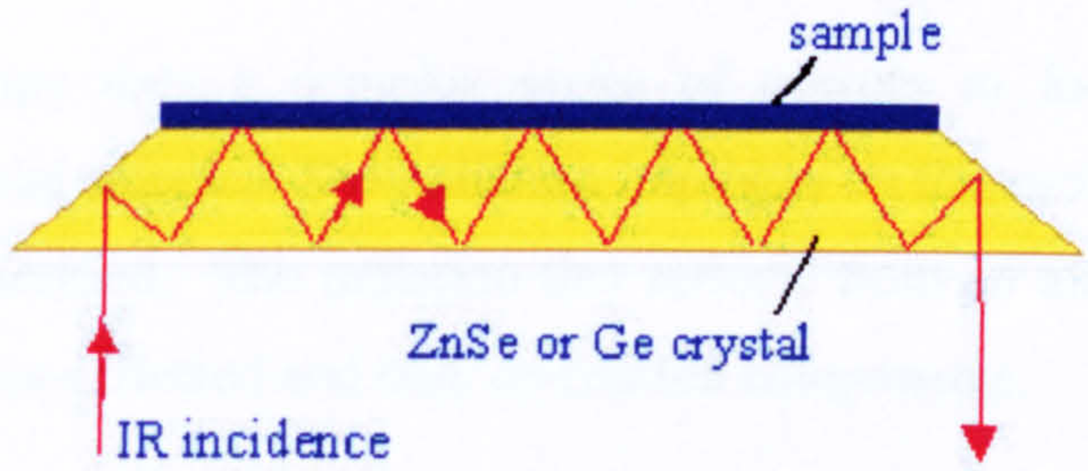


Figure 1.24. Diagram of an ATR-IR crystal and the IR beam reflection path[76]

The surface under investigation is pressed into intimate optical contact with the top surface of the crystal such as ZnSe, Ge, or a thallium compound named KRS-5. The IR beam from the spectrometer enters the crystal and is then reflected, penetrating into the sample a finite amount with each reflection along the top surface via the so-

called "evanescent" wave. At the output end of the crystal, the beam is directed out of the crystal and back into the normal beam path of the spectrometer.

To obtain internal reflectance, the incident angle must exceed the 'critical' angle, a function of the real parts of the refractive indices of both the sample and the crystal. The critical angle can be calculated through the following equation[77]:

$$\theta_c = \sin^{-1}(n_2/n_1)$$

Where $n_1$ is the refractive index of the crystal and $n_2$ is the refractive index of the sample. The evanescent wave decays into the sample exponentially with distance from the surface of the crystal over a distance in the order of microns, meaning that ATR-IR is only useful for analysing surfaces or thin films.

### *1.8.7 Diffuse Reflectance Ultraviolet-Visible Spectroscopy (DRUV)*

Due to the strong redox activity of chromium and its compounds, DRUV will be used to investigate possible changes in oxidation state. Additionally, the ligands bonded to chromium will also be investigated through this technique.

#### *1.8.7.1 Background*

DRUV spectroscopy uses a complex series of mirrors to focus the ultraviolet radiation onto a solid sample. The radiation impinges on the surface and is partially reflected and transmitted. The radiation that reflects from an absorbing material is composed of surface-reflected and bulk re-emitted components.

#### *1.8.7.2 Methodology*

The absorption of UV or visible radiation corresponds to the excitation of outer electrons. There are three types of electronic transition which can be considered[78];

1. Transitions involving p, s, and *n* electrons

2. Transitions involving charge-transfer electrons
3. Transitions involving *d* and *f* electrons

As Cr (VI) species have a d electron count of zero this means that d-d transitions cannot occur. Therefore, any peaks present in the UV-vis of Cr (VI) species must be from charge transfer transitions.

For a complex to demonstrate charge-transfer behaviour one of its components must have electron donating properties and another component must be able to accept electrons. Absorption of radiation then involves the transfer of an electron from the donor to an orbital associated with the acceptor occurring at high energy, normally appearing between 200-500nm.

### *1.8.8 $^{13}$Carbon Nuclear Magnetic Resonance ($^{13}$C-NMR)*

$^{13}$C-NMR will be used to monitor any polymerisations occurring in the primer and also model systems. At elevated temperatures, epoxies and phenolic epoxies polymerise and therefore, new carbon environments will be formed which can be analysed.

#### *1.8.8.1 Background*

NMR spectroscopy uses the principles first recorded by Purcell and Bloch in 1946. They noticed that magnetic nuclei, like $^{1}$H and $^{13}$C, could absorb RF energy when in a magnetic field of a specific strength i.e. in resonance.

#### *1.8.8.2 Methodology*

Depending on the local chemical environment that surrounds them, different $^{13}$C nuclei in a molecule resonate at different frequencies that is dependent on the strength of the magnetic field. To obtain independence from the field, the frequency is converted into a value known as the chemical shift which is reported as a relative measure from a reference resonance frequency (for $^{13}$C nuclei this is

tetramethylenesilane (TMS)). The chemical shift is calculated by the following equation[79]:

(Frequency of signal – Frequency of reference) / Frequency of field = Chemical shift

## 1.9 Project Aims

The primary aim of this research project is to increase the understanding of the functions of chromate in primer systems. This knowledge will then be taken into the second phase of the project and be used for the subsequent formulation of a novel, green alternative primer system.

Firstly, to increase the understanding of chromate an investigation will be carried out into the properties of the commonly used BR127 chromate containing primer system. This will be done by analysing the surface characteristics of industrially primed aluminium and also using spectroscopic techniques to investigate the actual primer formulation.

To further investigate the mechanisms by which chromium acts, model systems will be formulated which will be easier to analyse than the complex industrial formulation and therefore any changes in spectra will be more clearly observed. Many different analytical techniques will be used to analyse the model systems, which will look at both different chromates and different epoxies.

The analytical techniques found to be most successful for monitoring the chromium model systems will then be employed for the analysis of green alternative systems based on phosphate, tungstate and zirconate.

An additional investigation into surface pretreatments such as etching and anodisation will also be conducted. This will look into the changing properties of a treated surface over time and also if there is the possibility of combining the pretreatment and priming into a one-stage process.

## 1.10 References


1. Ransom, E.C.P., *Aircraft Engineering and Aerospace Technology*, 75, 6, 2003.
2. Hayward, K., *The British Aircraft Industry*, Manchester University Press, Manchester, 1989.
3. Clark, G., *Engineering Failure Analysis*, 12, 755, 2005.
4. Soutis, C., *Progress in Aerospace Sciences*, 41, 143, 2005.
5. Wang, J.T., Poe Jr.,C.C., Ambur, D.R., Sleight, D.W., *Composites Science and Technology*, 66, 2557, 2006.
6. Dill, H.G., *Earth-Science Reviews*, 53, 35, 2001.
7. Burkin, A.R., *Production of Aluminium and Alumina*, Chichester, 1987.
8. Wilquin, H., *Aluminium Architecture: Construction and Details*, 1st Edition, Birkhauser, Switzerland, 2001.
9. Massey, R., Taylor, D., *Aluminium in Food and the Environment*, Cambridge, 1989.
10. Hume-Rothery, W., *Theory of the Properties of Metals & Alloys*, The Institute of Metals, London, 1962.
11. Christian, J.W., *Theory of Transformations in Metals & Alloys*, 2nd Edition, Pergamon, Oxford, 1975.
12. Kaufman, J.G., *Introduction to Aluminum Alloys and Tempers*, Issue 1, ASM International, Ohio, 2000.
13. Kulinich, S.A., Shibata, J. Yamamoto, H. Shimada, Y. , *Applied Surface Science*, In Press, 2006
14. Shao, M., Fu, Y., Hu, R., Lin, C., *Materials Science & Engineering*, 2002.
15. Zhu, D., van Ooij, W.J., *Corrosion Science*, 2003, 45, 2163.
16. Alderliesten, R.C., Homan, J.J., *International Journal of Fatigue*, 28, 1116, 2006.
17. Vlot, A., *Glare: History of the Development of a New Aircraft Material*, Kluwer Academic Publishers, Dordrecht, Netherlands, 2001.
18. Stratmann, M., Frankel G.S., *Encyclopedia of Electrochemistry. Volume 4*, Wiley-VCH: Weinheim. 2003.

19. Scully, J.C., *The Fundamentals of Corrosion*, Butterworth-Heinemann, Oxford, 3rd Edition, 1990.
20. Evans, U.R., *An Introduction to Metallic Corrosion*, Edward Arnold, London, 1981.
21. University of Delaware, Sea Grant Marine Advisory Service.
22. Le Bozec, N., *Journal of the Electrochemical Society*, 149, 9, 2002.
23. *Corrosion, Failure Analysis and Metallography*, ASM International, New York, 1986.
24. VFF Guidance Sheet, *Filiform corrosion - Preventing filiform corrosion on finished aluminium parts*, 1997.
25. Lees, W. A., *International Journal of Adhesion and Adhesives,* 1, 241, 1981.
26. Blackman, B.R.K., Kinloch, A.J., *The durability of adhesive joints in hostile environments,* Elsevier ,Oxford, 2004.
27. Kinloch, A.J., *Adhesion and Adhesives: Science and Technology*, Chapman and Hall, 1987.
28. Kinloch, A.J., Gettings, M., *Journal of Materials Science*, 12, 2511, 1977.
29. Bhowmik, S., Bonin, H.W., Bui, V.T., Weir, R.D., *International Journal of Adhesion & Adhesives*, 26, 400, 2006.
30. Abel, M.-L., Kinloch, A.J., Shaw, S.J., Adams, A.N.N., Watts, J.F, *International Journal of Adhesion & Adhesives*, 26, 50, 2006.
31. ec.europa.eu/environment/chemicals/reach/reach_intro.htm
32. Comyn, J., *Adhesion Science*, RSC, London, 1997.
33. www.epa.gov/ttn/atw/hlthef/chromium.html
34. www.rohs.gov.uk
35. Rollinson, C.L., *Chemistry of Chromium, Molybdenum & Tungsten*, 1975.
36. Cotton, F.A., Wilkinson, G., Gaus, P., *Basic Inorganic Chemistry*, Wiley, Chichester, 1995.
37. McAughey, J.J., Rickeard, D.J., Bateman, J.R., Kwon, Y.K., *The Science of the Total Environment,* 71, 3, 317, 1988.
38. www.chromium-asoc.com/chromium/Chromium&Cement.pdf
39. Chromium based oxidation reactions, Acros Organics publication.
40. US National Toxicology Program Fact Sheet, 2003.
41. Wise Senior, J.P.,Wise, S.S., Little, J.E., *Mutation Research*, 517, 2002.

42. Bethencourt, M., Botana, F.J. Calvino, J.J., Marcos, M., Rodriguez-Chacon, M.A., *Corrosion Science*, 40, 11, 1998.
43. Deacon, G.B., Forsyth, C.M. Behrsing, T., Konstas, K., Forsyth, M., *Chemical Communications*, 23, 2820, 2002.
44. Muller, B., *Corrosion Science*, 46, 159, 2004.
45. Zhu, D., van Ooij, W.J., *Corrosion Science*, 45, 2177, 2003.
46. Watts, J., Abel, M-L., *Surface & Interface Analysis*, 29, 115, 2000.
47. Abel, M.-L., Allington, R.D., Digby, R.P., Porritt, N., Shaw, S.J., Watts, J.F. *International Journal of Adhesion & Adhesives*, 26, 2, 2006.
48. Abel, M.-L., Joannic, R., Fayos, M., Lafontaine, E., Shaw, S.J., Watts, J. F., *International Journal of Adhesion & Adhesives*, 26, 16, 2006.
49. Abel, M.-L., Rattana, A., Watts, J.F., *International Journal of Adhesion & Adhesives*, 26, 28, 2006.
50. Torry, S.A., Campbell,A., Cunliffe, A.V., Tod, D.A., *International Journal of Adhesion & Adhesives,* 26, 40, 2006.
51. Underhill, P.R., DuQuesnay, D.L., *International Journal of Adhesion & Adhesives*, 26, 62, 2006.
52. Rider, A.N., *International Journal of Adhesion & Adhesives*, 26, 67, 2006.
53. Choudhury, T., Jones, F.R., *International Journal of Adhesion & Adhesives*, 26, 79, 2006.
54. Underhill, P.R., DuQuesnay, D.L., *International Journal of Adhesion & Adhesives*, 26, 88, 2006.
55. Woods, G.A., Haq, S., Shaw, S.J., Raval, R., *International Journal of Adhesion & Adhesives*, 26, 94, 2006.
56. Jensen, R.E., Palmese, G.R., McKnight, S.H., *International Journal of Adhesion & Adhesives*, 26, 103, 2006.
57. Parkhill, R.L., et al, *Progress in Organic Coatings*, 41, 2001.
58. Anastas, P.T., Warner, J.C.; *Green Chemistry: Theory and Practice*, Oxford University Press, Oxford, 1998.
59. Gross, J.H., *Mass Spectrometry: A Textbook*, Springer, London, 1st Edition, 2006.
60. Tang, K., Smith, R.D., *Journal of the American Society for Mass Spectrometry*, 12, 3, 343, 2001.

61. Zeleny, J., *The Physical Review*, 3, 69, 1914.
62. Dole, M., *Journal of Chemical Physics*, 49, 2240, 1968.
63. Fenn, J.B., *Mass Spectrometry Review*, 9, 37, 1990.
64. Bruins, A.P., *Analytical Chemistry*, 59, 2642, 1987.
65. Briggs, D., Seah, M.P., *Practical Surface Analysis -Auger and X-ray Photoelectron Spectroscopy*, Wiley Interscience, Chichester, 2nd Edition, 1990.
66. Attard, G., Barnes, C., *Surfaces*, Oxford Chemistry Primers, Oxford, 1998.
67. Watts, J., Wolstenholme, J., *An Introduction to Surface Analysis by XPS and AES*, Wiley, Chichester, 1993.
68. Slater, E.M., Slater, H.S., *Light and Electron Microscopy*, Cambridge University Press, Cambridge, 1992.
69. Goodhew, P.J., Humphreys, J., Beanland, R., *Electron Microscopy and Analysis*, Taylor and Francis, London, 3rd Edition, 2000.
70. Russ, J.C., *Fundamentals of Energy Dispersive X-Ray Analysis,* Butterworth-Heinemann, Oxford, 1984.
71. Bell, D.C., *Energy Dispersive X-ray Analysis in the Electron Microscope,* Garland Science, London, 1st Edition, 2002.
72. Fuller, M.P., Griffiths, P. R., *Analytical Chemistry*, 50, 13, 1908, 1978.
73. www.nuance.northwestern.edu/keckii/ftir7.asp
74. Stuart, B.H., George, B., McIntyre, P., *Modern Infrared Spectroscopy*, Wiley, Chichester, 1996.
75. Öhman, M. et al, *Progress in Organic Coatings*, 57, 1, 78, 2006.
76. Bower, D.I., Maddams, W.F., *The Vibrational Spectroscopy of Polymers*, Cambridge University Press, Cambridge, Reprint Edition, 1992.
77. Urban, M.W., Vibrational Spectroscopy of Molecules and Macromolecules on Surfaces, Wiley-Interscience, Chichester, 1994.
78. Atkins, P., *Physical Chemistry*, Oxford University Press, Oxford, 7th Edition, 2001.
79. Sanders, J.K.M., Hunter, B.K., *Modern NMR Spectroscopy: A Guide for Chemists,* Oxford University Press, Oxford, 2nd Revised Edition, 1993.

# Chapter 2

# Experimental

## 2.1 Experimental for Chapter 3

### *2.1.1 Aluminium coating techniques*

#### *2.1.1.1 Dip coating*

1cm$^2$ coupons of AA2024-T3 were cut using a guillotine. The cut samples were held with tweezers and immersed in the BR127 primer solution in a watch glass for 15 seconds. The samples were then placed in an empty watch glass for 30 minutes to dry at room temperature and then cured at 120°C for 30 minutes in an oven.

#### *2.1.1.2 Brush coating*

1cm$^2$ coupons of AA2024-T3 were cut using a guillotine. Samples were coated with primer solution using a small paint brush and four strokes were made across the piece of aluminium to give approximately the same primer thickness verified by SEM.

### *2.1.2 Surface analysis*

#### *2.1.2.1 SEM and EDX analysis*

To achieve good conductivity, samples were plasma coated using an Agar Scientific gold sputtering machine under an argon atmosphere. These were then placed into a custom made multiple sample holder which was able to take seven samples. This was placed within a Sirion FEI microscope and UHV conditions were attained using an Edwards RV3 pump. Analysis was conducted using the standard FEI microscope operating software.

For EDX analysis, samples were not gold coated and measurements were conducted using an EDAX microanalyser and EDAX Genesis software.

#### *2.1.2.2 XPS analysis*

1cm$^2$ coupons of AA2024-T3 were cut by guillotine and brush coated with BR127 primer solution. Samples were run by Mr. Paul Elliott on a Kratos X-Ray Spectrometer using Mg Kα radiation.

### *2.1.3 IR analysis*

#### *2.1.3.1 Solution state IR*

Two drops of the solution under analysis were added to a circular NaCl disc. A second disc was placed on top of this one so that a thin film of solution was created between the two plates. To remove excess solution, the top disc was removed and cleaned so the film was of correct thickness for the IR beam to penetrate. The two NaCl plates were then positioned in a cell and analysed in transmission mode on a Bruker Equinox 55 IR spectrometer using Opus analytical software.

#### *2.1.3.2 DRIFT analysis*

8ml samples of the solution under analysis were pipetted into a 50ml one-necked round bottomed flask. The solvent was evaporated using a Buchi R110 rotary evaporator set at 60°C, leaving a powder in the flask. The powder was mixed with dry KBr crystals in a ratio of 1 part sample to 10 parts KBr. A pestle and mortar was used to grind the sample/KBr mix into an exceptionally fine powder which was then placed in a sample holder and analysed using standard DRIFT apparatus on a Bruker Equinox IR 55 spectrometer with Opus software.

#### *2.1.3.3 TG-IR analysis*

Shavings of BR127 primed AA2024-T3 were placed in a ceramic sample cup. Approximately 10mg of the sample was required and this was placed within a Netzsch STA-409 thermal analyser. This was connected to a Bruker Equinox 55 IR

spectrometer which was used to analyse gaseous species omitted during the temperature ramp.

### *2.1.4 $^{13}$C-NMR analysis*

An NMR sample tube was filled to a depth of 3cm with the sample under analysis. 5 drops of the deuterated NMR solvent to be used (normally either DMSO or methanol) was then added and the mixture was vigorously shaken. Analysis was carried out on a Jeol EX270 NMR, using 128 scans and Jeol analysis software.

### *2.1.5 UV-vis analysis*

#### *2.1.5.1 Solution state analysis*

For all analysis a Shimadzu UV-160A spectrometer using PC160 Plus software was used. To calibrate the spectrometer, two glass vials were filled with methanol to run a solvent-solvent baseline. 1.00ml samples of the solution under investigation were added to a vial and this was diluted to the top with methanol so that the absorption of the maximum did not go above 1.0.

#### *2.1.5.2 DRUV analysis*

DRUV spectra were obtained by taking 10.0ml samples of the model systems and evaporating the solvent on a Buchi R110 rotary evaporator. Using a small pestle and mortar, the evaporated solid was mixed with sodium chloride in a ratio of 1 part sample to 10 parts NaCl until the required amount was obtained to fit in the DRUV cell. All spectra were obtained on a Jasco V-550 UV-vis Spectrophotometer using Jasco Spectra Manager software on a Dell PC.

### *2.1.6 ESI-MS analysis*

5.00ml samples of the model system were withdrawn from the 250ml three-necked-round-bottomed flask. All samples were run by Dr. Trevor Dransfield on a VG Autospec Quadrupole high performance mass spectrometer. Both the positive and negative ion species were analysed in all cases.

### *2.1.7 Model system preparation*

The chromium model system was prepared by charging a 100ml conical flask with 1.00g of sodium chromate and 75.0ml of methanol. A PTFE magnetically stirred flea was added, as was a stopper to the flask, and the contents stirred on a magnetic stirrer for 16 hours at room temperature. After this time the mixture was then filtered using a grade 3 Whatman filter paper and Buchner funnel under vacuum to remove any non-dissolved chromate. This solution was then transferred into a 100ml three-necked-round-bottomed flask and 3.12ml cyclohexene oxide added by pipette. The system was then refluxed in an oil bath set to 100°C. An 8.00ml sample was removed by pipette after the immediate addition of the epoxide and further samples were removed from the solution at hour long intervals after that, until the reaction was stopped after 6 hours.

### *2.1.8 Model system – substrate reactions*

The experimental conditions outlined in section 7.17 were followed but 2.00g of neutral γ-alumina were added to the three-necked round bottomed flask in addition to the model system.

## 2.2 Experimental for Chapter 4

### *2.2.1 Further model system work*

To keep the concentration of chromate the same, different amounts of each species were added. As 1.00g (6.17mmol) of sodium chromate had been used in the previous experiments, this remained the same and therefore 1.20g of potassium chromate and 0.80g of lithium chromate were used.

Similarly, so that there was the same excess of epoxide in the formulations, the molar amount of cyclohexene oxide was used as a base to calculate the amounts of the other epoxides. 3.12ml (3.08mmol) of cyclohexene was used and therefore 3.52ml of styrene oxide and 3.20ml of epoxypentane.

### *2.2.2 DRUV analysis*

As different cations were used in experiments, the inert dissolution salt was changed to be the chloride species of the cation present in the model system, e.g. for the system involving lithium chromate and styrene oxide; lithium chloride was used as the dissolution salt.

### *2.2.3 Titrimetric determination of redox behaviour*

A stock solution of sodium chromate in methanol was made up by dissolving 25.0g of sodium chromate in 2.50l of methanol. 240ml of this solution was added to a three-necked round bottomed flask and to that 9.00ml of styrene oxide was added by pipette. A nitrogen gas input with a flow rate of 2.0 l/min was placed in one of the side arms of the flask. The solution was heated in an oil bath set at 100°C and 50.0 ml samples were taken at the beginning of reaction, after 6 hours and after 24 hours of reaction.

The 50.0ml of chromate solution were added to a 250ml conical flask and to this 50.0ml of a previously prepared 0.1M potassium iodide solution was added along with 2.00ml of concentrated hydrochloric acid. This mixture was then titrated against a 1.0M sodium thiosulphate solution. After enough thiosulphate had been added to turn the solution from orange to colourless, 2.00ml of a starch indicator solution was added. More thiosulphate was added to turn the mixture from blue to colourless signifying the end-point.

### *2.2.4 LC-MS analysis*

Analysis was carried out by ICI Measurement Science Group. Samples were analysed using a LC-MS with the source set to positive ion electrospray mode. An ultraviolet (UV) detector was positioned in series between the LC column and the mass spectrometer to gain quantitative results.

## 2.3 Experimental for Chapter 5

### *2.3.1 Alternative system work*

To maintain the same concentration of the alternatives in solution to the chromate concentration, different amounts of each species were added. As 6.17mmol of sodium chromate had been used, 2.04g of sodium tungstate dihydrate, 1.01g of sodium phosphate and 1.14g of sodium zirconate were used. The same procedure as stated in section 7.17 was then followed.

## 2.4 Experimental for Chapter 6

### *2.4.1 Surface treatments*

#### *2.4.1.1 Acid etching*

For the chromic acid etch (or Forest Product Laboratories [FPL] etch), 1cm$^2$ aluminium coupons was immersed in a solution consisting of 30g sodium dichromate, 60ml sulfuric acid and 340ml water and was heated at 68°C for 30 minutes. Samples were then removed from the acid and washed for 15 minutes in water.

The etched material needed to be washed with 2-butanone to remove any residual surface organics before use.

Similar procedures were followed for both the phosphoric and nitric acid etches, but here 1.0 molar acid was used.

#### *2.4.1.2 Anodisation*

This work was carried out at Imperial College, London. Strips of aluminium (AA2024-T3), 5cm wide, were initially placed in a tetrachloromethane cleaning bath that was heated until the solvent was boiling. The clean samples were removed, air dried and then placed in a phosphoric acid bath via an attached aluminium beam. A DC power supply, Iso-Tech IPS1603D, was then attached to the aluminium beam and a current passed through the samples. The applied voltage was always kept as close to 10V as possible and was active for two different lengths of time 10 minutes and 20 minutes. After the anodising was complete, the samples were rinsed in a water bath and then dried using an air circulating oven at approximately 60°C.

#### *2.4.1.3 Grit blasting*

Grit blasting was also conducted at Imperial College, London. Using 220-grit alumina powder at a pressure of 0.4MPa, the aluminium surface was bombarded until the surface appeared to be completely matt.

### *2.4.2 Application of model coatings*

A standard model system based on sodium chromate, cyclohexene oxide and methanol (see 7.1.1) was formulated and brush coated to 1cm$^2$ samples of grit blasted AA2024-T3.

### *2.4.3 Attenuated Total Internal (ATR) IR Spectroscopy*

0.1mm thick aluminium foil samples were cut to be 50mm in length and 15mm in width. The samples were (pre-) treated then placed on top of a KRS-5 ATR crystal and finally positioned within a sample holder which was placed in a Bruker equinox 55 IR spectrometer using OPUS software. Liquid nitrogen was added to a MCT detector to increase the energy throughput of the spectrometer.

### *2.4.4 Spectroscopic marker*

#### *2.4.4.1 Preparation of Trioctylammonium hydrogen sulphate*

A 500ml, one-necked round-bottomed flask equipped with a magnetic stirrer bar was charged with 2.093g of $[(n\text{-}C_8H_{17})_3NCH_3]Cl$ (5.17mmol), 100g of 49% $H_2SO_4$ (0.51mol) and 100ml of toluene. The biphasic mixture was vigorously stirred at room temperature for 12 hours. The aqueous phase was removed and 100g of 49% $H_2SO_4$ (0.51mol) was added to the organic phase and the mixture vigorously stirred at room temperature for 12 hours. The organic phase was separated, dried over $Na_2SO_4$ for 24 hours and then filtered. Toluene was removed under pressure to give $[(n\text{-}C_8H_{17})_3NCH_3]HSO_4$ as a semi-crystalline solid.

#### *2.4.4.2 Epoxidation of trans-3-pentenenitrile*

A 50ml round-bottomed flask was charged with 0.132g (0.4mmol) of $Na_2WO_4.2H_2O$, 0.093g (0.2mmol) of $[(n\text{-}C_8H_{17})_3NCH_3]HSO_4$ 3.49ml of 30%$H_2O_2$/phosphate solution (in a ratio 7:3 of 0.1M $H_3PO_4$ in $H_2O_2$ and 0.1M $NaH_2PO_4$ in $H_2O_2$). The mixture was vigorously stirred at room temperature for 10 minutes and then heated at 70°C. To this, 1.94ml (20mmol) of trans-3-pentenenitrile was added. The reaction mixture was vigorously stirred for 2 hours at 70°C. This procedure was then scaled up by a factor of ten to generate a larger volume of the epoxynitrile compound.

# ***Chapter 3***

# ***Industrial primer and model system***

## 3.1 Introduction

Cytec's BR127 primer has been used on nearly every single commercial and military aircraft manufactured since its introduction onto the adhesives market approximately three decades ago[1]. It combines both unparalleled corrosion resistance with outstanding adhesion promotion and can be applied both for use with adhesives or as a protective coating outside bonded areas.

The primer itself consists of both complex epoxy resin and solvent systems, and strontium chromate (figure 3.01); the latter being believed to give the compound many of its excellent, market-leading properties[1].

| **Compound** | **Composition (Weight %)** |
|---|---|
| 2-Butanone | 58.2 |
| Tetrahydofuran | 17.9 |
| Diacetone alcohol | 13.4 |
| Strontium chromate | 2.0 |
| Phenolic epoxy resin | Proprietary |
| Phenolic resin | Proprietary |

Figure 3.01. Formulation of BR127[2]

The primer is normally applied via a spray coating technique under stringent safety conditions due to its highly carcinogenic nature. After application, the compound can be cured prior to bonding at a variety of cure cycles, ranging from 4 hours at 80°C to 30 minutes at 120°C. After curing the material can be kept indefinitely and will prevent hydrolysis of the reactive oxide layer beneath it.

An example of the properties the primer brings to an adhesive system can be seen in figure 3.02, where a comparison is made on lap shear samples (a commonly employed adhesive test) between two different generation chromate primers and an epoxy based aerospace adhesive.

| Exposure time | Lap Shear Strength / MPa | |
|---|---|---|
| | BR123 Primer | BR127 Primer |
| Initial | 40.6 | 39.2 |
| After 30m days | 24.1 | 40.6 |
| After 90 days | 10.1 | 34.3 |
| After 180 days | 0.0 | 30.9 |

Figure 3.02. Table showing the increased adhesive properties given by BR127[3]

In both cases the samples were FPL etched, 2024-T3 clad aluminium bonded with a 120°C cure elastomer modified epoxy adhesive. The samples were then subjected to salt spray tests, meaning these values give a good indication of both the adhesive and corrosion resistive properties afforded by the primer.

## 3.2 Analysis of BR127 industrial primer

### *3.2.1 Solution phase analysis*

To try and understand the function of chromate in the industrial primer, the BR127 solution was analysed by liquid IR spectroscopy (figure 3.04). As can be seen from the spectrum, there is a high concentration of organic compounds. However, the commonly observed chromate band which normally appears at approximately 900-1000cm$^{-1}$ cannot be seen. This is because the concentration of strontium chromate in the industrial primer is very low in comparison to that of the organic species. Figure 3.05 shows a DRIFT spectrum of strontium chromate and the peaks which will be present in the BR127 but are covered by the stronger organic based ones.

| Bond | Compound Type | Frequency range, $cm^{-1}$ |
|---|---|---|
| C-H | Alkanes | 2960-2850 stretch<br>1470-1350 scissoring and bending |
| | $CH_3$ Umbrella Deformation | 1380 - Doublet - isopropyl, *t*-butyl |
| C-H | Alkenes | 3080-3020 stretch<br>1000-675 bend |
| | Aromatic Rings | 3100-3000 stretch |
| C-H | Phenyl Ring Substitution Bands | 870-675 bend |
| | Phenyl Ring Substitution Overtones | 2000-1600 - fingerprint region |
| C-H | Alkynes | 3333-3267 stretch<br>700-610 bend |
| C=C | Alkenes | 1680-1640 stretch |
| C-O | Epoxides | 900-950 stretch |
| C=C | Aromatic Rings | 1600, 1500 stretch |
| C-O | Alcohols, Ethers, Carboxylic acids, Esters | 1260-1000 stretch |
| C=O | Aldehydes, Ketones, Carboxylic acids, Esters | 1760-1670 stretch |
| | Monomeric -- Alcohols, Phenols | 3640-3160 stretch |
| O-H | Hydrogen-bonded -- Alcohols, Phenols | 3600-3200 stretch |
| | Carboxylic acids | 3000-2500 stretch |
| N-H | Amines | 3500-3300 stretch<br>1650-1580 bend |
| C-N | Amines | 1340-1020 stretch |
| C≡N | Nitriles | 2260-2220 stretch |
| Cr-O | Chromates | 850-970 stretch<br>1370-1450 1st overtone |

Figure 3.03. Table showing commonly occurring infrared absorption frequencies

As can be seen from figure 3.03, the spectrum of BR127 primer shows a strong O-H stretch at $3500cm^{-1}$, both C-H stretches and bends at $2900cm^{-1}$ and $1450cm^{-1}$ respectively, a strong C=O stretch absorbance at $1650cm^{-1}$ and also peaks corresponding to C-O stretches around the $1200cm^{-1}$ area. The complexity of this spectrum indicates the presence of many organic compounds.

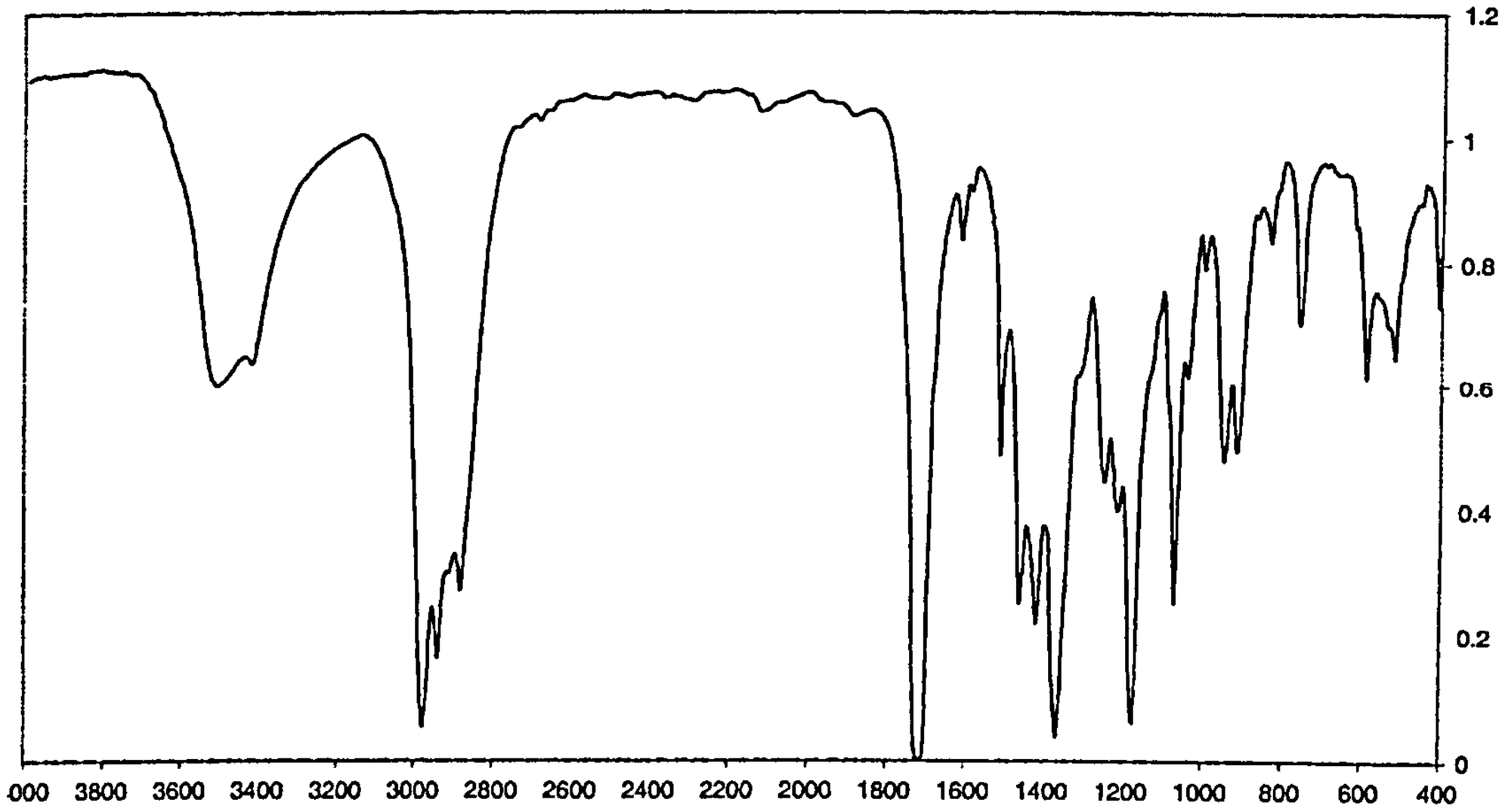


Figure 3.04. FTIR liquid thin film spectrum of BR127 primer

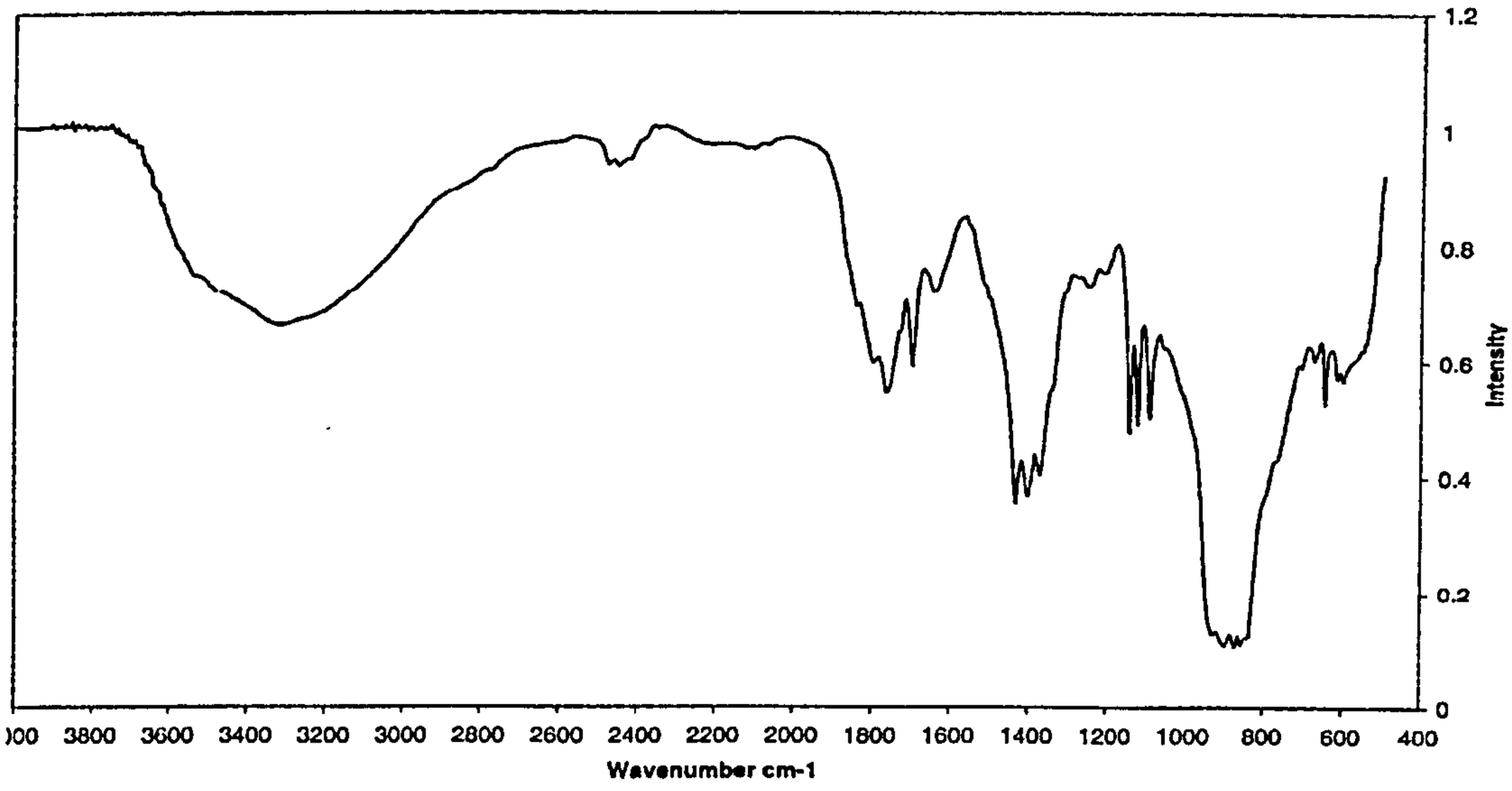


Figure 3.05. DRIFT IR spectrum of strontium chromate

A further technique that was used to analyse the industrial primer was $^{13}$C-NMR, (figure 3.06). Again, this technique shows that there are a large number of different organic species in the system, however, again, due to the low concentration of the chromate no effect of this compound (e.g. significant change in chemical shift) can be observed.

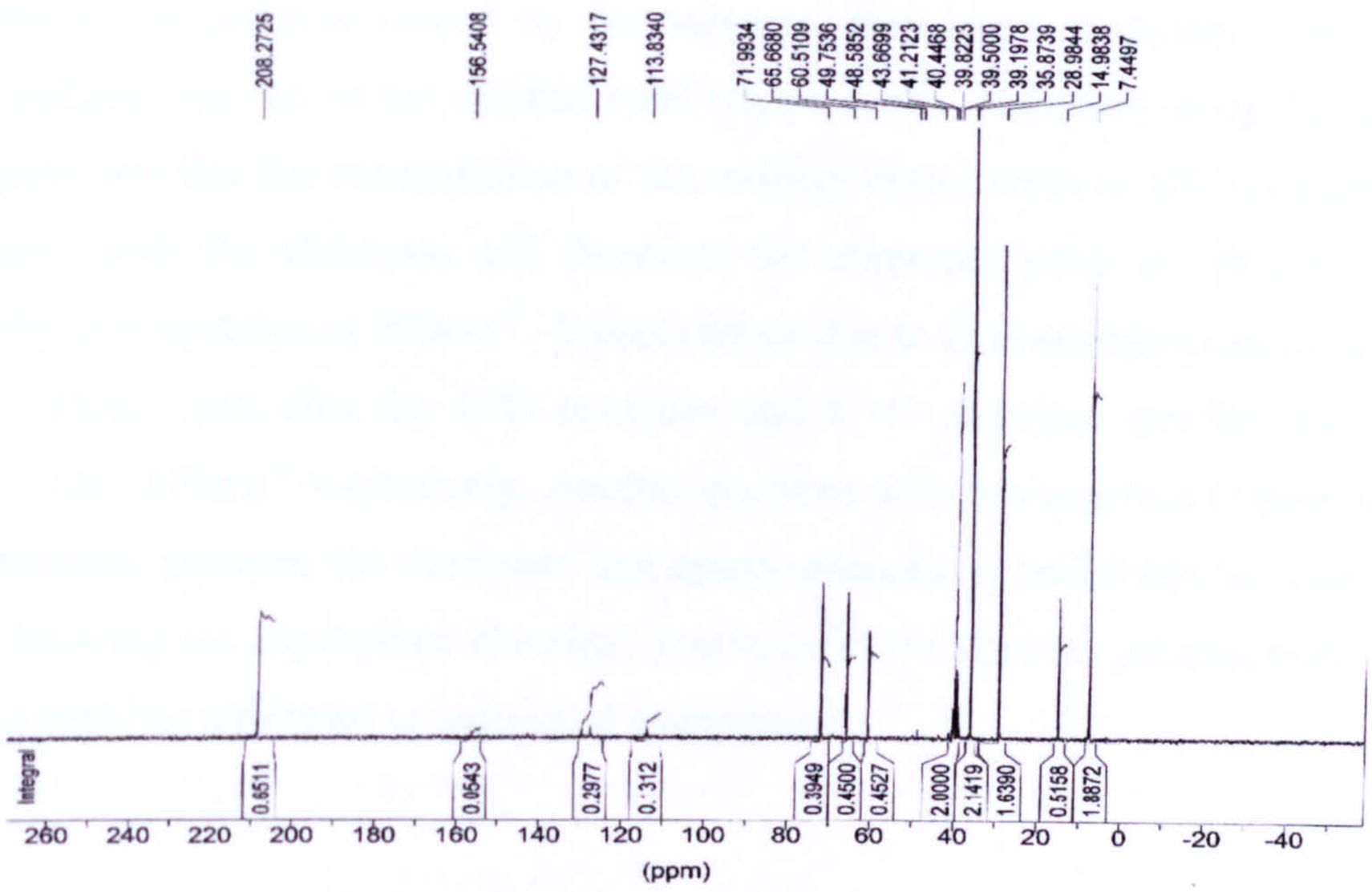


Figure 3.06. $^{13}$C-NMR of BR127 Primer in $d_6$ DMSO

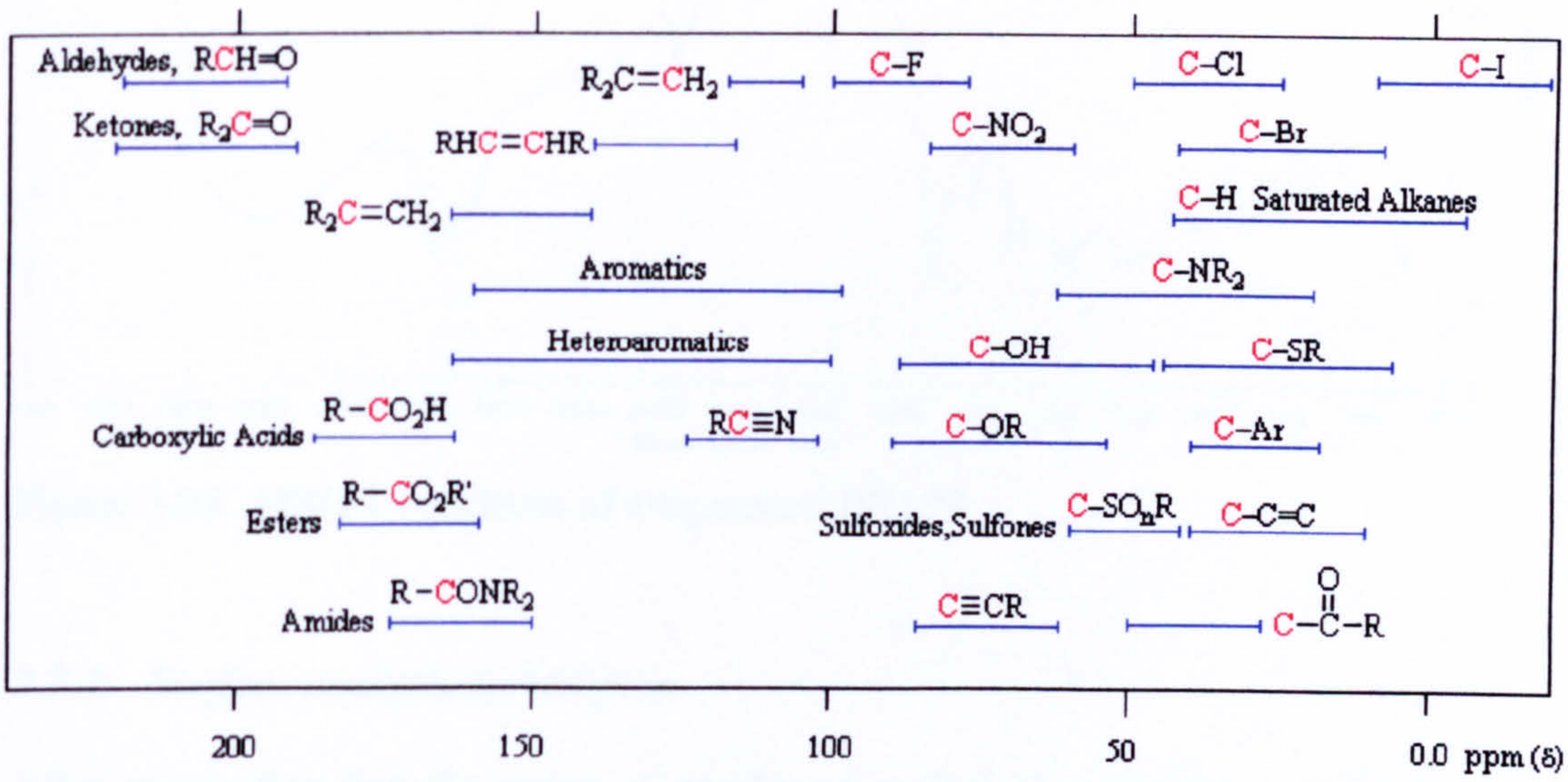


Figure 3.07. Chart showing commonly occurring $^{13}$C-NMR chemical shifts

As can be seen from figure 3.07, BR127 shows the corresponding frequencies for different saturated alkane peaks at 7ppm, 14ppm and 30ppm. C-OH groups peaks are also present between 40-50ppm, and aromatic carbons are also present at 113ppm, 127ppm and 156ppm.

To eliminate the problem caused by the solvents, they were evaporated off and DRIFT analysis was run on the residual solid (figure 3.08). However, it can be seen from figure 3.03 that the concentration of the residual epoxy resin is still too high in comparison with the chromate and therefore the chromate peak at ~900cm$^{-1}$ is masked by C-O stretches at 950cm$^{-1}$. Intense bands due to O-H stretches can be seen at 3300-355cm$^{-1}$ and also the C-H stretches and C=O stretches can be seen at 2900cm$^{-1}$ and 1670cm$^{-1}$ respectively. Another problem with this was that if there had been a reaction between the chromate and epoxy-phenolic it could not be seen as without knowing the appropriate chemical structures of the epoxies present, none of the peaks could be attributed to individual components.

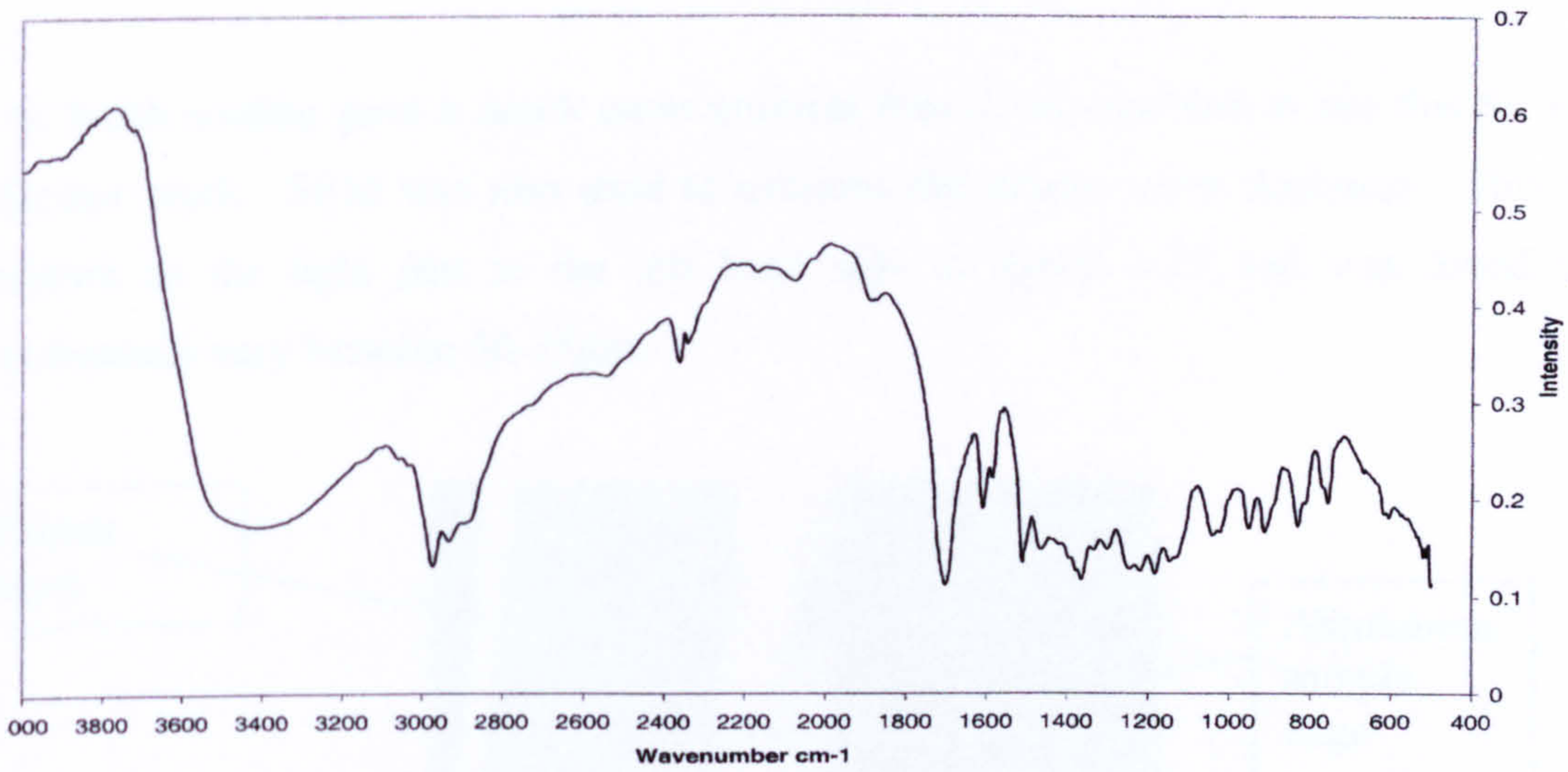


Figure 3.08. DRIFT spectrum of evaporated BR127

### *3.2.2 Surface analysis techniques*

After concluding that the range of employed analytical methods was unsuitable, it was decided to use some surface analysis techniques to see if chromate species were more readily observable.

Using the BR127 primer and aluminium alloy 2024-T3 (the current aerospace grade used on wings and fuselages), two different coating techniques were investigated. Due to safety concerns, the industrial method of spraying could not be used so samples were either dipped into the solution and removed or were brush coated. The resultant cured samples were analysed by SEM (figures 3.09a & 3.09b).

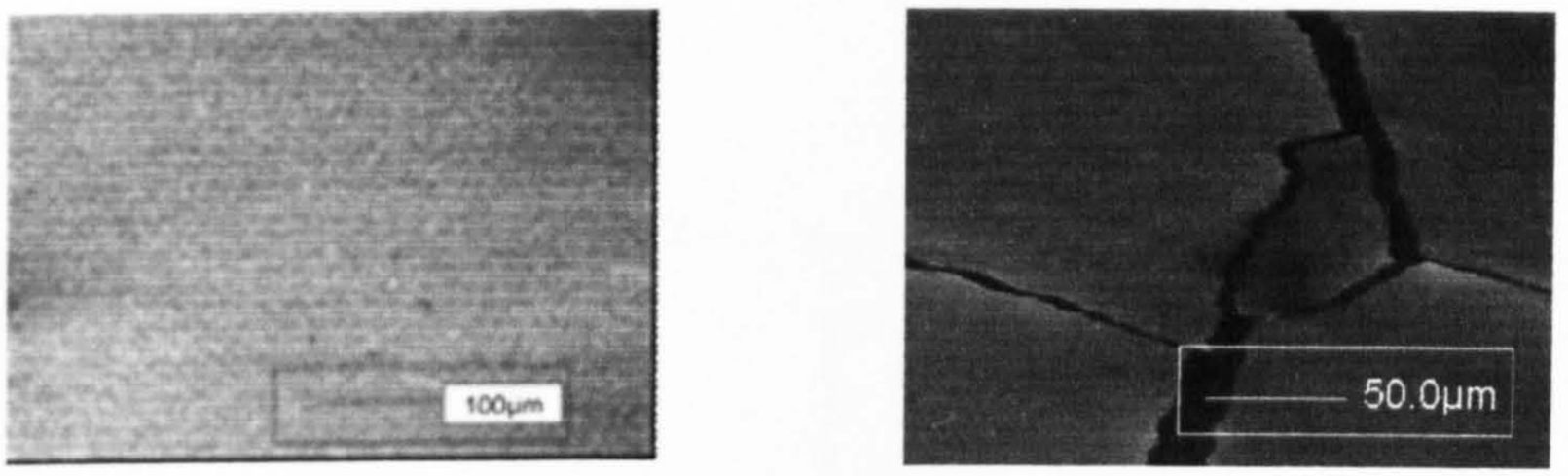


a b

Figure 3.09. SEM images obtained at 10kV and a) 1000x magnification and b) 2000x magnification of a) a brush primer coated aluminium surface and b) a dip primer coated aluminium surface

As brush coating gave a much more uniform film it was decided to use this for all further work. SEM was also used to examine the primer layer thickness. This is shown as the light part to the left hand side of figure 3.10 and was found to commonly vary between 50-75µm.

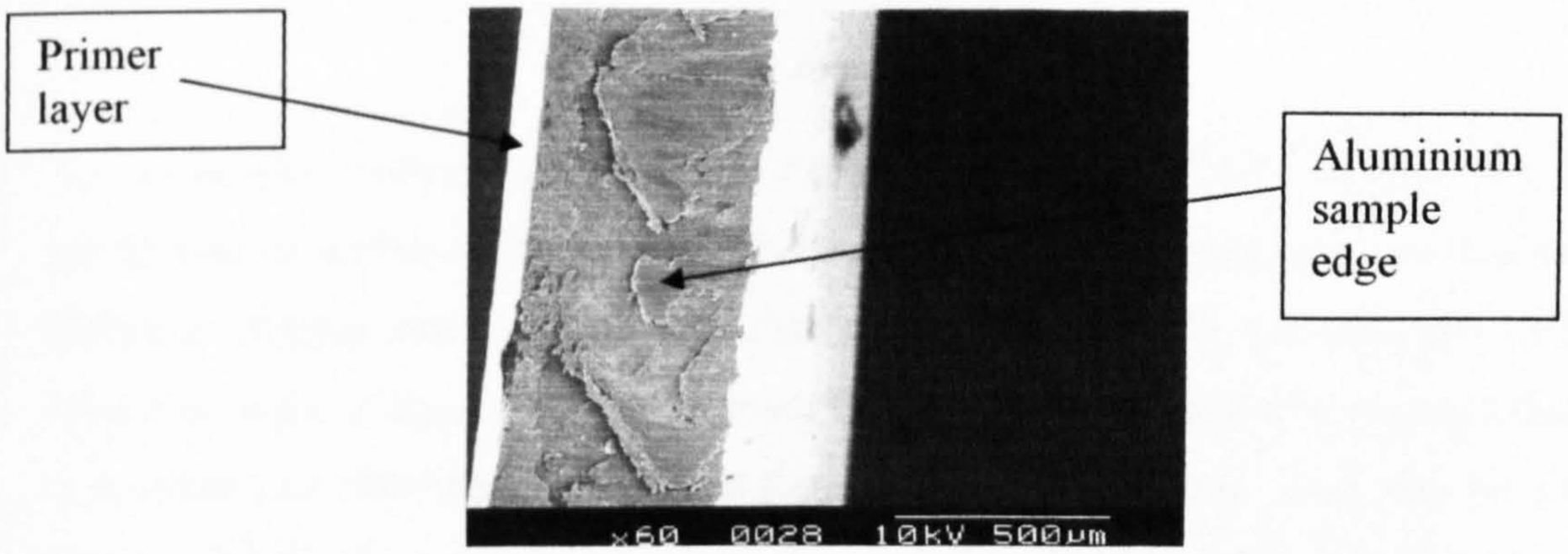


Figure 3.10. SEM image obtained at 10kV and 60x magnification showing the edge of brush coated, primed aluminium

However, the film thickness obtained through brush coating is considerably higher than the desired film thickness which is achieved using the industrial spray technique[3].

This experimentally obtained film thickness provided a problem for the extremely sensitive XPS technique which was used to analyse the brush primed aluminium.

This technique showed that there is no chromate present at the surface of the primed layer (figure 3.11).

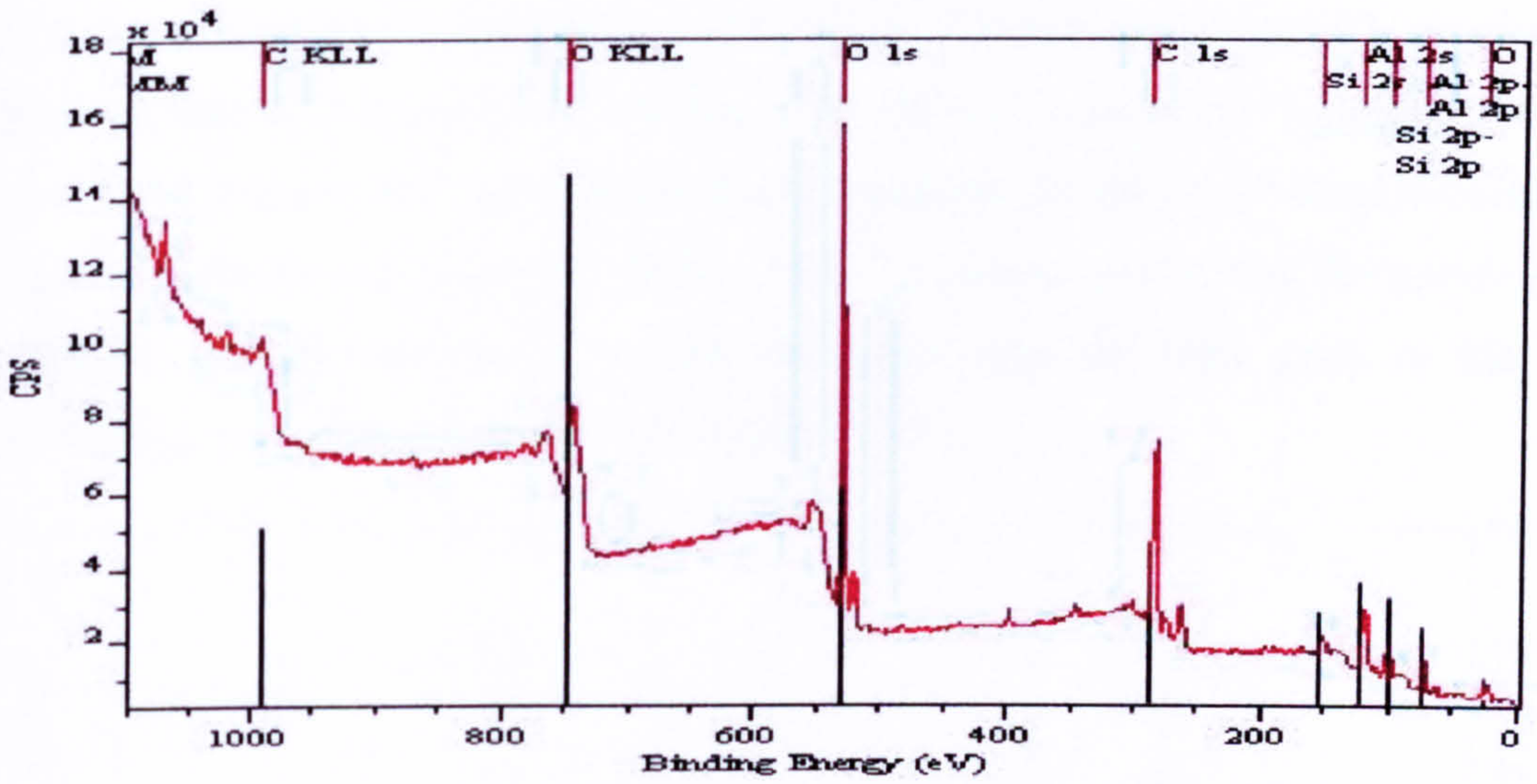


Figure 3.11. XPS of brush coated primed aluminium

As can be seen from the spectrum, only organics (C 1s and C KLL) and silicon and aluminium impurities from the atmosphere are present. Chromium appears at several different binding energies in XPS that correspond to different electron shells. However, none of these peaks are present in the XPS results and this suggests that it is possible that chromate is present at the metal-primer interface. It is also possible that the level of chromate is below the detection limits of the spectrometer or alternatively that it is surrounded by an organic polymer layer. This is quite important in trying to determine the mechanism of action of chromate as it suggests that chromate is not present at one of its most likely positions; the surface.

A further surface technique used to try and locate the chromate was attenuated total internal reflection spectroscopy (ATR). However, the energy of the beam was not great enough to give any informative readings and larger samples of material needed to be observed. From the results obtained it appeared that only the organic species were visible and that again this was not the most suitable technique of analysis.

Another infrared technique which was used in the analysis of the primed aluminium was thermo-gravimetric-IR (TG-IR). This technique uses a combination of thermal analysis equipment, combined in series with an infrared spectrometer to monitor the gaseous species evolved under heating[4]. To observe volatile species coming off the surface aluminium foil had to be used as a substitute for the metal sheet because this increased the ratio of primer to metal. This experiment proved that there were many different species leaving the surface throughout heating, with some of the most interesting evolving at around 400°C (figure 3.12).

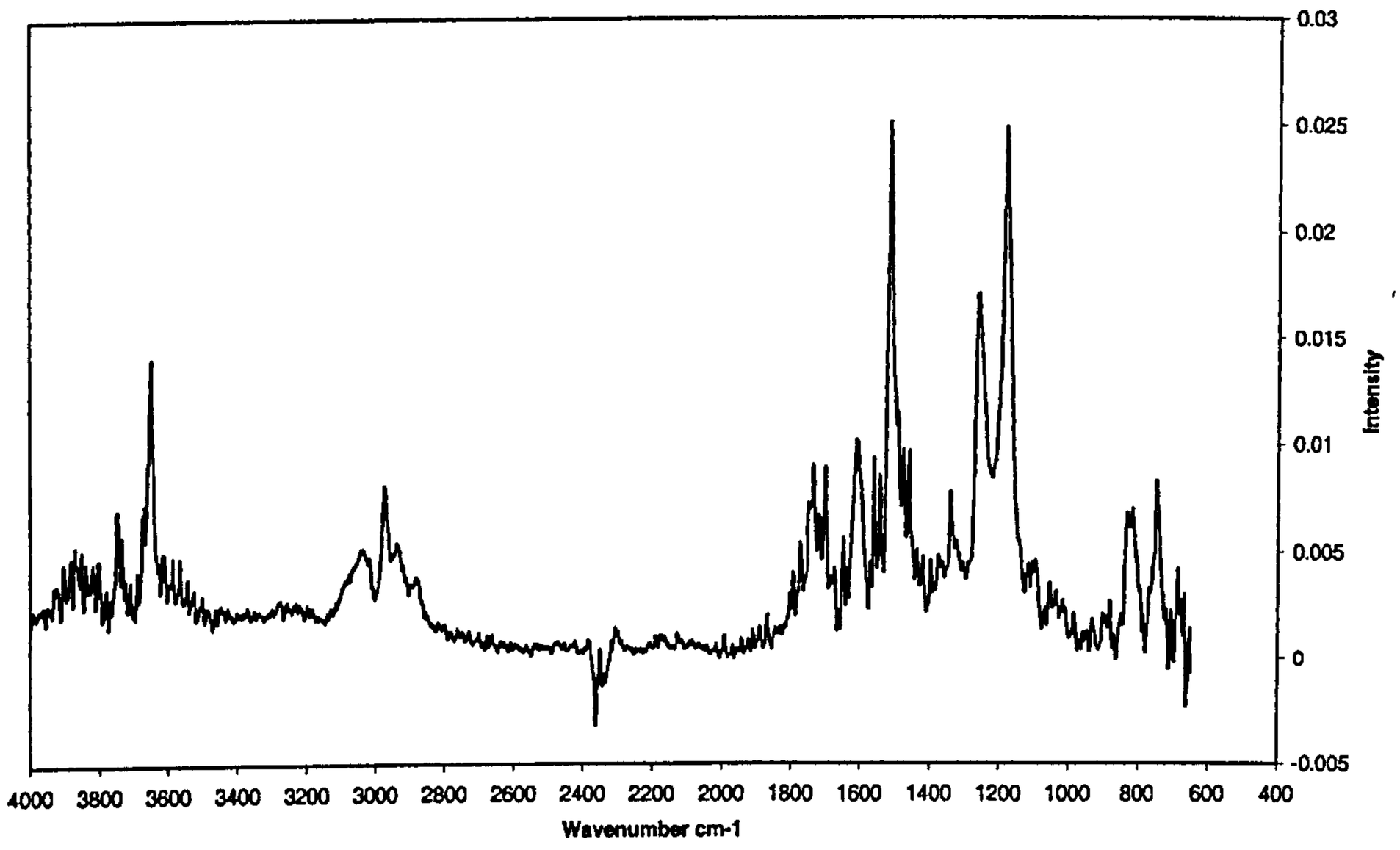


Figure 3.12. TG-IR showing organic vapour species at 400°C

This appears similar to what would be expected for a phenolic compound[5]. Unfortunately, due to the complexity of the system and not knowing some of the actual materials in the primer it is difficult to assign all of the peaks present, however some of the peaks are typical of common organic compounds. Figure 3.03 shows that the sharp peak at 1480 $cm^{-1}$ indicates the C–C stretch of an aromatic ring[6] with the corresponding C-H stretching modes of the ring at approximately 3650$cm^{-1}$ and 3000$cm^{-1}$. The sharp peaks at approximately 1200$cm^{-1}$ are consistent with the stretching mode of a C-O group[7], in this case corresponding to the epoxide groups in the compound.

### *3.2.3 EDX Analysis*

After some FPL etched, chromic acid anodised, industrially spray coat primed aluminium was obtained from Cytec Engineered Materials, EDX analysis was conducted, allowing the primer-metal interface to be analysed. Initially an accelerating voltage of 5kV was employed as this was the standard of the machine. However, this meant that only elements which emit X-rays of up to 5keV energy could be observed (figure 3.13).

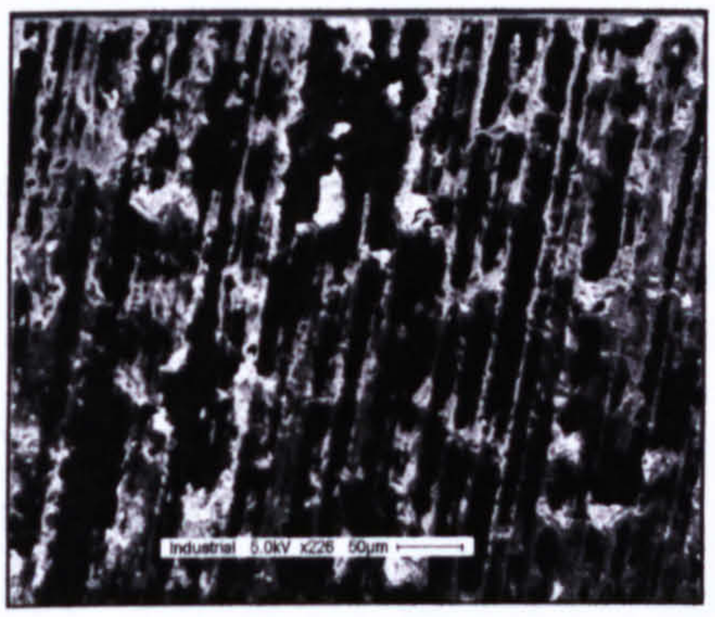


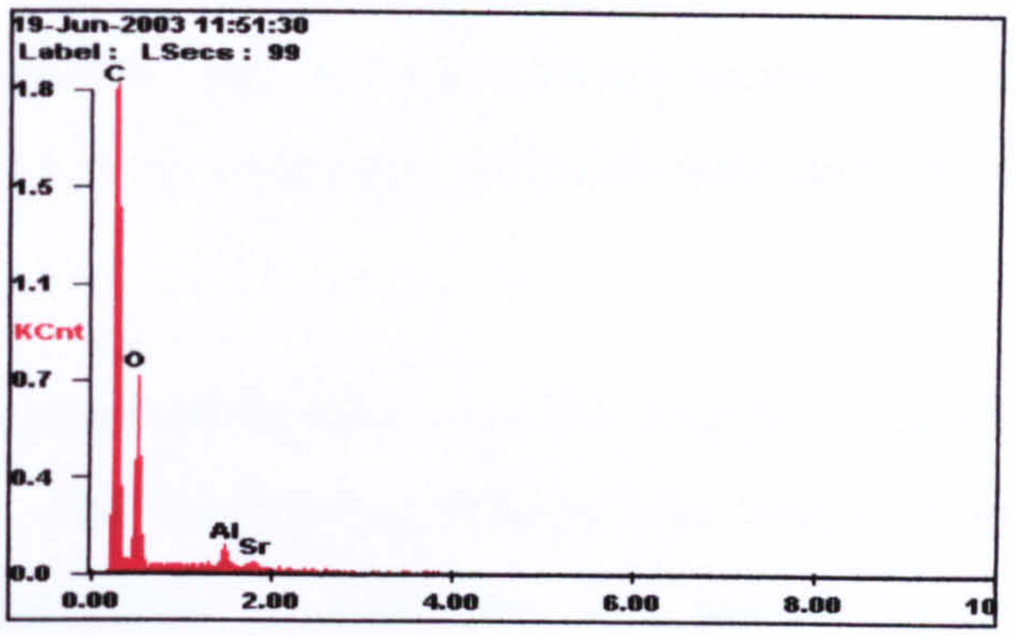


| *Element* | *Wt%* | *At%* |
|---|---|---|
| ***C*** | 74.33 | 82.71 |
| ***O*** | 17.69 | 14.78 |
| ***Al*** | 03.78 | 01.87 |
| ***Sr*** | 04.20 | 00.64 |

Figure 3.13. SEM image obtained at 5kV and 200x magnification and EDX analysis of an industrially primed AA2024-T3 surface

Therefore, chromium, which emits X-rays of 5.4keV is absent from this first spectrum. When the accelerating voltage was increased to 10kV (figure 3.14) the chromium can clearly be observed.

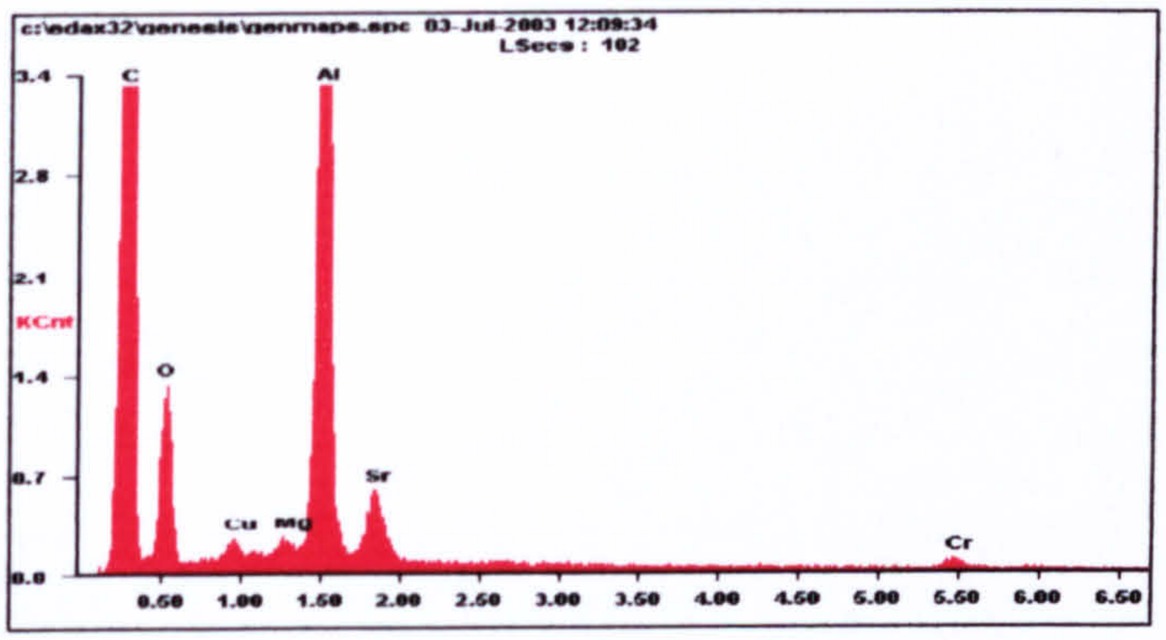


| *Element* | *Wt%* | *At%* |
|---|---|---|
| *C K* | 62.39 | 80.55 |
| *O K* | 05.13 | 04.97 |
| *CuL* | 00.95 | 00.23 |
| *MgK* | 00.54 | 00.35 |
| *AlK* | 18.85 | 10.84 |
| *SrL* | 04.57 | 00.81 |
| *CrK* | 07.56 | 02.26 |

Figure 3.14. EDX analysis of industrially primed aluminium using a 10kV electron beam

Although the chemical formula of strontium chromate is $SrCrO_4$, it can be seen in figure 3.14 that the concentrations of strontium and chromium do not appear in a 1:1 ratio. This is possibly due to inaccuracies in the technique, with chromate been more sensitive to analysis than strontium.

In an attempt to accurately locate the chromium in relation to the interface a depth profile investigation was carried out. The accelerating voltage was increased in 0.2kV increments between 7.8kV and 12kV. However, this proved to be unsuccessful as increasing the voltage only increased the amount of aluminium observed.

To look more closely at the interface, a cross section of the aluminium was taken. To increase the resolution of the image, the sample had been gold coated which interfered with the quantitative analysis. It appears that there are three main areas along the edge (figure 3.15).

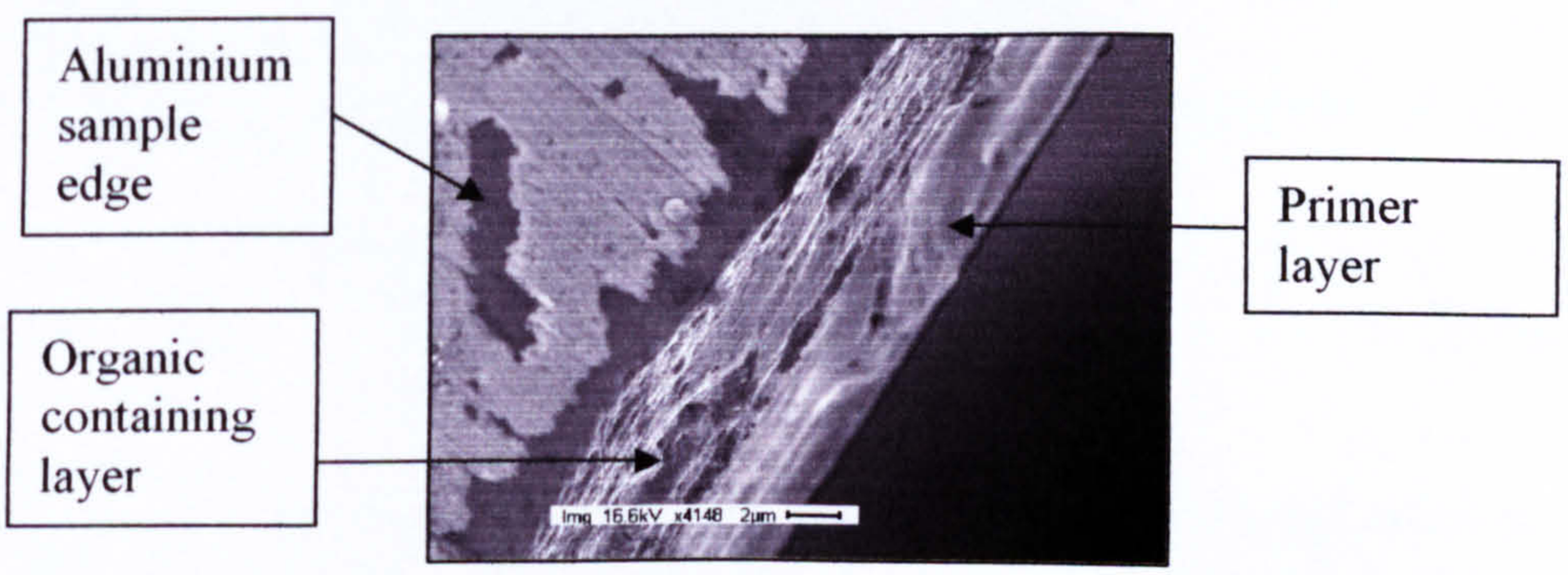


Figure 3.15. SEM image obtained at 10kV and 4000x magnification of the industrially primed aluminium edge

The first major area (to the left) is the aluminium alloy. The section to the right, approximately 3μm thickness, is the primer layer. This is evident from a spectrum at higher magnification (figure 3.16) which shows the presence of both strontium and chromium.

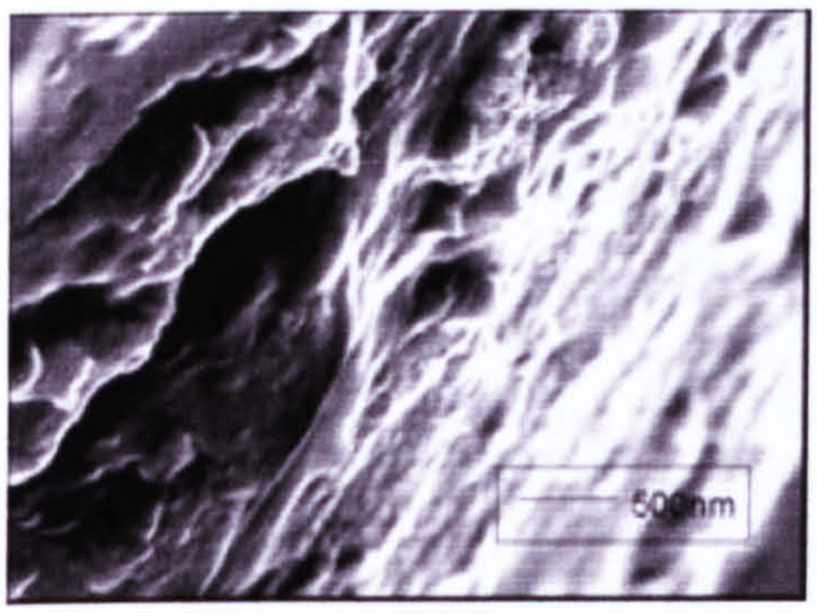


| *Element* | *Wt%* | *At%* |
|---|---|---|
| *C K* | 32.52 | 55.10 |
| *O K* | 04.10 | 05.21 |
| *CuL* | 03.69 | 01.18 |
| *MgK* | 01.24 | 01.04 |
| *AlK* | 47.62 | 35.92 |
| *SrL* | 01.37 | 00.32 |
| *AuM* | 08.76 | 00.90 |
| *ClK* | 00.24 | 00.14 |
| *CrK* | 00.47 | 00.18 |

Figure 3.16. SEM image obtained at 10kV and 15000x magnification and EDX analysis of the edge of the chromate containing primer coating

However, it is the middle section of figure 3.15 that is of most interest as it appears to be neither the aluminium nor the primer (figure 3.17). From the SEM picture it seems to have a similar surface morphology to the coated material but the EDX analysis states that it does not contain any strontium or chromium.

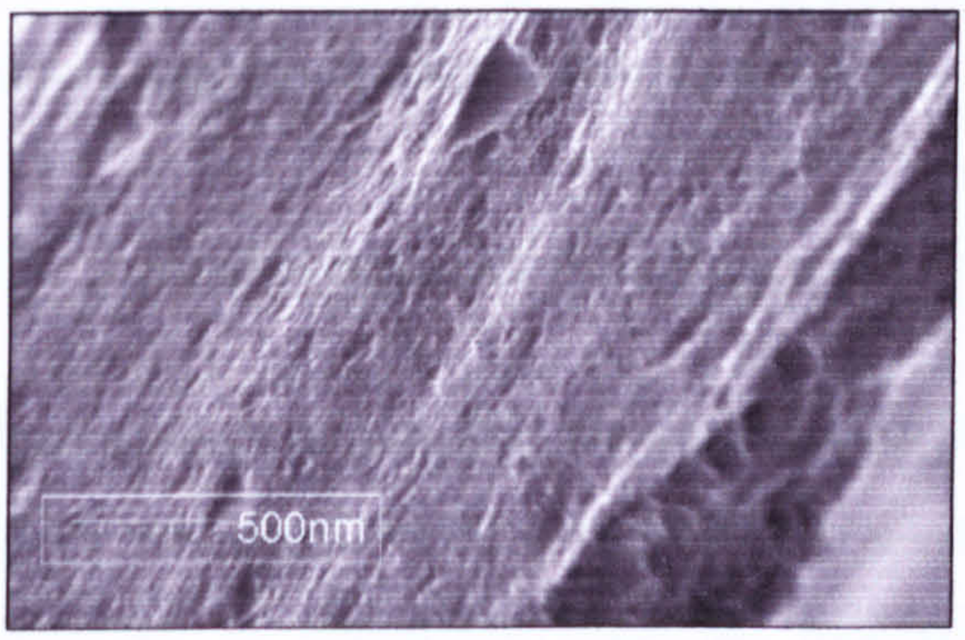


| *Element* | *Wt%* | *At%* |
|---|---|---|
| *C K* | 39.13 | 67.66 |
| *O K* | 04.69 | 06.08 |
| *CuL* | 01.50 | 00.49 |
| *MgK* | 00.57 | 00.49 |
| *AlK* | 29.03 | 22.34 |
| *AuM* | 24.37 | 02.57 |
| *CaK* | 00.71 | 00.37 |

Figure 3.17. SEM image obtained at 10kV and 15000x magnification and EDX analysis of the organic section between the aluminium surface and primer coating

As the middle section is primarily organic based (39.13 Wt%) carbon, it means that this could not be the anodised oxide layer. It is possible that this could be part of the surface that has not been coated by the all of the constituent chemicals of the primer.

As can be seen in figure 3.13, the aluminium surface is not uniformly covered by the primer coating. This is better illustrated in figure 3.18, where it can clearly be seen that there are areas where the yellow colour of the primer is absent. However, it is possible that there is some residual epoxy on the aluminium and this could be the reason that the area in question shows organic character under EDX analysis.

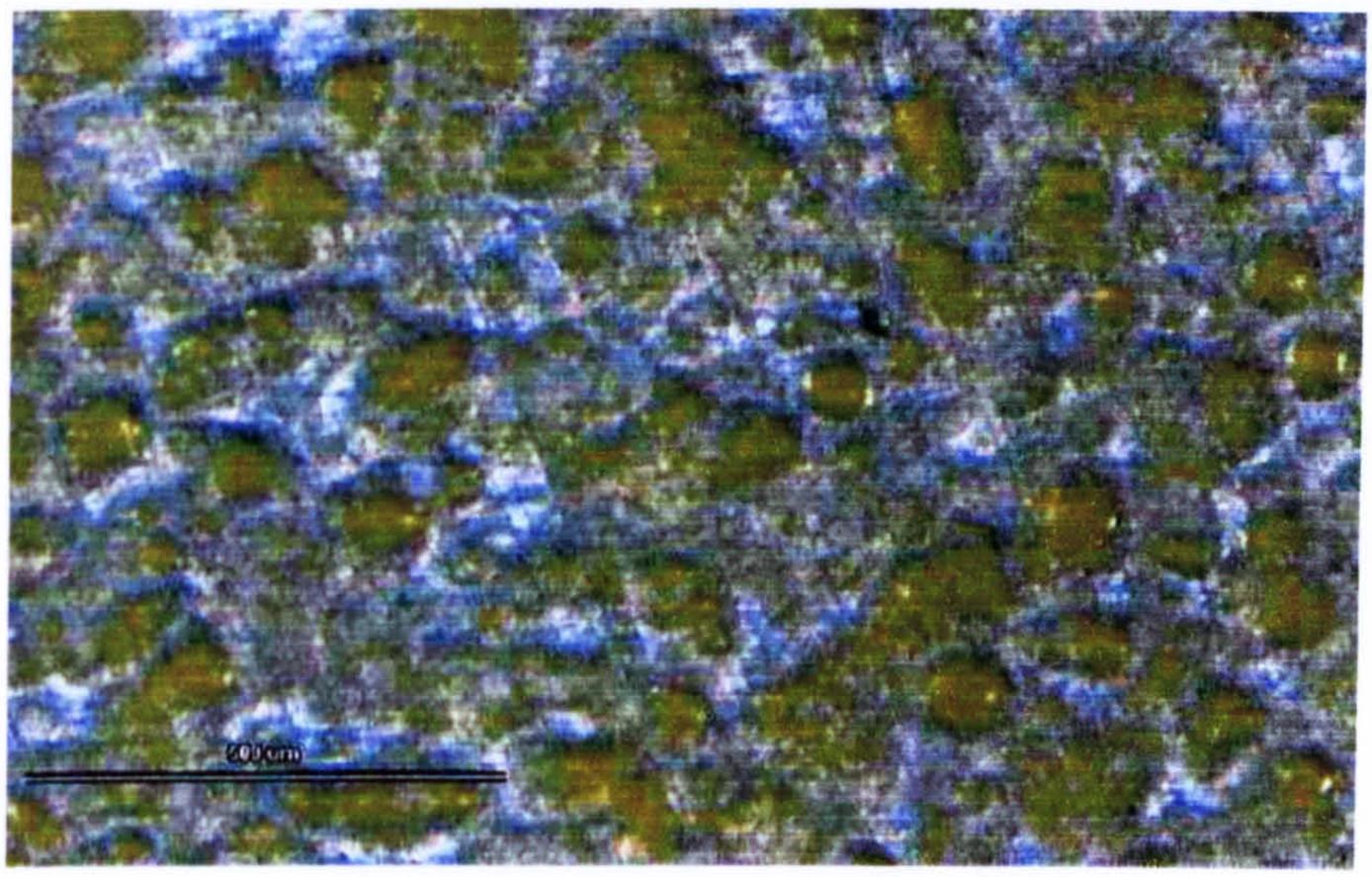


Figure 3.18. Optical micrograph image of BR127 primed aluminium[8]

The absence of chromium from parts of the image suggests that it remains mobile after application of the primer and could therefore explain why no chromium peaks were present in the XPS studies carried out.

## 3.3 Model System Development

In an attempt to simplify the complicated industrial system, a model was generated which was based on the industrial primer compound. Model systems are commonly employed in chemistry when an increase in the understanding of a complex mechanism is being investigated. Regularly applied substitutions include; the replacement of polymeric species with much lower molecular weight monomers, the use of powdered oxide species in place of solid substrates and the use of low boiling point solvents to aid both analysis and the experimental procedures being followed.

The major problem with the industrial compound was in the use of strontium chromate and its apparent lack of solubility in commonly used, low boiling point solvents. Therefore, the strontium derivative (5.90mmol $l^{-1}$) was replaced with the more soluble sodium chromate compound (7.09mol $l^{-1}$). Another problem was the use of the epoxy resins. Due to their complex structures (figure 3.19) easy analysis by available spectroscopic techniques was difficult, literature does provide details of characterisation[9] but for this investigation their complexity meant mechanistic theories were hard to generate. The development of the model system was based on the idea of carrying out a fundamental study using a much more simple epoxide, cyclohexene oxide (figure 3.20), to be used as a replacement. Subsequently, the change in both chromate and epoxide meant that the three high-boiling point solvent system was replaced with methanol, again, enabling for much easier analysis.

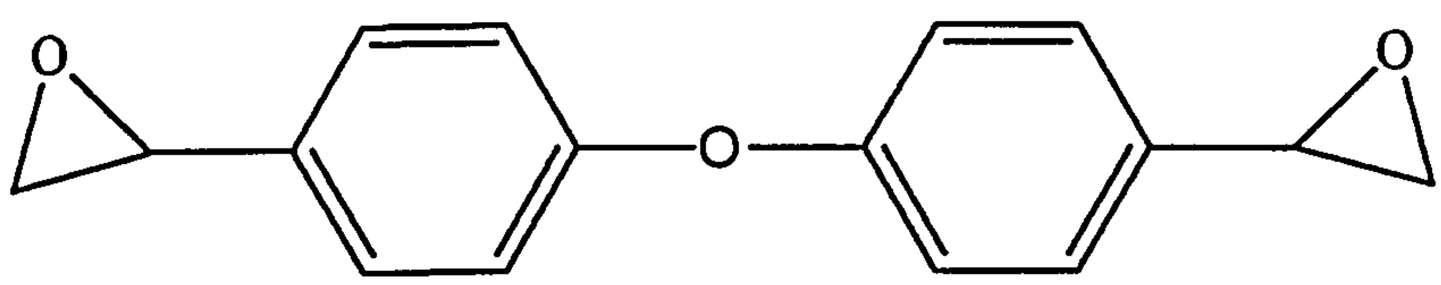


Figure 3.19. Probable structure of one of the epoxy resins used in BR127[9]

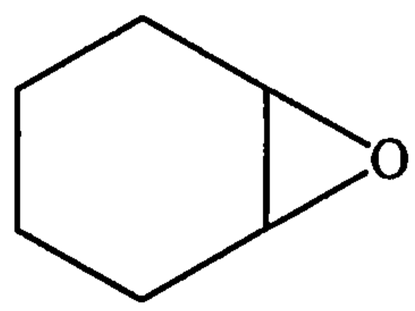


Figure 3.20. Structure of cyclohexene oxide

### *3.3.1 Model system analysis*

To maintain similar chemistry to the industrial formulation, the concentrations of chemicals in the model system were kept in the same ratio, therefore, a large molar excess of epoxide was used in comparison to the chromate. These two compounds were dissolved in methanol and the reaction was conducted at both elevated (carried out under reflux conditions) and room temperatures.

Various different analytical techniques were employed to investigate the model system meaning that the most successful ones could be used for all future analysis.

### *3.3.1.1 UV-vis Spectroscopy*

Initially, UV-vis spectroscopy was used to investigate the model system reaction over time. A sample was taken at the beginning of the reaction and then every hour for 6 hours. As can be seen from figures 3.21 and 3.22, there appears to be no change in the spectra when the system was left at room temperature.

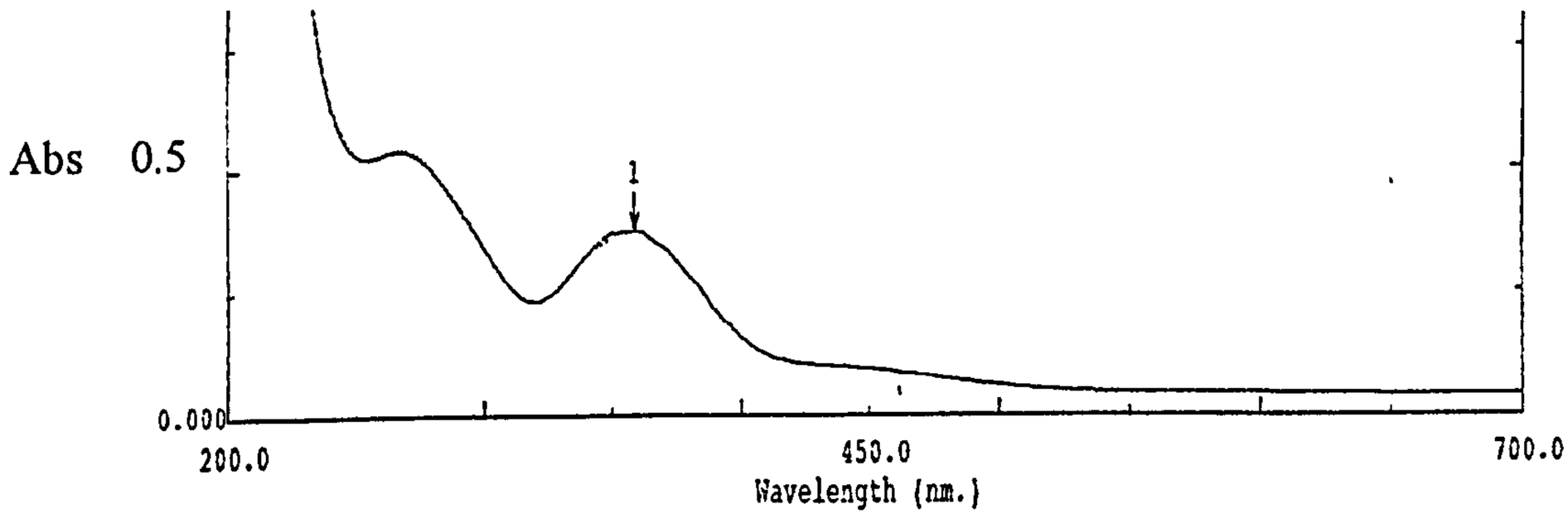


Figure 3.21. UV-vis spectrum of the reaction between $Na_2CrO_4$ and cyclohexene oxide at room temperature after 0 hours

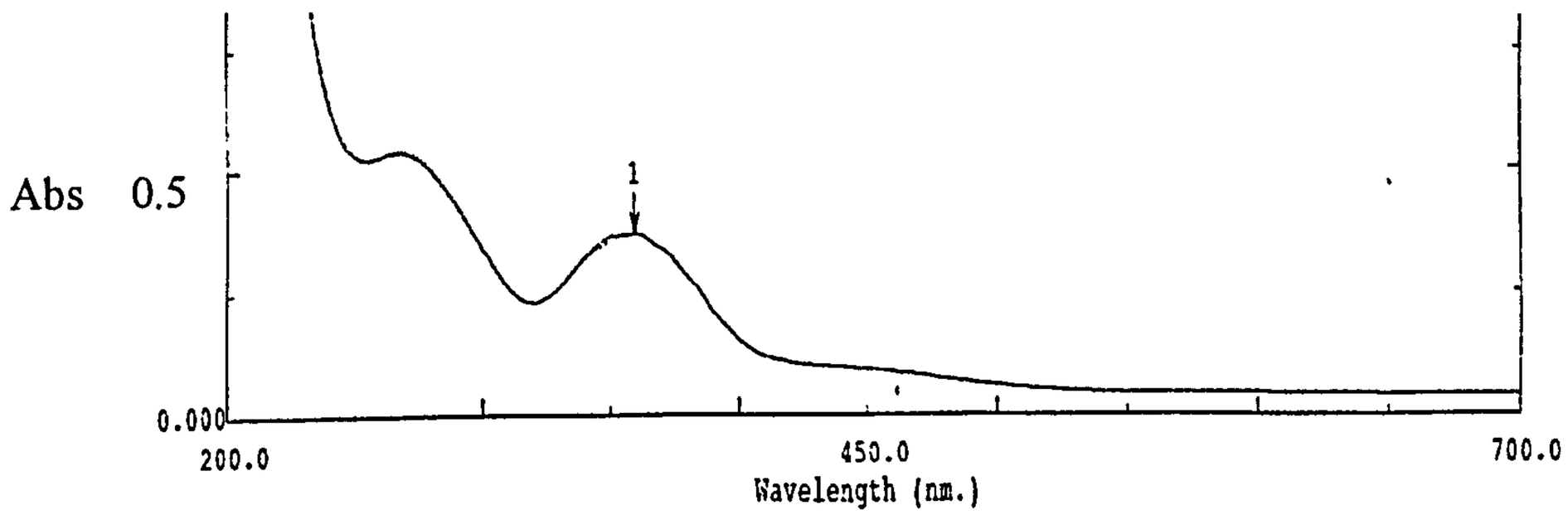


Figure 3.22. UV-vis spectrum of the reaction between $Na_2CrO_4$ and cyclohexene oxide at room temperature after 6 hours

However, when the system was heated to reflux conditions, there is a new absorbance peak appearing at approximately 450nm (figure 3.23).

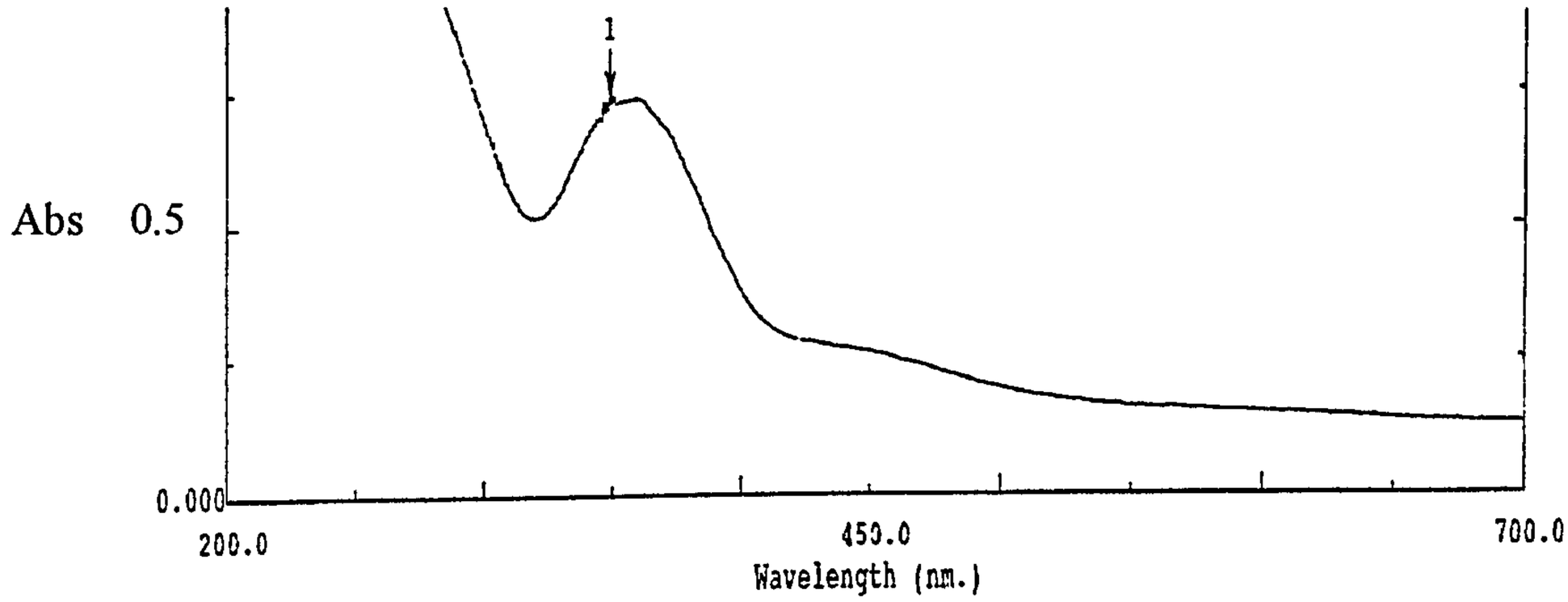


Figure 3.23. UV-vis spectrum of the reaction between $Na_2CrO_4$ and cyclohexene oxide at refluxed at 60°C after 6 hours

As chromium VI is a very powerful oxidising agent[10,11], it is possible that this peak is due to the presence of a reduced form of chromium. The most probable of these would be chromium III as it is the most stable form[11,12]. Another possibility is that there has been a reaction to form a dichromate compound. However, since the chromate-dichromate equilibrium is pH dependent and the formation of dichromate requires highly acidic conditions this seems unlikely[13]. Additionally, neither of these compounds shows a peak in exactly the same UV-vis region, which means it is probable that the reaction is leading to the formation of a different species. One such possibility is that an organochromate may have been formed.

### *3.3.1.2 Organochromates*[14,15,16]

Organochromium compounds are quite commonly employed in the field of catalysis[17], where their chemistry is analogous to that of Grignard reagents[18], providing methods for addition of organic nucleophiles to electrophiles. The key significance of organochromium chemistry, however, is the relatively soft nature of the reagents themselves; the only electrophiles they will react with are aldehydes, thus making them extremely chemioselective.

However, most examples of organochromium compounds are based on the metal been in either the chromium II or chromium III oxidation state[19]. Due to the ability of chromium VI to oxidise many organic species, there appears to be no mention in the current literature of organochromium (VI) compounds, probably due to their instability.

### *3.3.1.3 ESI-MS*

The model system was also studied by electrospray ionisation mass spectrometry. Similar conditions were used and the reaction analysed after 6 hours (figure 3.24).

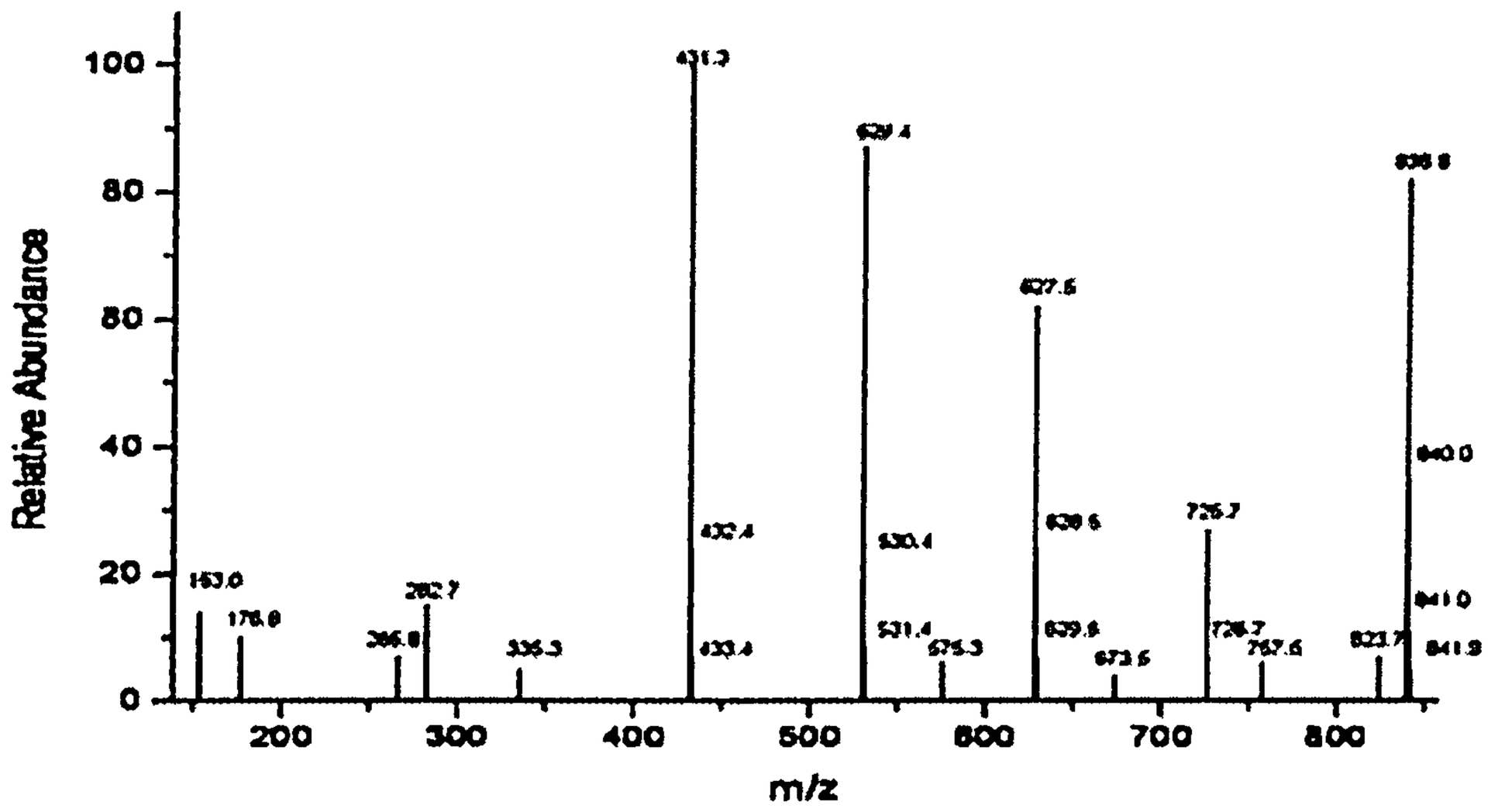


Figure 3.24. ESI-MS of sodium chromate, cyclohexene oxide and methanol, refluxed at 60°C for 6 hours

The results suggest that some oligomerisation has occurred. This is evident as there is a recurring loss of 98 mass units in the following pattern:

$$725 - 627 - 529 - 431$$

98 corresponds to the mass of the molecular ion of the cyclohexene oxide molecule (see figure 3.25) so it is probable that this is oligomerising. If it is taken that there is a loss of a further 3 of these units this leaves a mass of 137. $CrO_4^{2-}$ has a mass of

116 leaving a value of 21. A sodium atom has a mass of 23 which could account for this (allowing for some error in the MS readings) and suggests the possibility of a compound with the structure shown below (figure 3.26).

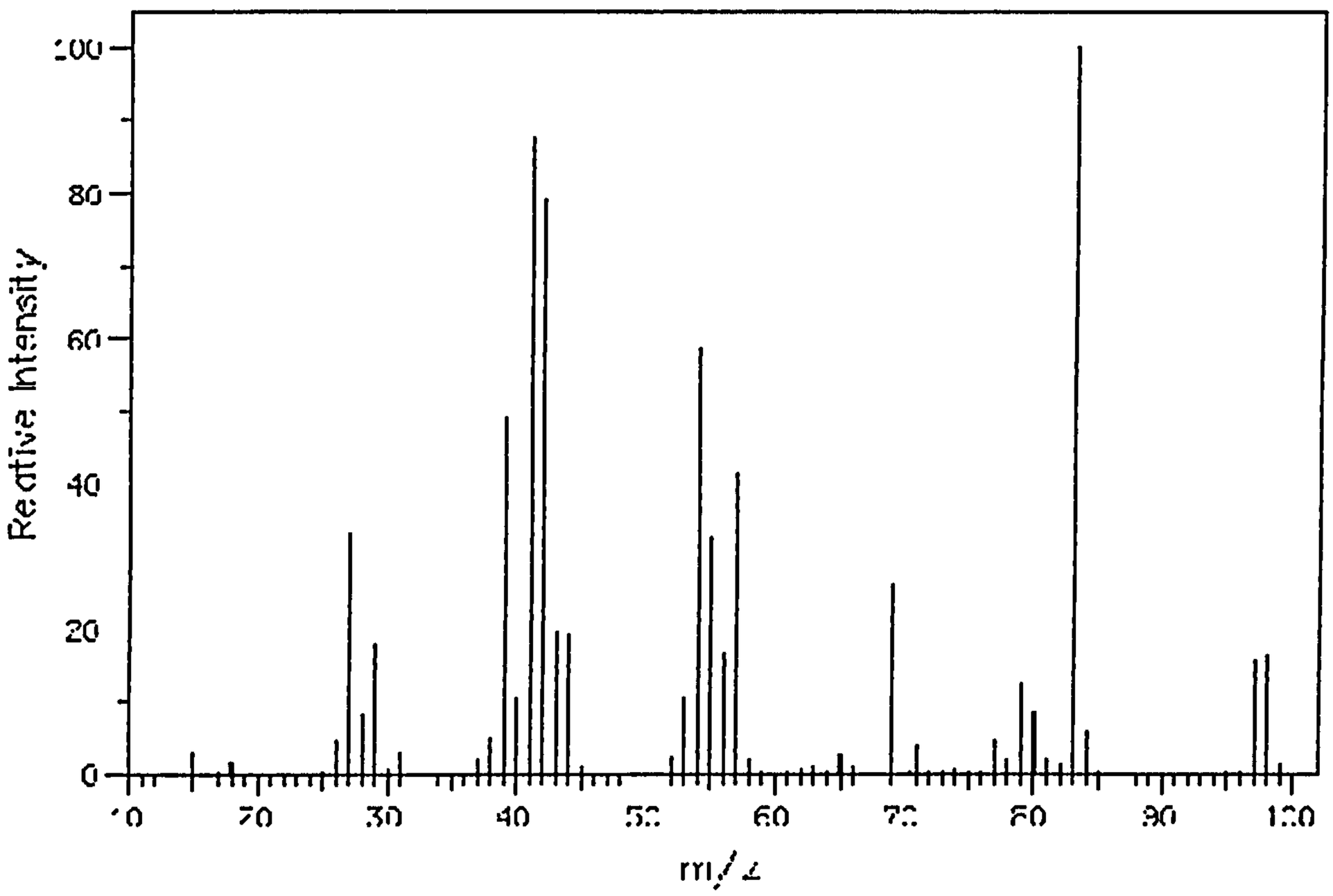


Figure 3.25. Mass spectrum of Cyclohexene oxide

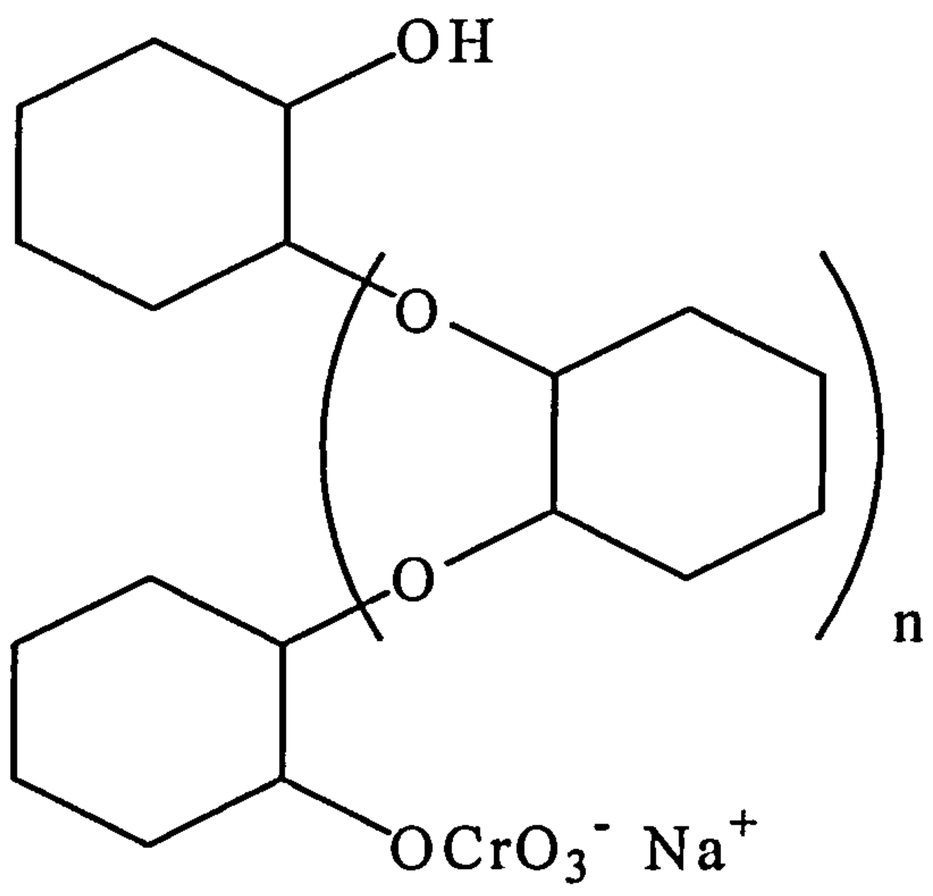


Figure 3.263. Structure of possible organochromate species

If a structure such as that shown in figure 3.26 did form, it would mean that the chromate in the primer formulation was acting as a curing agent. This makes sense as in most epoxy adhesive formulations an amine curing agent is often added. As this is absent from chromate primers, it suggests that the chromate possibly carries out this function.

#### *3.3.1.4 IR spectroscopy*

For further confirmation of this organochromate species, IR studies were conducted on the model system reaction. To eliminate the large peaks of the methanol from the spectrum, this was evaporated on a rotary evaporator and the solid analysed (figure 3.27).

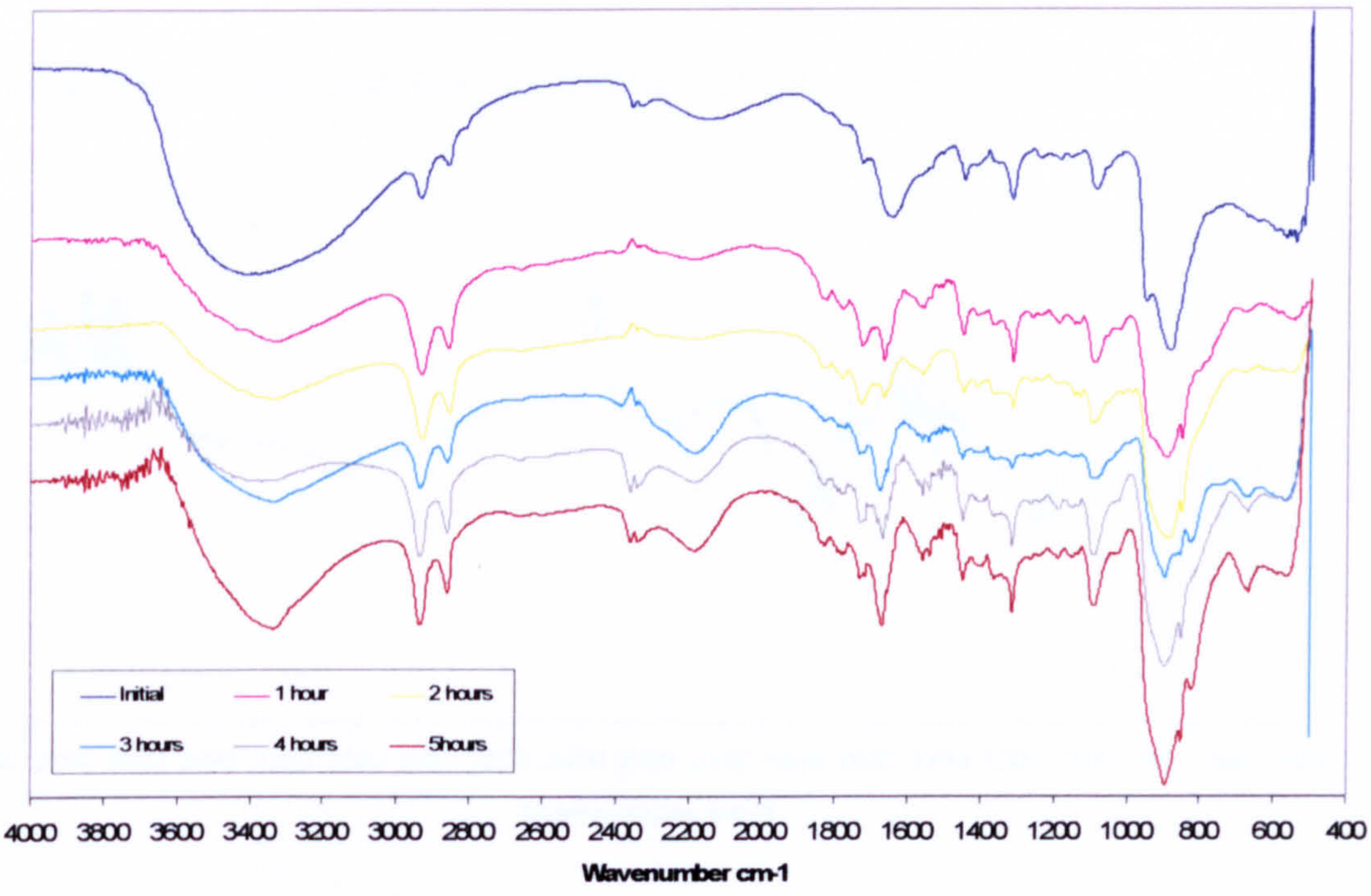


Figure 3.27. DRIFT analysis over a 5 hour time range refluxed at 60°C

There appears to be two main areas of change in the spectra. Firstly there are differences at approximately 1650-1800cm$^{-1}$ and since there are no active modes in this area of the cyclohexene oxide (see figure 3.28), it can be assumed that these

changes are due to a change in structure of the chromate as this is IR active in that region (figure 3.29).

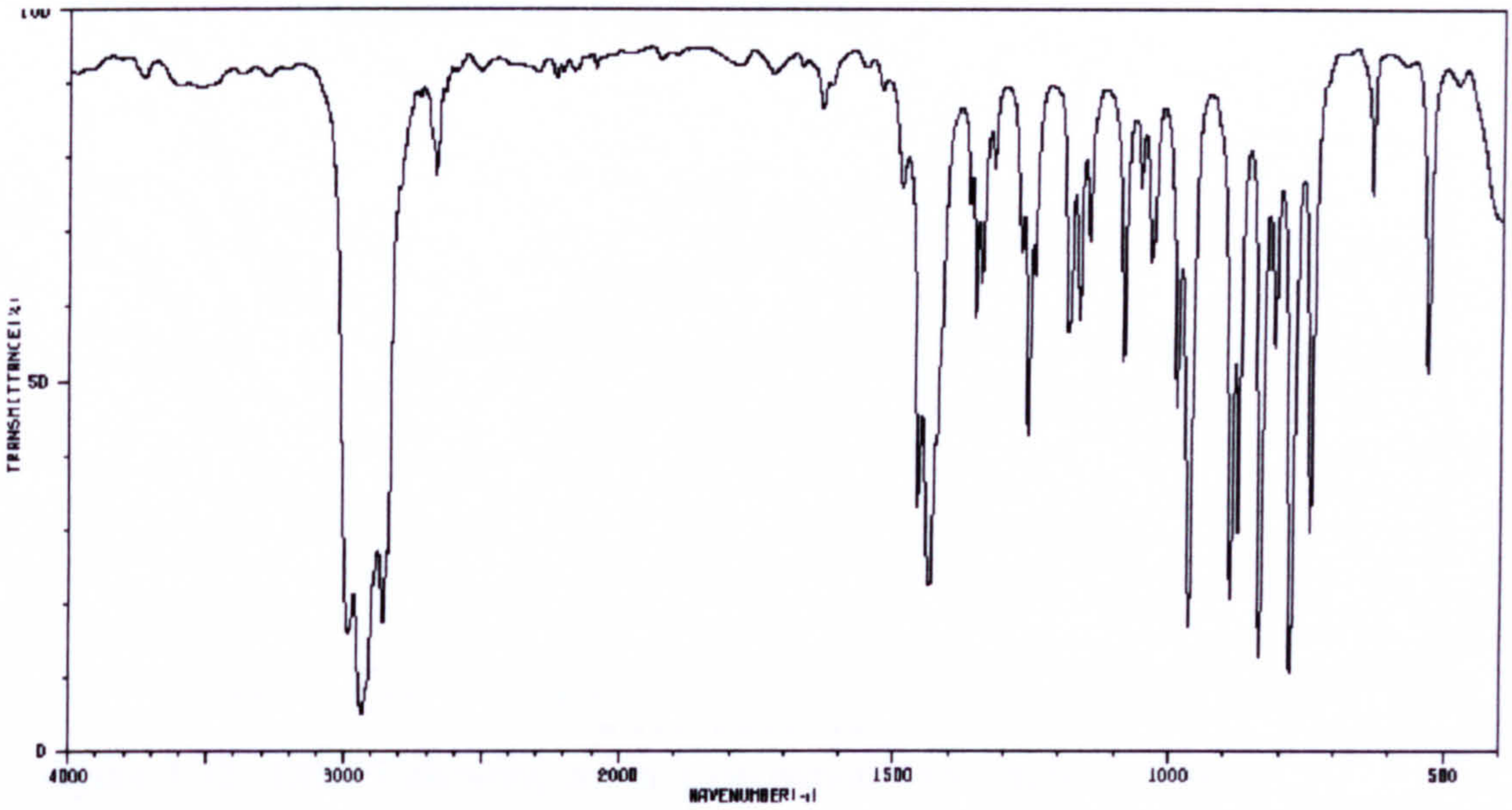


Figure 3.28. FTIR liquid thin film spectrum of cyclohexene oxide

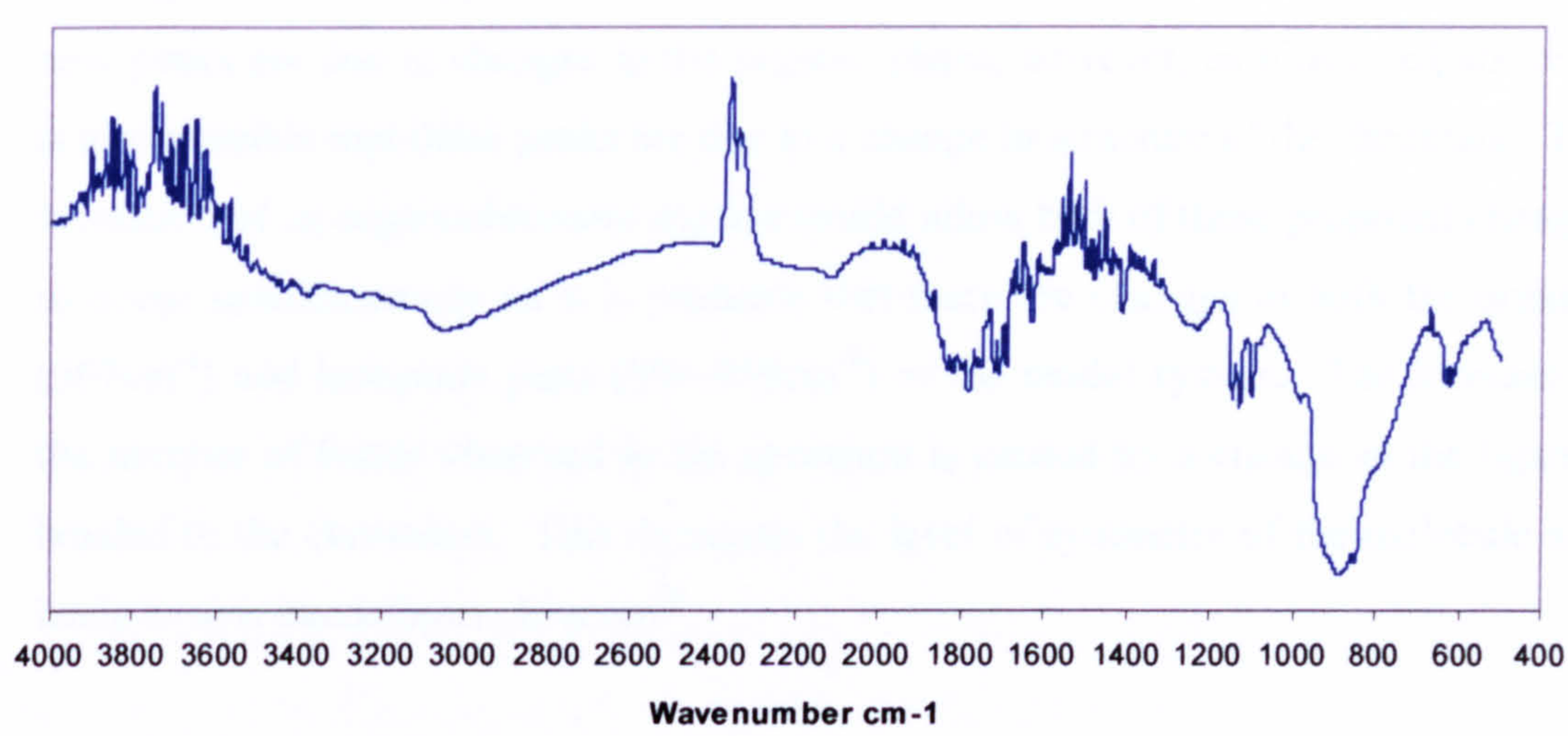


Figure 3.29. DRIFT spectrum of sodium chromate

The second part of the spectra that shows changes is around the 650-900cm$^{-1}$ range. On enlarging this region (figure 3.26) there are two major changes occurring with time. There are new peaks forming at approximately 875cm$^{-1}$ and also at 675cm$^{-1}$.

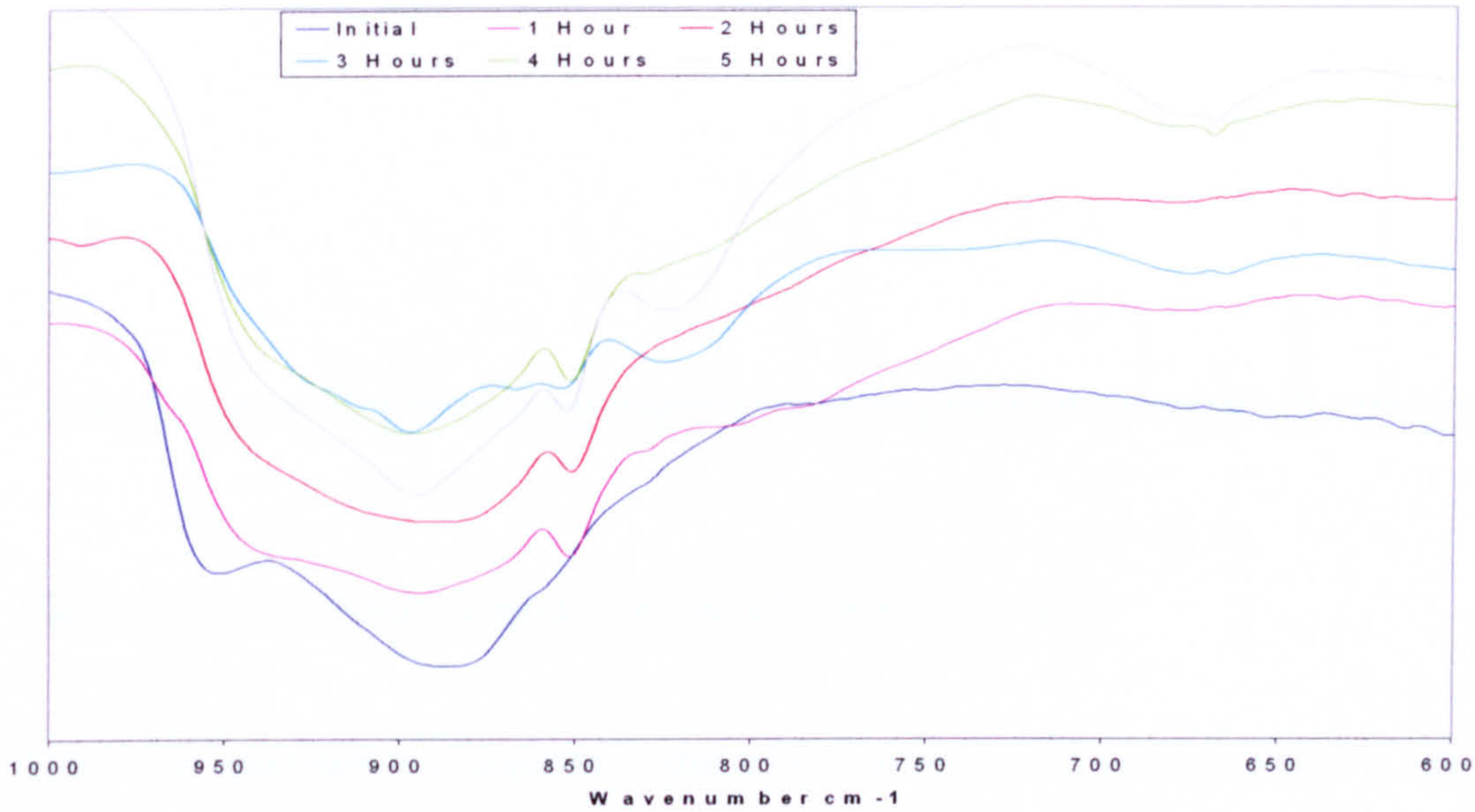


Figure 3.30. DRIFT showing zoom in on region between 600-1000cm$^{-1}$

Even though the IR spectrum of cyclohexene oxide is quite complex in this region (see figure 3.28), it appears that these are indeed new peaks. It could be that these new peaks are due to changes in the organic phase; however, as illustrated above, it is also possible that these peaks are due to a change in structure of the chromate. The formation of an organochromate species would allow both of these proposed changes to occur simultaneously so it is probable that there are changes in both the organic (667cm$^{-1}$) and inorganic parts (800-950cm$^{-1}$) of the model system. The increase in the number of bands observed in the spectrum is caused by a change in the ligands bonded to the chromium. This decreases the level of symmetry of the molecule and leads to new bands been observed[20].

### *3.3.1.5 NMR spectroscopy*

$^{13}$C-NMR was also employed to investigate the possibility of the formation of a new species. The chromate, epoxide and methanol mix was refluxed and a sample analysed after 6 hours (figure 3.31).

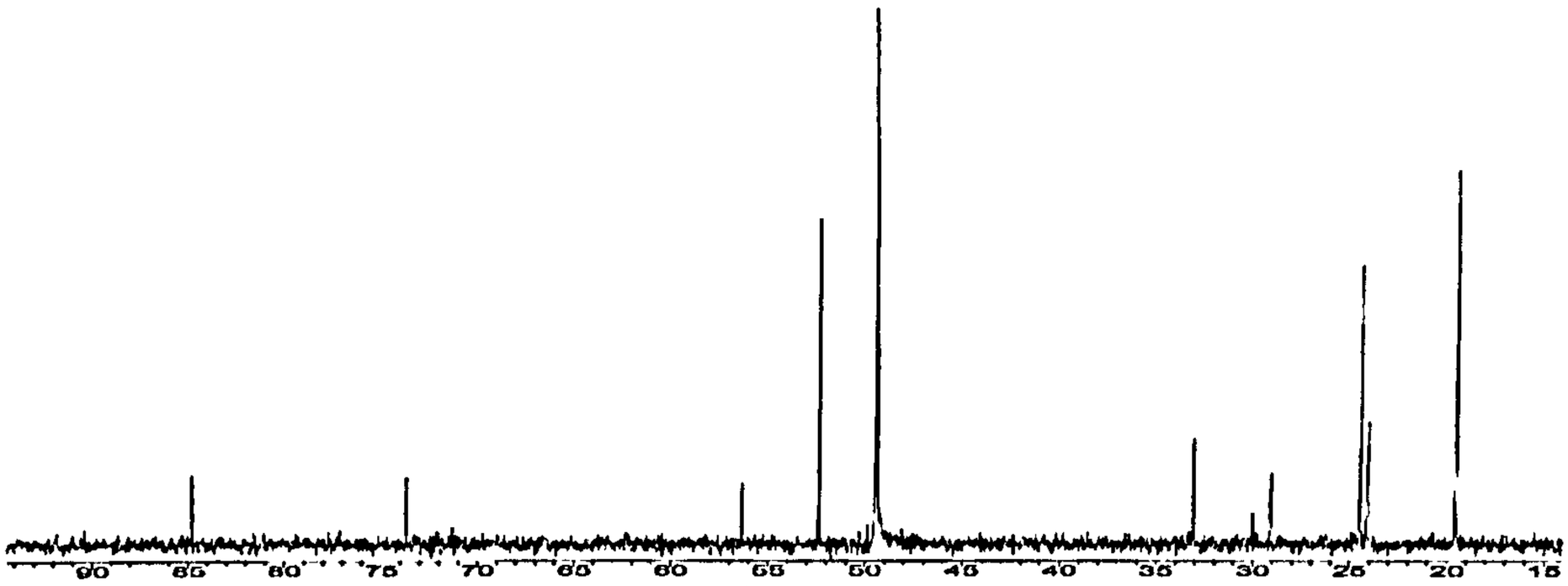


Figure 3.31. $^{13}$C-NMR of model system after 6 hours at 60°C

When this spectrum is compared to that of the non-refluxed system (figure 3.32) and cyclohexene oxide control (figure 3.33) it is clear that there are 6 new peaks.

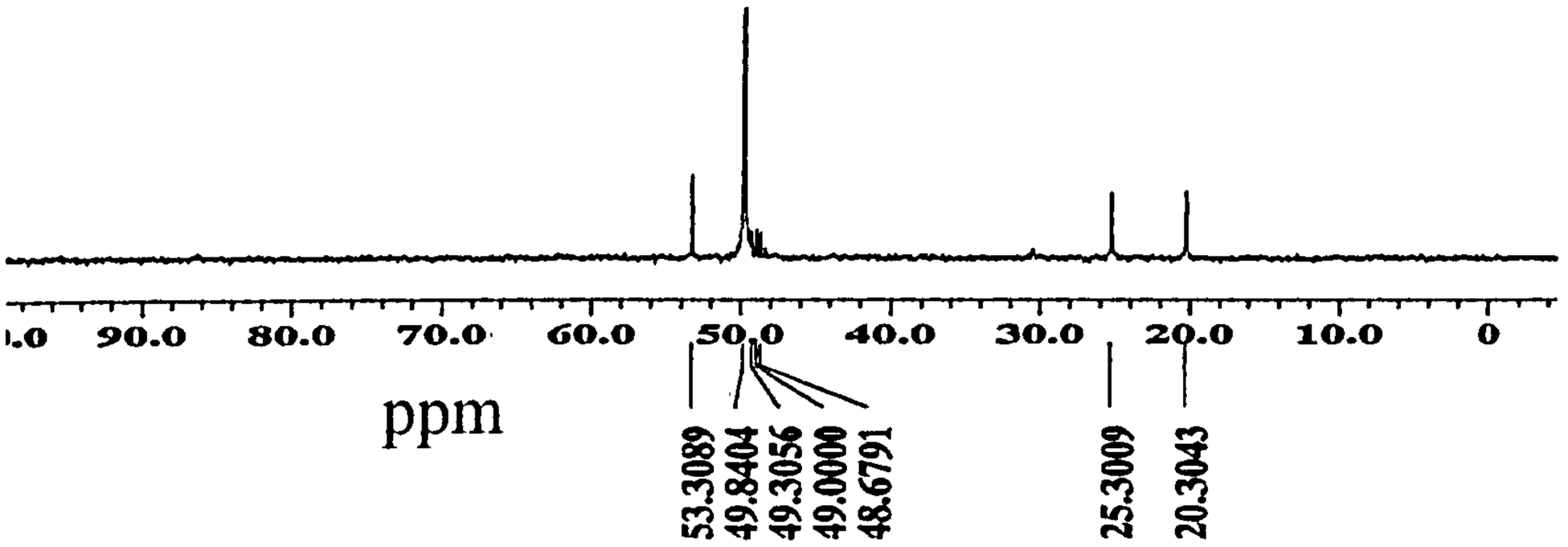


Figure 3.32. $^{13}$C-NMR of model system at the start of the reaction

Unfortunately, it is difficult to tell whether any of these peaks are due to the presence of an organochromate or simply an effect of the chromate acting as a catalyst for the homopolymerisation of the epoxide. Figure 3.07 suggests that the presence of the new peaks at 27ppm and 33ppm are due to the formation of new aliphatic carbon environments and the new peak at approximately 57ppm could either be due to a C-O-C bonding system or a C-OH bond. However, all these peaks would be present in both an organochromate and a homopolymerised epoxy.

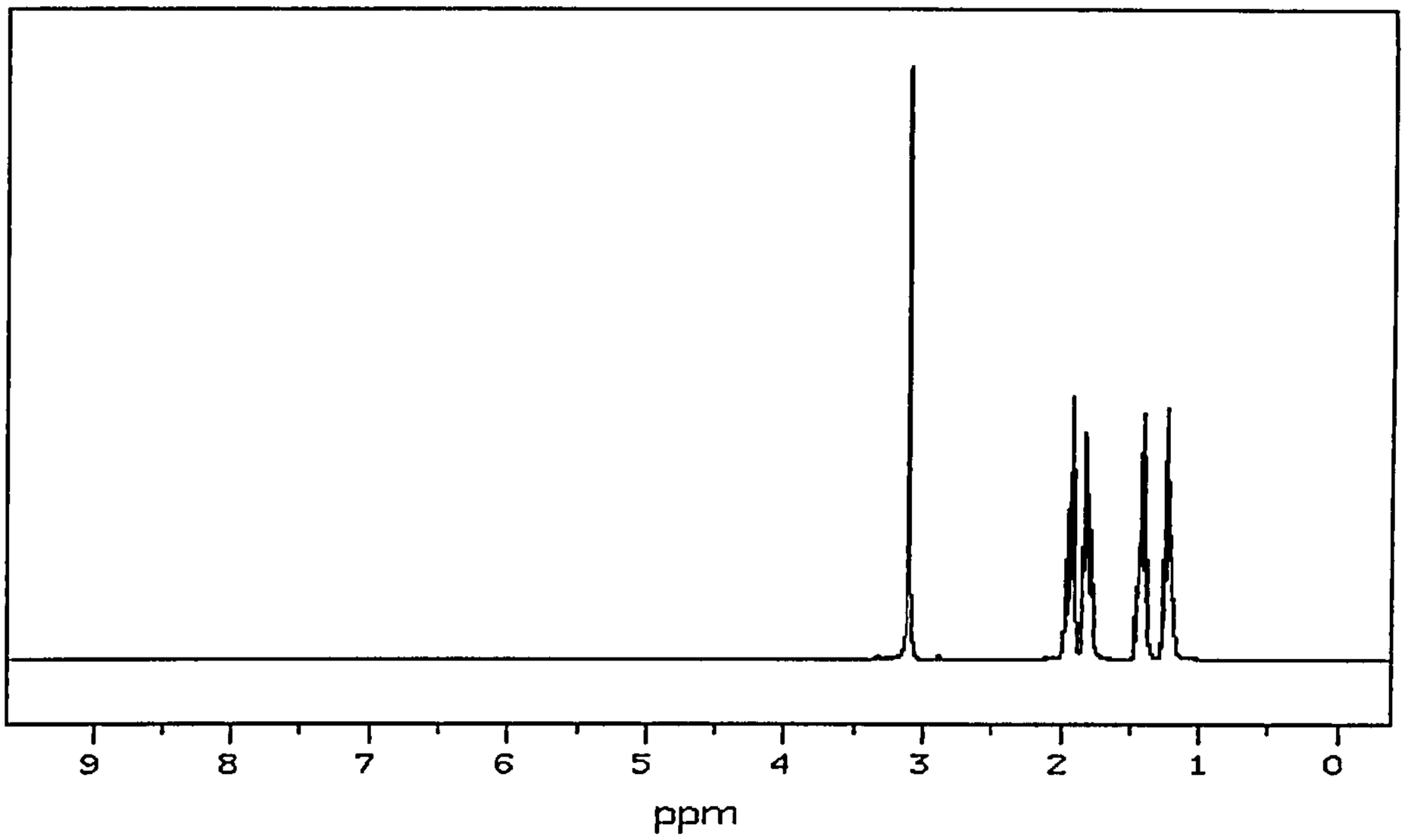


Figure 3.33. $^{13}$C-NMR spectrum of cyclohexene oxide

The peaks with the largest chemical shifts, 85ppm and 73ppm are most likely due to a carbon closely bonded to a metal; however, it is also possible that these carbon atoms could be directly attached or in close proximity to oxygen atoms (figure 3.07) which would have a similar effect on the chemical shift.

This does not mean that an organochromate has not formed. The high concentrations of organic compounds in the system mean that it would be extremely difficult to see an organochromate in such a small quantity.

## 3.4 Model system – substrate interactions

The model system was also used to coat aluminium surfaces. However, due to the high volatility of the methanol solvent, whenever the coated samples were placed under UHV conditions the film evaporated from the surface giving an uneven coating. This meant that techniques such as XPS were unsuitable to analyse the coated samples.

To observe possible interactions between the model system and a substrate, it was decided to conduct the reaction in the presence of neutral γ-alumina powder and monitor any possible reaction by Diffuse Reflectance UV-vis Spectroscopy. As well as alleviating the problem described above, using aluminium oxide greatly increases the number of active groups on the substrate and therefore, any effect would be much more easily observed.

Figure 3.34 shows the differences obtained in the model reaction when alumina was present and when absent. As can be seen from the two spectra, there is clearly a new peak formed at approximately 440nm. It is possible that this new peak is due to an interaction between the chromate and functional groups on the surface of the alumina. It is therefore possible that similar reactions occur on the surface of the aluminium sheet but as the concentration of functional groups is much lower, the effects are not observable in the DRUV spectrum.

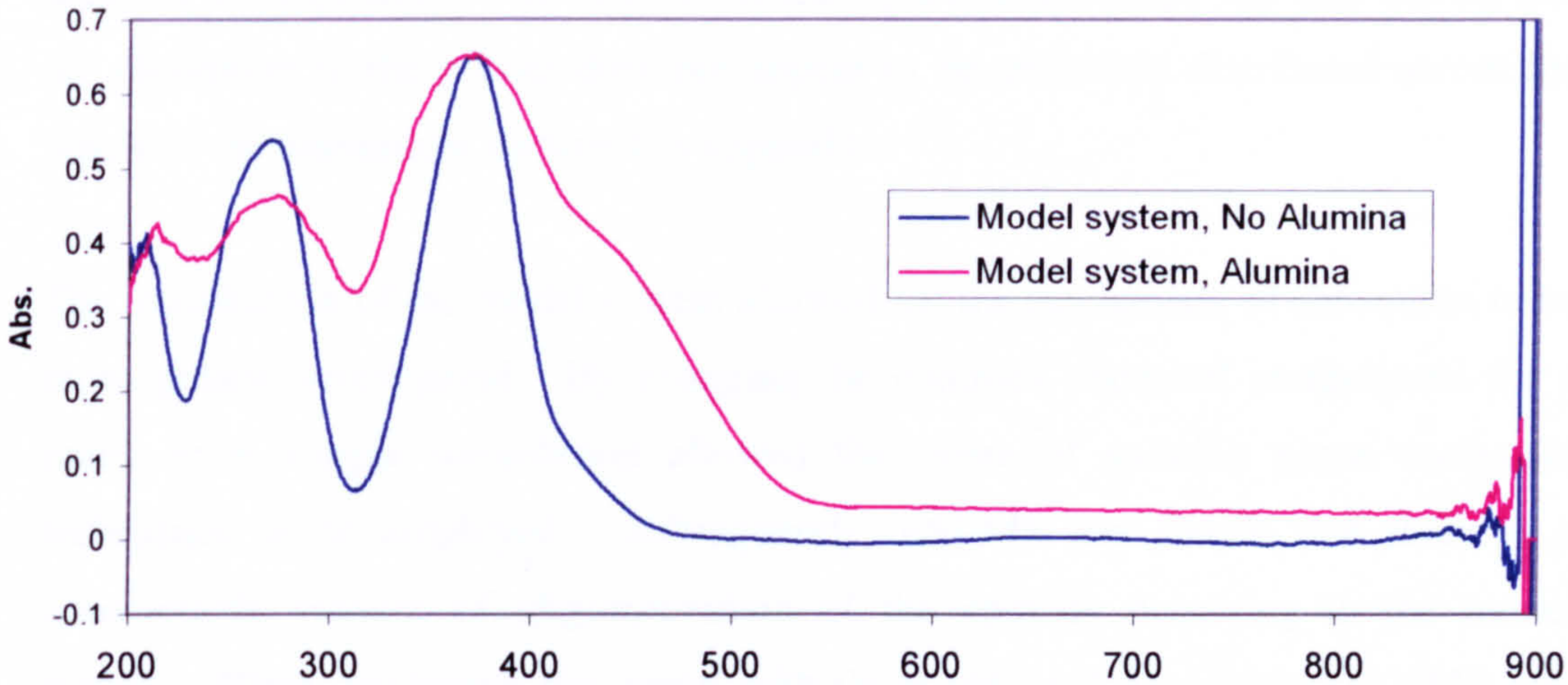


Figure 3.34. DRUV spectra showing the effect of adding alumina to the model system reaction after 6 hours at 60°C

As stated in Chapter 1, literature shows that there are silane containing systems which react to form interfaces with bonding such as Al – O – Si[21,22]. Therefore, it is

possible that in chromium primer systems there would be an interface which would contain Al – O – Cr groups.

## 3.5 Conclusions

From this series of experiments it has been possible to draw several conclusions. The most obvious of these is that it is possible to say that the industrial primer is difficult to study due to its high complexity. This has been proven by analysing the compound with several different solution phase analytical techniques and also when analysing the primer applied to an aluminium substrate.

The most successful technique for analysing the industrial primer was EDX. This was the only technique that showed chromium present and also showed that it was unlikely to be in the top most surface layers of the primer coating. This was further suggested by the absence of chromium from the XPS analysis that was carried out, although it is possible in this case that the chromium is surrounded by organic compounds which would prevent it from been observed. Additionally, the EDX analysis in conjunction with both SEM and optical microscopy has also shown that the chromium in the primer does not appear to be uniformly distributed across the whole of the aluminium surface it is applied to.

The introduction of the model system allowed for the mechanism of chromium to be more greatly investigated. By changing the complex chemical components for a much more simple formulation allowed the range of solution phase analytical techniques to be employed. Subsequently, ESI-MS has shown that there is a considerable amount of oligomerisation of the epoxide occurring in the model system. When combining this result with those obtained from both $^{13}$C-NMR and DRIFTS it appears that there are definitely new species generated from the reaction. As there are changes in both the organic and inorganic phases of the system happening concurrently, it is possible that an organochromate species has been formed. It is also probable that this new species is acting as a catalyst for the opening of the epoxide ring.

It has also been shown that there is a possible reaction between the chromate in the system and alumina when it was added as a substrate. This suggests that chromate may act in a similar fashion to silane compounds in the presence of an aluminium substrate, leading to the formation of an Al-O-Cr bonding network.

## 3.6 References


1. www.cytecengineeredmaterials.com
2. BR127$^{+}$ Corrosion Inhibiting Primer, 10% Solids, Material Safety Data Sheet.
3. Cytec Engineered Materials BR127 Primer Product Data Sheet.
4. Nouwen, R., Mullens,J., Franco, D., Yperman, J., Van. Poucke, L.C., *Vibrational Spectroscopy*, 10, 2, 291, 1996.
5. Wang, M., *Polymer,* 46, 21, 9202, 2005.
6. Royal Society of Chemistry, Infrared Spectroscopy, 2002.
7. Volland,W., *Organic Compound Identification Using IR Spectroscopy*, 1999.
8. Cytec Engineered Materials Internal Report, 2003.
9. Boerio, F.J., Hong, P.P., *Materials Science and Engineering A,* 126, 1, 245, 1990.
9. Shan, L., *Journal of Polymer Science Part B: Polymer Physics*, 37, 19, 2815, 1999.
10. Das, A. K., *Coordination Chemistry Reviews,* 248, 81, 2004.
11. Cotton, F.A., Wilkinson, G., *Advanced Inorganic Chemistry, Wiley,* 1999.
12. Mertz, W., *Physiological Reviews*, 49, 2, 163, 1969.
13. O'Hare P.A.G., Boerio, J., *The Journal of Chemical Thermodynamics,* 7, 12, 1195, 1975.
14. Petrou, A., Vrachnou-Astra, E., *Inorganica Chimica Acta,* 39, 161, 1980.
15. González, I.C., Forsyth, C.J., *Tetrahedron Letters,* 41, 3805, 2000.

16. Servi, S., Topaloglu, C., *Molecules*, 9, 22, 2004.

17. Smith, K.M., *Coordination Chemistry Reviews,* 250, 9-10, 1023, 2006.

18. Comina, P.J., Hodgson, D.M., *Tetrahedron Letters,* 15, 50, 9469, 1994.

19. Betz, P., *Organochromium π-complexes, Tetrahedron Letters*, 1991-1993.

20. Atkins, P., *Physical Chemistry*, Oxford University Press, Oxford, 7th Edition, 2001.

21. Watts, J., Abel, M-L., *Surface & Interface Analysis*, 29, 115, 2000.

22. Abel, M.-L., Allington, R.D., Digby, R.P., Porritt, N., Shaw, S.J., Watts, J.F. *International Journal of Adhesion & Adhesives*, 26, 2, 2006.

23. van Ooij, W.J., *Tsinghua Science & Technology*, 10, 6, 639, 2005.

# Chapter 4

# Further model system

## 4.1 Introduction

After promising results from the initial work carried out on the model system (see Chapter 3), it was decided to extend this area of study. A series of experiments was designed which would investigate the effects of different chromates and their reactions with various epoxides.

The chromates investigated were; sodium chromate, potassium chromate and lithium chromate, all being readily available, inexpensive, and not containing a strongly associating cation.

The epoxides investigated were cyclohexene oxide, styrene oxide and 1,2-epoxypentane (figure 4.01).

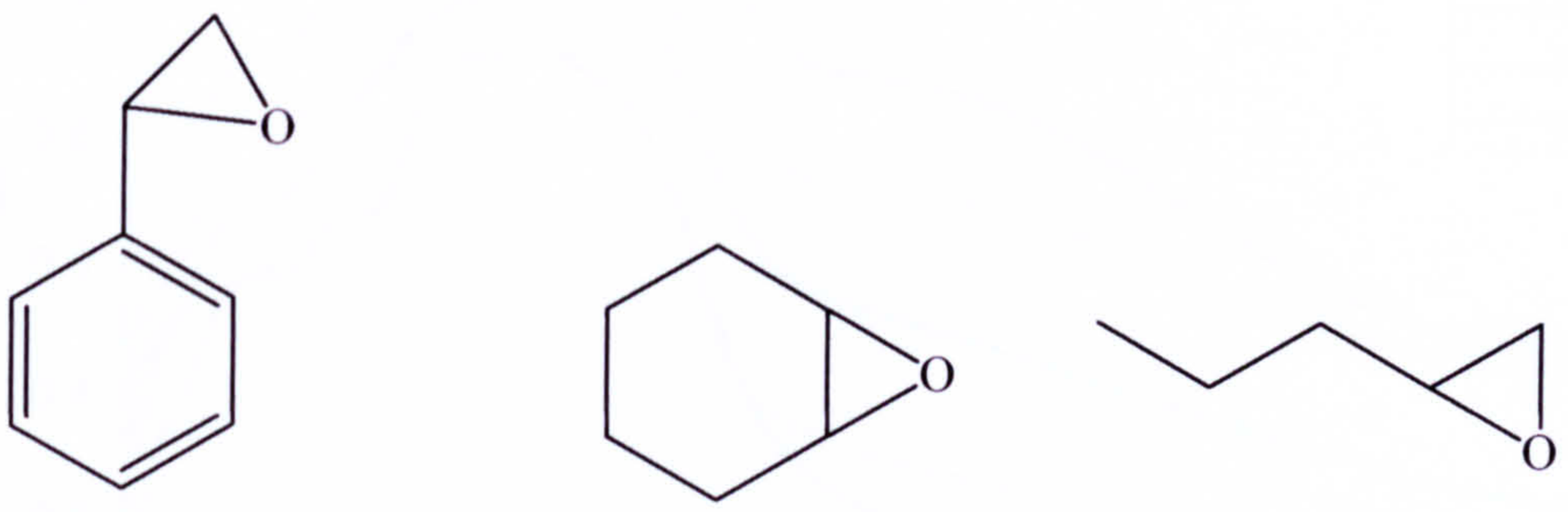


Styrene oxide Cyclohexene oxide 1,2-Epoxypentane

Figure 4.01. Structures of epoxides used in model system

It was thought that these epoxides would give a good balance to the investigation (one cyclic, one aromatic, one aliphatic) whilst remaining similar in structure to the complex epoxy resins used in the industrial system.

In addition to this primary investigation, the effects of time, temperature and chromate concentration were also investigated.

In keeping with the findings from the initial model compound work, the analytical techniques employed remained the same but the focus was more driven towards DRUV and ESI-MS, which proved to be informative in terms of observing changes on interaction with epoxies.

## 4.2 DRUV Analysis

The first number of reactions carried out under reflux at 60°C for 6 hours and subsequently analysed by DRUV were between cyclohexene oxide and sodium chromate (figure 4.02).

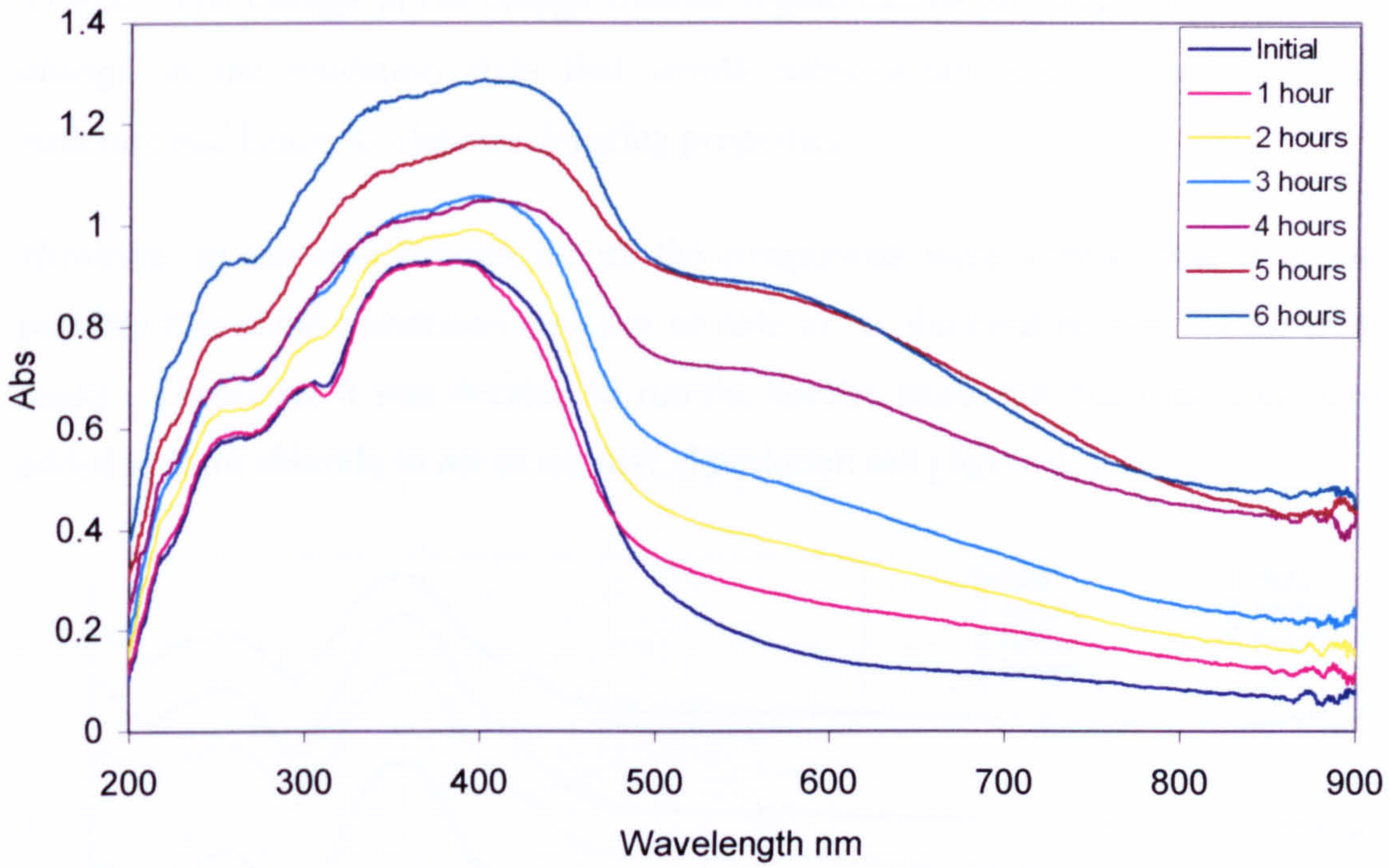


Figure 4.02. DRUV spectrum showing changes in the reaction between cyclohexene oxide and $Na_2CrO_4$ over a 6 hour period at 60°C

In analysing the spectrum for the initial run (Time=0), the dark blue line, it appears that there are 5 peaks in the 200-500nm range. The first peak is at 215nm, the second and 245nm, the third at 295nm, the fourth at 340nm and the fifth at 410nm. As stated before these peaks must all be due to charge transfer transitions and they are all in the correct energy range[1]; however, as stated in the literature, charge transfer transitions tend to be unique to the compounds under investigation so are

difficult to assign, although peaks at 250nm, 360nm and 480nm have been shown to be due to charge transfer transitions between $O^{2-}$ and the $Cr^{6+}$ of the tetrahedral chromate group[2,3].

Figure 4.02 also shows that there are changes occurring in the DRUV over time. At approximately 575nm there is a substantial new peak forming that, because it is at lower energy, is less likely to be due to a charge transfer transition. This means that there is a possible change in the oxidation state of the chromium which would allow a d-d transition to be possible. There are also significant changes in the charge transfer region where after 6 hours it appears that there are only 4 peaks present; the first peak at 220nm, the second at 250nm, the third at 340nm and the fourth at 415nm. The change in the charge transfer region can be attributed to the probable change in the oxidation state that would subsequently change the chromate's structure and hence its electron donating properties.

However, as the absorbencies for all the compounds were very intense it seemed possible that some transitions may not be able to be observed because of the broad peaks. Therefore, it was decided to run the spectra again but this time with some added sodium chloride to act as an inert, dissolution salt (figure 4.03).

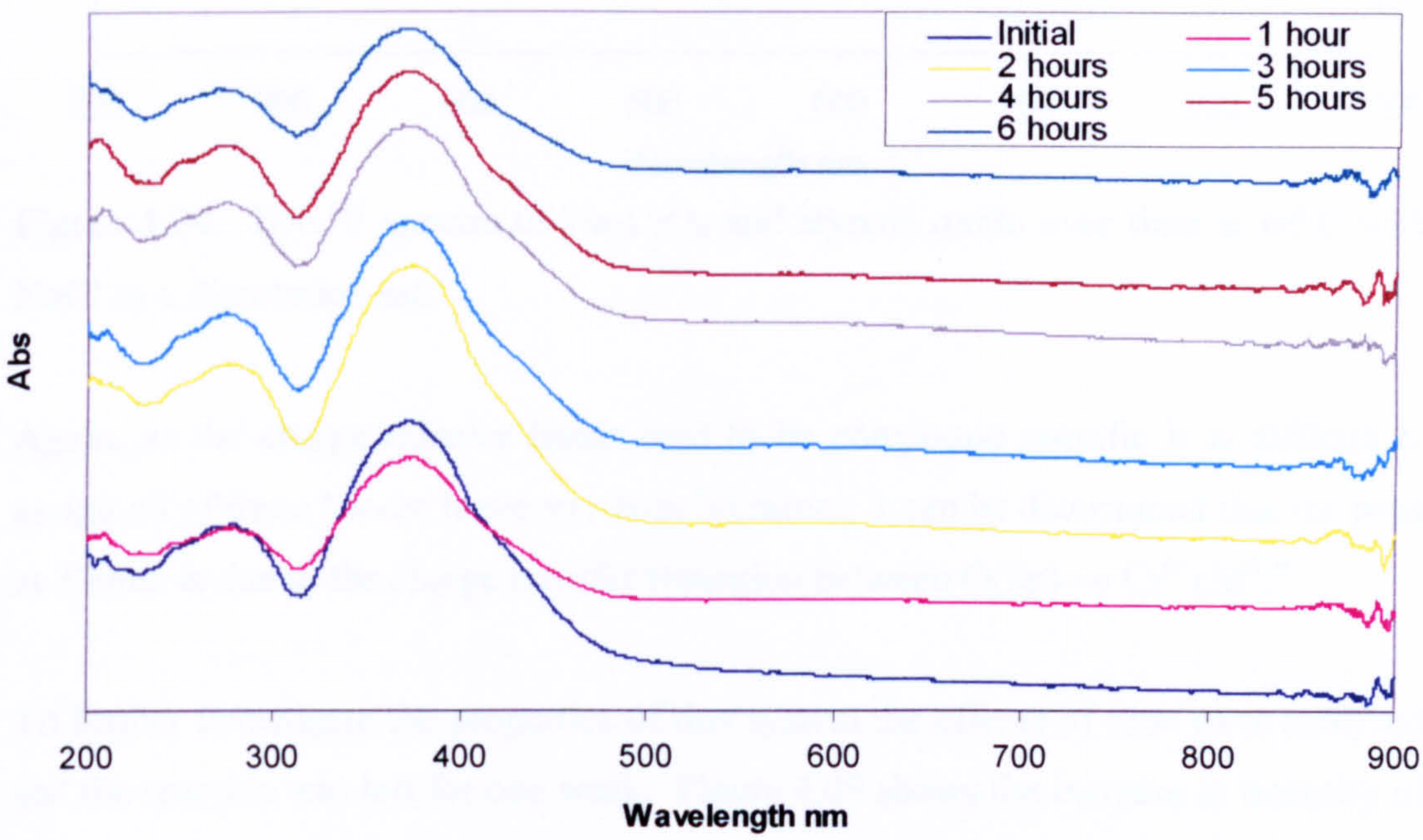


Figure 4.03. DRUV spectra showing the effect of adding NaCl to act as an inert, dissolution salt

It is evident that the addition of the dissolution salt makes the spectra clearer. However, the new peak that appeared in figure 4.02 at approximately 575nm is not present any more. This suggests that whatever this peak is due to is in very low concentration or has a very low extinction coefficient.

When using a different system, sodium chromate with styrene oxide, similar spectra were obtained showing peaks in the charge-transfer energy region but also new peak formation at 575nm was observed (figure 4.04).

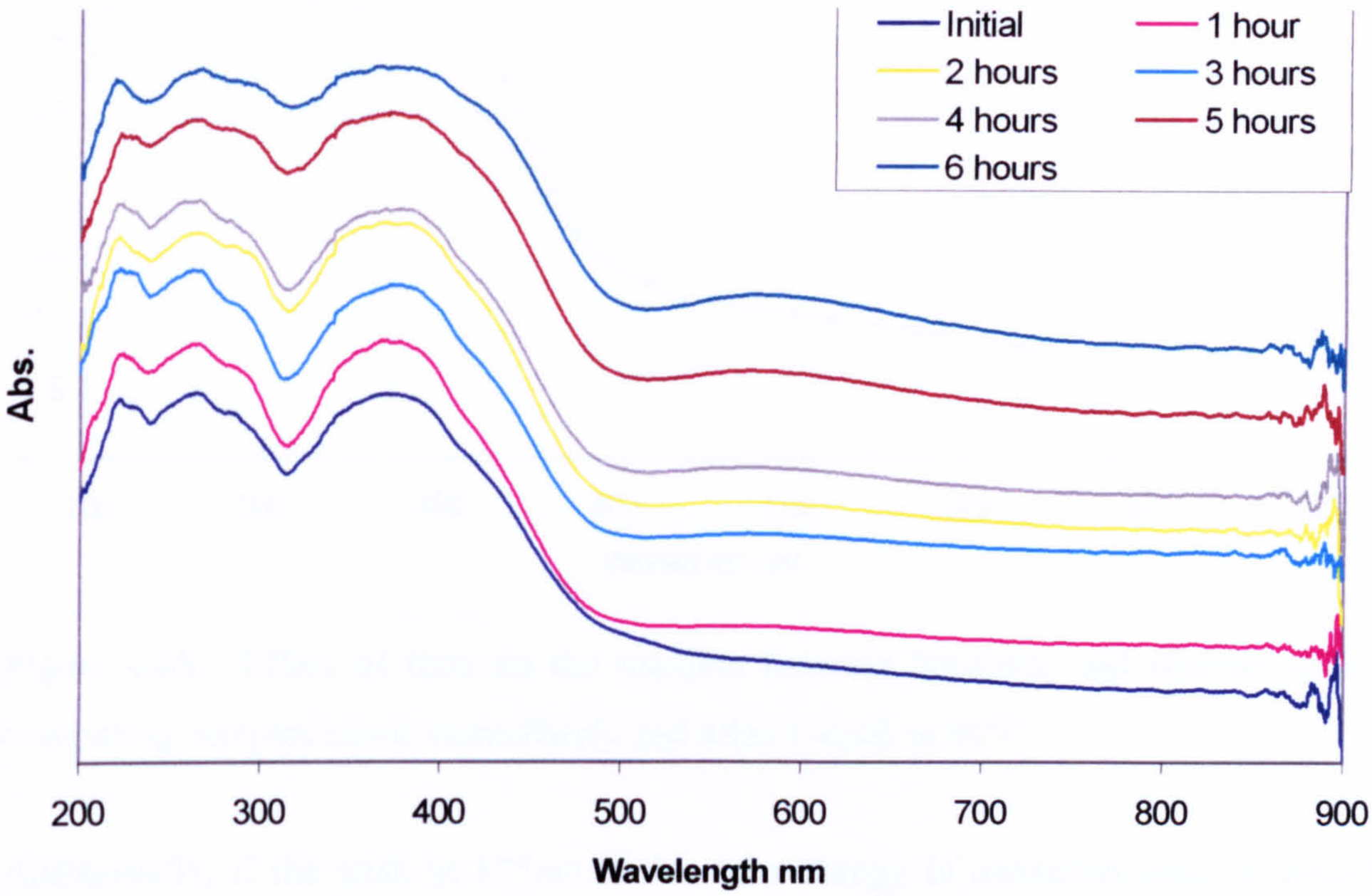


Figure 4.04. DRUV spectra of $Na_2CrO_4$ and styrene oxide over time at 60°C with NaCl as a dissolution salt

Again, as the charge transfer bands tend to be compound specific it is difficult to assign all of these bands; however, from literature, it can be determined that the peak at 370nm is due to the charge transfer transition between $O(2p) \rightarrow Cr^{6+}(3d^0)^4$.

To further investigate the properties of this system the effects of time were analysed and the reaction was left for one week. Figure 4.05 shows the increase in intensity of the peak at 575nm and also a large change in the charge-transfer area. The decrease in intensity of the peak at 370nm suggests that the compound undergoes fewer O(2p)

$\rightarrow Cr^{6+}(3d^0)$ charge transfer transitions. A simple explanation for this would be that the complex has a lower concentration of chromium VI as a result of a redox reaction, which suggests that the peak at 575nm could be due to a d-d transfer.

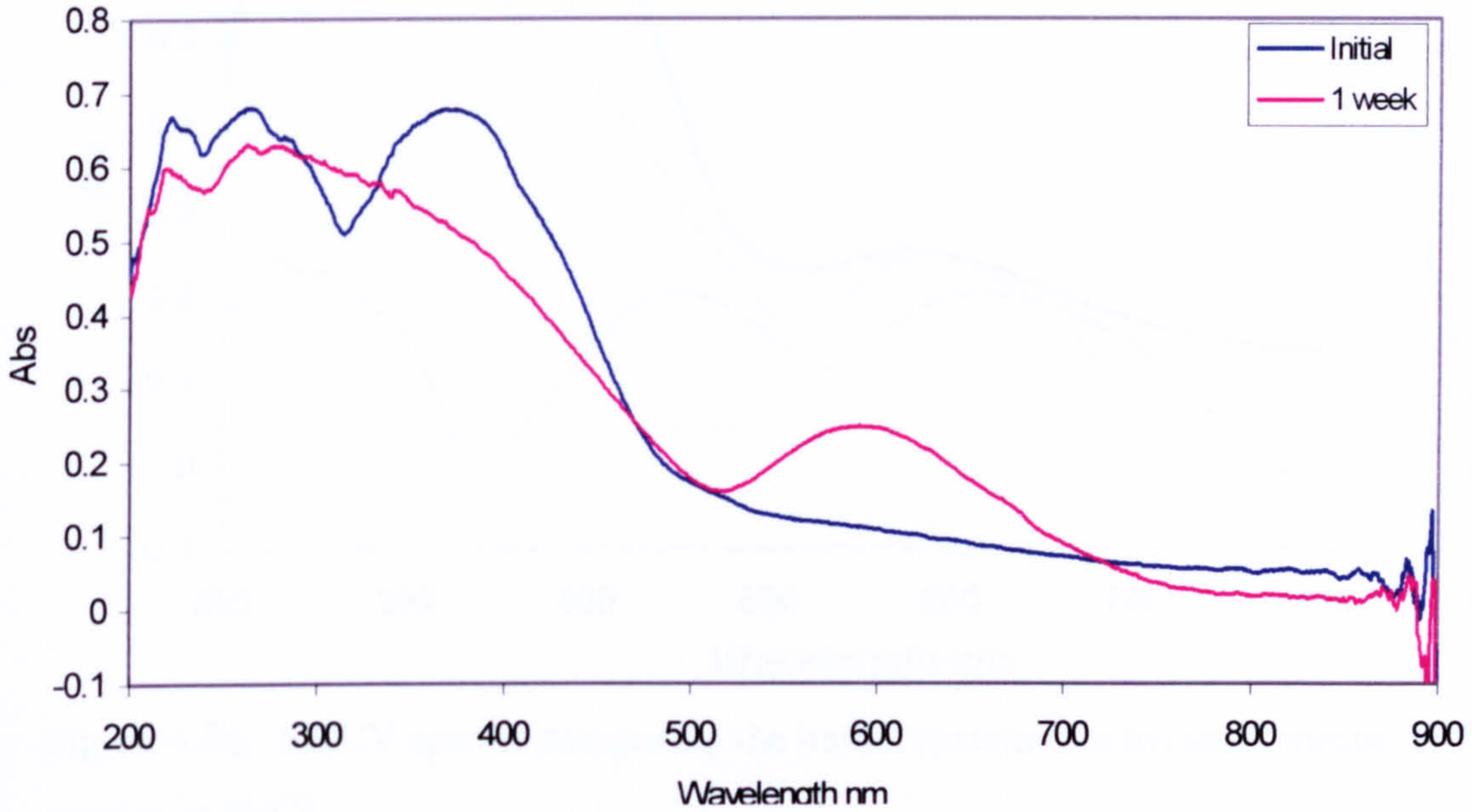


Figure 4.05. Effect of time on the reaction between $Na_2CrO_4$ and styrene oxide, comparing samples taken immediately and after 1 week at 60°C

Additionally, if the peak at 575nm is due to a change in oxidation state, it would mean that the ligand environments around the chromate would change and this may alter the position and intensities of the charge-transfer transitions.

To investigate the possibility that a redox reaction had occurred, a simple comparison can be made by looking at the DRUV spectra of the model system and that of a trivalent species of chromium. Figure 4.06 shows the spectrum of chromium (III) chloride with NaCl added as a dissolution salt. The spectrum illustrates some charge transfer activity and two major peaks at 440nm and 610nm that are characteristic of trivalent chromium in an octahedral coordination[5]. Although the 610nm peak is in the vicinity to that of the model system at 575nm it is not exactly the same. This could be due to a difference in ligand environment or it could be due to the fact the

chromium has not been reduced all the way down to the trivalent species and is instead in an oxidation state of either IV or V.

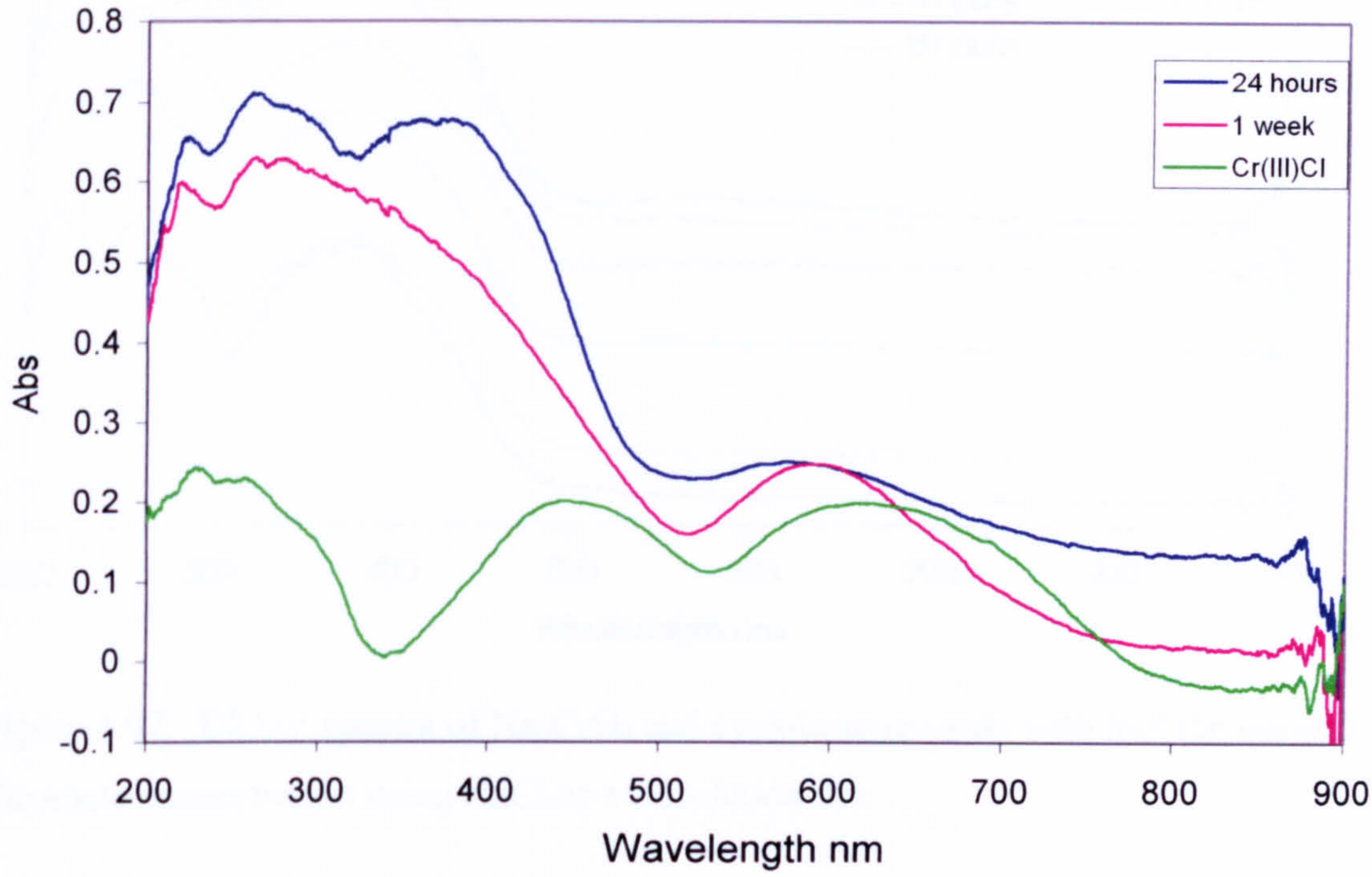


Figure 4.06. DRUV spectra comparing the model system to a trivalent chromium III species in NaCl

Literature states that some chromium III complexes do possess peaks at around 570nm[6] and $Cr(H_2O)_6$ shows a peak at exactly 575nm; however; it is still possible that a rarer chromium IV or V species has been formed. Although much less common than hexavalent and trivalent species, both chromium IV and chromium V have been studied[7,8]. However, this has been done more from a biochemistry perspective rather than purely chemistry orientated as these species are important in the mutagenic mechanism of chromium reduction in the human body[9]. Further experimentation illustrated that chromate concentration also had an impact on the peak at 575nm. Figure 4.07 shows that by halving the amount of chromate in the reaction, the peak is still present but it is of much lower intensity. This suggests that this peak is almost certainly due to the chromate and not because of other changes to the organic species present.

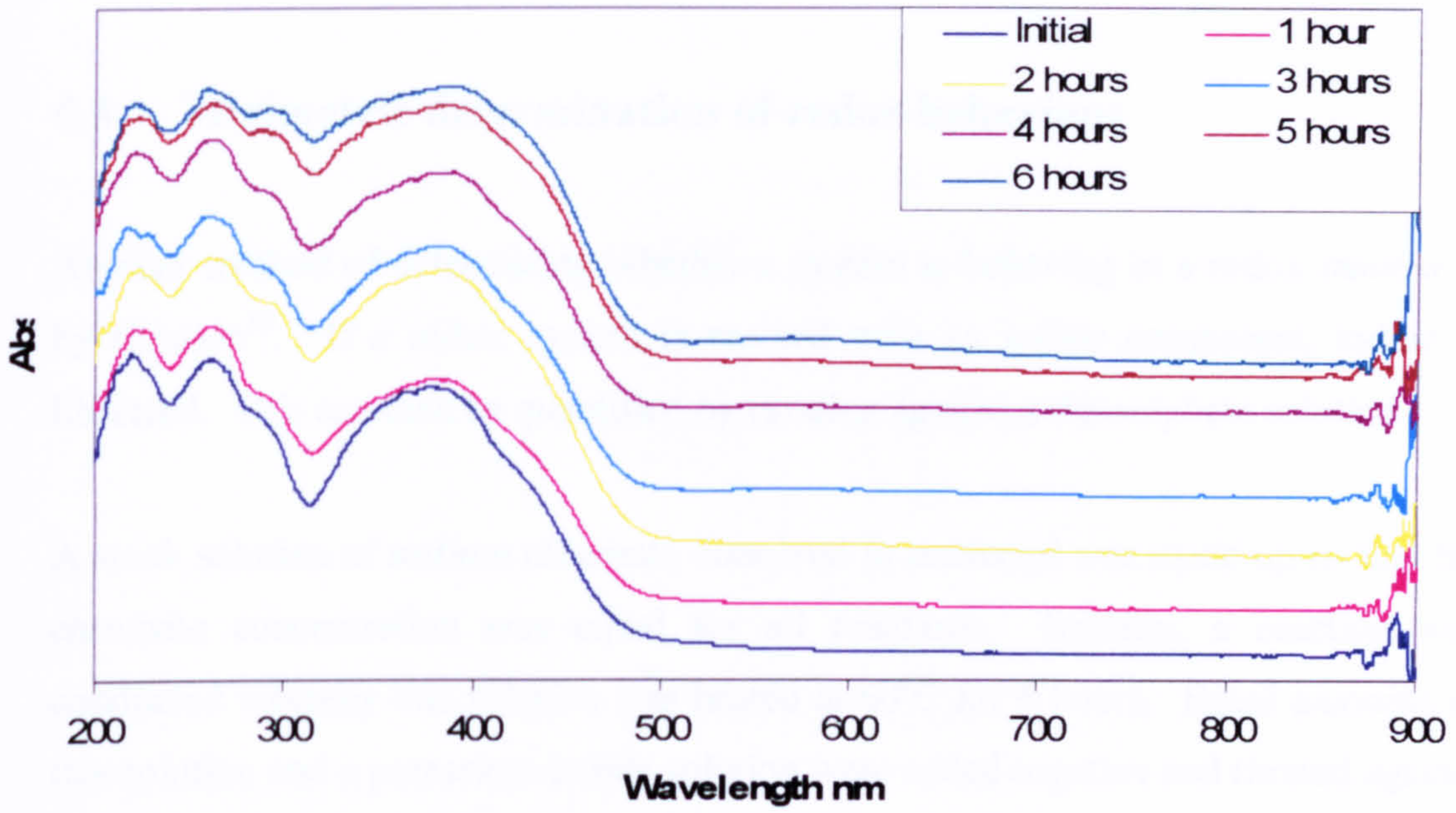


Figure 4.07. DRUV spectra of $Na_2CrO_4$ and cyclohexene oxide with half the normal chromate concentration using NaCl as a dissolution salt

Similar results have also been generated with the two other chromates, potassium and lithium. However, the effects of these are slower in the formation of the new peak than sodium, suggesting that the cation has some influence on the chemistry taking place (figure 4.08), although relative solubilities might also be relevant.

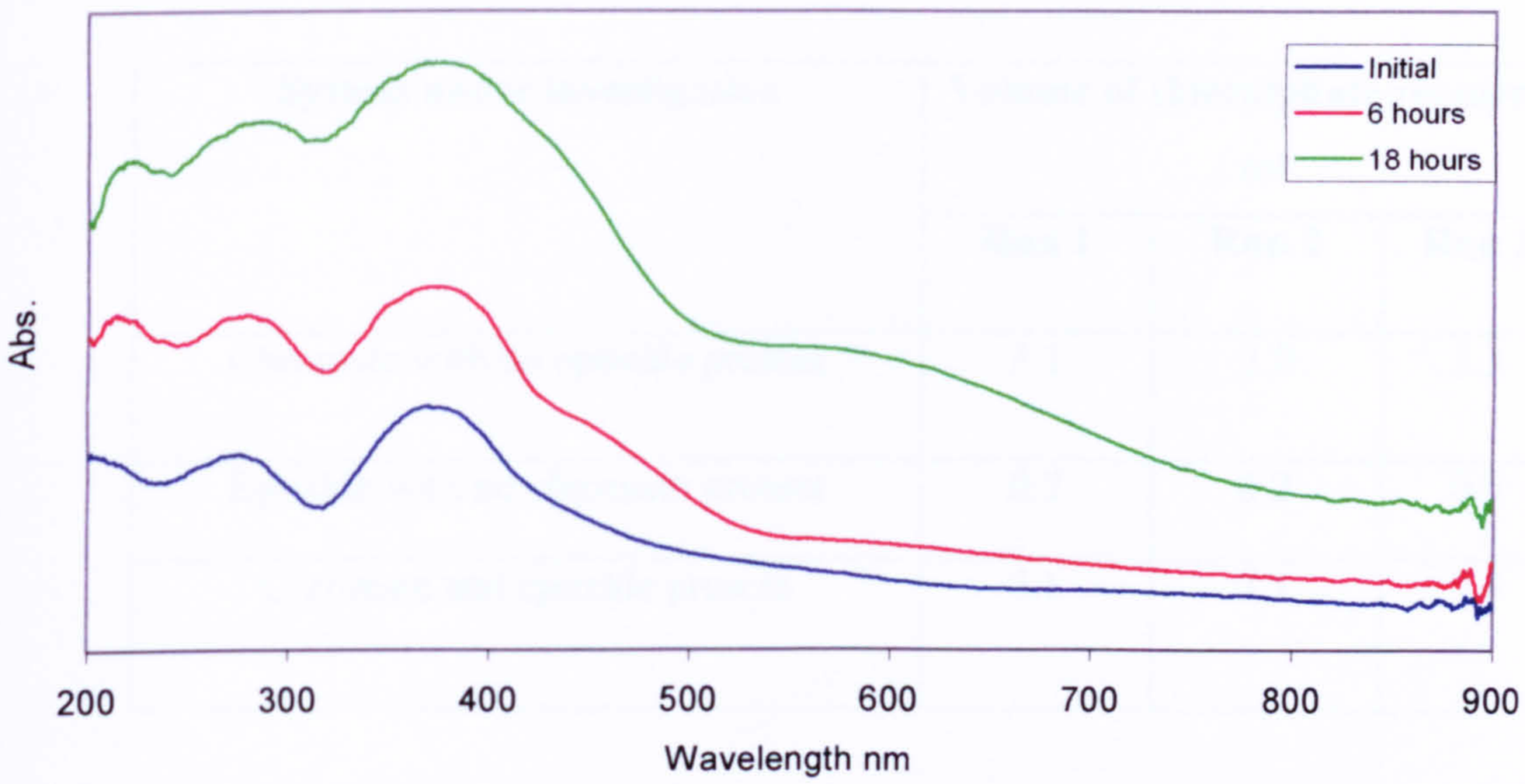


Figure 4.08. DRUV spectra for the reaction between $Li_2CrO_4$ and cyclohexene using NaCl as a dissolution salt

## 4.3 Titrimetric determination of redox behaviour

Another method of determining whether a system is behaving in a redox manner is by titration[10]. If a redox system is reacted with an iodide compound, iodine is liberated. This can then be quantified by titrating against a thiosulphate solution

A stock solution of sodium chromate dissolved in methanol was made up so that the chromate concentration was equal for all reactions. Initially, a reaction was conducted whereby this solution was heated at 60°C for 6 hours. Equal amounts of this solution and a potassium iodide solution were added together and titrated against sodium thiosulphate. HCl was added to give acidic conditions (otherwise there is a reaction of the liberated iodine into unstable hyperiodite[11]) and a starch based indicator used to monitor the end point of the titration (blue to colourless). Following this, a similar reaction was conducted using the same chromate / methanol solution, but this time an excess of cyclohexene oxide was introduced. An experiment in the absence of chromate was also carried out to show that no redox reaction occurred when chromium was absent. The results of the titration can be seen in figure 4.09.

| **System under investigation** | **Volume of thiosulphate required / ml** | | |
|---|---|---|---|
| | **Run 1** | **Run 2** | **Run 3** |
| Chromate with no epoxide present | 3.1 | 3.0 | 3.3 |
| Epoxide with no chromate present | 0.2 | 0.2 | 0.3 |
| Chromate and epoxide present | 7.1 | 7.1 | 7.4 |

Figure 4.09. Table showing the results of the redox titrations

As can be seen from the results in figure 4.09 there is a significant difference in the volume of thiosulphate required when the epoxide is present. The most probable explanation for this is that, as earlier hypothesised, the chromate is oxidising the epoxide into an alcohol or ketone species and therefore reducing its own oxidation state from chromium VI.

## 4.4 ESI-MS Analysis

Similarly to DRUV, initial work concentrated on the sodium chromate and cyclohexene oxide reaction (figure 4.10).

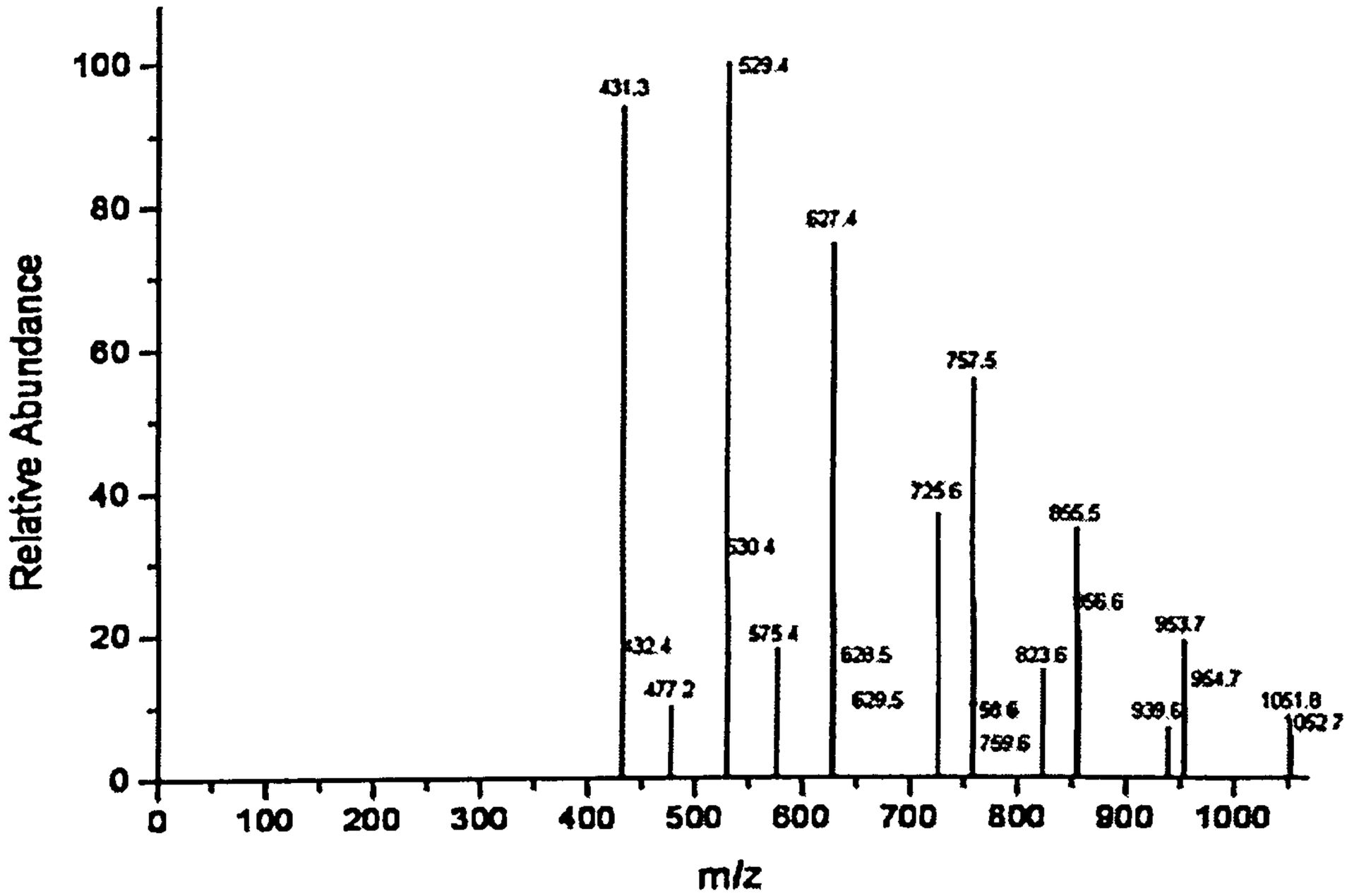


Figure 4.10. ESI-MS of the reaction between $Na_2CrO_4$ and cyclohexene oxide at 60°C after 6 hours

The spectrum shows two major series of peaks. Both of these series have characteristic fragmentation patterns with recurring losses of 98, corresponding to the mass of the cyclohexene oxide (see figure 3.25). This illustrates that it is likely that

the reaction is initiating oligomer formation. If this is the case it is probable that the chromate ion is acting as a Lewis acid to catalyse the epoxide ring opening, possibly leading to the formation of an organochromate species (figure 4.11).

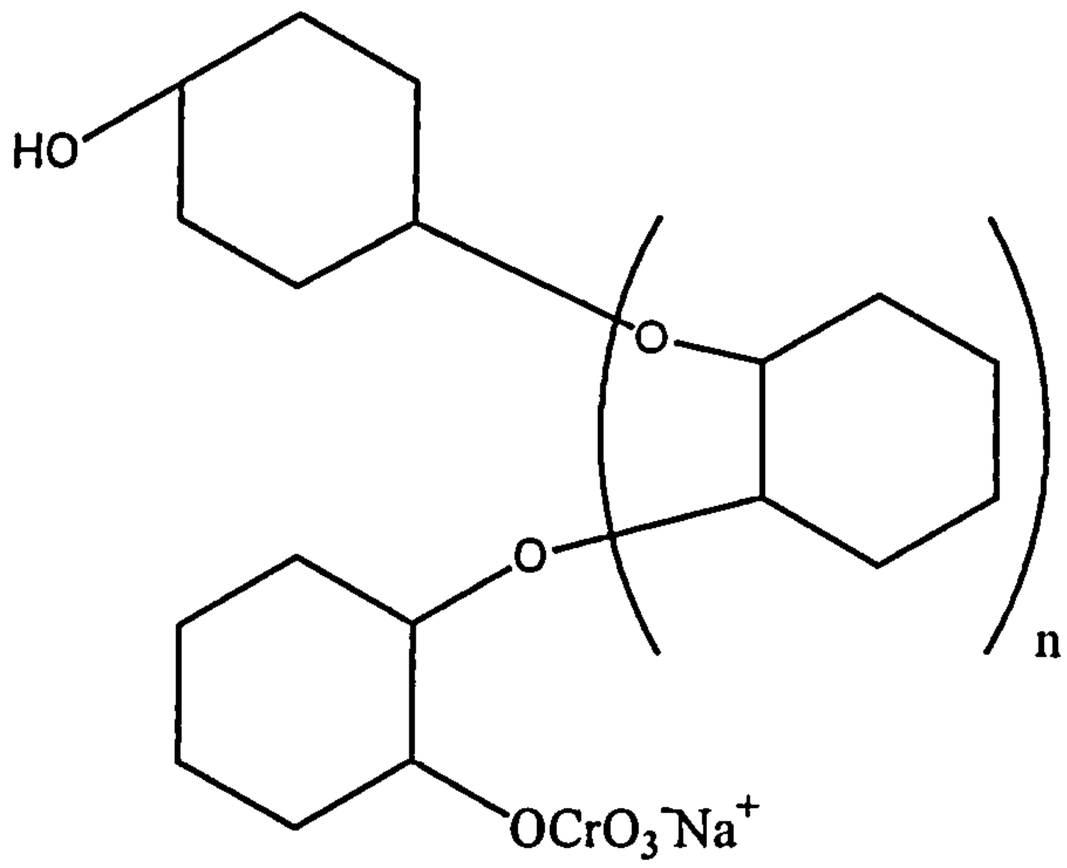


Figure 4.11. Structure of possible organochromate species

However, unlike the results obtained from the initial model system, figure 4.10 does not show a mass loss of 15m/z from 838 to 823. Instead of this suggested methyl end capping we see a completely new second series starting at 757m/z (32m/z higher than the peak at 725m/z) with increases of 98 up to 1051m/z. It is probable that this increase of 32m/z is due to either; oxidation of the cyclohexane ring or there is some complexation with methanol occurring.

A similar reaction was conducted using styrene oxide in place of cyclohexene oxide (figure 4.12). As can be seen from the spectrum, the second series present in figure 4.11 that shows an increase of 32m/z is not observed in this system. This is probably due to the styrene oxide been more readily prone to oligomerise compared to the cyclohexene oxide. Any oxidised products would be present in low concentrations which would not necessarily be easily observed using ESI-MS.

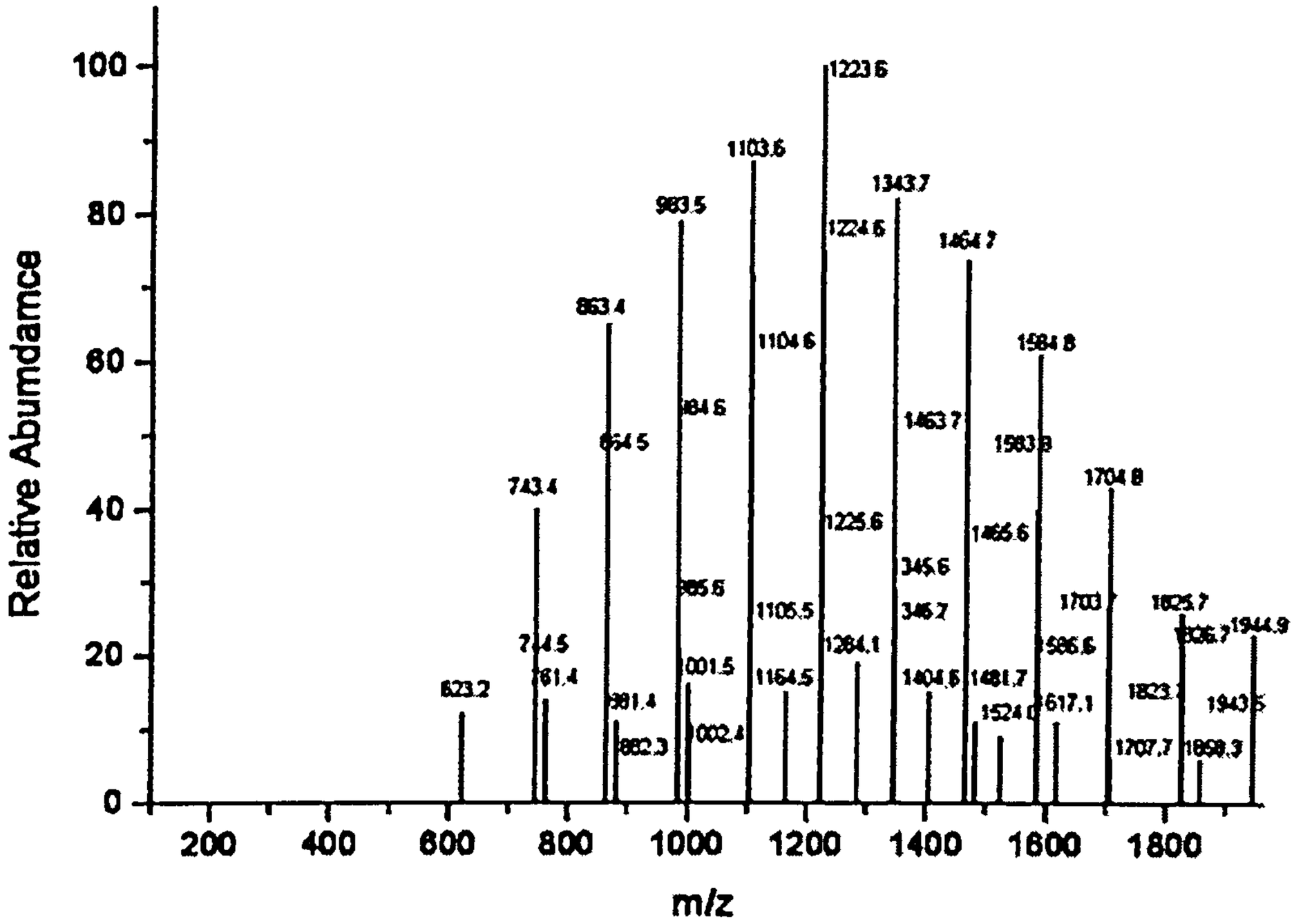


Figure 4.12. ESI-MS spectrum for the reaction between sodium chromate and styrene oxide

### *4.4.1 Liquid chromatography mass spectrometry(LC-MS) analysis*

To investigate the possibility of an oxidation reaction occurring, a further mass spectrometry technique was employed. ICI's Measurement Science Group was employed to use Liquid Chromatography - Mass Spectrometry (LC-MS)[12,13] to observe the reactions between both sodium chromate with cyclohexene oxide and sodium chromate with styrene oxide.

For the reaction involving the styrene oxide, the LC-MS data suggests that there are four distinct series of oligomers present (Figure 4.13 series A – D). It can be observed from these structures that there is one oxidised species (structure C) present; however, the other compounds are primarily based on the oligomerisation

theme. This explains why there is no second series in the sodium chromate-styrene oxide ESI-MS spectrum.

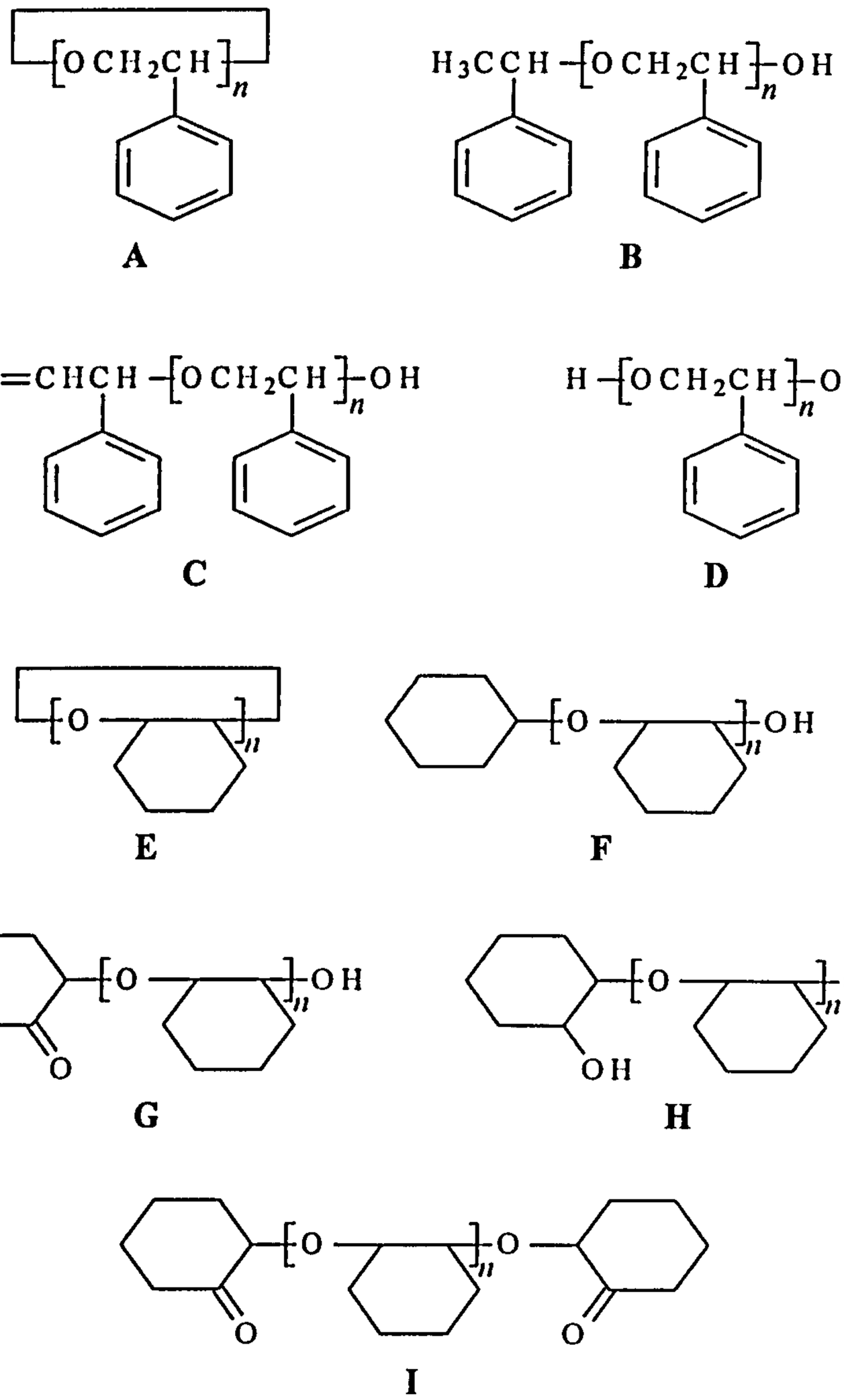


Figure 4.13. Structures of major oligomers formed in the reactions between sodium chromate with styrene oxide and sodium chromate with cyclohexene oxide

When observing the cyclohexene oxide reaction, the LC-MS data suggests that these samples contain nine different oligomeric series. The structures of five of these series are shown in figure 4.13 (Series E – I). In addition to these, Series J (oligomer molecular weight is 32Da higher than that of the equivalent Series E oligomer) and

Series K (oligomer molecular weight is 48Da higher than that of the equivalent Series E oligomer) could be oxidised forms of Series G.

The confirmation of the presence of oxidised species in both systems corresponds suitably with the results from the DRUV analysis which showed a reduction in the chromium's oxidation state. Combining the two results illustrates that there is a redox reaction occurring.

### *4.4.2 Further ESI-MS analysis*

By using different chromate species in the model system, it is clear that there is only one cation in the structures that the signals are due to. Figure 4.14 shows that with the reaction of potassium chromate there is a series of peaks beginning 16 m/z higher than that for sodium. (The series of peaks from 431m/z is still present due to some residual sodium model system in the spectrometer.)

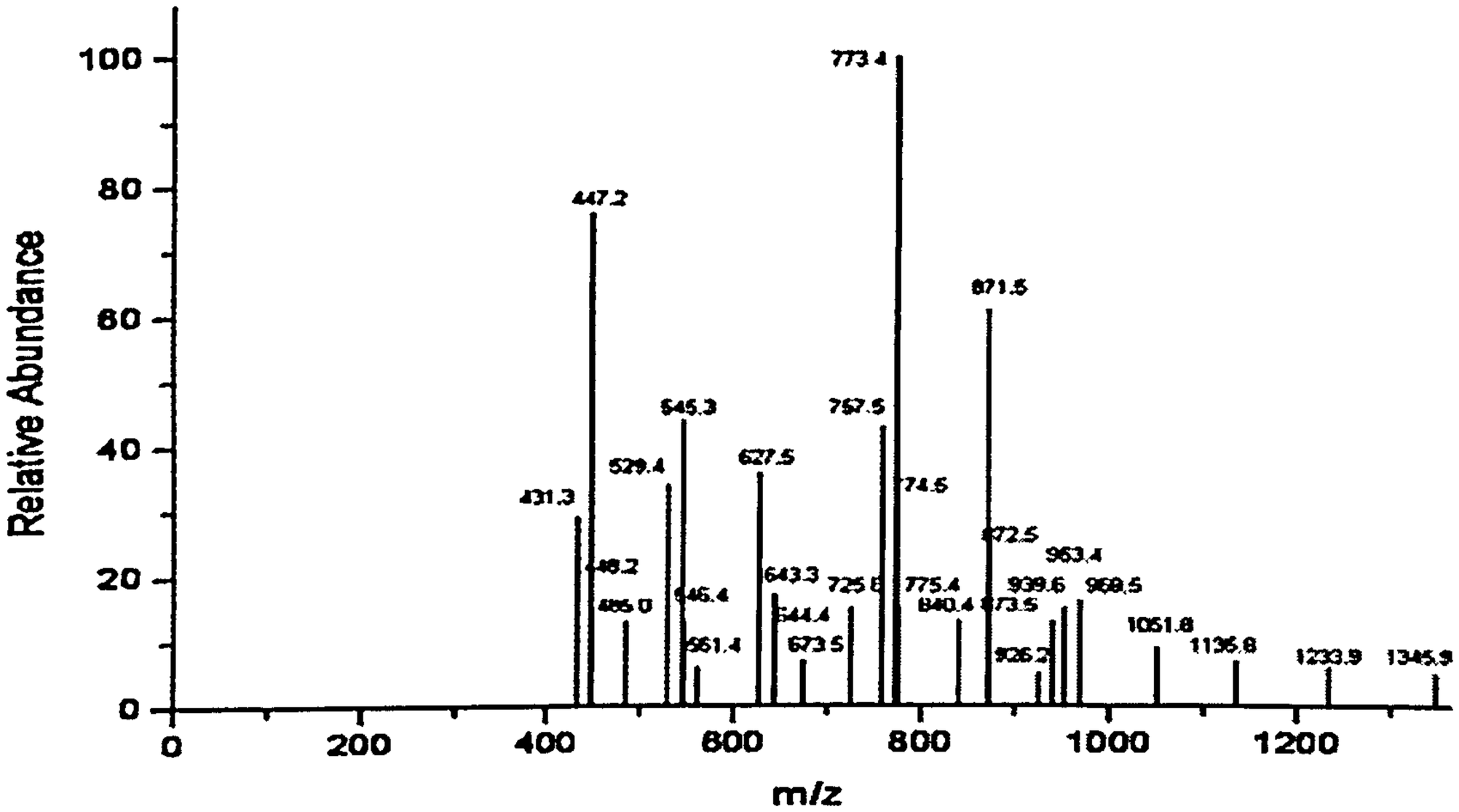


Figure 4.14. ESI-MS after reaction between $K_2CrO_4$ and cyclohexene oxide after 6 hours at 60°C

Similarly, figure 4.15 shows the comparable effect of using lithium where the series of peaks begins at 415 m/z.

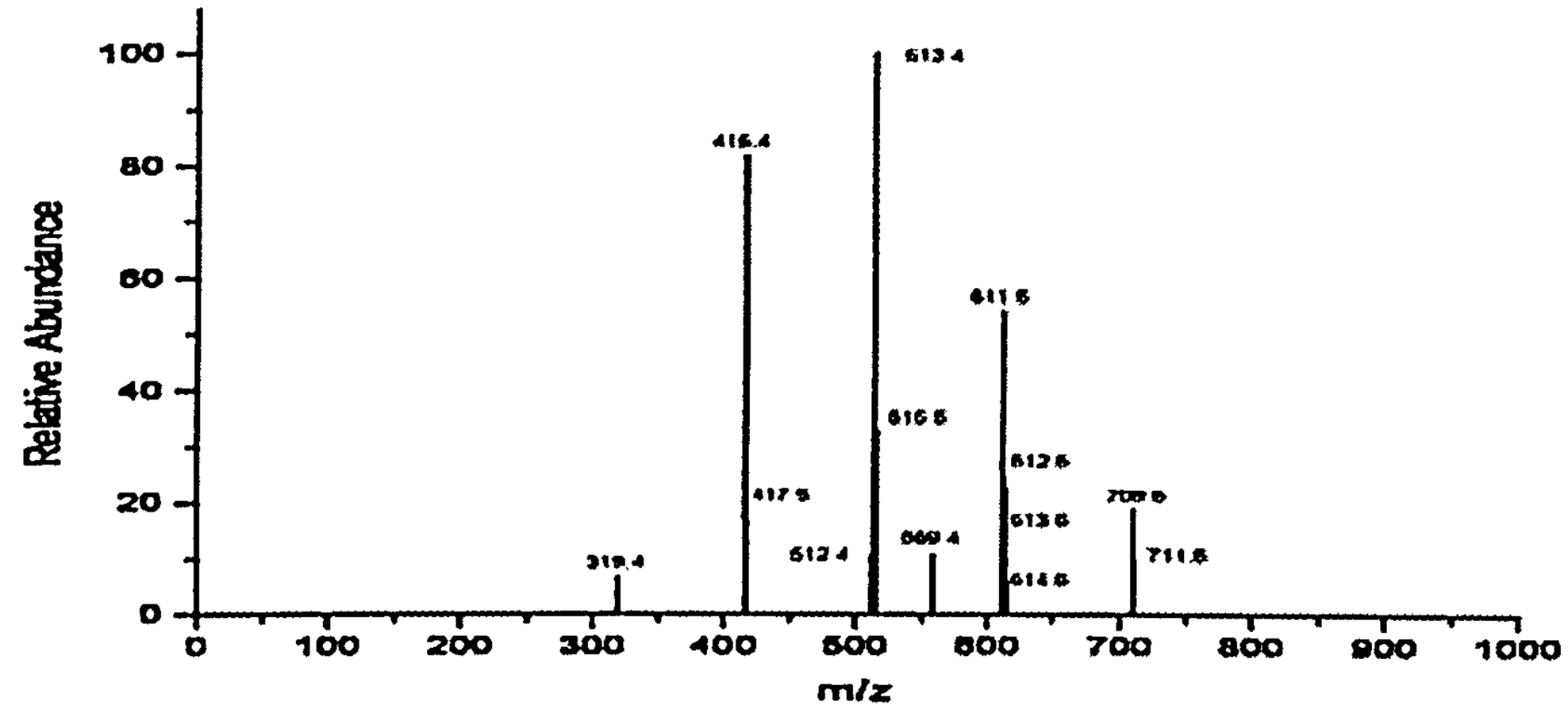


Figure 4.15. ESI-MS showing the effect of using $Li_2CrO_4$ in the model system after 6 hours at 60°C

There appears to be much fewer species formed in the reaction when lithium chromate is used, suggesting that it is a weaker Lewis acid catalyst than either the sodium or potassium based chemicals. Its lower reactivity cannot be due to the relative solubilities of the compounds as the potassium chromate is the least soluble of the three.

When investigating the effect of time on the model system, a completely new series of peaks is visible (figure 4.16).

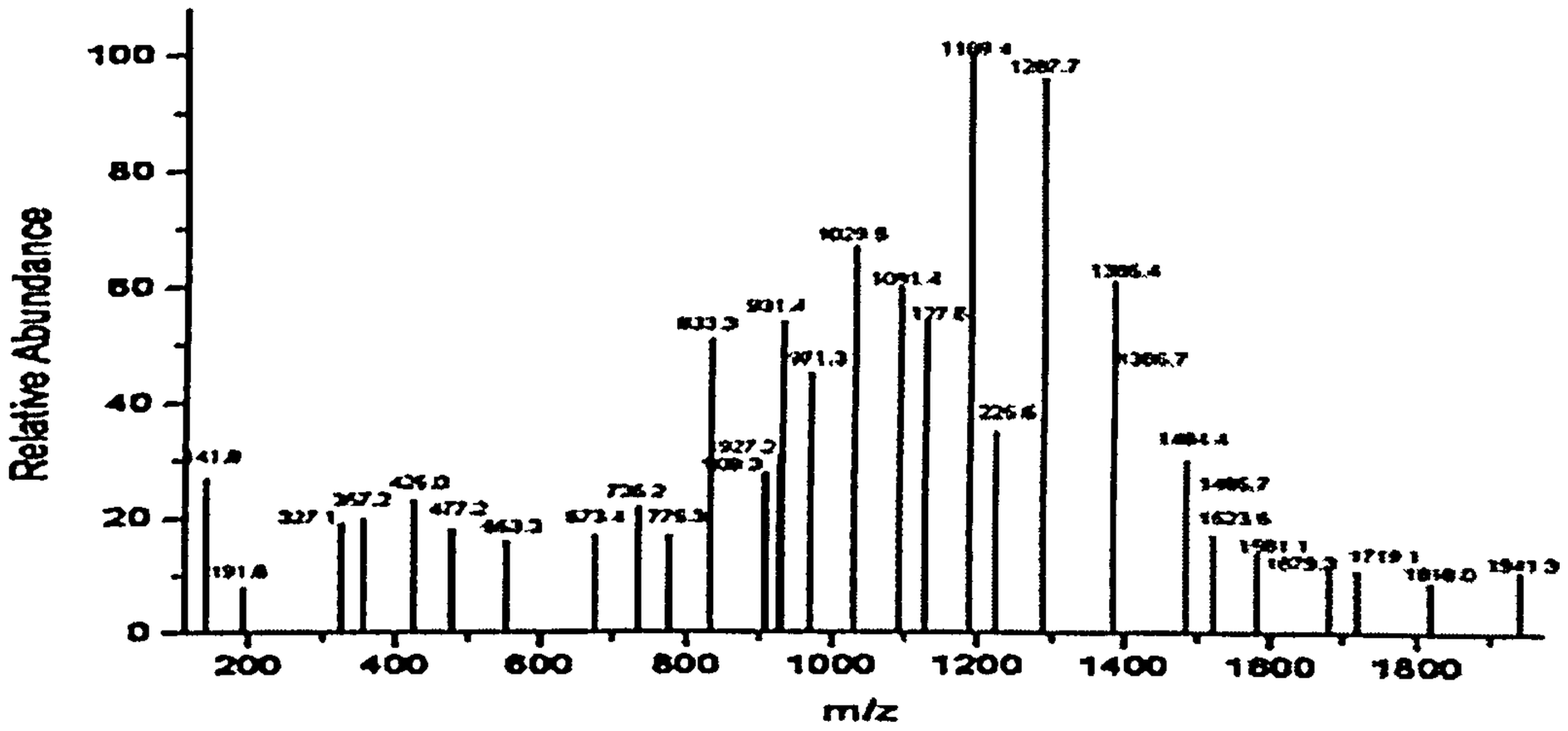


Figure 4.16. ESI-MS of $Na_2CrO_4$ model system after refluxing for 1 week at 60°C

This agrees with the work carried out using DRUV spectroscopy in that there are large changes in both spectra (i.e. changes in the charge-transfer region in the DRUV spectrum). There are also similarities to figure 4.10 in that there are losses of 98m/z but the peaks are at higher values. This is often seen in polymerisation reactions where the polymer chain length (and therefore molecular weight) increases with time[14]. Changes in the chain length would alter the ligand field environment causing differences in DRUV so the two sets of results concur.

However, when looking at the effect of temperature on the system, results from the two techniques differ greatly. Where DRUV showed that there was no reaction at low temperature, ESI-MS shows that the same structures are present in solution (figure 4.17).

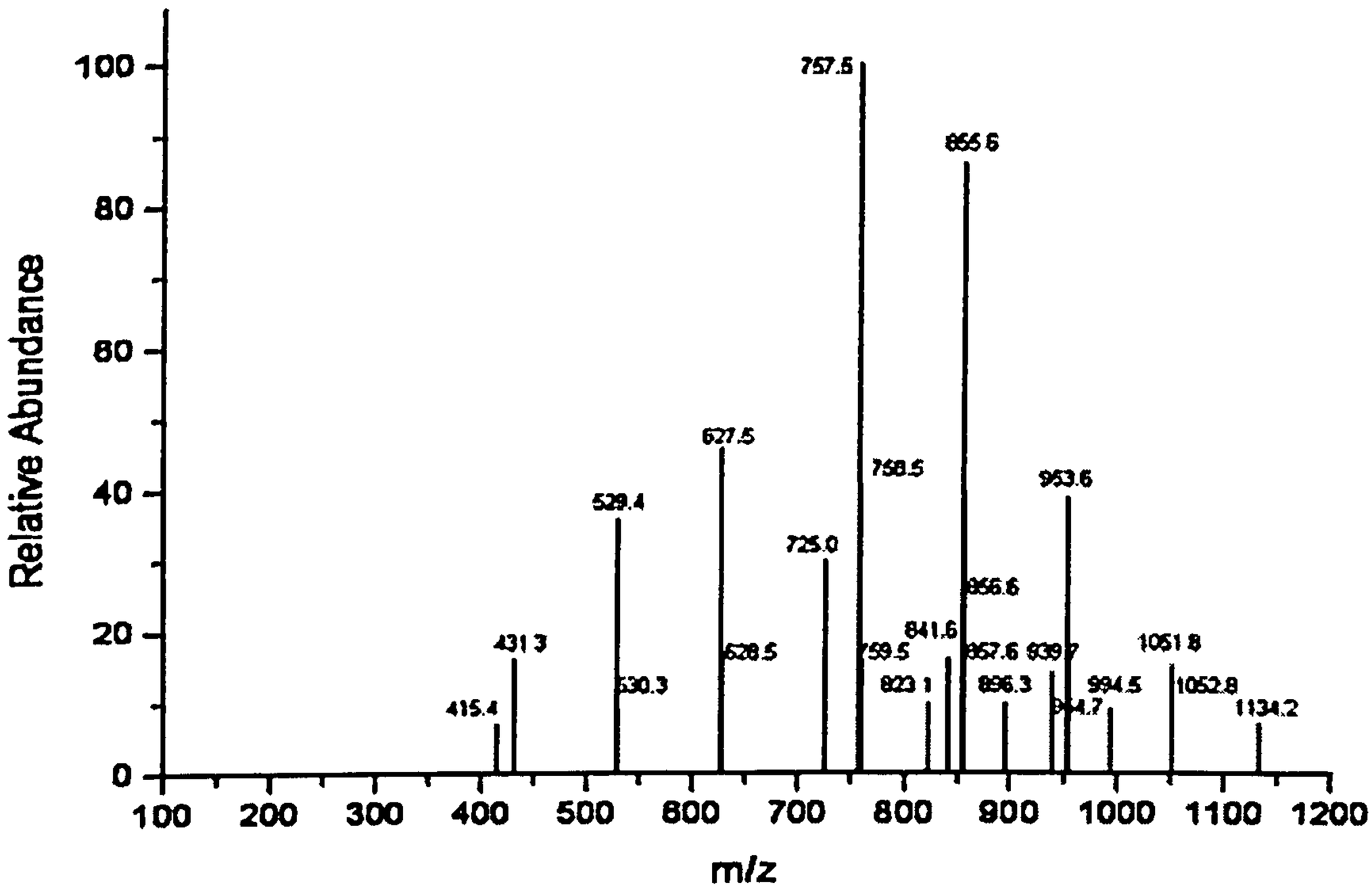


Figure 4.17. ESI-MS at 30°C showing the effect of temperature on the model system

Due to the increased sensitivity of ESI-MS over DRUV it could be possible that these compounds are in such low concentration that they do not appear to be present in the DRUV spectra.

Similar results were obtained when looking at the effect of chromate concentration. Again, half the normal chromate concentration was used but this time the same results occurred as for the usual concentration (figure 4.18).

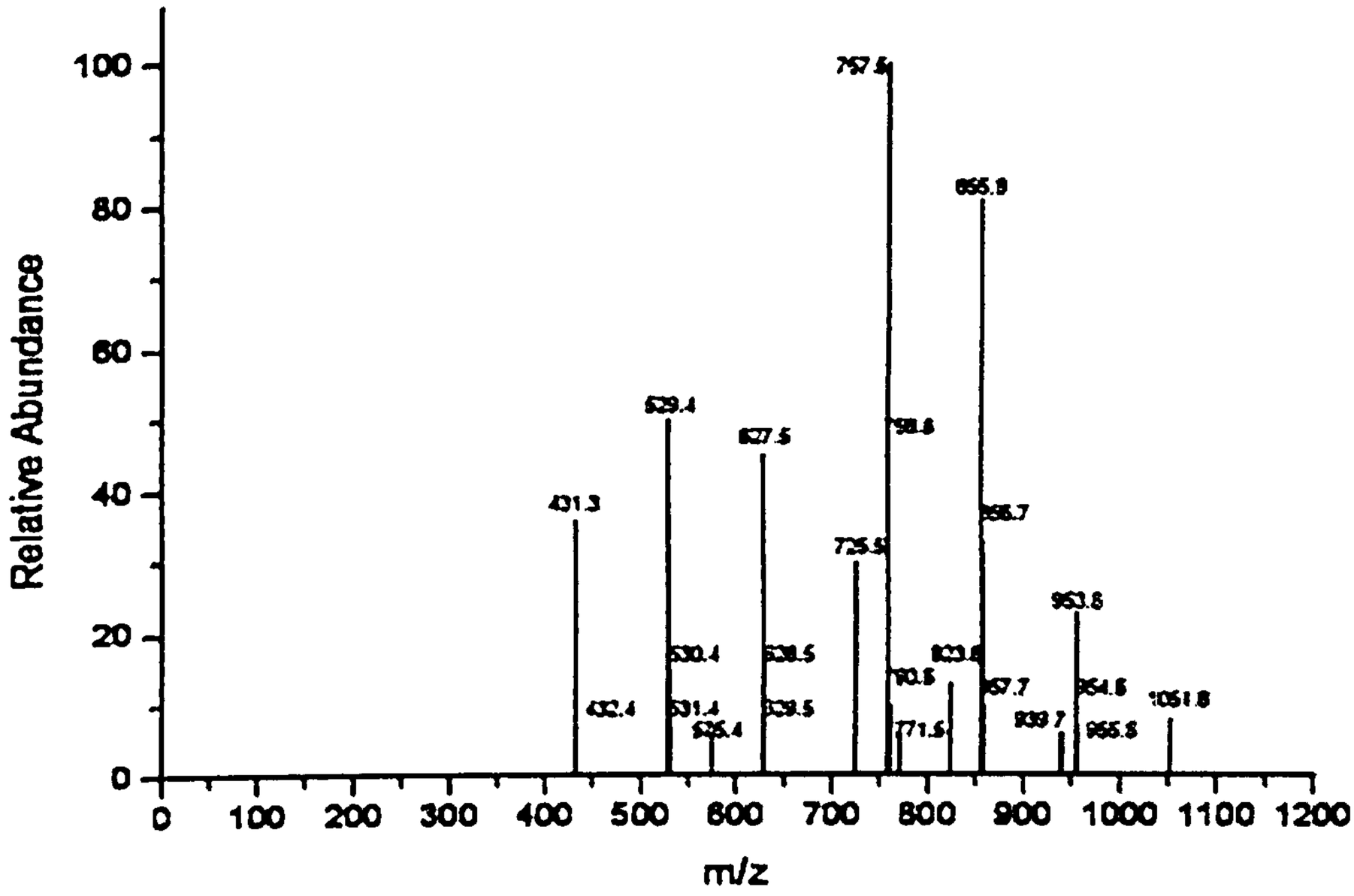


Figure 4.18. ESI-MS showing the effect of using half the normal chromate concentration after 6 hours at 60°C

It is again possible that the extra sensitivity of ESI-MS means that these compounds are present in the DRUV but they are in too low concentration to be observed.

## 4.5 NMR analysis

The theory of oligomerisation was strengthened by conducting $^{13}$C-NMR throughout the reactions. Figure 4.19 shows the $^{13}$C-NMR spectrum of sodium chromate and cyclohexene oxide before the reaction was initiated. The spectrum is assigned in figure 4.20. When compared to the spectrum after 6 hours (figure 4.21) it is clear that there is no change in the position of the peaks. However, after 24 hours under reflux conditions, there are several new peaks in the spectrum (figure 4.22).

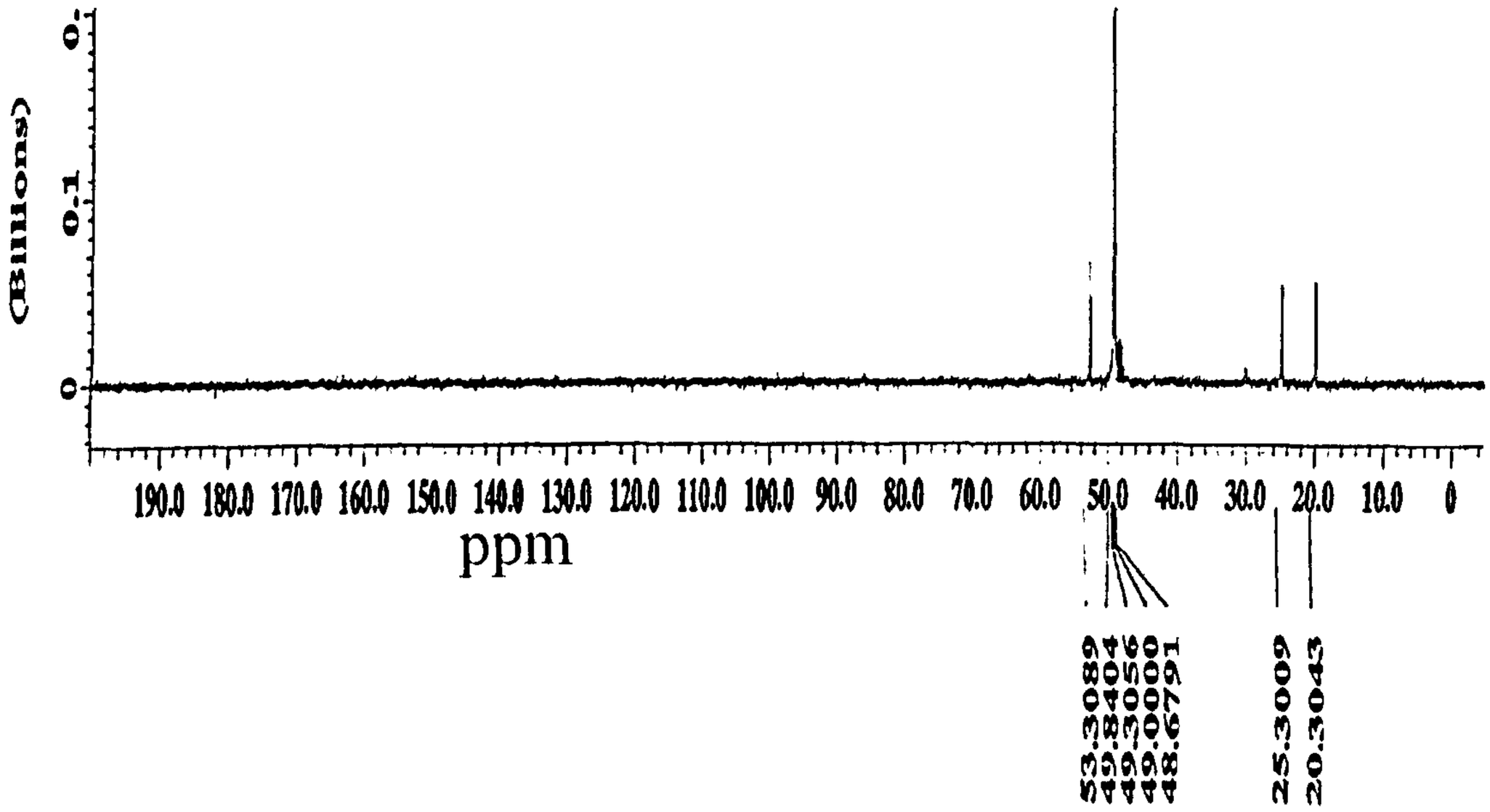


Figure 4.19. $^{13}$C-NMR spectrum of sodium chromate and cyclohexene oxide after 0 hours

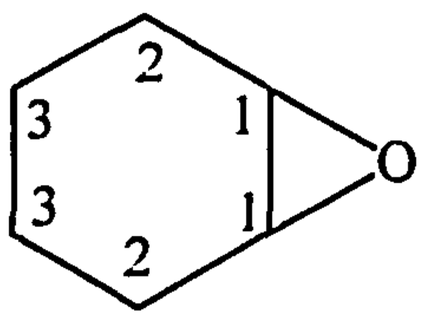


| Carbon number | δ/ppm |
|---|---|
| 1 | 53.3 |
| 2 | 25.3 |
| 3 | 20.3 |

Figure 4.20. Table for peak assignment of sodium chromate and cyclohexene oxide after 0 hours

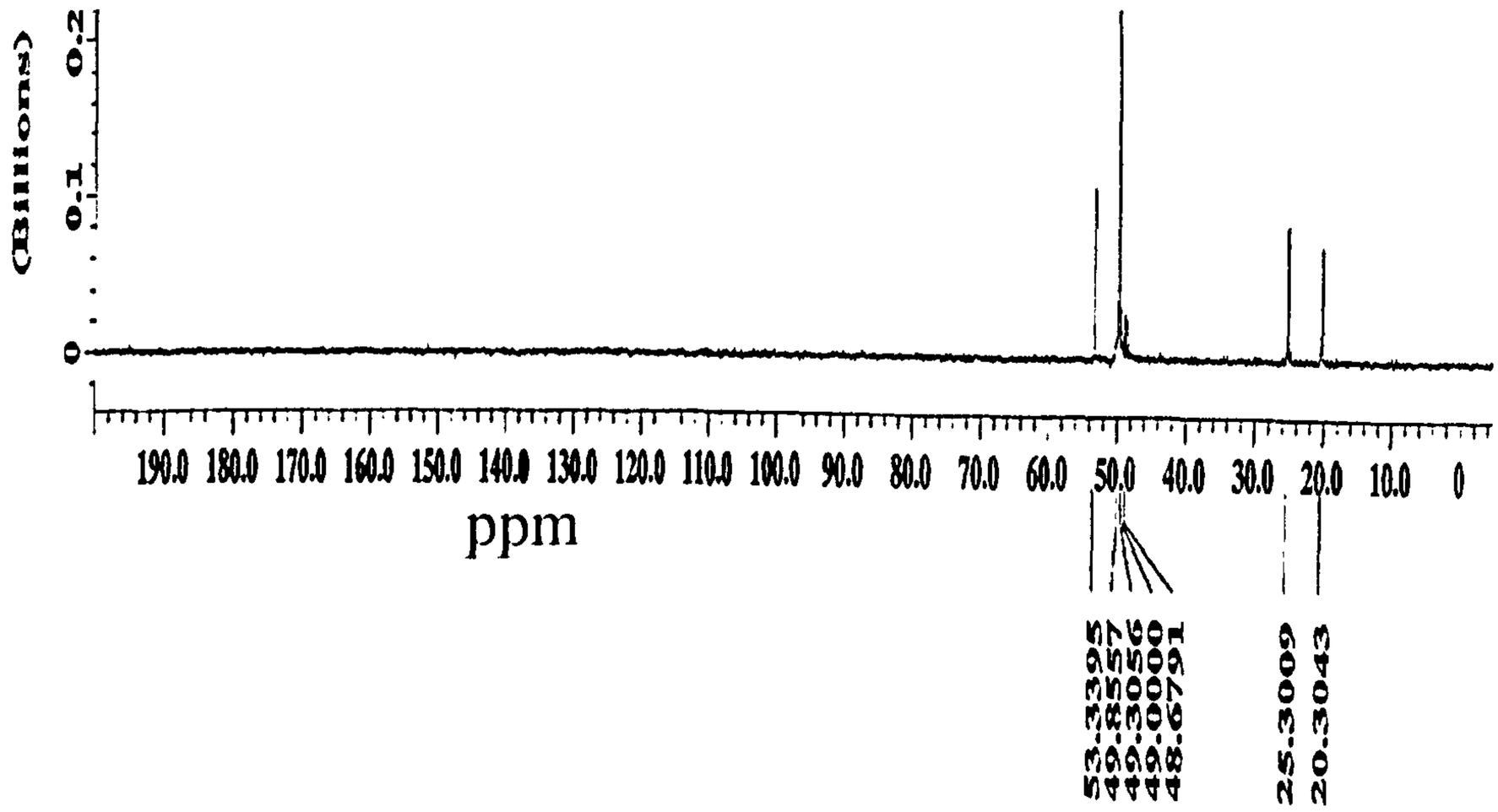


Figure 4.21. $^{13}$C-NMR spectrum of sodium chromate and cyclohexene oxide after 6 hours

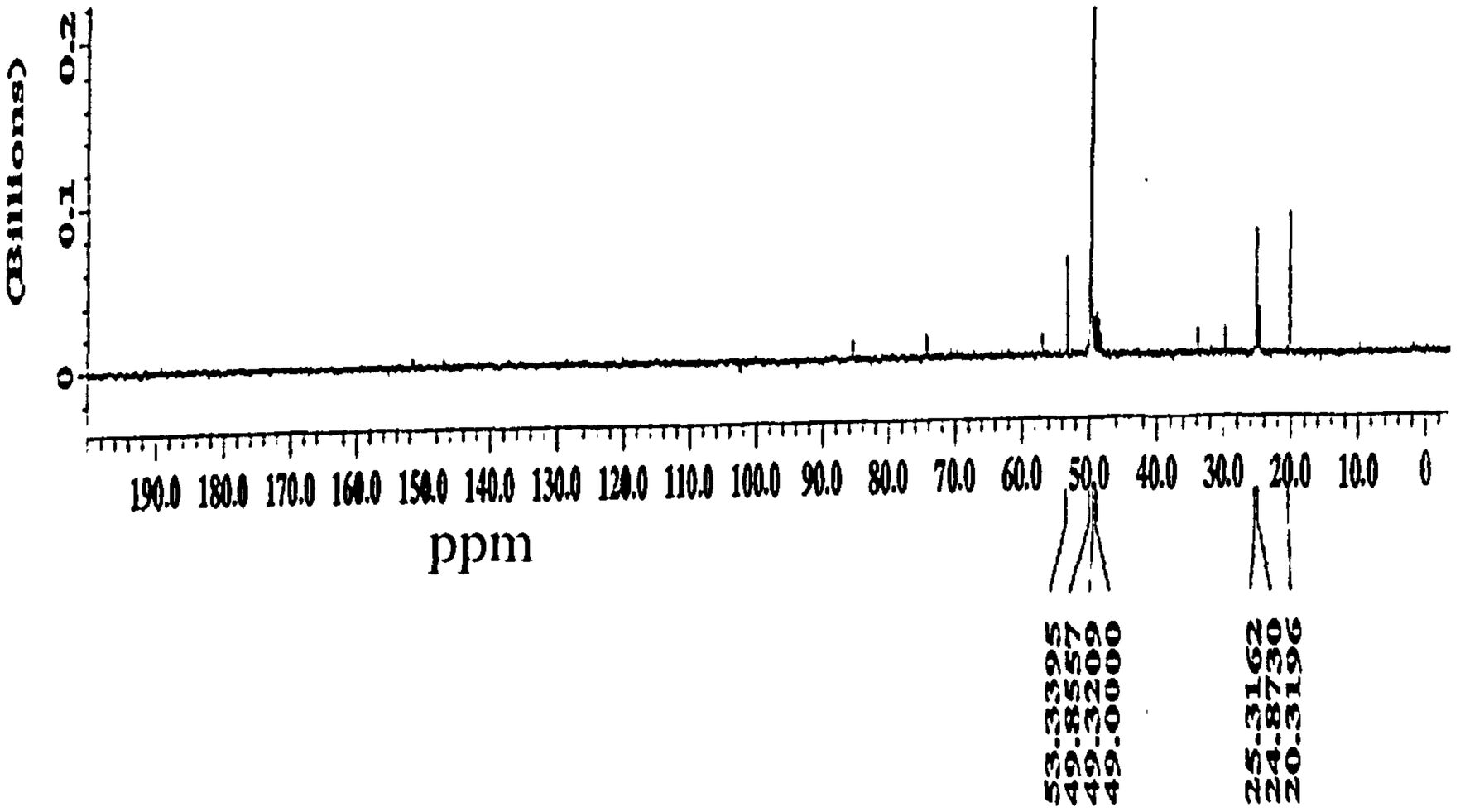


Figure 4.22. $^{13}$C-NMR spectrum of sodium chromate and cyclohexene oxide after 24 hours

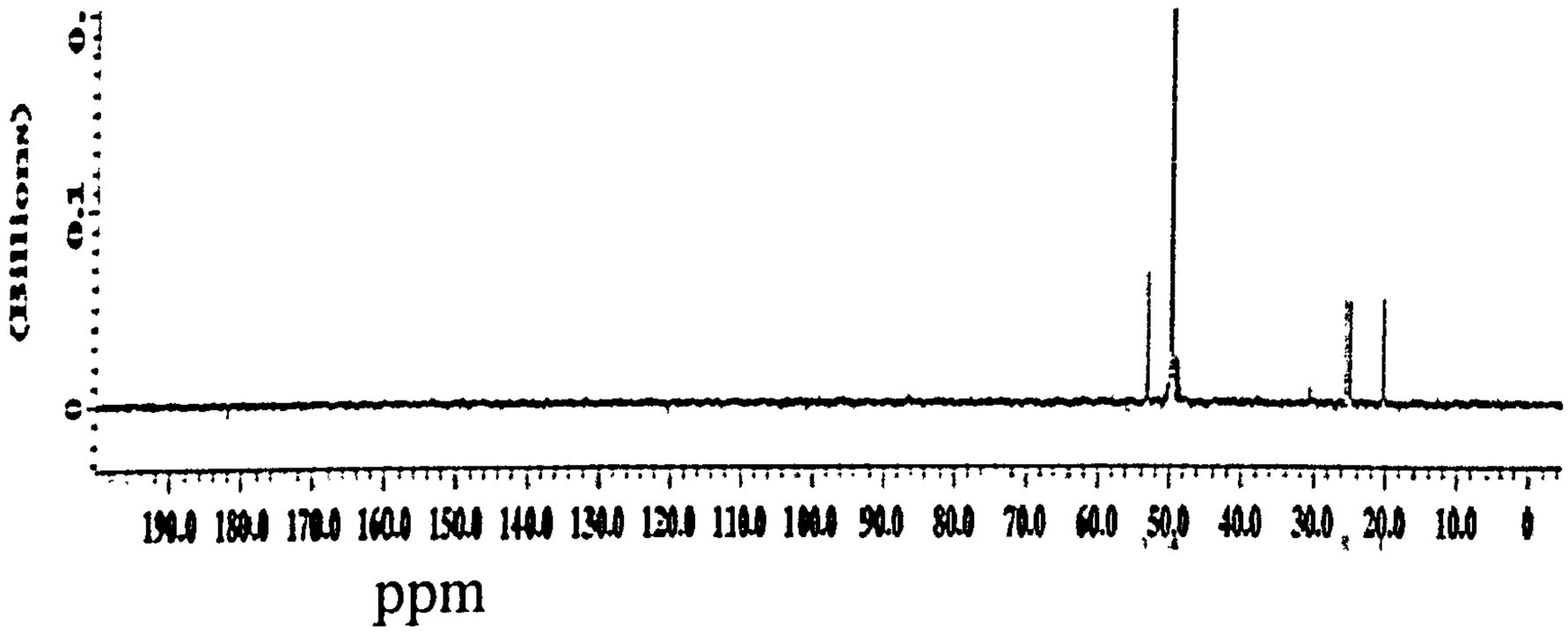


Figure 4.23. $^{13}$C-NMR spectrum of control experiment of cyclohexene oxide and methanol refluxed at 60°C for 24 hours

As can be seen from figure 4.23 when the control experiment was run in the absence of chromate, no new peaks were formed, suggesting that chromate is acting as a catalyst for reaction.

NMR spectra predicting calculations[15] were used to aid the assignment of these new peaks and a table of the results is shown below (figure 4.24).

$$\Delta_c = -2.3 + \Sigma z + \Sigma S + \Sigma K$$

Where: $z$ is a substituent constant

$S$ is a steric correction

$K$ is a conformational increment for γ-substituents

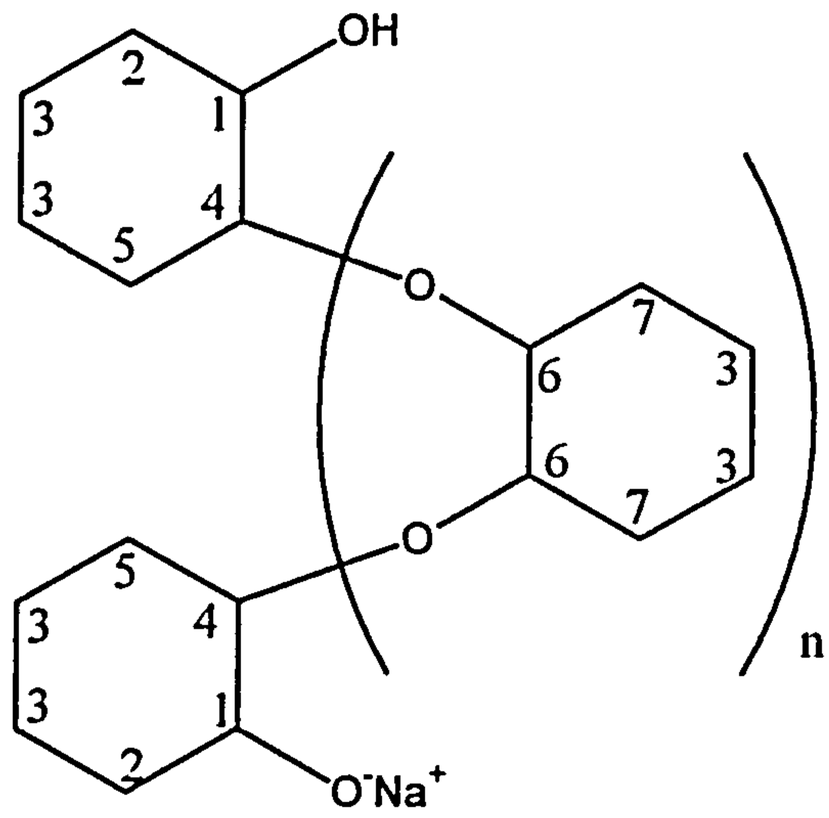

| Carbon number | Theoretical δ/ppm | Real δ/ppm |
|---|---|---|
| 1 | 77 | 74.2 |
| 2 | 34 | 33.8 |
| 3 | 26 | 25.3 |
| 4 | 87 | 85.5 |
| 5 | 31 | 29.8 |
| 6 | 75 | 83.0 |
| 7 | 25 | 24.7 |

Figure 4.24. Table for the peak assignment of sodium chromate and cyclohexene oxide after 24 hours

As can be seen, the calculated values for the proposed theoretical structure correspond quite favourably with the real values, showing results within approximately 2-3ppm in most cases. The only result that is inaccurate is for the carbon next to the oxygen atoms of the opened up epoxide. The electron withdrawing (deshielding) effect of these oxygens can vary considerably from system to system[16] depending on conditions such as conjugation or steric/conformational effects and therefore the exact position of these carbons is difficult for the software to estimate[16].

These results suggest that the oligomerisation theory is highly probable. However, the other structures reported in the LC-MS and the oxidation products in the ESI-MS are not observed, suggesting that these species are in extremely low concentration.

Further experiments were carried out with both lithium and potassium chromates and the same results were obtained. However, when styrene oxide was used instead of cyclohexene oxide, the $^{13}$C-NMR analysis showed that a reaction had taken place after 6 hours. Figures 4.25-4.27 show the spectra for the reaction between lithium chromate and styrene oxide.

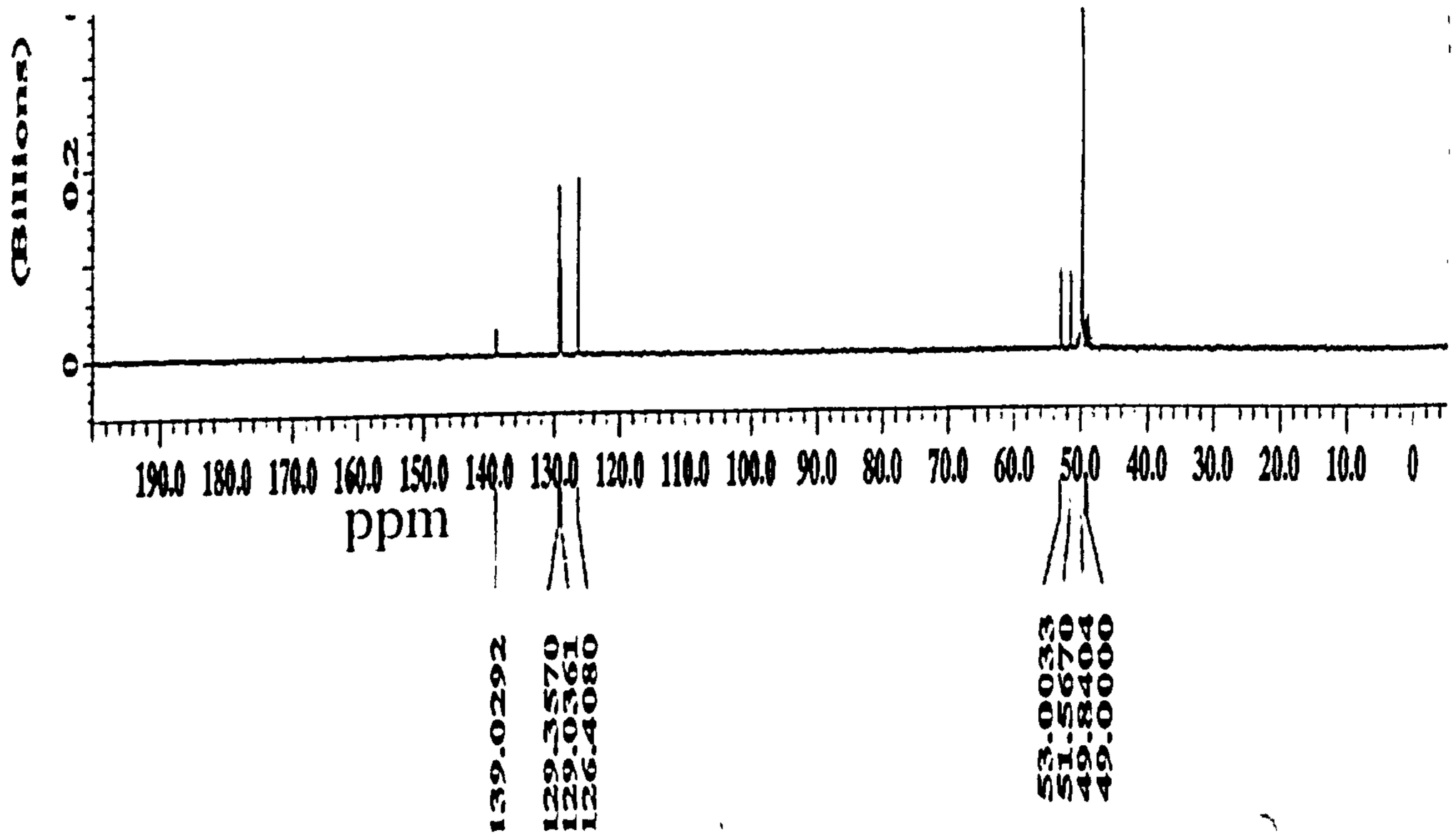


Figure 4.25. $^{13}$C-NMR spectrum of lithium chromate and styrene oxide after 0 hours at 60°C

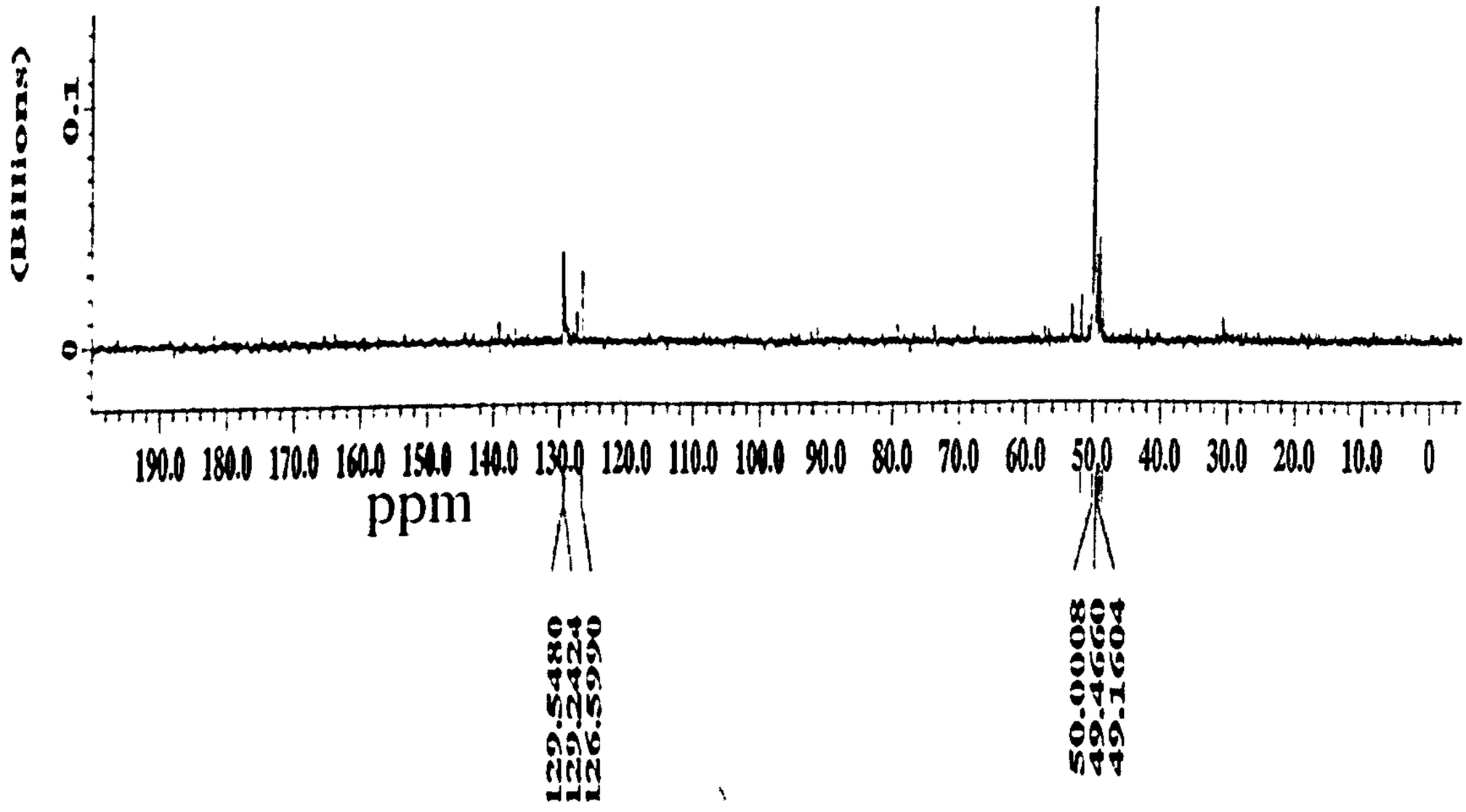


Figure 4.26. $^{13}$C-NMR spectrum of lithium chromate and styrene oxide after 6 hours at 60°C

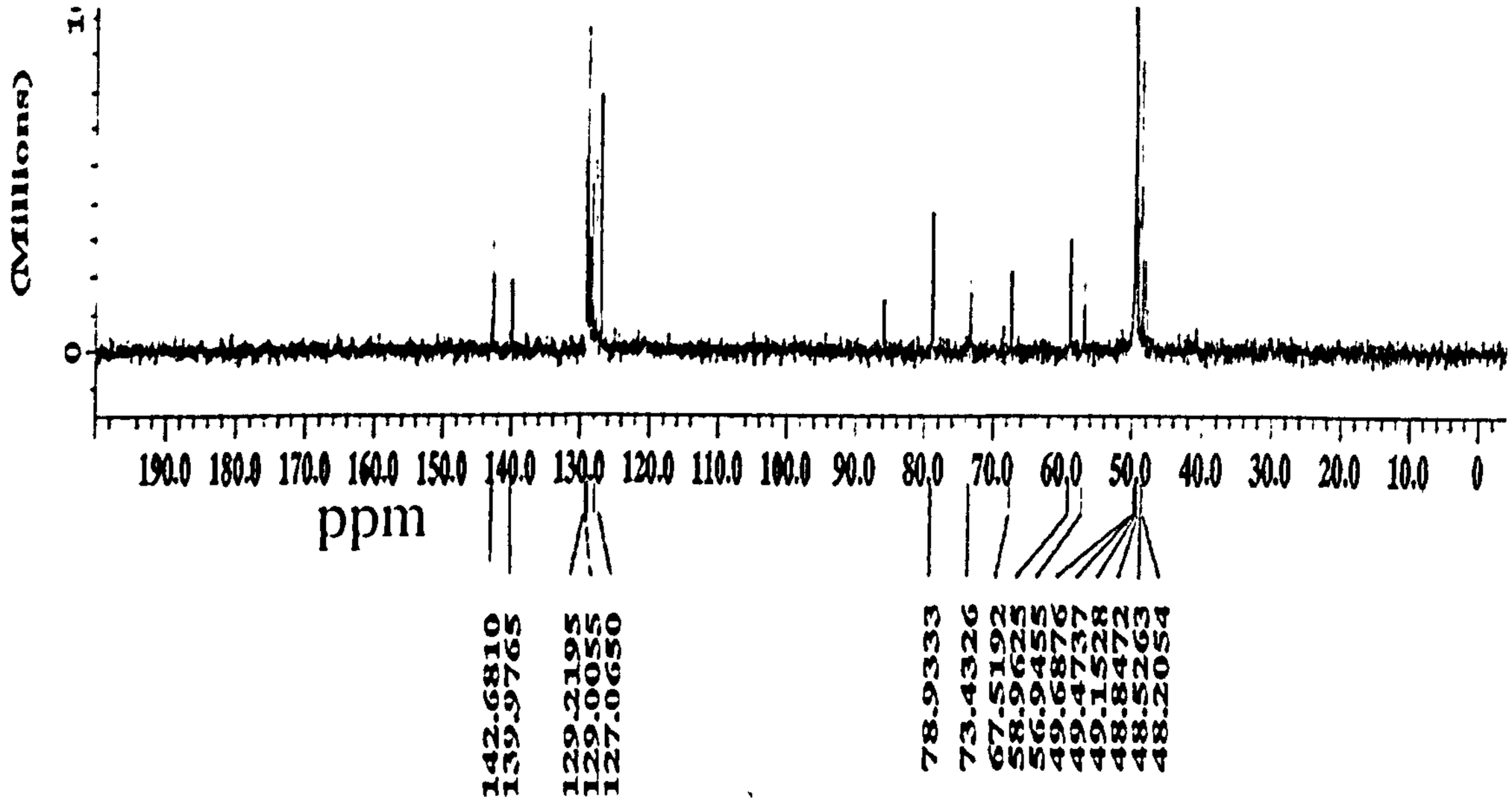


Figure 4.27. $^{13}$C-NMR spectrum of lithium chromate and styrene oxide after 24 hours at 60°C

The increased reactivity observed in the styrene oxide system is common in styrene based systems as they have a propensity for polymerisation. This is due to the large stabilisation energy afforded by the aromatic ring close to the reactive centre of the structure[18].

## 4.6 DRIFT-IR analysis

The final technique that was used to observe the chromate and epoxide reaction was IR. DRIFT-IR was used to monitor the individual components to eliminate the strong effect the solvent could have on the spectrum.

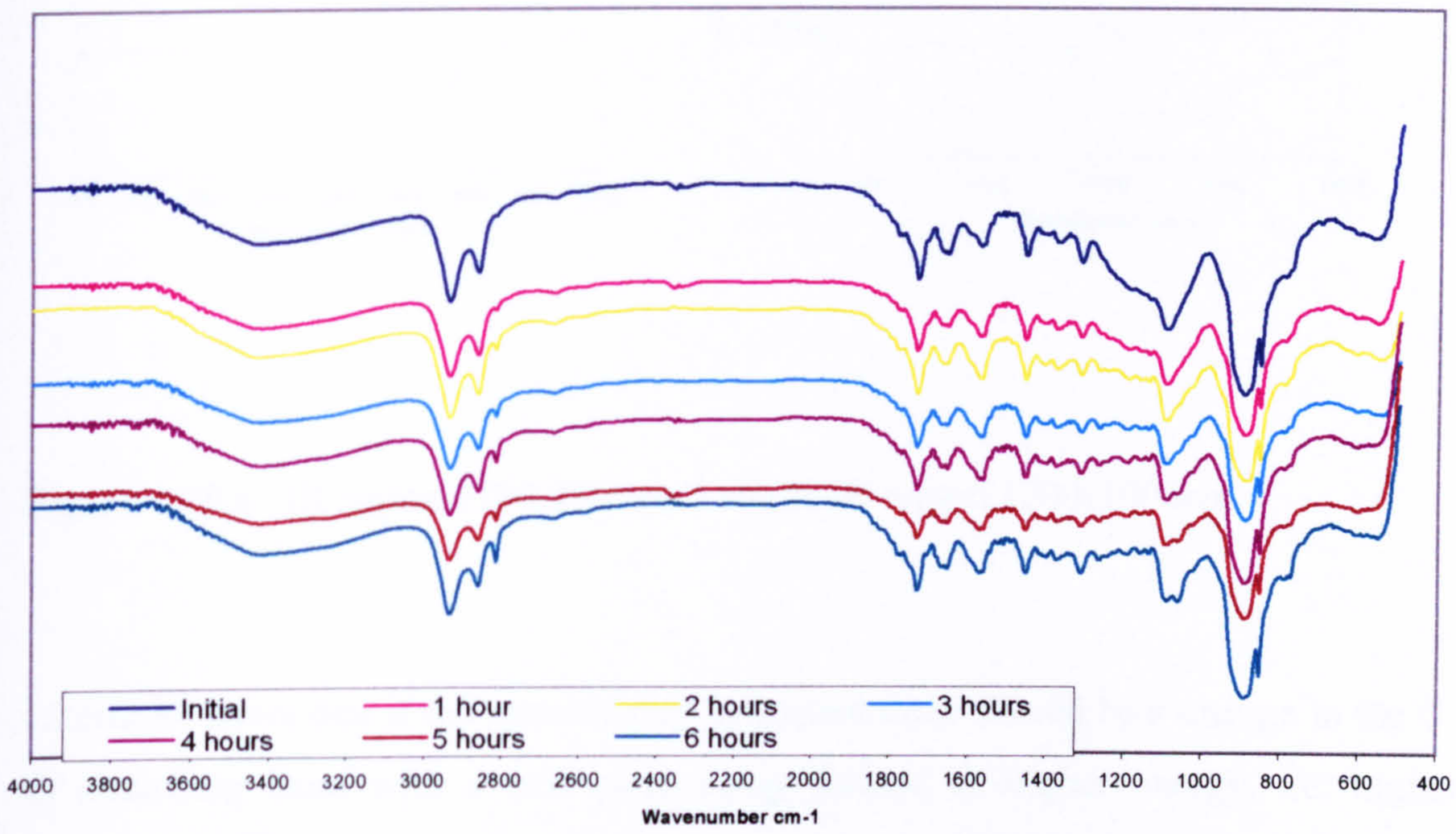


Figure 4.28. DRIFT spectra showing the reaction between $KCrO_4$ and cyclohexene oxide over 6 hours at 60°C

Figure 4.28 shows spectra for the reaction between potassium chromate and cyclohexene oxide and the way that it evolves over time. It is clear that there are two main areas of change in the spectrum. The first of these is in the C-H stretching band and the growth of a new peak at 2813cm$^{-1}$ (figure 4.29a). The second is in the C-O band at 1083cm$^{-1}$ [18] with a new peak arising at 1052cm$^{-1}$ (figure 4.29b).

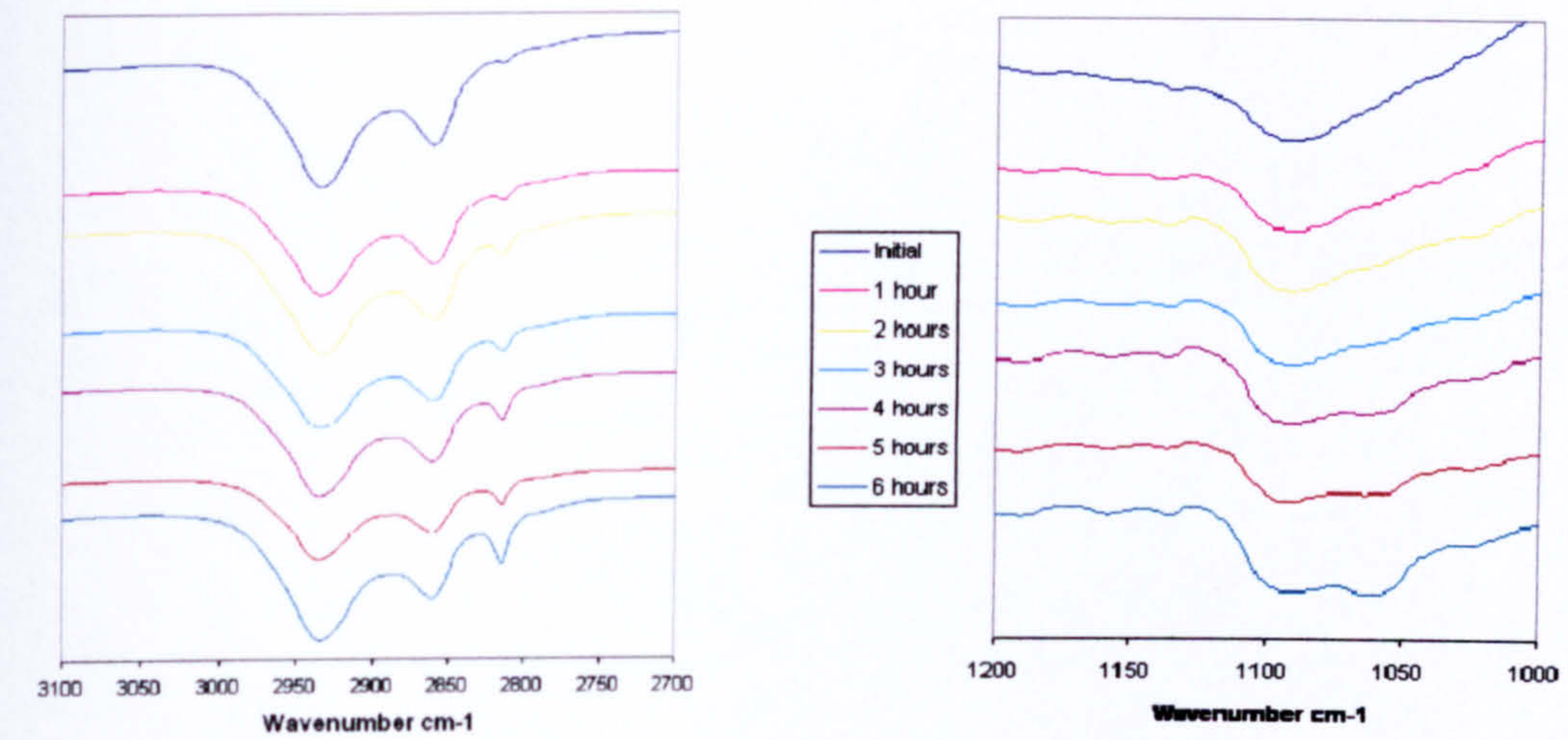


Figure 4.29 a. IR region 3100-2700cm$^{-1}$ and b. IR region 1200-1000cm$^{-1}$

Literature states that if the epoxide ring is opened there should be a change in the C-O stretching band with a new peak being formed at higher energy, i.e. higher wavenumber[20]. This is because there is a release of the strain energy from the opening of the epoxide ring. However, in the results obtained, the new peak is at a lower wavenumber (1052cm$^{-1}$) compared to that of the original peak at 1083cm$^{-1}$. It must be noted, though, that this is not the only peak present in IR spectroscopy due to the epoxide band; a further peak should appear at 963cm$^{-1}$ [21]. However, in this system this peak would be obscured by the broad chromate band and is therefore not visible, but if it was there the new peak at 1052cm$^{-1}$ would be at higher energy compared to this. Previous studies have shown that the depletion of the oxirane ring C-O-C bonding structure is also a way of monitoring oligomerisation of epoxies, however, this peak is at 914cm$^{-1}$ and therefore obscured by the broad chromate band.

The change in the C-H region can also be attributed to the opening of the epoxide ring. In contrast to the C-O group, the new C-H peak appears at lower energy (2813cm$^{-1}$). One possible reason for this is because the release of strain of the oxygen from the epoxide group allows for easy hydrogen bonding (figure 4.30).

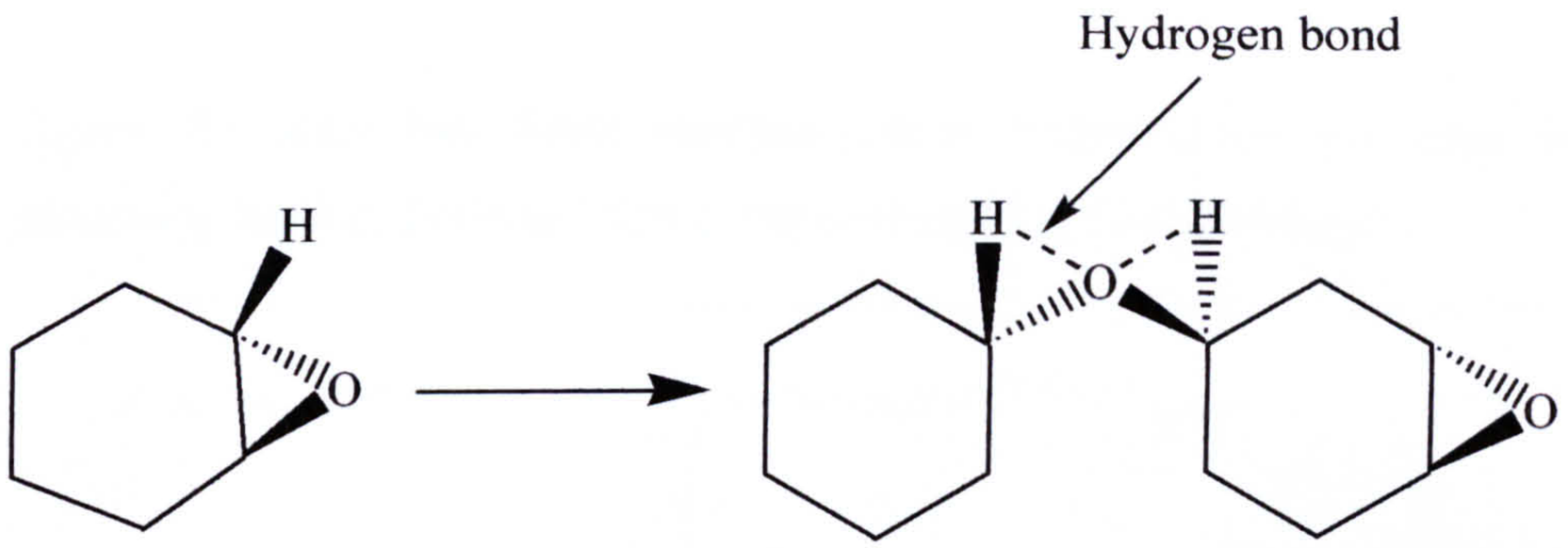


Figure 4.30. Diagram showing the possibility for hydrogen bonding after opening the epoxide ring

However, the formation of intramolecular hydrogen bonds is unlikely so another possible explanation is that this peak is due to one of the by-products formed from the reaction. Figure 4.13 shows various other species present after reaction, so it is possible that one of these new hydrogen environments is the cause of the new peak.

Similar results have been observed for the other systems investigated. Figure 4.31 shows the DRIFT spectra for the reaction between sodium chromate and epoxypentane.

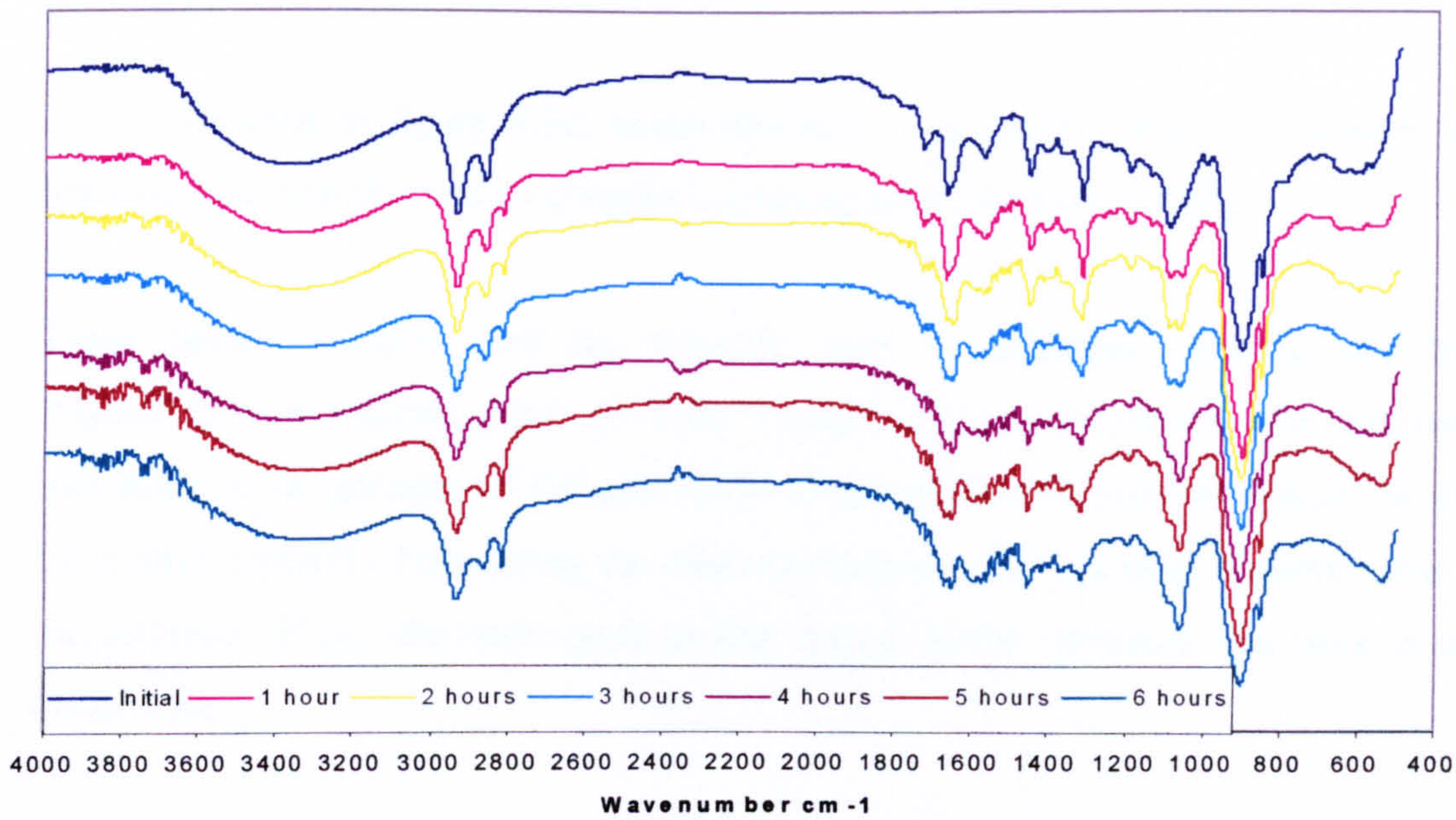


Figure 4.31. DRIFT spectra of the reaction between $Na_2CrO_4$ and epoxypentane over 6 hours at 60°C

Again, the same two major changes can be observed i.e. a change in the C-H stretching band at 2813cm$^{-1}$ and in the C-O band at 1080-1050cm$^{-1}$.

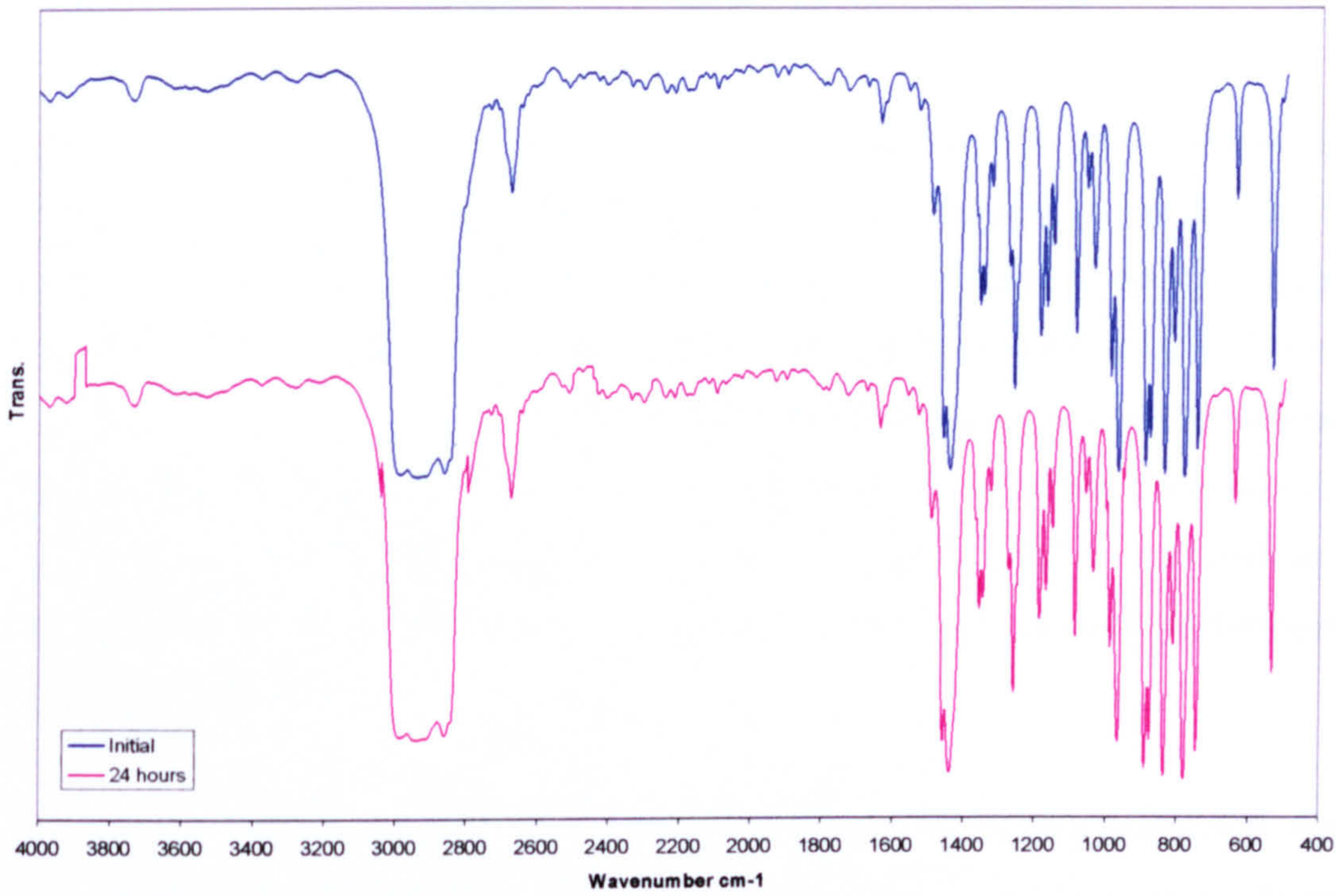


Figure 4.32. FTIR Transmission liquid thin film spectrum of cyclohexene oxide and methanol control experiment before reflux and after 24 hours refluxing at 60°C

As can be seen in figure 4.32, when chromate was emitted from the system, the infrared spectrum showed no changes occurring after 24 hours at 60°C

These results confirm that the epoxide ring is definitely opening and that oligomerisation is taking place, probably catalysed by the presence of the chromate. The decrease in intensity of the commonly observed oxirane peak at 914cm$^{-1}$ would be another method of observing the oligomerisation of the epoxide, however, due to the intensity of the chromate peak in this region in the spectrum this peak is not observable

## 4.7 Conclusions

The application of various different analytical procedures has lead to several different conclusions being drawn from this series of experiments.

Firstly, the combined findings from the UV-vis spectroscopy and titrimetric studies have shown that over time there is a redox reaction occurring in the model system. This has been illustrated through the observation of new peaks in the UV-vis spectra caused by the presence of d-d electron transitions; not available in Cr (VI) species. Also, the large increase in the amount of thiosulphate consumed in the presence of epoxide in the titrimetric data illustrates that there is a definite reduction of the chromium. This is not surprising as when analysing the LC-MS results it can be seen that there are many different oxidised species formed from the reaction between the chromate and epoxide.

Through the use of ESI-MS, $^{13}$C-NMR, and DRIFTS, it has been shown that there is significant oligomerisation of the epoxide occurring. This has been illustrated through the presence of the series of peaks due to the repeating mass unit of the epoxide in the ESI-MS. Additionally, the formation of new peaks visible in $^{13}$C-NMR spectroscopy and their subsequent identification using NMR spectra predicting calculations confirms that an oligomer has been formed. The fact that this oligomer formation did not occur when the chromate was absent (see figures 4.23 and 4.32) is important as it suggests that Cr (VI) is acting as a catalyst for the ring opening reaction and subsequent oligomerisation of the epoxide. Chromium compounds have been shown in the literature to behave as epoxide ring opening catalysts[21] and it appears that this is occurring here.

The results obtained from the ESI-MS and LC-MS experiments suggest that either chromate is not in the final oligomeric species, or that it is not present in great amounts. This has been shown through the presence of the associated cation (which is present in the same concentration as the chromate) in the ESI-MS, and also by the absence of chromate in any of the structures determined through LC-MS. However,

this does not mean to say that the presence of an organochromate species can definitely be ruled out; it may just be present in very low concentration.

## 4.8 References


1. Banwell, C.N., McCash, E.M., *Fundamentals of Molecular Spectroscopy*, McGraw Hill, London, 1994.
2. Weckhuysen, B.M., Verberckmoes, A.A., Buttiens, A.L., Schoonheydt,R.A., *Journal of Physical Chemistry*, 98, 2, 579, 1994.
3. Yamashita, H., Yoshizawa, K., Ariyuki, M., Higashimoto, S., Che, M., Anpo, M., *Chemical Communications*, 435, 2001.
4. Bensalem, A., Weckhuysen, B.M., Schoonheydtet, R.A., *Journal of Physical Chemistry B,* 101, 2824, 1997.
5. Subrahmanyam, C., Louis, B., Rainone,F., Viswanathan, B., Renken, A., Varadarajan, T.K., *Applied Catalysis A: General,* 241, 205, 2003.
6. Shores, M.P., Berseth, P. A., Long, J. R., *Inorganic Synthesis*, 34, 149, 2004.
7. Signorella, S., Garcia, S., Rizzotto, M., Levina, A., Lay, P. A., Sala, L. F., *Polyhedron*, 24, 1079, 2005.
8. Geiger, D.K., *Coordination Chemistry Reviews,* 172, 157, 1998.
9. Levian, A., Lay, P., *Coordination Chemistry Reviews*, 249, 281, 2005.
10. Greenwood, N. N., Earnshaw, A., *Chemistry of the Elements*, Butterworth-Heinemann, Oxford, UK, 2nd Edition, 1997.
11. Vogel, A.I., *Quantitative Chemical Analysis*, Longman Scientific & Technical, Harlow, 5th Edition, 1989.
12. Willoughby, R., Sheehan, E., Mitrovich, S., *A Global View of LC/MS*, Global View Publishing, Pittsburgh, 1998.
13. Sparkman, O.D., *Mass Spectrometry Desk Reference,* Global View Publishing, Pittsburgh, 2nd Edition, 2006.
14. Billmeyer, F.W., *Textbook of Polymer Science*, 3rd Edition, John Wiley & Sons Inc., New York, 1984.

15. Williams, D.H., Fleming, I., *Spectroscopic Methods in Organic Chemistry*, McGraw-Hill, London, 1995.
16. Harwood, L., Claridge, D., *Introduction to Organic Spectroscopy*, Oxford University Press, Oxford, 1995.
17. Bagno, A., Saielli, G., Scorrano, G., *Chemistry a European Journal*, 7, 1652, 2001.
18. Sykes, P., *A Guidebook to Mechanism in Organic Chemistry*, Longman, Harlow, 6th Edition, 1986.
19. Memarian, H.R., Nikpour, F., *Molecules, 7*, 63, 2002.
20. Cambie, R.C., Denny, W.A., *Australian Journal of Chemistry*, 28, 5, 1153, 1975.
21. Park, J.S., Kwak, G.H., Seo, M.K., Lee, J.R., *Journal of Polymer Science Part B: Polymer Physics*, 39, 3, 326, 2000.
22. Ironmonger, A., Stockley, P., Nelson, A., *Organic Biomoecular Chemistry*, 3, 250, 2005.

# ***Chapter 5***

# ***Alternatives***

## 5.1 Introduction

As stated in Chapter 1, there has been much previous research into the area of chromate replacement. Further alternatives suggested to those already mentioned include molybdates, titanates and lanthanum based coatings.

### *5.1.1 Molybdates*

Molybdates have been extensively tested as alternatives due to their oxidising power and the stability of their reduction products, which form a passivating layer[1]. They have low toxicity and have been shown to improve the pitting resistance of aluminum by changing its pitting potential to more noble values[2,3]. Further recent work states that in the presence of an etched surface the molybdenum is reduced from the +6 state to the +4 state, suggesting that a level of redox activity is useful for successful corrosion protection[4].

### *5.1.2 Titanates*

Titanate coupling agents are widely available[5,6] and have been proven to illustrate a high level of interactivity between themselves and free protons at an inorganic interface (figure 5.01).

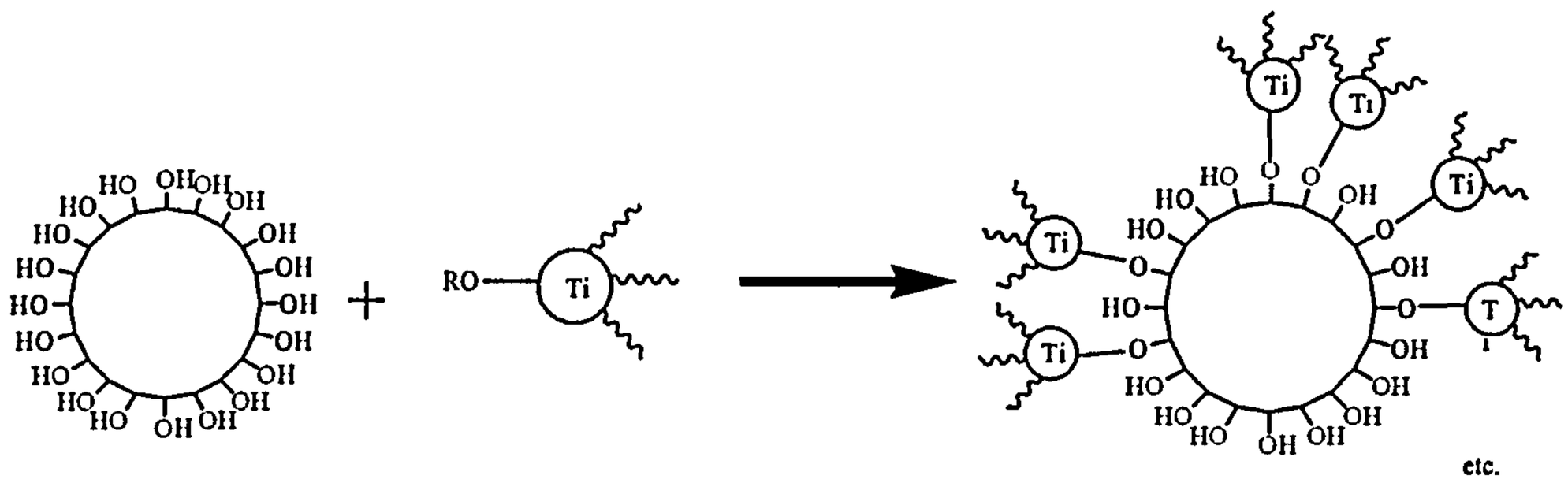


Figure 5.01. Diagram showing the reaction between a triorganofunctional titanate and the surface of a proton bearing inorganic[7]

This mechanism results in the formation of monomolecular layers on the surface, allowing surface energy modifications to occur and is believed to take place through the following mechanism:

$$MOH + \mathbf{R'O}\text{-}Ti(O\text{-}X\text{-}R\text{-}Y)_3 \rightarrow MO\text{-}Ti(O\text{-}X\text{-}R\text{-}Y)_3 + \mathbf{R'OH}$$

Where, M = substrate, H = surface proton, R'O = monohydrolysable group, Ti = tetravalent titanium, X = binder, R = thermoplastic, Y = thermoset

### *5.1.3 Lanthanum derivatives*

Surface treatments based on lanthanide salts, which are both economic and ecologically viable, have been considered a good alternative to chromate processes since the late '80s. Lanthanide salt treatments are able to protect most aluminium alloys through the formation of insoluble hydroxides over cathodic sites present on the metal surface; thus stopping the cathodic reaction of the corrosion process[8,9].

Recent studies have led to many researchers using lanthanum–cerium treatments since it was found that these elements behave in a more effective way than other rare earths.

### *5.1.4 Criteria for substitution*

In analysing the results obtained from the chromate model system, it was suggested that any successful alternative must possess three major chemical characteristics.

The first of these that it must be able to act as a Lewis acid catalyst to encourage the formation of epoxide oligomers, important in the curing mechanism of the primer.

The second key factor is that the alternative should be able to form a strong Al-O-X bond, where X is the alternative. This is so that any replacement would be able to successfully form a similar compound to the suggested chromium product (figure

5.02), which may be formed from the reaction between a chromate-epoxy oligomer and the aluminium surface.

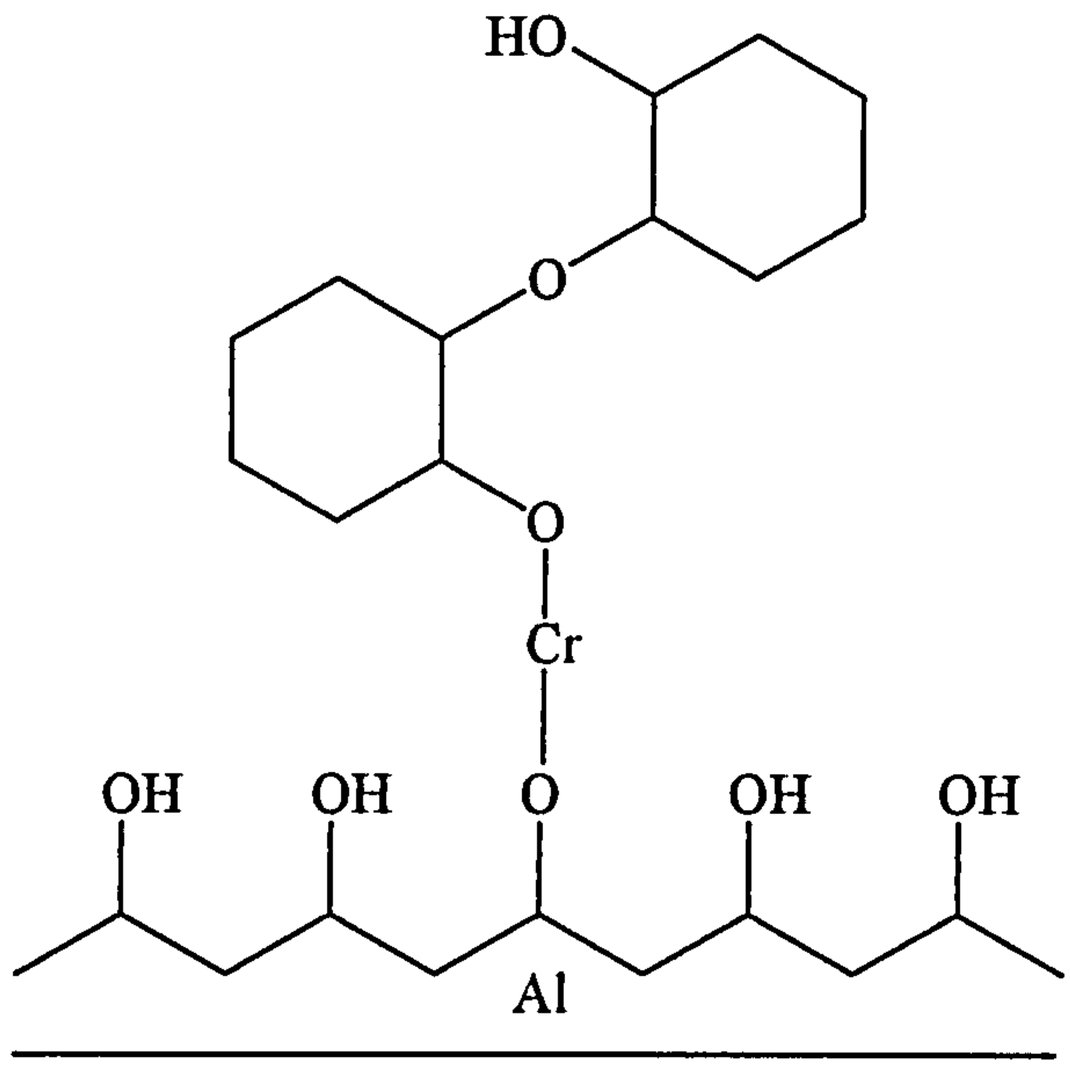


Figure 5.02. Suggested chromate product

These two factors must be combined with the final key point, which is that the alternative must be environmentally benign.

It is also possible that a level of redox activity would be advantageous, as it has been observed in the chromate model system.

Obviously, there are many elements that cover all three of these points. Figure 5.03, shows a version of the periodic table that illustrates both groups of elements offering a fully green solution and groups of non-environmentally friendly elements that would accomplish the first two factors from above.

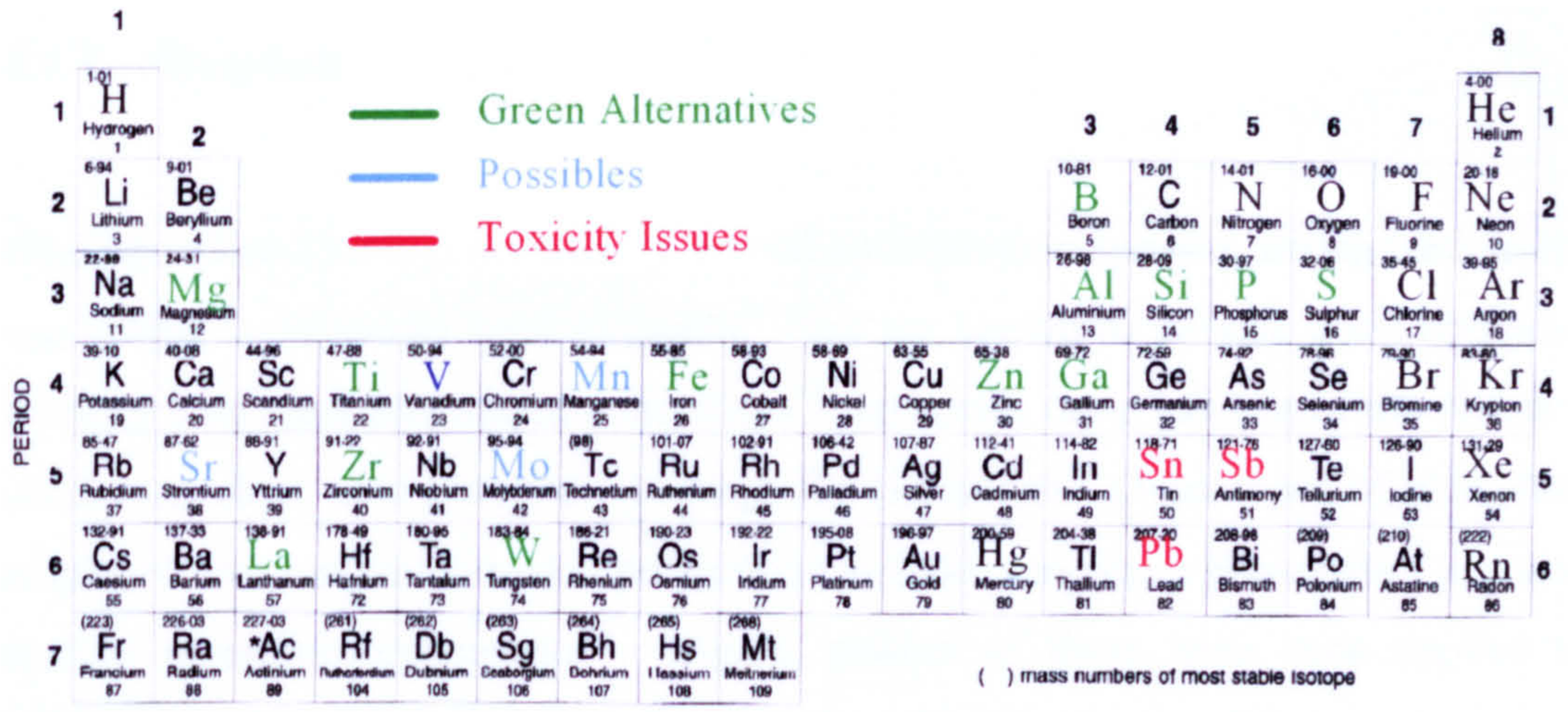


Figure 5.03. Periodic table showing possible green alternatives

The blue coloured elements in figure 5.03 are ones which may well achieve all the major points from above, however, either their toxicity might be too high (strontium), or their ability to act as a Lewis acid might not be great enough (manganese).

From all the possible green alternatives, it was decided to pick three to investigate in greater detail. So as to encompass as great a range as possible for the study, the elements were chosen from across the periodic table. The chosen elements were selected as they had all previously demonstrated a level of corrosion resistance in one field or another and therefore were believed to be amongst the more realistic replacements to chromate.

### *5.1.5 Phosphate*

Zinc phosphate coatings are used in several anticorrosion systems, dating back to the mid 1980s[10]. Primarily used in paints[11] they are known to provide good corrosion resistance on steel and magnesium alloys[12]; however, there has been little research conducted about zinc phosphate coatings for aluminium. Other types of phosphate employed from an anticorrosion perspective include manganese phosphate[13] and also sodium monoflurorophosphate[14]. Again, neither of these have been applied to aluminium alloys, however, phosphoric acid anodisation is one of the most common electrochemical pretreatments employed on aluminium in both the aerospace and automotive industries. Through this process, although the major anticorrosion mechanism is the substantial aluminium oxide layer formed, it is likely that some phosphate remains on the surface or embedded in the alumina layer.

### *5.1.6 Tungstate*

As tungsten belongs to the same group of elements as chromium, it has been suggested that it would provide similar levels of adhesion promotion and corrosion resistance[15]. Tungstate coatings were first reported in the early 1980s[16], but tungsten's corrosion inhibitive properties were well known in the '50s[17]; however, they have not been investigated in as much detail as phosphate or molybdate coatings. Sodium tungstate has been the most studied compound in this family and several papers have shown this to be moderately successful in inhibiting corrosion[18]. However, other research indicates that using tungstate alone is not suitable as it is extremely expensive and does not have the oxidising ability for successful corrosion inhibition[19]. The authors go on to suggest that combining tungstate with a strong oxidising agent such as potassium iodate, provides a strong oxide layer that is able to passivate the substrate's surface.

### *5.1.7 Zirconate*

Zirconate compounds are currently been investigated in great detail. The major compound of interest is zirconium tetrapropoxide[20], an organic based zirconium compound, which is used substantially in sol-gel coatings[21]. Other compounds that have been investigated are zirconium fluoride[22] and zirconium nitride[23]. However, there are also commercially available coupling agents based on zirconate. The US based Kenrich Petrochemicals, Inc. produce several complex organozirconate structures such as Cycloneopentyl, cyclo(dimethylaminoethyl)pyrophosphate zirconate (figure 5.04).

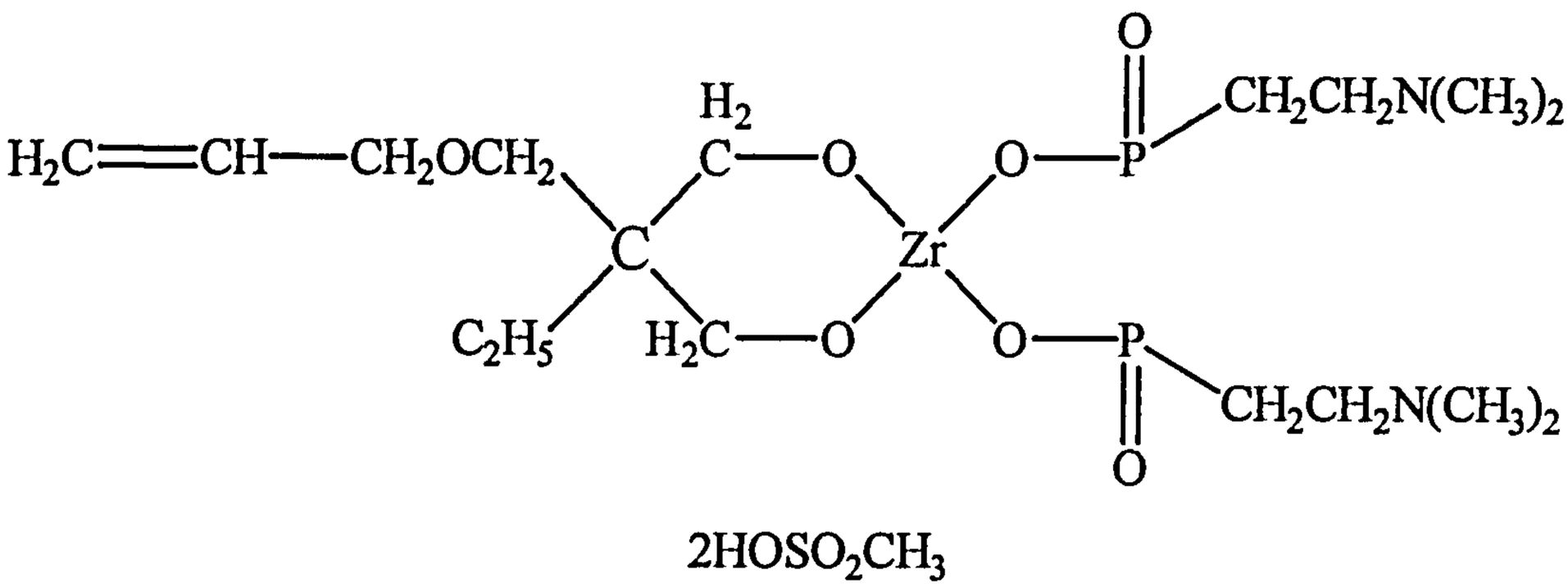


Figure 5.04. Structure of Cycloneopentyl, cyclo(dimethylaminoethyl)pyrophosphate zirconate[7]

One of the major advantages in using zirconate based compounds is that they are able to broaden upon the basis of silanes. This means that as well as reacting in a similar fashion to silanes, they are able to provide novel opportunities for adhesion between a wide range of materials such as metal substrates[24] and fluorinated polymers[25] through the formation of zirconium(VI) organofluoride.

## 5.2 Methodology

Although the chosen alternatives had illustrated a certain level of ability to act as chromate replacements; to investigate whether they behaved in a similar chemical manner, the same procedures and analytical techniques were employed as those that had been used for chromate. For each of the three alternatives, the sodium salt was chosen as these all possessed adequate solubilities in methanol. Cyclohexene oxide and styrene oxide were again used as the epoxides; however, due to mostly unsuccessful formulations with epoxypentane, no further work was conducted using this reactant. So as to keep all of the analytical data meaningful, the same concentrations of all chemicals were used for each of the three alternatives as had been used with chromate.

## 5.3 DRUV Analysis

### *5.3.1 Phosphate analysis*

As UV-vis analysis had been particularly successful in the observation of changes in the chromate systems, it was initially decided to apply this technique to each of the alternatives.

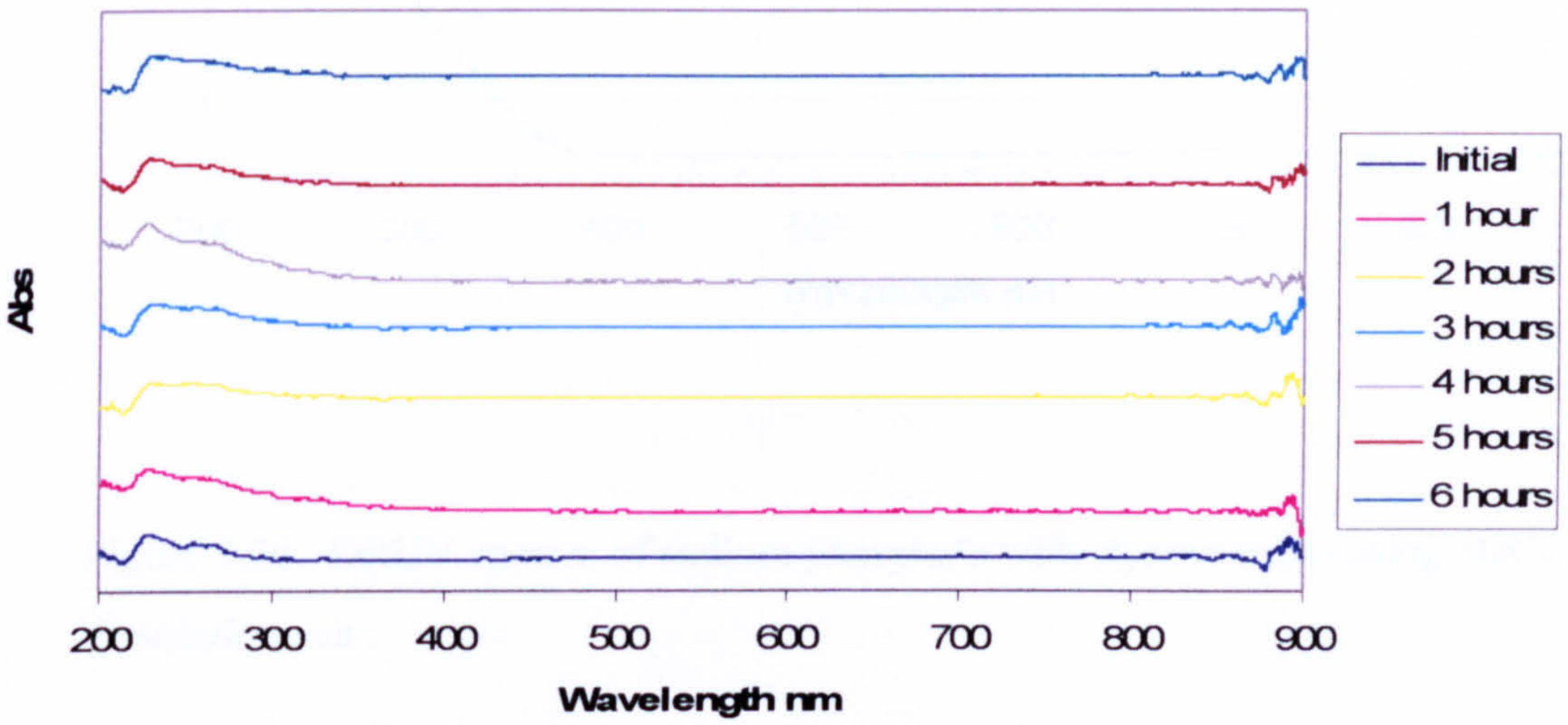


Figure 5.05. DRUV spectra of sodium phosphate with cyclohexene oxide using NaCl as a dissolution salt

Initially, the phosphate system was investigated. Figure 5.05 shows the DRUV spectra over a 6 hour period for the refluxing of sodium phosphate and cyclohexene oxide. It can be observed that there is a reduction in the relative intensity of the peak at 260nm after the procedure was ceased. This suggests that there is a reaction occurring between the two compounds; however, the changes are quite small and not of the same intensity to those observed when chromate was studied.

As more clear changes had been observed when chromate reacted with styrene oxide, it was decided to run sodium phosphate with this epoxide (figure 5.06).

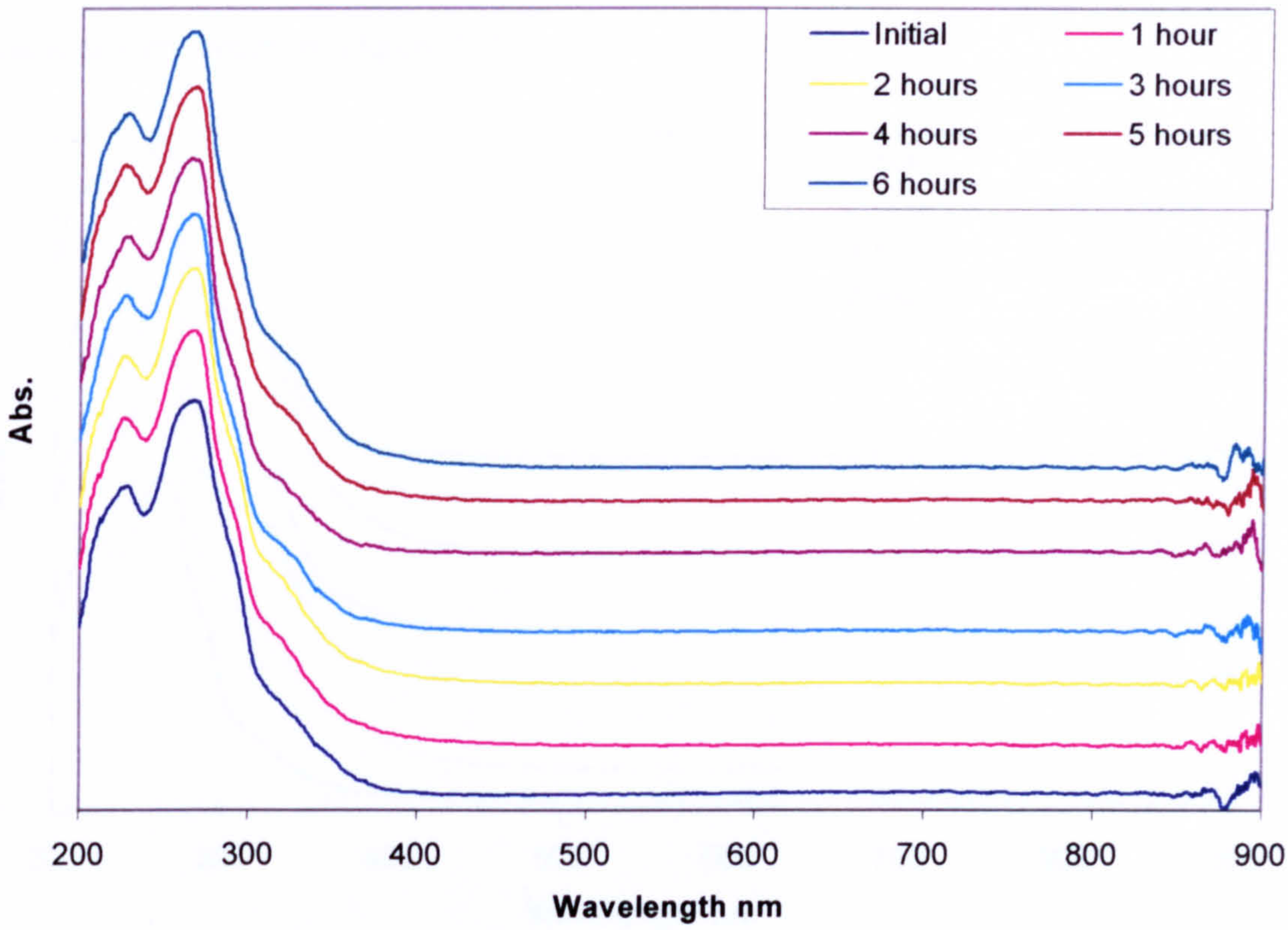


Figure 5.06. DRUV spectra of sodium phosphate with styrene oxide using NaCl as a dissolution salt

Figure 5.06 suggests DRUV shows little or no reaction occurs between the sodium phosphate and styrene oxide over a period of 6 hours as there are no changes in peak

shape or any new peaks emerging. Additionally, after continuing the reaction over a 24 hour period there was still no change in the spectrum.

It is probable that the results from the styrene oxide are more reliable than those obtained with cyclohexene oxide as the peak intensities are far greater and therefore any changes that would be observed would be far clearer.

### *5.3.2 Tungstate analysis*

When the same process was carried out using sodium tungstate, much clearer changes were observed (figure 5.07).

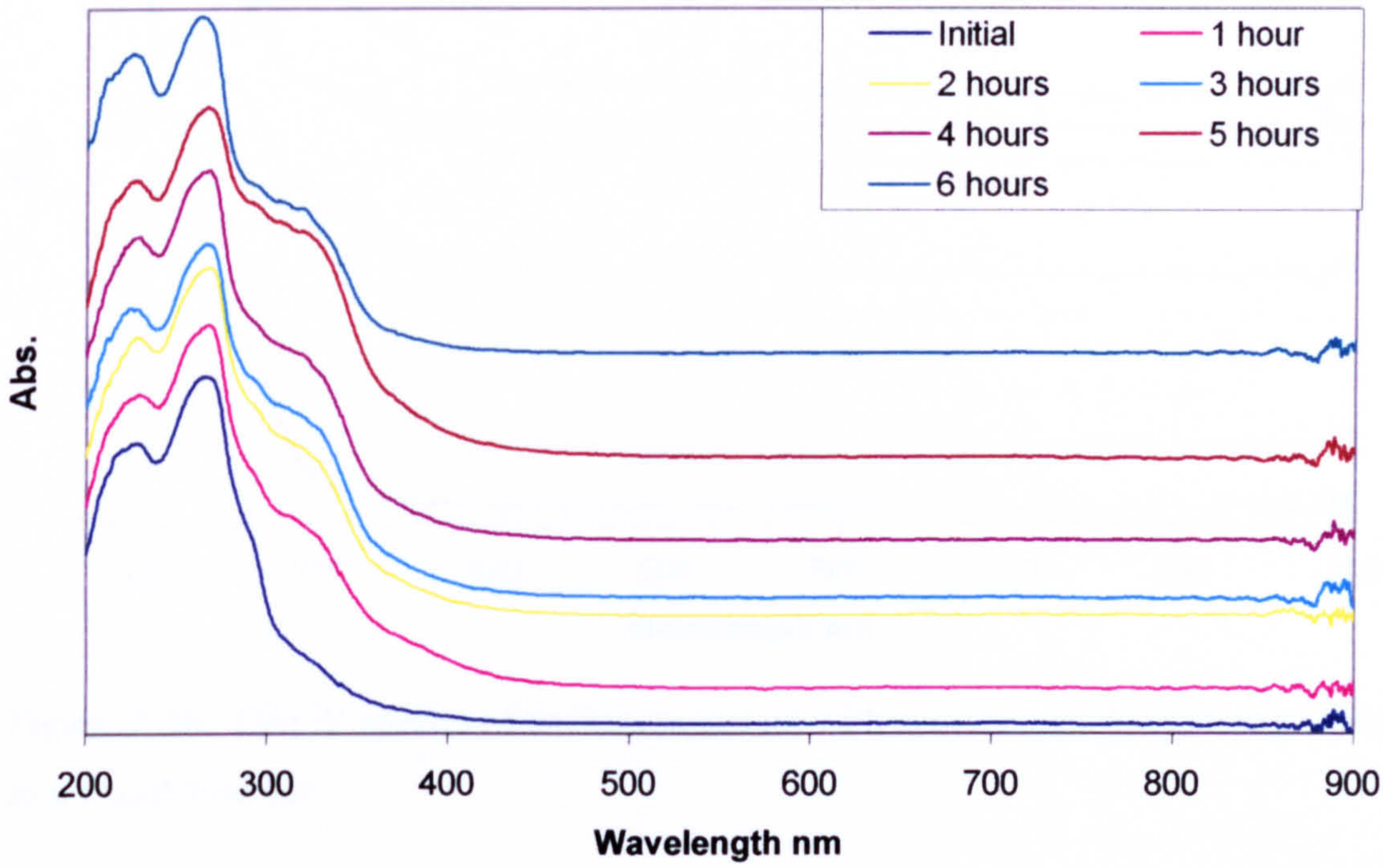


Figure 5.07. DRUV spectra of sodium tungstate with styrene oxide using NaCl as a dissolution salt

As can be seen from the DRUV spectra, there is a new peak forming at approximately 320nm suggesting that there is definitely a reaction occurring between the tungstate and the epoxide. However, what is surprising is that the peak gains almost its maximum intensity after 1 hour of reaction. This is surprising as in the

reactions involving chromate, all the changes in UV had been particularly time dependent and had all progressed over longer periods.

When the epoxide was changed to cyclohexene oxide, a similar observation was made (figure 5.08). Again, a definite reaction can be seen due to new peak formation at approximately 320nm, and similarly to styrene oxide, the reaction appears to have gone to completion after 1 hour.

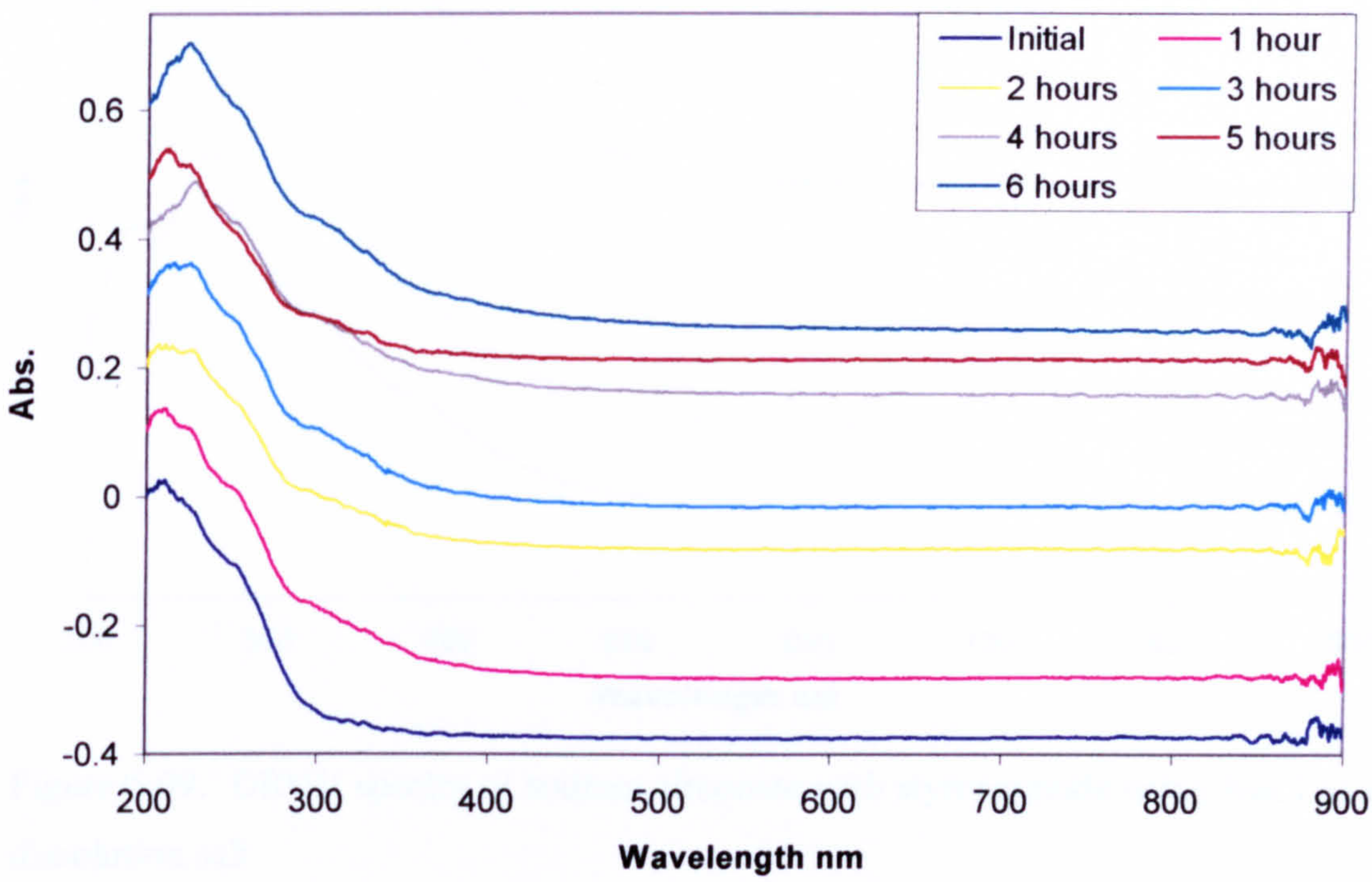


Figure 5.08. DRUV spectra of sodium tungstate with cyclohexene oxide using NaCl as a dissolution salt

It is likely that the new peaks formed in both the reactions with sodium tungstate are due to change transfer transitions. The reason for this is due to the fact that they appear at too high energy to be caused by d-d transitions.

As there are no other changes to the tungstate spectra, particularly in the d-d electron transfer region, it can be suggested that although tungstate performs some form of reaction with epoxides, it does not offer the same type of redox chemistry that chromate exhibits.

### *5.3.3 Zirconate analysis*

Through looking at the DRUV spectra obtained in the system of sodium zirconate and styrene oxide (figure 5.09) it appears that the activity of zirconate is higher than that of tungstate.

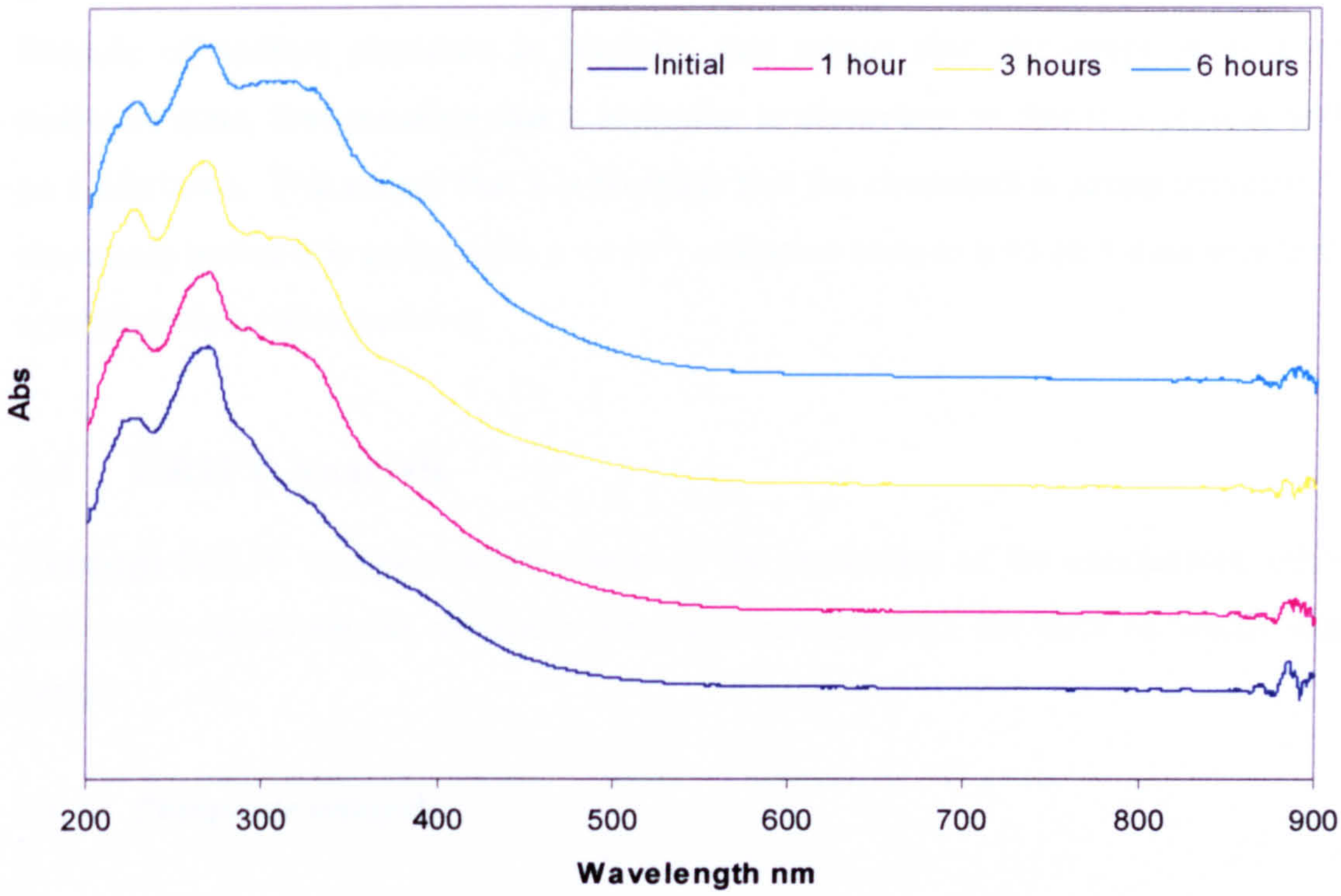


Figure 5.09. DRUV spectra of sodium zirconate with styrene oxide using NaCl as a dissolution salt

As can be seen from the DRUV spectra, there are three major changes occurring over the 6 hour period. The first of these is the large change in peak shape at approximately 320nm. Although this peak is in the same position as that in the tungstate system, here it increases in intensity over time.

The second major change is the growth of the peak at approximately 375nm. This band changes from been shoulder like at the start of the reaction to been quite an intense peak after approximately 5-6 hours.

The third major change is that the starting point of the series of peaks moves to a higher wavelength as the reaction progresses. After 6 hours, the initiation point of the peaks is approximately 560nm as opposed to 500nm for the system at 0 hours. This suggests that there is another peak of low intensity present at 560-500nm after 6 hours. A peak in this region in UV spectroscopy is most commonly attributed to a d-d transition[26]. Although zirconium is in group IV in the periodic table, as the formula of sodium zirconate is $Na_2ZrO_3$ this means that zirconium is in a +4 oxidation state, thus meaning that it is similar to chromium in that it is present with no d-electrons. This means that it is probable that the zirconium is acting similarly to chromium in that it is going from a +4 ($d^0$) oxidation state to a +3 ($d^1$) state with both operating via a redox pathway.

## 5.4 DRIFT Analysis

Although DRUV was particularly useful in the evaluation of the alternatives, other techniques employed on chromate were also investigated, the first of which was DRIFT.

### *5.4.1 Phosphate analysis*

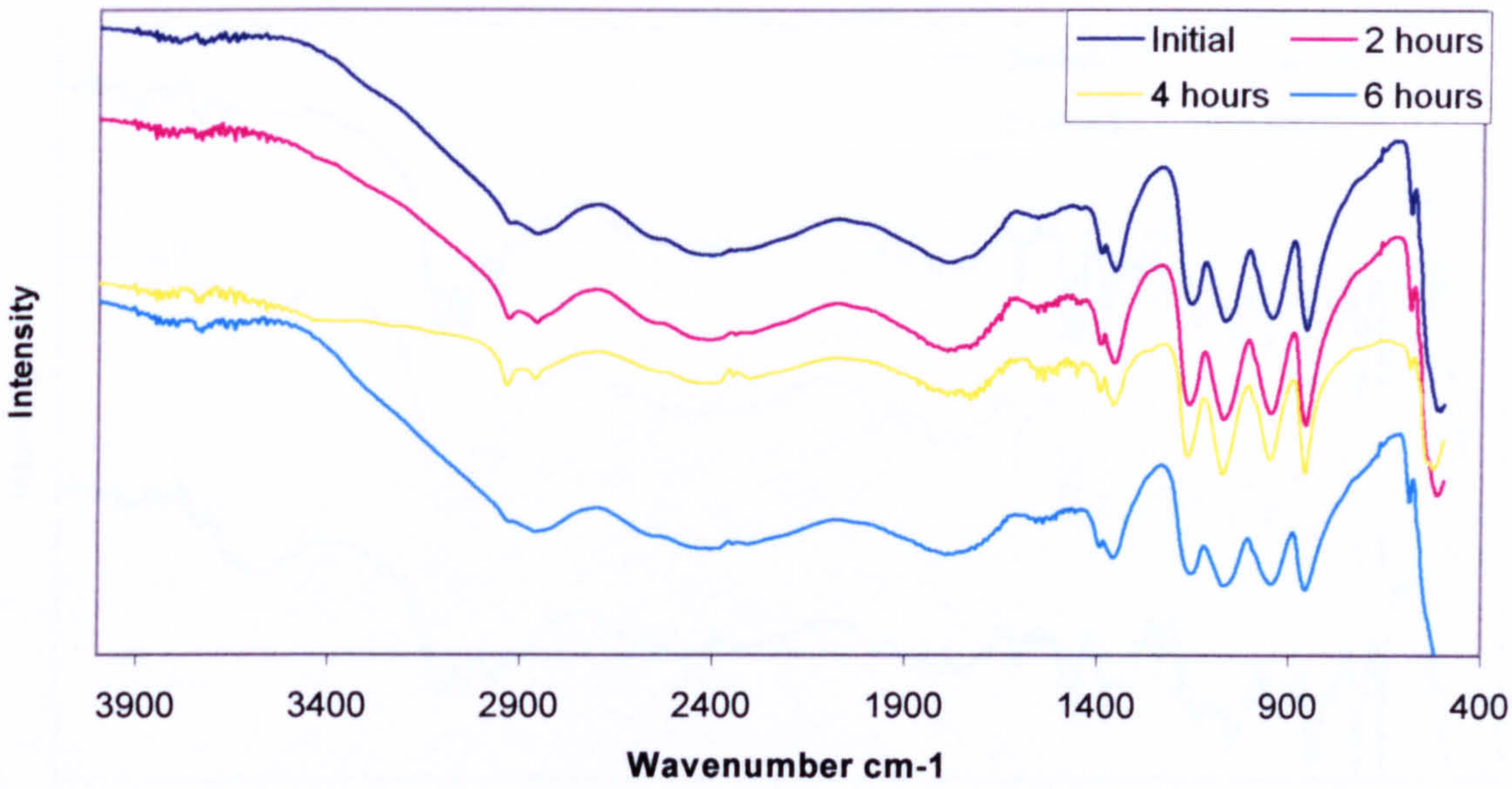


Figure 5.10. DRIFT spectra of sodium phosphate with cyclohexene oxide

When the phosphate system was analysed by IR, results were obtained that lead to similar conclusions to those observed through DRUV. Figure 5.10 illustrates that there is no observable reaction between the two compounds over the 6 hour period. However, it appears that the peaks in the 800-1200cm$^{-1}$ region are very broad and it is probable that these peaks are due to the phosphate as opposed to any of the organic species (figure 5.11).

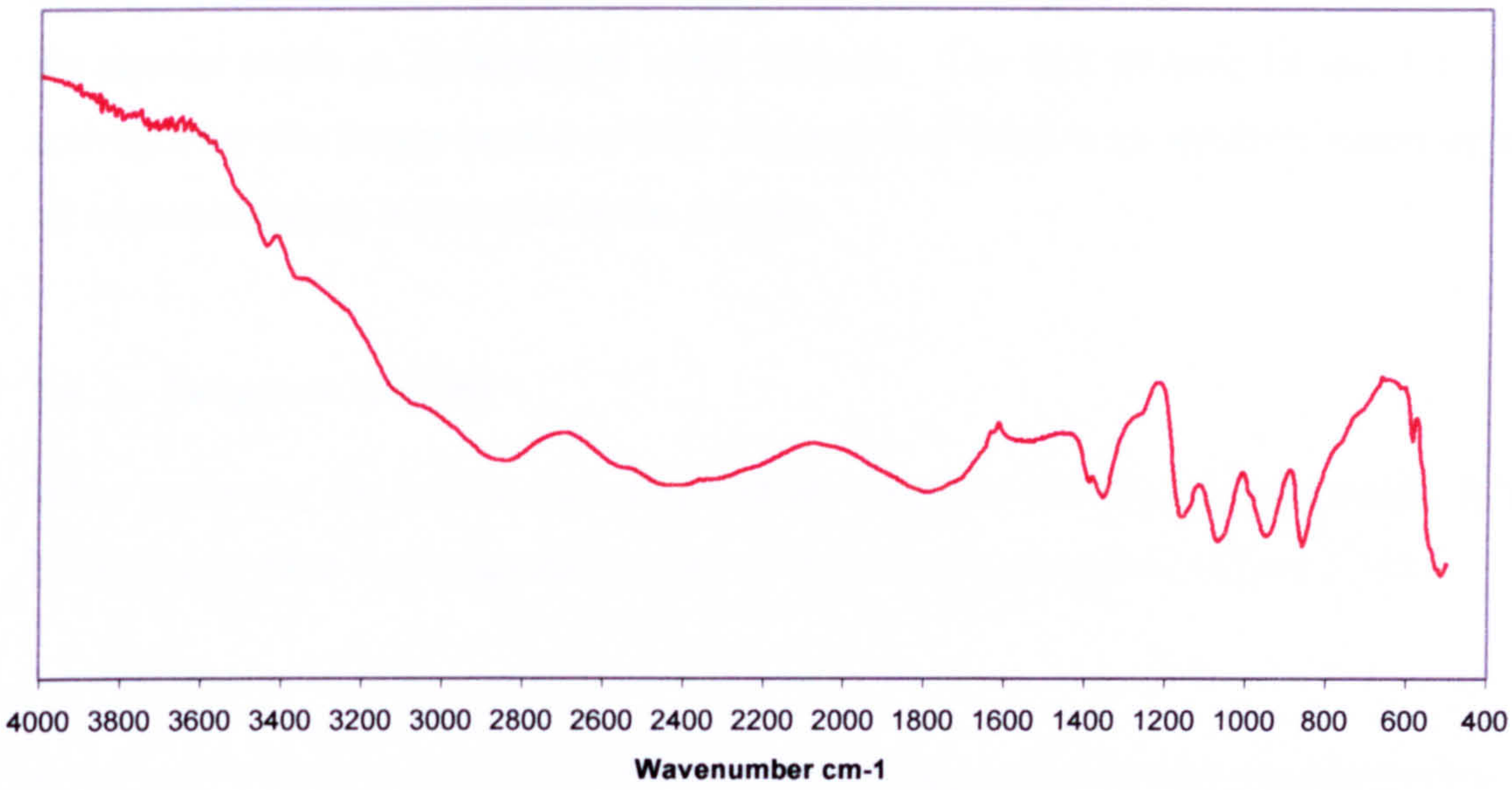


Figure 5.11. DRIFT spectrum of sodium phosphate

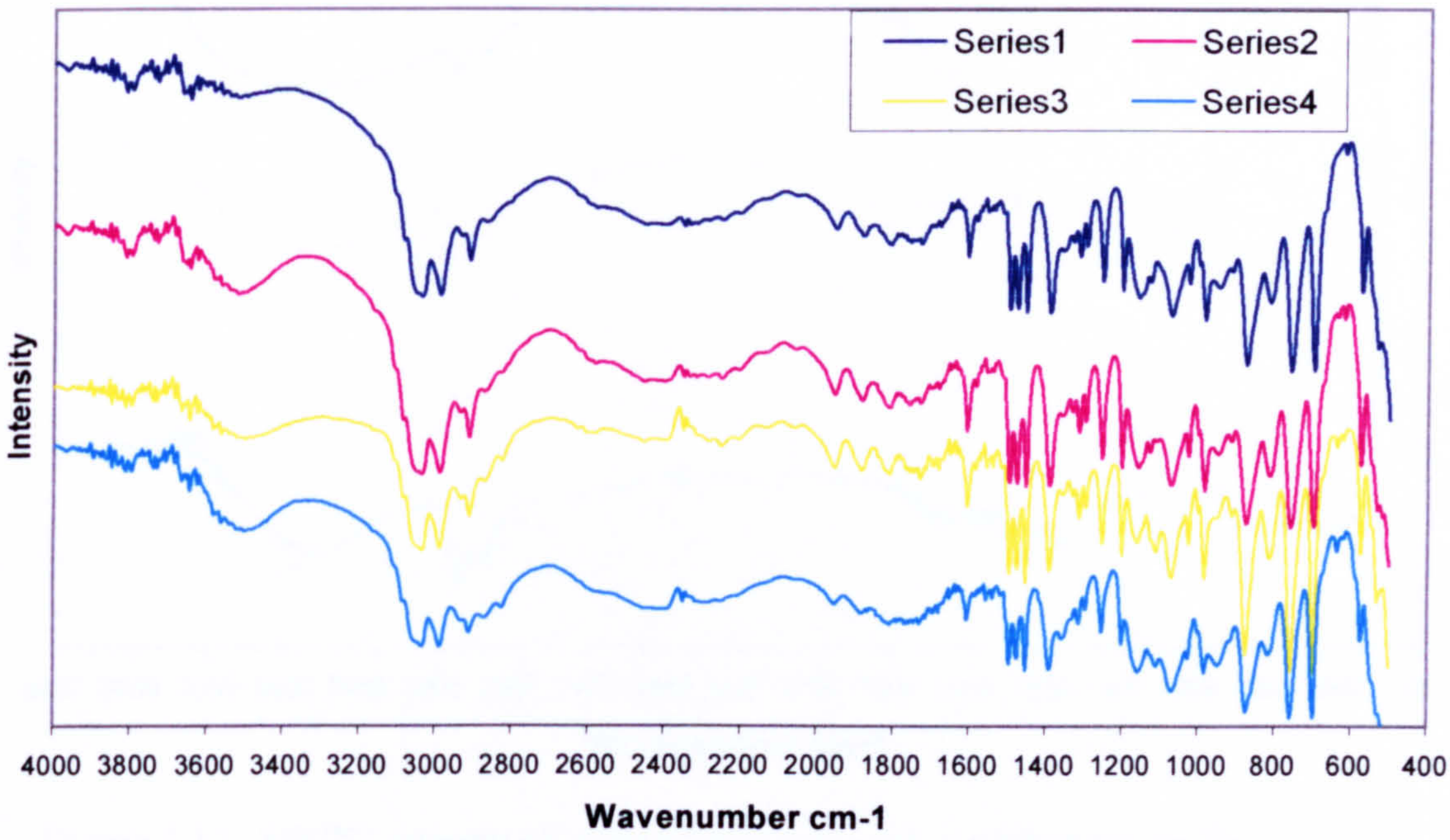


Figure 5.12. DRIFT spectra of sodium phosphate with styrene oxide

When the cyclohexene oxide was replaced with styrene oxide the organic peaks of the epoxide were able to be observed (figure 5.12). However, it is clear from these spectra that there are no changes occurring, be it peak shape changes or new peak formation, in the IR over a 6 hour period.

A further investigation was conducted to see whether a reaction occurred over a 24 hour period, however, there were still no detectable changes in the spectra for either the styrene oxide or cyclohexene oxide systems. The lack of both IR and UV-vis activity over this longer period of time suggests that there is no reaction occurring at all when phosphate is included in the system.

### *5.4.2 Tungstate analysis*

When analysing the system including sodium tungstate and cyclohexene oxide, it is immediately clear that tungstate is more active than the phosphate (figure 5.13).

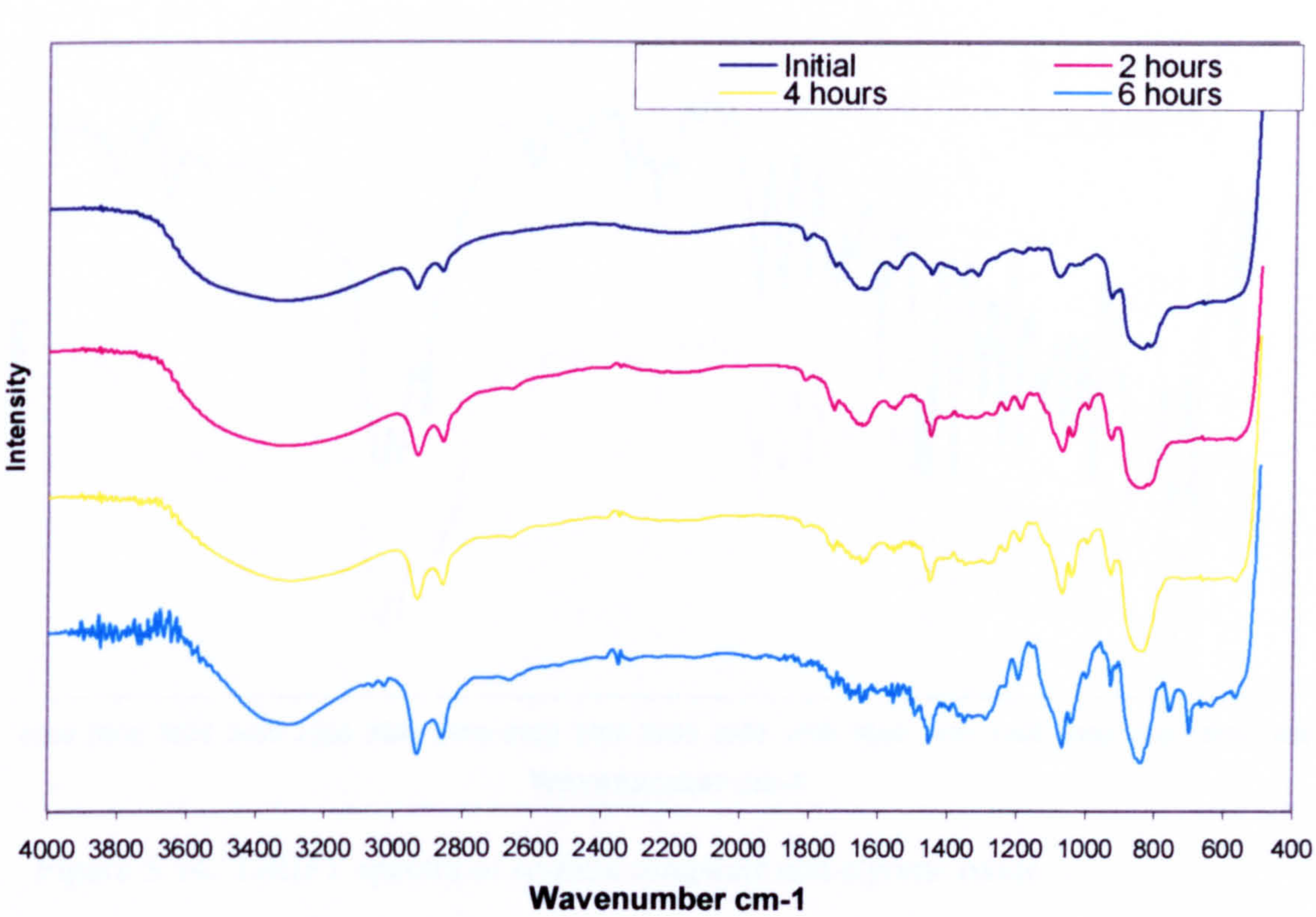


Figure 5.13. DRIFT spectra of sodium tungstate with cyclohexene oxide

It can be observed in the DRIFT spectra that there is a new peak forming at 995cm$^{-1}$. It is likely that this is due to the opening of the epoxide ring[27]. Other changes in the spectrum are those associated with the broad tungstate peak at approximately 830cm$^{-1}$ [28]. This region changes from two distinct peaks in the 0 hour spectrum into one sharp peak after 6 hours. This suggests that there is a change in the tungstate molecule which could be due to an alteration in the shape and hence oxidation state.

The sharp peaks at 700cm$^{-1}$ and 750cm$^{-1}$ in the spectrum after 6 hours are due to residual methanol in the sample.

When sodium tungstate was refluxed with styrene oxide, small changes were visible in the DRIFT spectra at 1350cm$^{-1}$ and 1030cm$^{-1}$ (figure 5.14). Both of these peaks have been shown to correspond to a change in the C-O region, due to the opening up of the epoxide ring[29,30]. The corresponding epoxide change in the cyclohexene oxide reaction suggests that tungstate is working in a similar manner to how chromate operates.

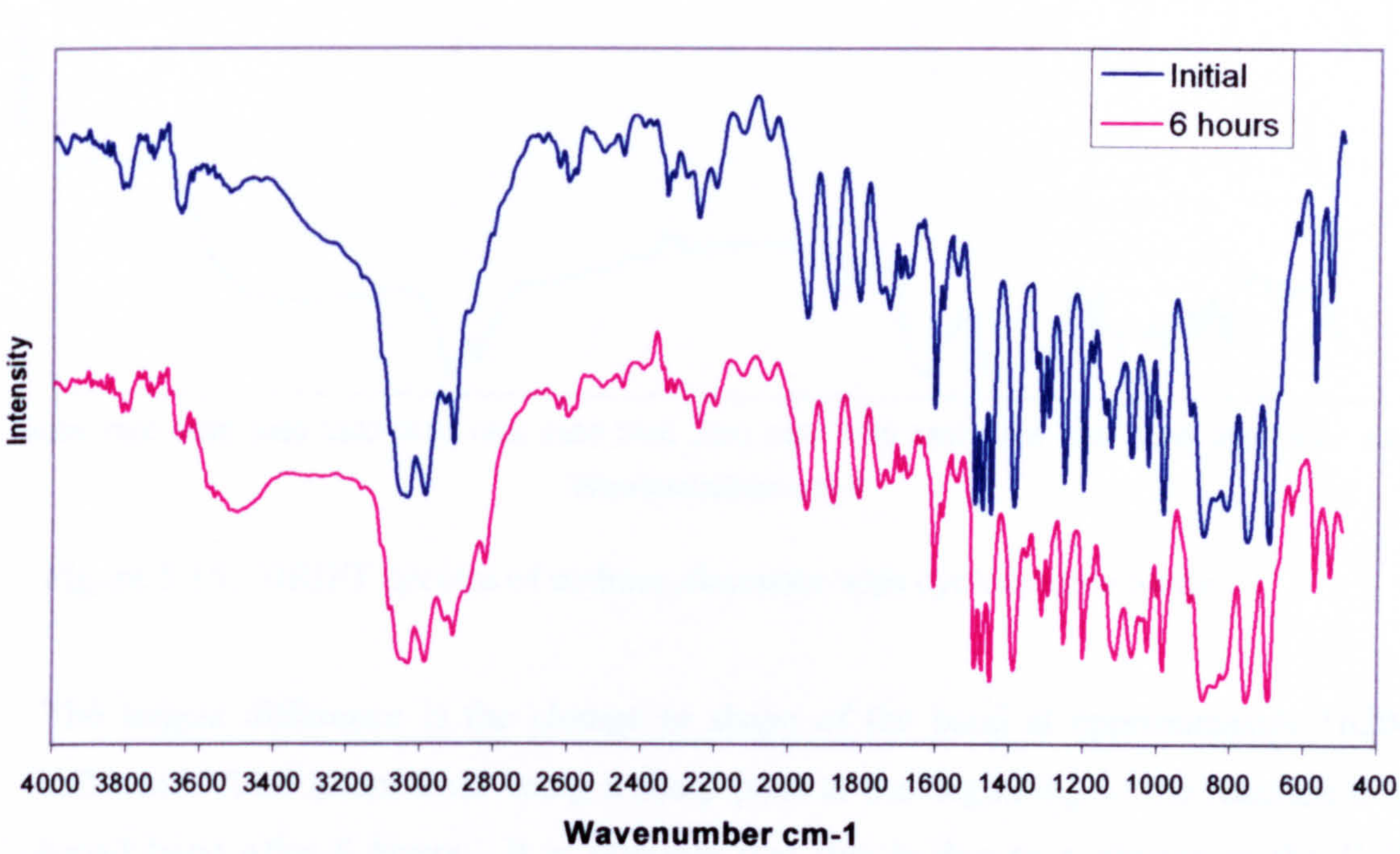


Figure 5.14. DRIFT spectra of sodium tungstate and styrene oxide

### *5.4.3 Zirconate analysis*

As the DRUV analysis had shown zirconate to be the most reactive of the three alternatives, it was proposed that this would be confirmed through IR. It was hoped that there would be more substantial changes in the spectra than those observed for either phosphate or tungstate.

Figure 5.15 shows the spectrum for sodium zirconate and cyclohexene oxide. It is noticeable that there are more substantial changes than in the phosphate and tungstate spectra.

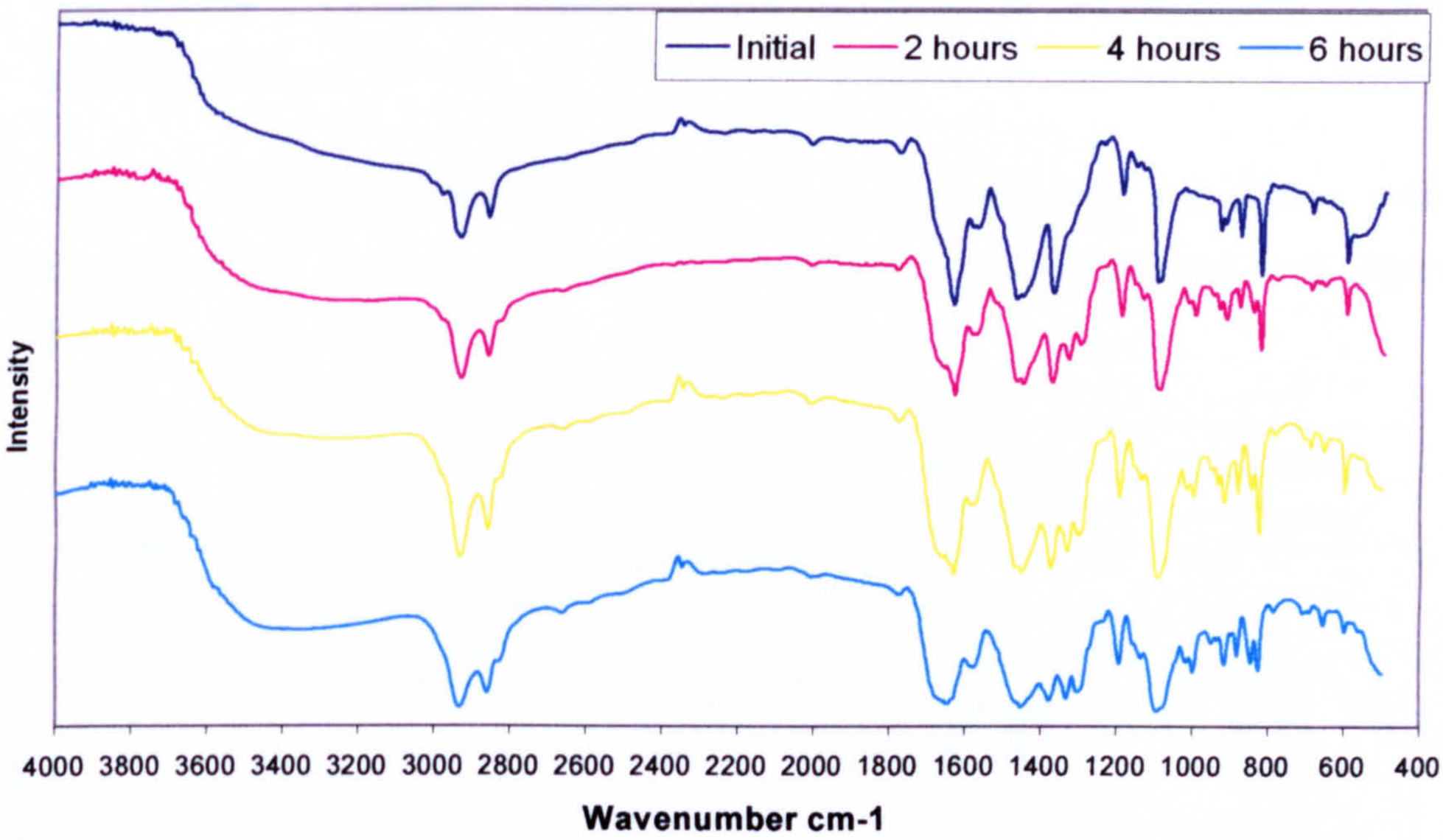


Figure 5.15. DRIFT spectra of sodium zirconate with cyclohexene oxide

The largest difference is the change in shape of the band at approximately 1620-1630cm$^{-1}$. This alters from being a sharp peak at the beginning of the reaction to a broad band after 6 hours. It is possible that this is due to a change in the O-H bending mode. However, it is difficult to attribute signals to certain peaks in this particular area of the infrared spectrum and it is therefore possible that this change in shape is due to the formation of various oxidised products as was seen in the LC-MS experiments in Chapter 4. It is probable that if zirconate is acting in a similar method

to chromate then carbonyl species would be formed following the oxidation of the cyclohexene oxide ring and C=O species would show a signal at this point in the IR.

Another large change occurs in the spectra at approximately 1325cm$^{-1}$ and 1295cm$^{-1}$. At the beginning of the reaction, DRIFT shows that there are shoulders visible at these regions. However, after 2 hours the peaks are clearly visible and become stronger after 4 and 6 hours respectively. The increasing intensity of these peaks is due to alterations in the compound's structure due to the opening of the epoxide ring[31] as figure 3.03 shows, this area of the spectrum is where ether linkages are present.

The spectra also show strong O-H stretches at 3500cm$^{-1}$, C-H stretches at 2920cm$^{-1}$ and 1950cm$^{-1}$. The strong peak at 1074cm$^{-1}$ is due to the Zr-O stretching mode in sodium zirconate.

When analysing the DRIFT spectra for the sodium zirconate and styrene oxide system, similar results can be seen as when cyclohexene oxide was used (figure 5.16).

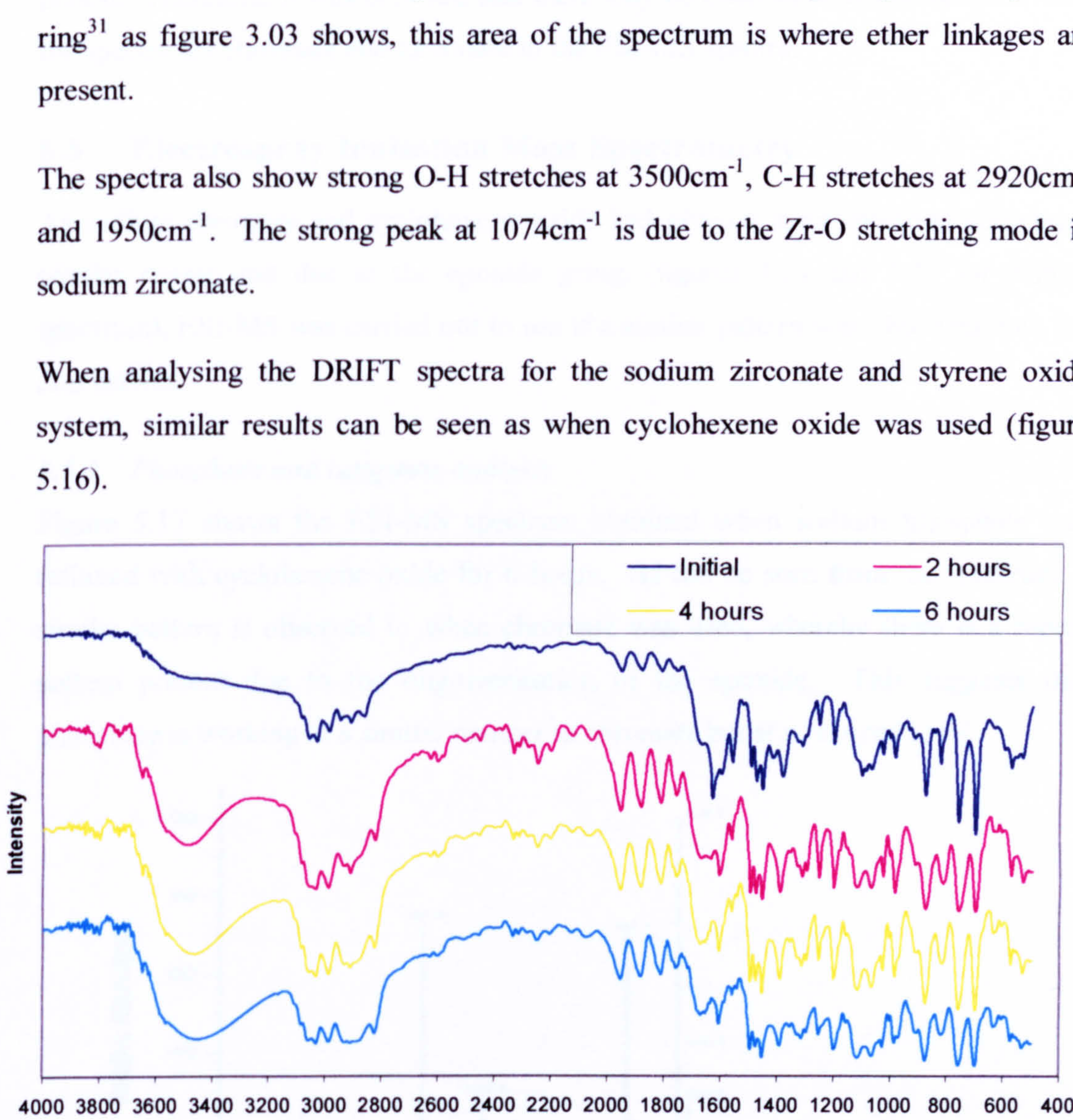


Figure 5.16. DRIFT spectra of sodium zirconate with styrene oxide

Again, there is a large change in the spectra at approximately 1630-1640cm$^{-1}$, however, this time there are new peaks arising at 1100cm$^{-1}$. These latter changes are again due to the opening of the epoxide ring but are at a different energy from those in the cyclohexene oxide spectra due to the change in group that the epoxide is attached to. It appears from the DRIFT spectra that the effects caused by zirconate are complete after 2 hours as there is little or no change to the spectra after this time. This was different to chromate where changes could still be observed after the 6 hour period. Therefore, it was believed that there may be observable differences between the spectra for chromate and zirconate in the ESI-MS spectra.

## 5.5 Electrospray Ionisation Mass Spectrometry

As sodium chromate and cyclohexene oxide had given a mass spectrum showing a regular repeat unit due to the epoxide group (figures 3.24 and 3.25 for control spectrum), ESI-MS was carried out to see if a similar pattern was observed with the alternatives.

### *5.5.1 Phosphate and tungstate analysis*

Figure 5.17 shows the ESI-MS spectrum obtained when sodium phosphate was refluxed with cyclohexene oxide for 6 hours. As can be seen from the spectrum, a similar pattern is observed to when chromate was used, whereby there is a repeat pattern present due to the oligomerisation of the epoxide. This suggests that phosphate is working in a similar manner to chromate but at a reduced level.

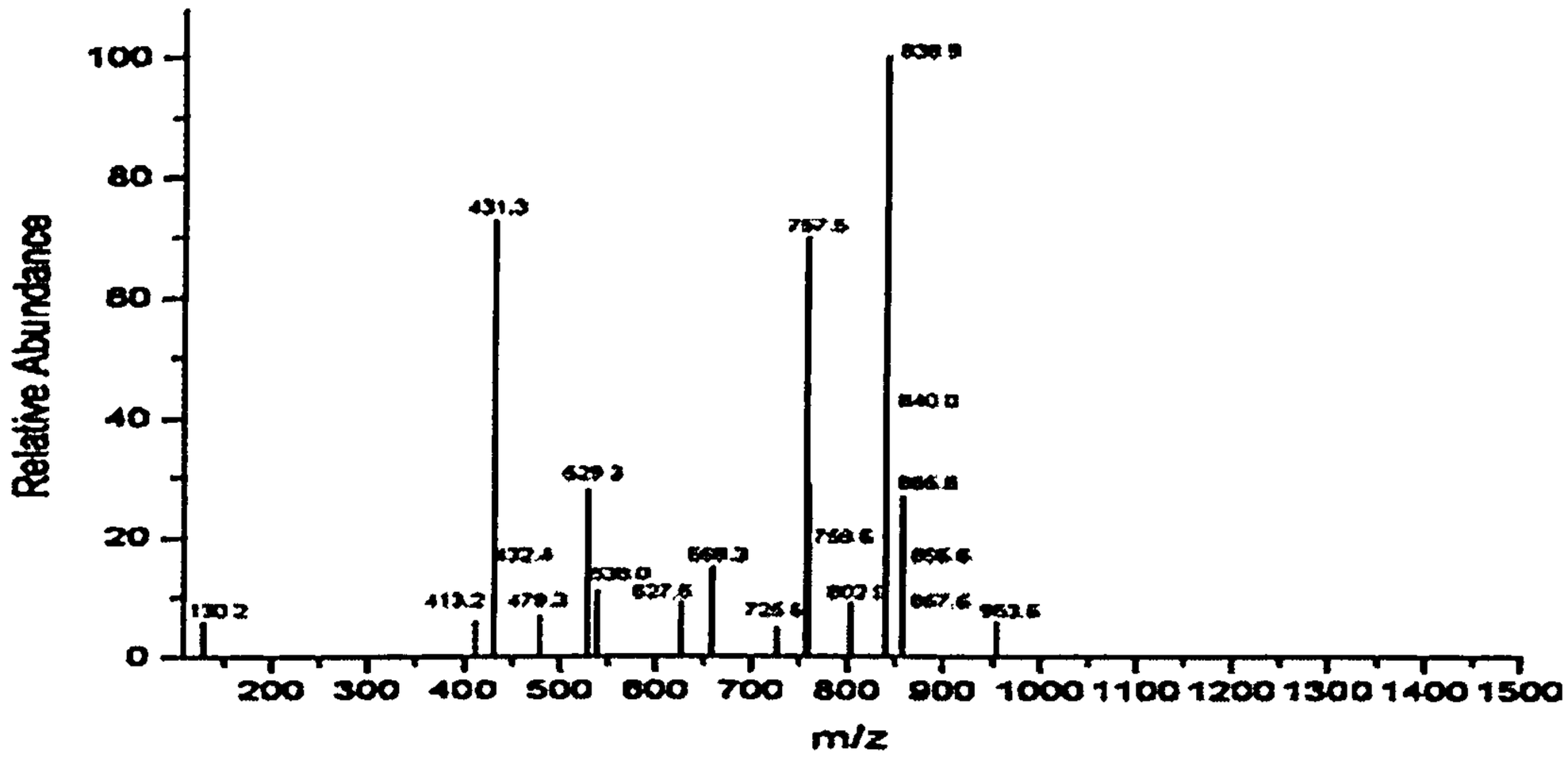

Figure 5.17. ESI-MS spectrum of sodium phosphate and cyclohexene oxide after 6 hours at 60°C

The spectrum is very similar to the original result obtained in Chapter 2 whereby there is a series of repeat units 431-529-627-725 followed by a large peak at 838 suggesting that this oligomer has a methyl end capping group attached to it. A similar result was observed when phosphate was replaced with tungstate (figure 5.18) again suggesting that tungstate is performing in a similar manner to chromate.

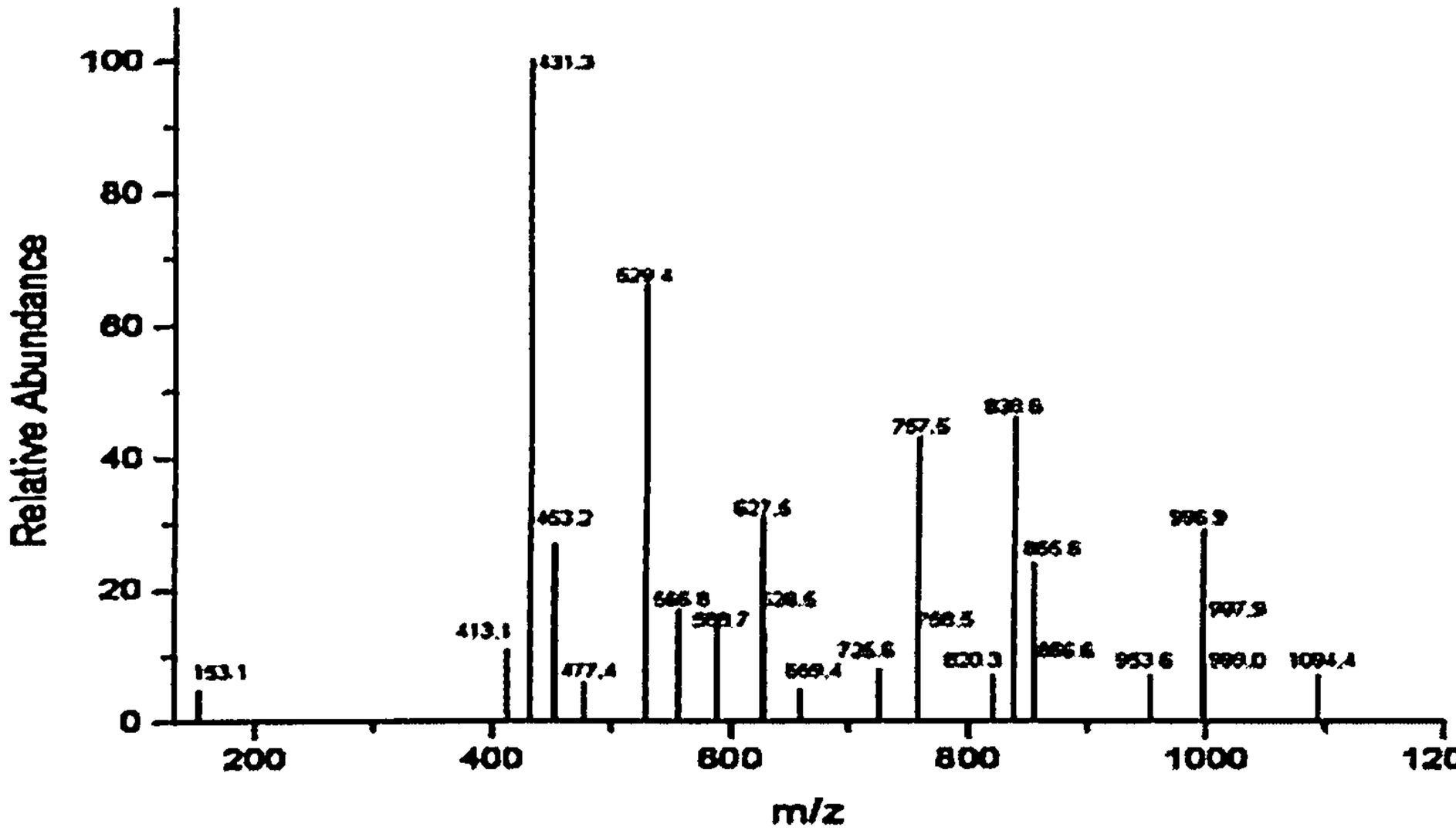


Figure 5.18. ESI-MS spectrum of sodium tungstate and cyclohexene oxide after 6 hours at 60°C

### *5.5.2 Zirconate analysis*

However, when sodium zirconate was refluxed with cyclohexene oxide, a completely different spectrum was observed (figure 5.19). In this instance, although the repeating pattern observed with the other compounds was present, there were also many other intense peaks. The appearance of these additional peaks suggests that although zirconate is acting in a similar manner to chromate it works much more quickly and is causing further extensive fragmentation of the molecules. This confirms what was observed in the IR experiments whereby the effects from the zirconate have subsided after 2 hours.

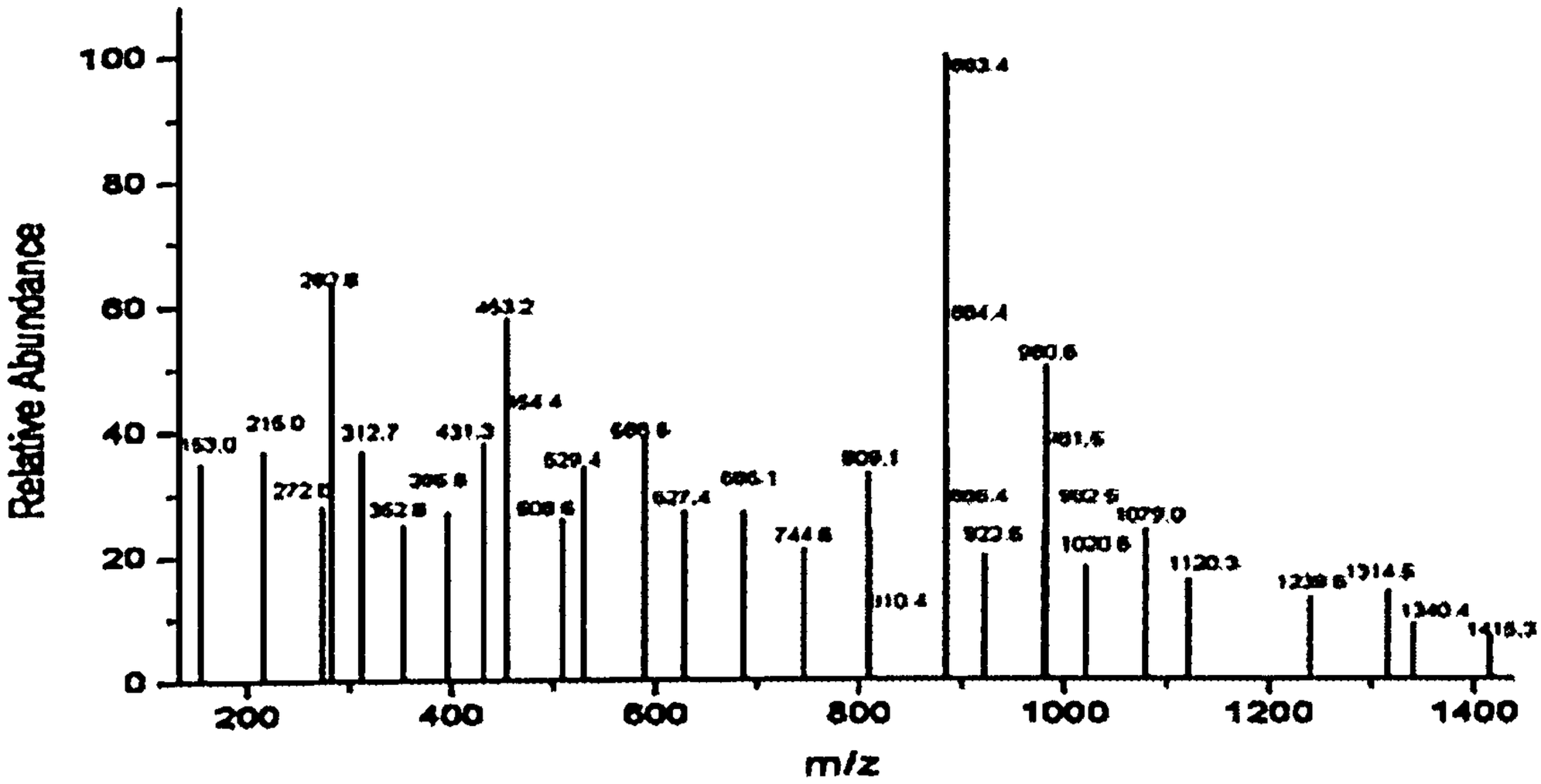


Figure 5.19. ESI-MS spectrum of sodium zirconate and cyclohexene oxide after 6 hours at 60°C

To investigate whether zirconate was acting in a kinetically greater way to chromate and the other alternatives or whether its mechanism was completely different, a further experiment was conducted. Here, the system was refluxed for one hour and then analysed immediately by ESI-MS (figure 5.20).

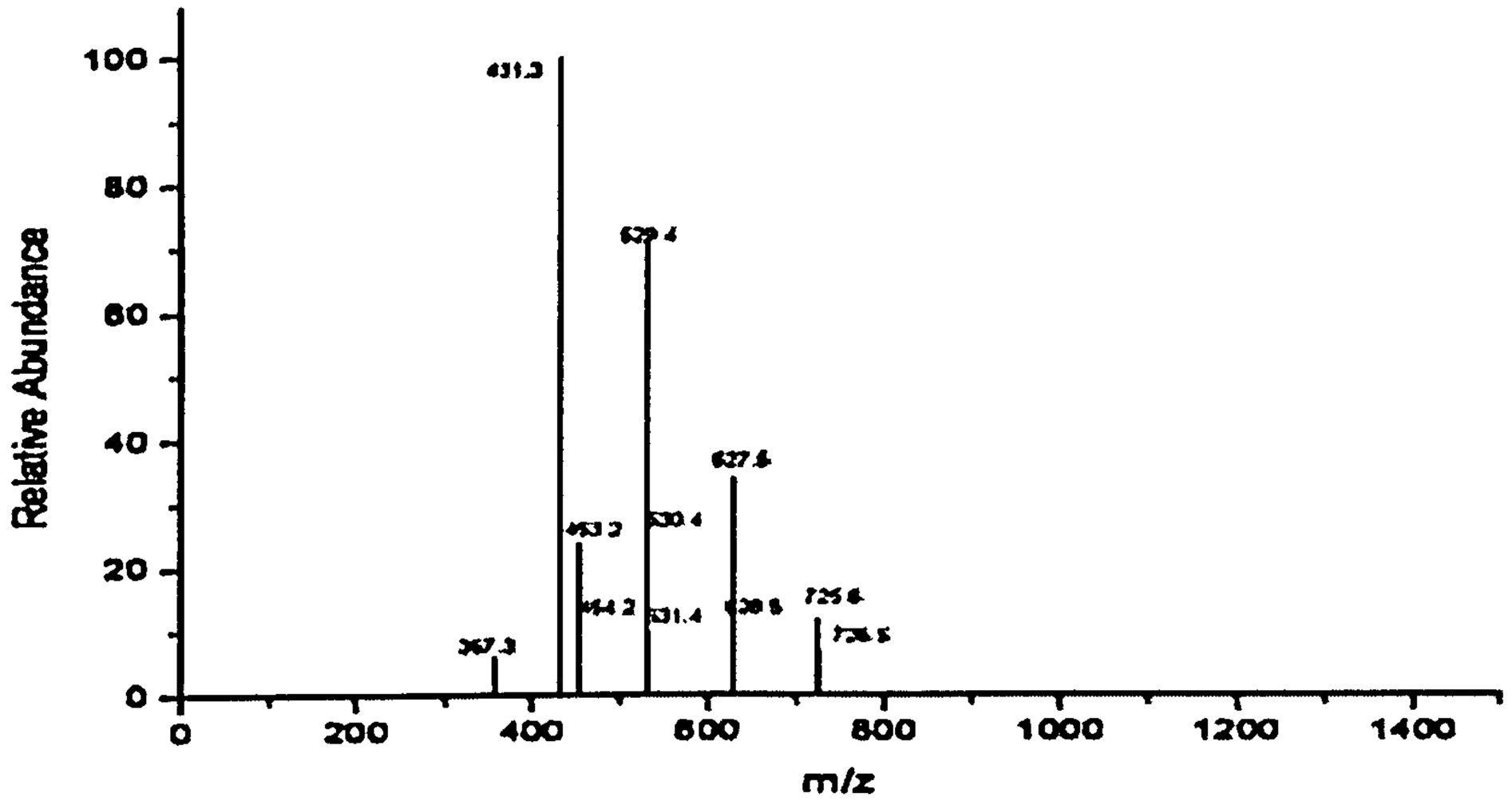


Figure 5.20. ESI-MS spectrum of sodium zirconate and cyclohexene oxide refluxed for 1 hour at 60°C

Since the spectrum obtained is very similar to those of chromate and the other alternatives it is clear that the differences in figure 5.19 are merely due to the fact that zirconate reacts with cyclohexene oxide at a much higher rate than the other compounds.

As the increased rate of reaction had been illustrated through both IR spectroscopy and mass spectrometry, it was believed that it would also be observable through $^{13}$C-NMR spectroscopy which had effectively shown the epoxide oligomerising in the chromate system.

## 5.6 $^{13}$C-NMR Spectroscopy

The chromate system involving styrene oxide had given changes of a greater intensity in $^{13}$C-NMR compared to the cyclohexene oxide system and it was therefore decided to concentrate on this for investigating the potential of the alternatives.

### *5.6.1 Phosphate analysis*

Since phosphate had shown some activity by ESI-MS analysis it was believed that $^{13}$C-NMR would also give a positive outcome due to it being one of the best methods for observing oligomerisation with chromate.

As with the chromate system no changes were observed in the NMR when using phosphate after 6 hours of refluxing. However, similarly to chromate, after 24 hours, several new peaks could be seen (figures 5.21 a & b).

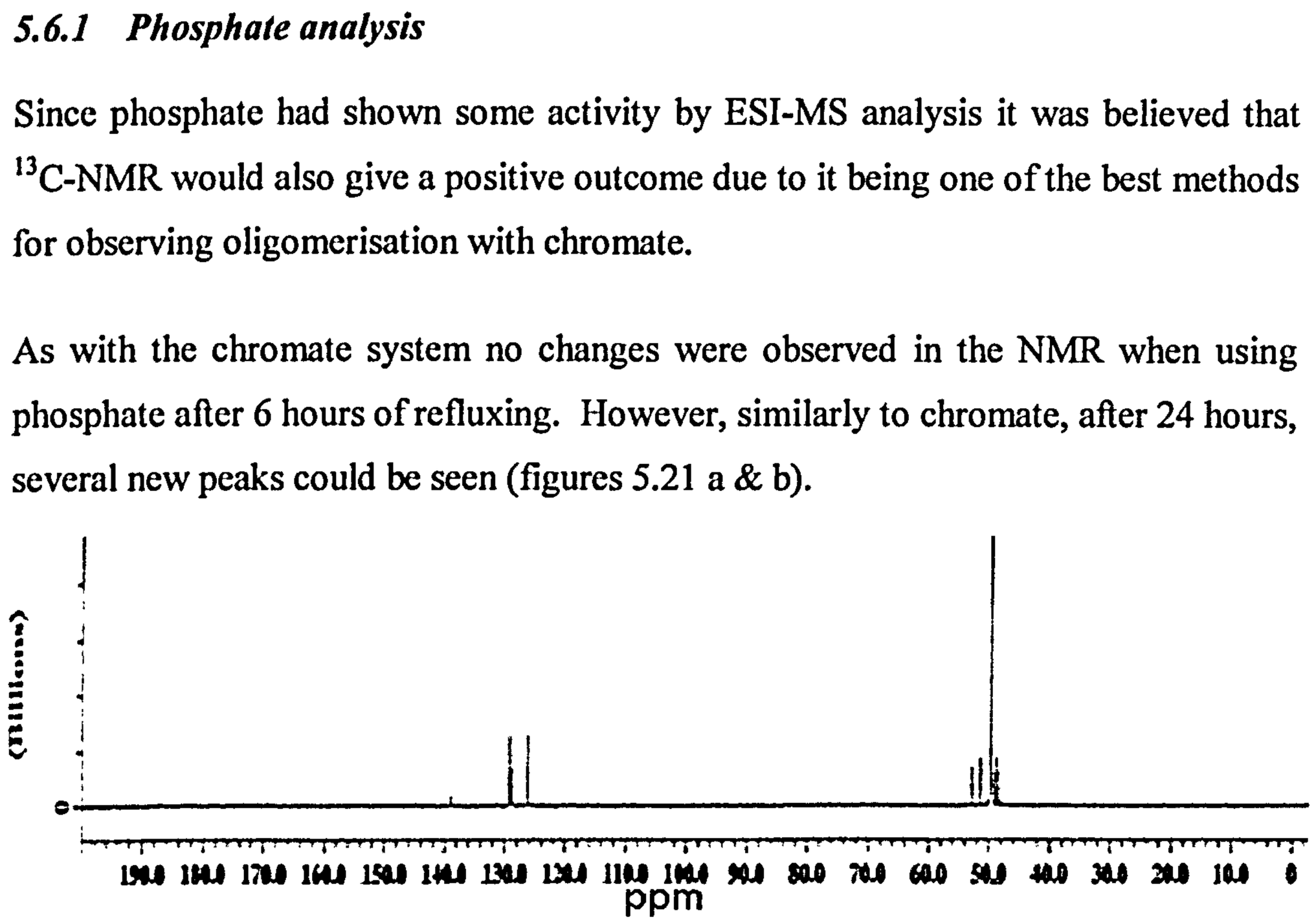


Figure 5.21a. $^{13}$C-NMR spectrum of sodium phosphate and styrene oxide at the beginning of reaction

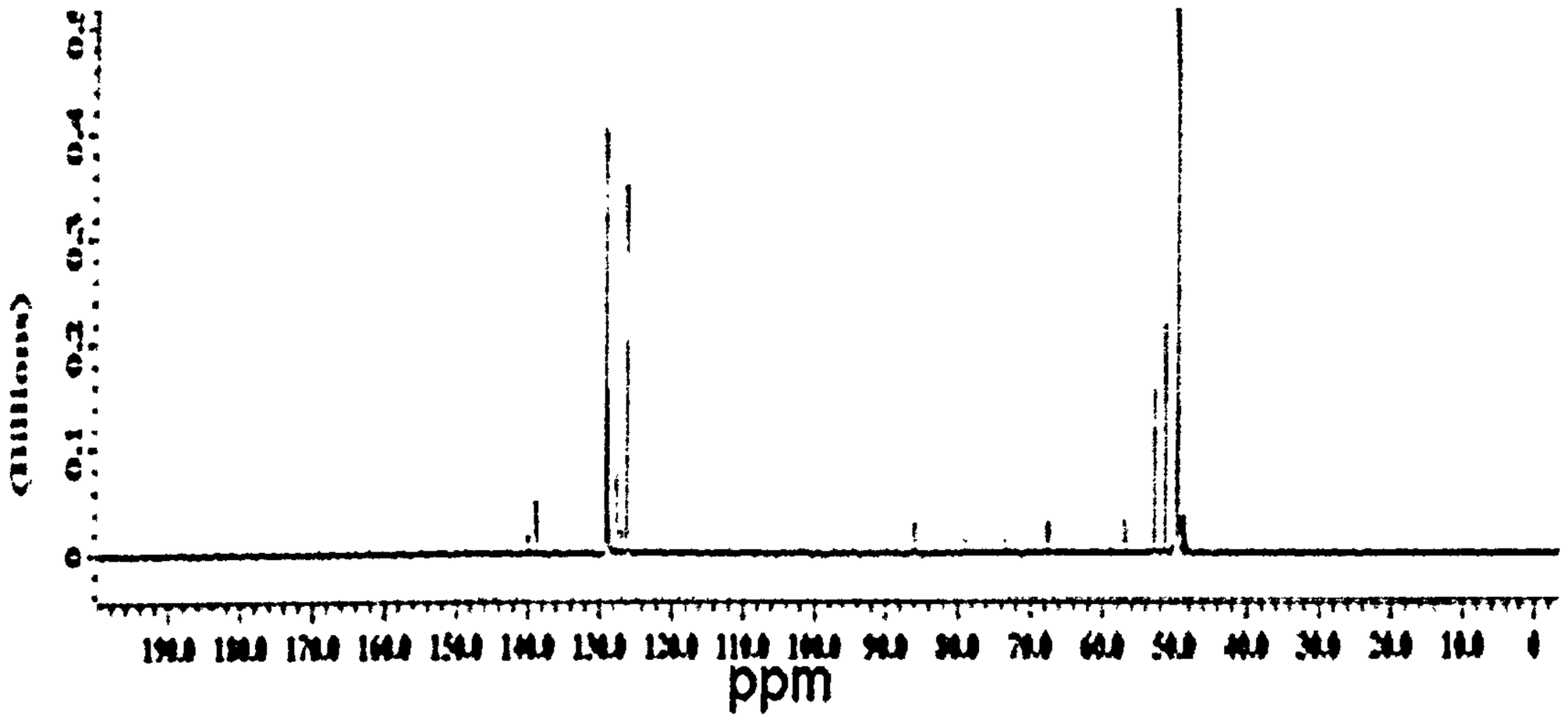


Figure 5.21b. $^{13}$C-NMR spectrum of sodium phosphate and styrene oxide after 24 hours of refluxing at 60°C

The new peaks occur in the same positions as peaks in the chromate system spectrum and therefore it is possible to say that phosphate may be acting in the same manner.

### *5.6.2 Tungstate analysis*

When phosphate was substituted with tungstate, a similar result was obtained, i.e. there was no reaction after 6 hours but after 24 hours new peaks assigned to oligomerisation could be observed (figure 5.22).

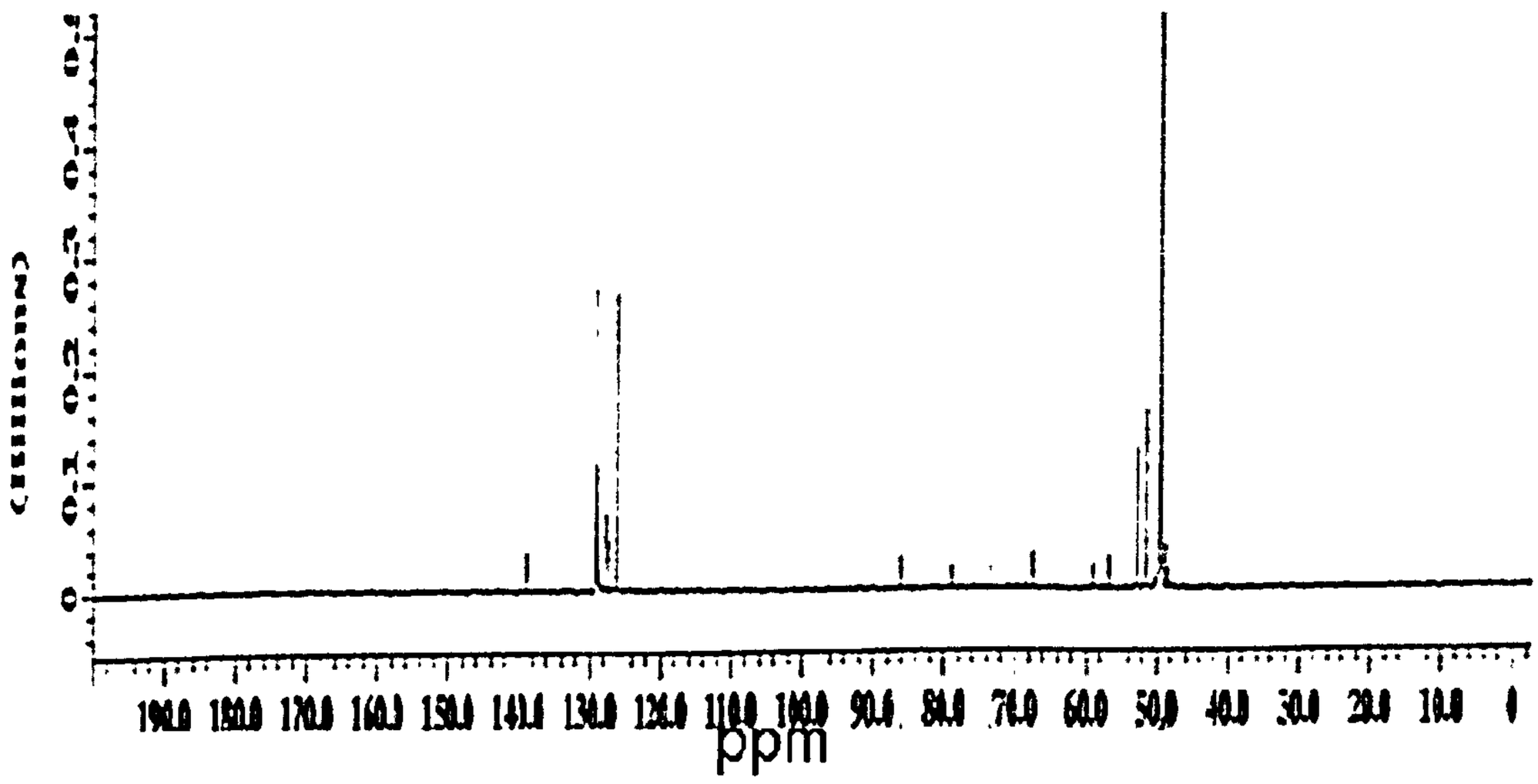


Figure 5.22. $^{13}$C-NMR spectrum of sodium tungstate and styrene oxide after 24 hours of refluxing

### *5.6.3 Zirconate analysis*

However, when zirconate was used, major differences were seen when compared to the chromate and other alternative systems. Whereas none of the other compounds had shown any activity using NMR after 6 hours of refluxing, zirconate showed similar changes as were observed with DRIFT and ESI-MS. As can be seen in figure 5.23, the same peaks due to oligomerisation are present after 6 hours of refluxing.

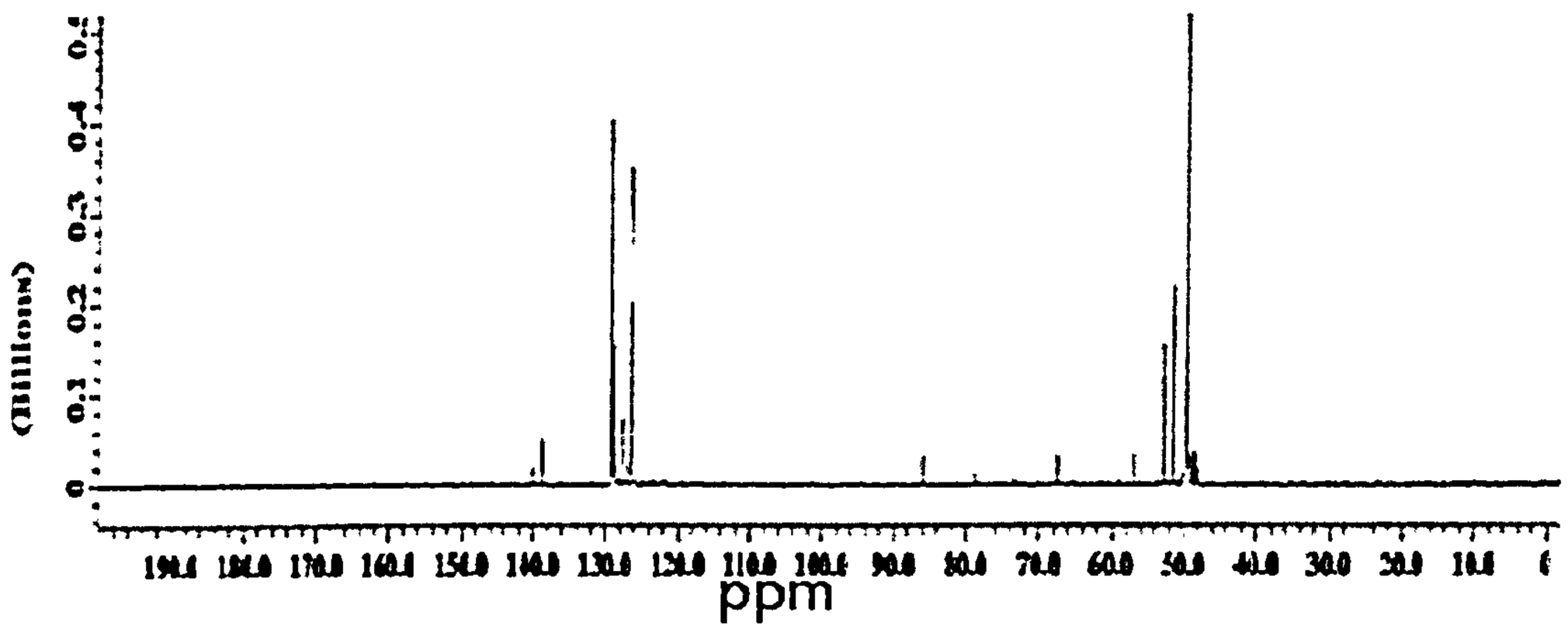


Figure 5.23. $^{13}$C-NMR spectrum of sodium zirconate and styrene oxide after 6 hours of refluxing

After further time refluxing there were no additional changes to the NMR spectrum confirming that the oligomerisation was complete. However, after a shorter period of reaction, only 3 hours, the same oligomerisation peaks were visible at lower intensity (figure 5.24).

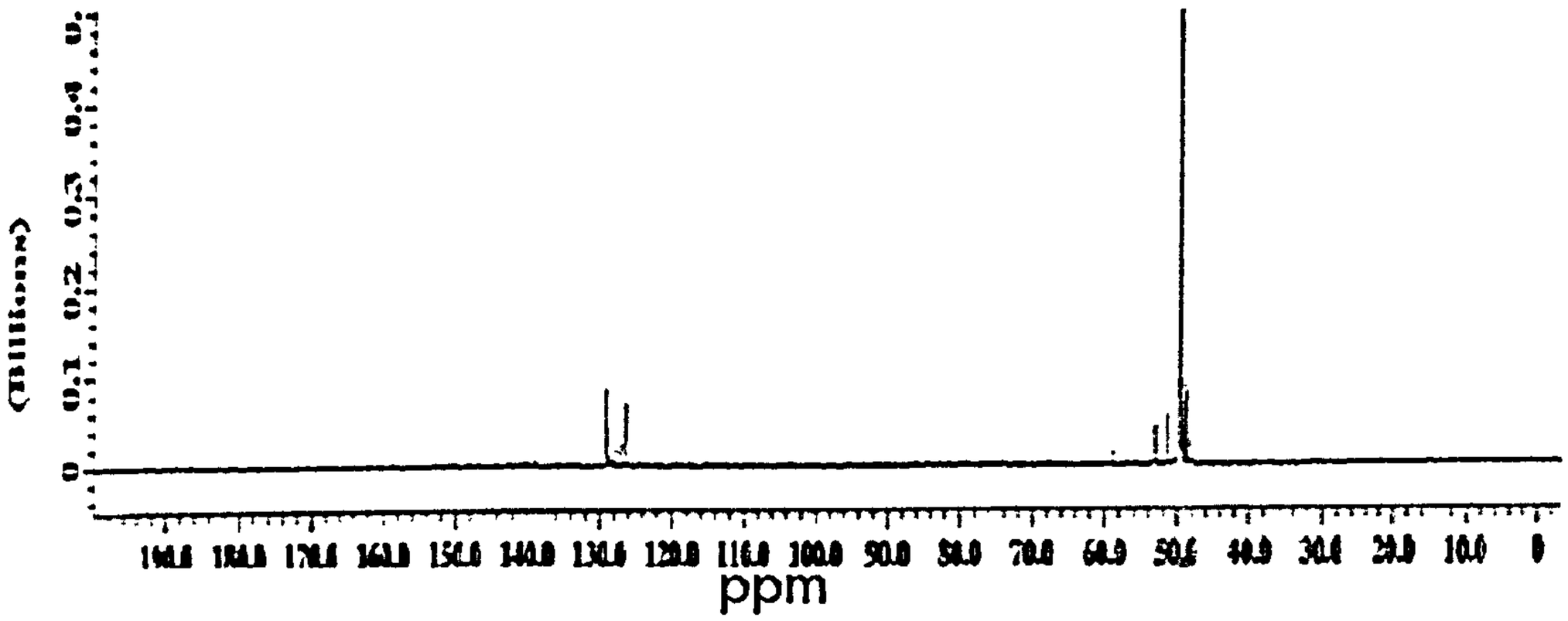


Figure 5.24. $^{13}$C-NMR spectrum of sodium zirconate and styrene oxide after 3 hours of refluxing

The presence of the oligomerisation peaks after this short period of time agrees with the results from the other analytical techniques used, suggesting that zirconate carries out the same functions as chromate but at a higher rate.

## 5.7 Conclusions

It is believed that to be a replacement for chromate, any successful alternative must possess three major chemical characteristics; the ability to act as a Lewis acid catalyst for the oligomerisation of epoxides, to have a strong Al-O-X bond and to be environmentally benign. It is also thought that a certain level of redox activity may be important to the process as this was observed with chromate. From this series of experiments and the resulting analysis, several conclusions can been determined as to the success of the three tested alternatives.

Firstly, it is clear that all three of the chosen alternatives have some effect on the chemical behaviour of the epoxide. However, from the results obtained it is also apparent that each of the alternatives behaves with differing amounts of success.

Of the three alternatives, phosphate appears to be the least likely to be a successful alternative. This is because of its lack of redox activity illustrated in DRUV spectroscopy and its apparent lack of activity in DRIFTS through which changes had been observed in the chromate system. However, phosphate does show similar levels of activity to chromate in $^{13}$C-NMR and ESI-MS suggesting that it is able to function as an effective Lewis acid catalyst for the oligomerisation of the epoxides.

Tungstate appears to be the second most successful alternative of those tested. DRUV analysis shows a low level of reactivity between the tungstate and the epoxide, however, the lack of a substantial change in the d-d transition region suggests that there is no redox reaction occurring. Changes in the C-O region and the corresponding new peaks in $^{13}$C-NMR & peak pattern in ESI-MS suggest that tungstate is acting in a similar fashion to chromate in that it is again able to act as a Lewis acid catalyst for the ring opening oligomerisation of the epoxides.

By analysing the results with time it is also possible to say that both phosphate and tungstate work on a similar kinetic scale to chromate with respect to their catalytic properties of epoxides.

When observing the analytical results, it is immediately clear that of the three tested alternatives, zirconate would be the most successful replacement for chromate. This is because it shows quite a high level of activity in the DRUV spectra, some of which is probably due to a redox reaction with zirconium passing from a +4 state to a +3 state. There are also clear changes in the C-O region in the DRIFT spectra corresponding to the opening of the epoxide ring. However, the key factor to its success is that kinetically speaking, zirconate acts on a greater level to chromate and the other two alternatives tested. This is observed in both $^{13}$C-NMR where zirconate showed peaks due to oligomerisation after a much shorter time, 6 hours as opposed to 24 hours, and ESI-MS where zirconate illustrated the distinctive oligomerisation pattern after 1 hour instead of 6 hours that the other compounds had shown.

## 5.8 References


1. Hamdy, A.S., *Progress in Organic Coatings,* 56, 2-3, 146, 2006.
2. Emregul, K.C., Aksut, A.A., *Corrosion Science*, 45, 2415, 2003.
3. United States Patent, Number 6468364.
4. Twite, R.L., Bierwagen, G. P., *Progress in Organic Coatings,* 33, 91, 1998.
5. Monte, S.J., Sugerman, G., *Titanate Coupling Agents in Coatings*, 1979.
6. Monte, S.J., Sugerman, G., *Modern Paint and Coatings*, April 1980.
7. Ken React Reference Manual, Kenrich Petrochemical, Inc.
8. Pardo, A., *Electrochimica Acta*, 2006 In Press.
9. Bethencourt, M., Aballe,A., Botana, F.J., Marcos, M., *Journal of Alloys and Compounds,* 323–324, 855, 2001.

10. Freeman, D.B., *Phosphating and Metal Pre-treatment*, Industrial Press Inc, 1986.
11. Menke, J.T., *Products Finishing*, 5660, 1994.
12. Sun, X., Susac, D., Li, R., Wong, K.C., Mitchell, K.A.R., Foster, T., *Surface and Coatings Technology,* 155, 46, 2002.
13. Morks, M.F., *Materials Letters,* 58, 26, 3316, 2004.
14. Ngala, V.T., Page, C.L., Page, M.M., *Corrosion Science*, 45, 1523, 2003.
15. Shibli, S.M.A., Saji, V.S., *Corrosion Science*, 47, 2213, 2005.
16. Van de Leest, R.E., Krijl, G., *Thin Solid Films*, 72, 2, 237, 1980.
17. Robertson, W.D., *Journal of the Electrochemical Society*, 98, 94, 1951.
18. Guannan, M., Li, X., Qu, Q., Zhou, J., *Corrosion Science* 48, 445, 2006.
19. Sastri, V.S., Bednar, J.S., *Materials Performance,* 29, 5, 44, 1990.
20. Voevodin, N.N., Grebasch, N.T., Soto, W.S., Kasten, L.S., Grant, J.T., Arnold, F.E., Donley, M.S., *Progress in Organic Coatings,* 41, 287, 2001.
21. Guinebretiere, R., Soulestin, B.,Dauger, A., *Thin Solid Films,* 319, 197, 1998.
22. Verdier, S., Van Der Laak, N., Dalard, F., Metson, J., Delalande, S., *Surface & Coatings Technology*, 200, 2955, 2006.
23. S. Mokerji, MascoTechInc., *Zirconium Nitride Coating,* U.S. Patent 6,168,242, Jan. 2, 2001.
24. Monte, S.J., Sugerman, G., *New Neoalkoxy Titanate and Zirconate Coupling Agents*, 1985.
25. Harasek, S., Wanzenboeck, H.D., Basnar,B., Smoliner, J., Gornik, E., Brenner, J., Stoeri, H., Bertagnolliet, E., *Thin Solid Films*, 414, 199, 2002.
26. Banwell, C.N., McCash, E.M., *Fundamentals of Molecular Spectroscopy*, McGraw Hill, London, 1994.
27. Memarian, H.R., Nikpour, F., *Molecules, 7*, 63, 2002.
28. Zorina, M.L., Syritso, L.F., *Journal of Applied Spectroscopy*, 16, 6, 1972.
29. Cambie, R.C., Denny, W.A., *Australian Journal of Chemistry*, 28, 5, 1153
30. Fooken, U., Liebezeit, G., *An IR Study of Humic Acids in Soils and Sediments*, Wilhelmshaven, Germany.
31. Qu, X., Wirsén, A., Albertssonet, A.C., *Journal of Applied Polymer Science*, 74, 13, 3186, 1999.

# Chapter 6

# Surface treatment

## 6.1 Introduction

As mentioned in Chapter 1, one of the simplest ways of generating superior adhesion performance is by altering the surface morphology of the metal substrate. In anodising aluminium, the naturally occurring aluminium oxide layer is made thicker by passing a current through an acidic solution, with the aluminium object serving as the anode (the positive electrode). The current releases hydrogen at the cathode (the negative electrode) and oxygen at the surface of the aluminium anode, creating a build up of aluminium oxide[1].

Conditions such as acid concentration, solution temperature and current must be controlled to allow the formation of a consistent oxide layer, which can be many times thicker than would otherwise be formed. Changes in these conditions can initiate the electrolyte used to cause impurities to arise in the oxide, resulting in a reduction of its beneficial properties[2].

The presence of the oxide layer increases both the hardness and the corrosion resistance of the aluminum surface. This is achieved by the formation of microscopic structures, each having a central hexagonal pore. These pores are also the reason that an anodized part can take on color in the dyeing process[3].

However, although the mechanism of anodisation is reported in the literature[4,5], there are still some issues that are unclear with respect to the properties achieved by the process.

This chapter will cover two such issues which arose from one of the network meetings that took place during the research. The first of these is the fact that there is a decrease in the adhesive performance of the anodised material with time, meaning that industrial manufacturers will not bond or apply primer coatings more than 3 hours after anodisation. The second issue is whether the anodisation process

can be used in conjunction with an organic based compound to provide a one-step alternative to the current pretreatment-priming procedure.

## 6.2 Experimental work

### *6.2.1 Acid etching*[6,7,8]

To gain a thorough understanding of the subject area, work began by looking at the most basic areas of surface pretreatment. Initially, simple chemical treatments such as etches in chromic acid, nitric acid and phosphoric acid were carried out using 1.0M acids at room temperature. On addition of aluminium to the acids, both chromic[6] and nitric appeared to show no effect to the metal. However, when the aluminium was added to the phosphoric acid, there was immediate effervescence which corresponds to a reaction occurring on the surface of the metal.

On removing the aluminium from the acids, the chromic and nitric treated samples still showed a glossy, shiny surface. The phosphoric acid treated sample, however, possessed a matt surface.

When the samples were observed in the SEM (figure 6.01), under low resolution all three samples showed similar roughened surfaces.

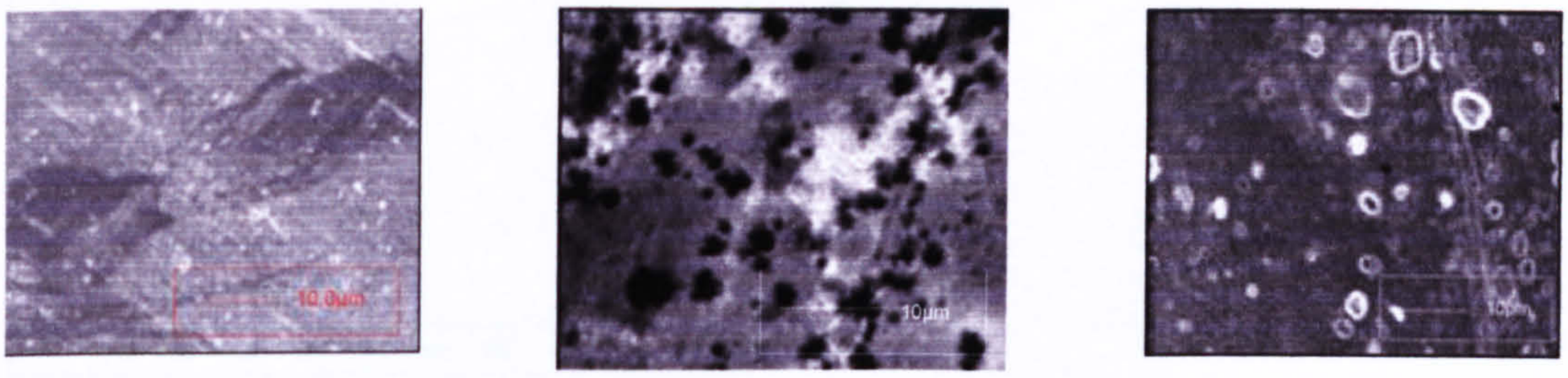


a b c

Figure 6.01. SEM images obtained at 10kV and 1000x magnification showing the effect of different acid etches on AA2024-T3 a. chromic b. nitric c. phosphoric

All three samples showed a surface that was covered with areas of micro roughness. However, when observed under higher resolution, the phosphoric acid treated sample showed a much more ordered surface (figure 6.02). Literature states that the other

two acids should give similar effects, however, in this study, only phosphoric acid gave this effect.

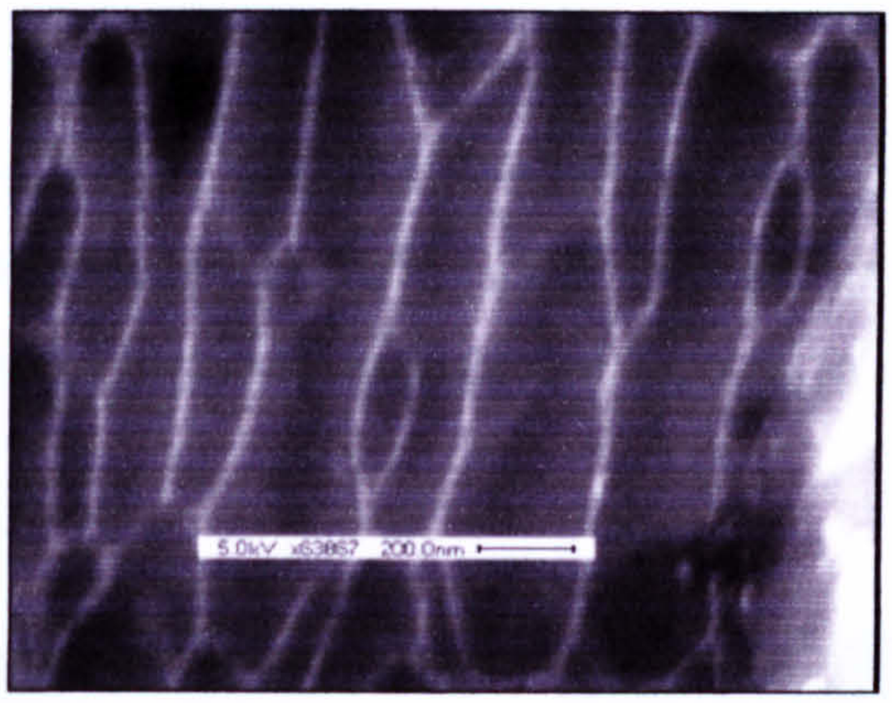


Figure 6.02. High resolution SEM obtained at 5kV and 63867x magnification of phosphoric acid etched AA2024-T3

EDX analysis of the sample (figure 6.03) showed an oxygen content of 14.19At% and an aluminium content of 76.95At% at the surface of the sample. Carbon is present in the analysis due to probable adsorption of organic species from the laboratory atmosphere onto the treated surface.

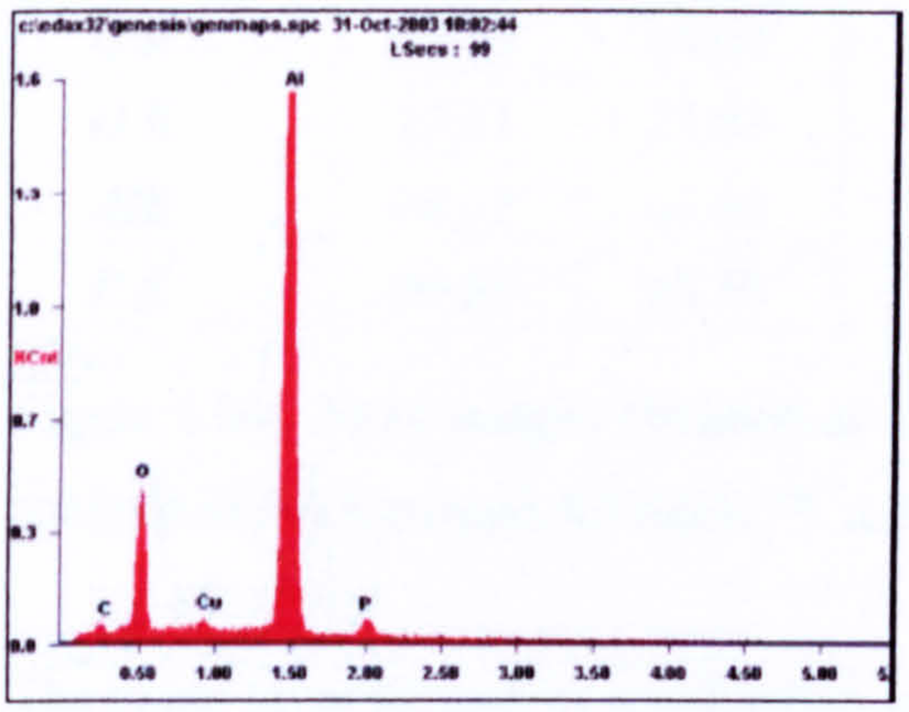


| *Element* | *Wt%* | *At%* |
|---|---|---|
| ***C K*** | 02.28 | 04.76 |
| ***O K*** | 09.05 | 14.19 |
| ***CuL*** | 01.65 | 00.65 |
| ***AlK*** | 82.76 | 76.95 |
| ***P K*** | 04.25 | 03.45 |

Figure 6.03. EDX analysis of the phosphoric acid etched AA2024-T3

A highly ordered surface, such as that achieved in this study by the phosphoric acid etch is more preferable for bonding as it allows more mechanical interlocking to occur[9]. To gain further uniformity of the surface an electrochemical treatment can be used called anodisation which has also been investigated.

### *6.2.2 Anodisation*[5,8,9]

Samples of AA2024-T3 were treated by phosphoric acid anodisation (PAA) using Boeing BAC 5555 specification for either 10 or 20 minutes to investigate the effect of anodisation time on the properties of the oxide layer formed (figure 6.04).

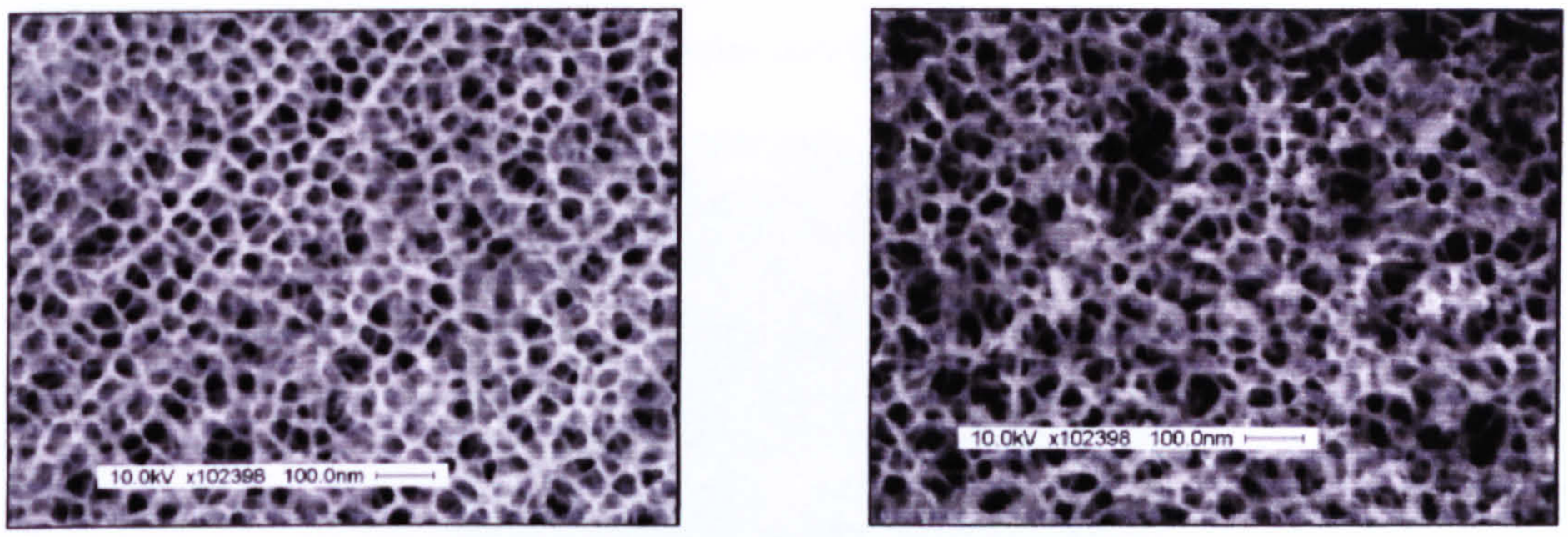


a

| *Element* | *Wt%* | *At%* |
|---|---|---|
| *C K* | 07.59 | 14.07 |
| *O K* | 17.11 | 23.83 |
| *AlK* | 74.61 | 61.61 |
| *P K* | 00.69 | 00.50 |

b

| *Element* | *Wt%* | *At%* |
|---|---|---|
| *C K* | 04.34 | 08.11 |
| *O K* | 21.59 | 30.30 |
| *AlK* | 73.44 | 61.12 |
| *P K* | 00.64 | 00.46 |

Figure 6.04. SEM images obtained at 10kV and 102398x magnification and EDAX analysis of PAA treated AA2024-T3. a. 10mins and b. 20mins

The oxide layer formed by anodisation is extremely uniform and highly ordered[8] in a hexagonal pipe packed structure with a pore size of approximately 40nm.

In comparing the two different samples there appears to be little difference in either their chemical composition or morphology of the oxide layer. The increase in oxygen concentration suggests that the oxide layer is of slightly greater thickness after 20 minutes anodising but the pore size is approximately the same.

However, in comparison with the etched sample there is a large difference between the oxygen concentrations. As the PAA oxygen concentration is approximately double that of the etched sample, it is probable that the oxide layer is twice the thickness.

### *6.2.3 Grit blasting*[7,10]

The commonly used technique of grit-blasting was also used to observe its effect on adhesion. Grit-blasting is used to remove the first few layers of the aluminium surface thus providing an exceptionally clean layer to be anodised. It also provides great roughness which allows for greater mechanical interlocking (figure 6.05).

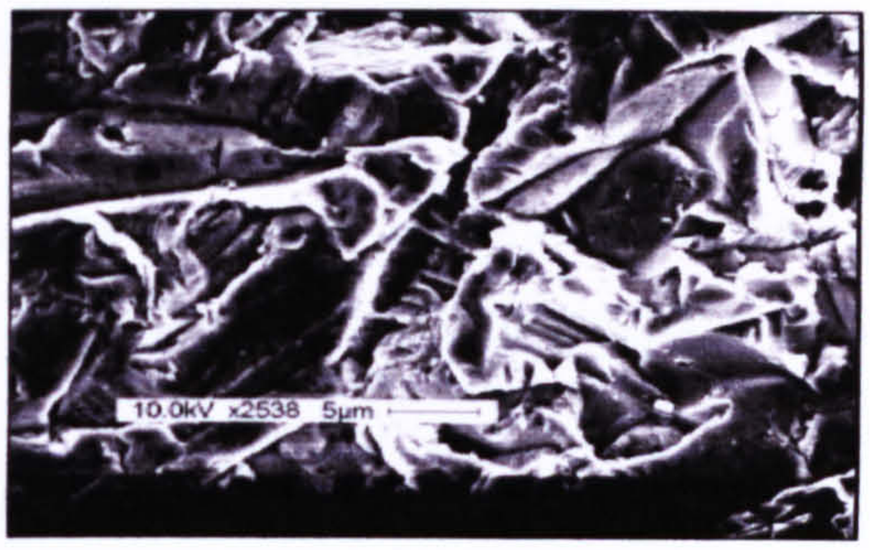


Figure 6.05. SEM image obtained at 10kV and 2538x magnification showing the effect of grit blasting on AA 2024-T3

However, with this increase in surface roughness comes a randomness that, when analysed provides a less ordered oxide layer (figure 6.06).

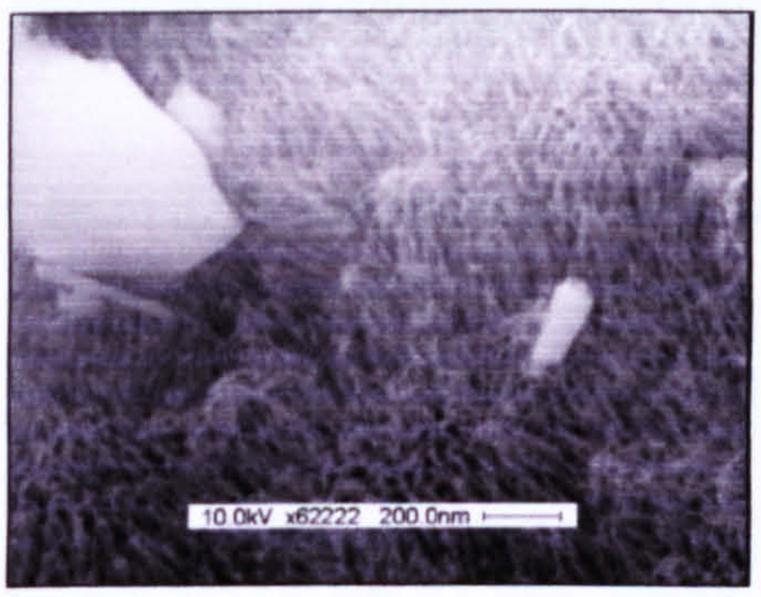


| *Element* | *Wt%* | *At%* |
|---|---|---|
| ***C K*** | 05.68 | 09.73 |
| ***O K*** | 35.48 | 45.58 |
| ***AlK*** | 57.57 | 43.86 |
| ***P K*** | 01.26 | 00.84 |

Figure 6.06. SEM image obtained at 10kV and 62222x magnification and EDAX analysis showing the effect of phosphoric acid anodisation on grit blasted AA2024-T3

The oxygen concentration achieved by anodising after grit-blasting was again substantially larger than that of the purely anodised material.

### *6.2.4 Effects of model coating*

To give an indication of the adhesive properties achieved by electrochemical pretreatment, a layer of the chromate containing model system was applied to differently treated substrates. Through application of the model coatings it was clear that the surface pretreatment has a large effect on the adhesion properties. When the coating of the sodium chromate and cyclohexene oxide system was added to an untreated AA2024-T3 surface and placed under the UHV conditions of the SEM, the coating came away from the surface and only the bare aluminium could be seen. When the same coating was applied to the grit-blasted and anodised sample, good adhesion was achieved and a coating of almost uniform thickness observed (figure 6.07).

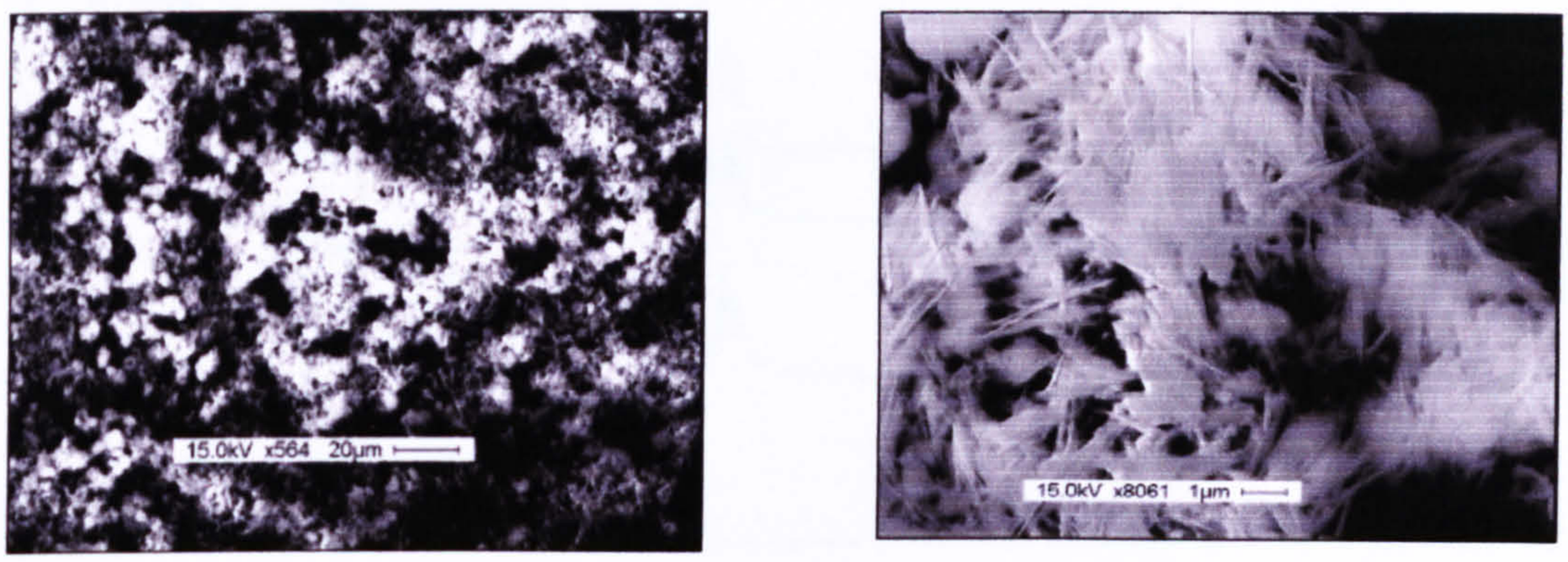


a b

Figure 6.07. SEM images obtained at a. 15kV and 564x magnification and b. 15kV and 8061x magnification showing the sodium chromate, cyclohexene oxide model on grit-blasted, anodised AA2024-T3

Figure 6.07b shows that unlike the industrially primed sample (figure 3.11), the model coating is highly crystalline. As the cyclohexene oxide used in the model system is much less viscous than the industrial epoxy resins it is not able to form a substantial layer over the chromate. Therefore, the characteristic crystals of the sodium chromate are easily observed.

## 6.3 Aging studies of the anodised aluminium surface

To study the surface of the aluminium over time, ATR spectroscopy was employed. This technique is sensitive to approximately 2μm deep[11] and is therefore useful in looking at the chemistry occurring on the metal surface.

Samples of 0.1mm aluminium foil were anodised using laboratory apparatus available under conditions similar to those used at Imperial College (15V DC, 20mins, 25°C) and were then left for various amounts of time under atmospheric conditions. Spectra were taken and the results can be seen in figure 6.08.

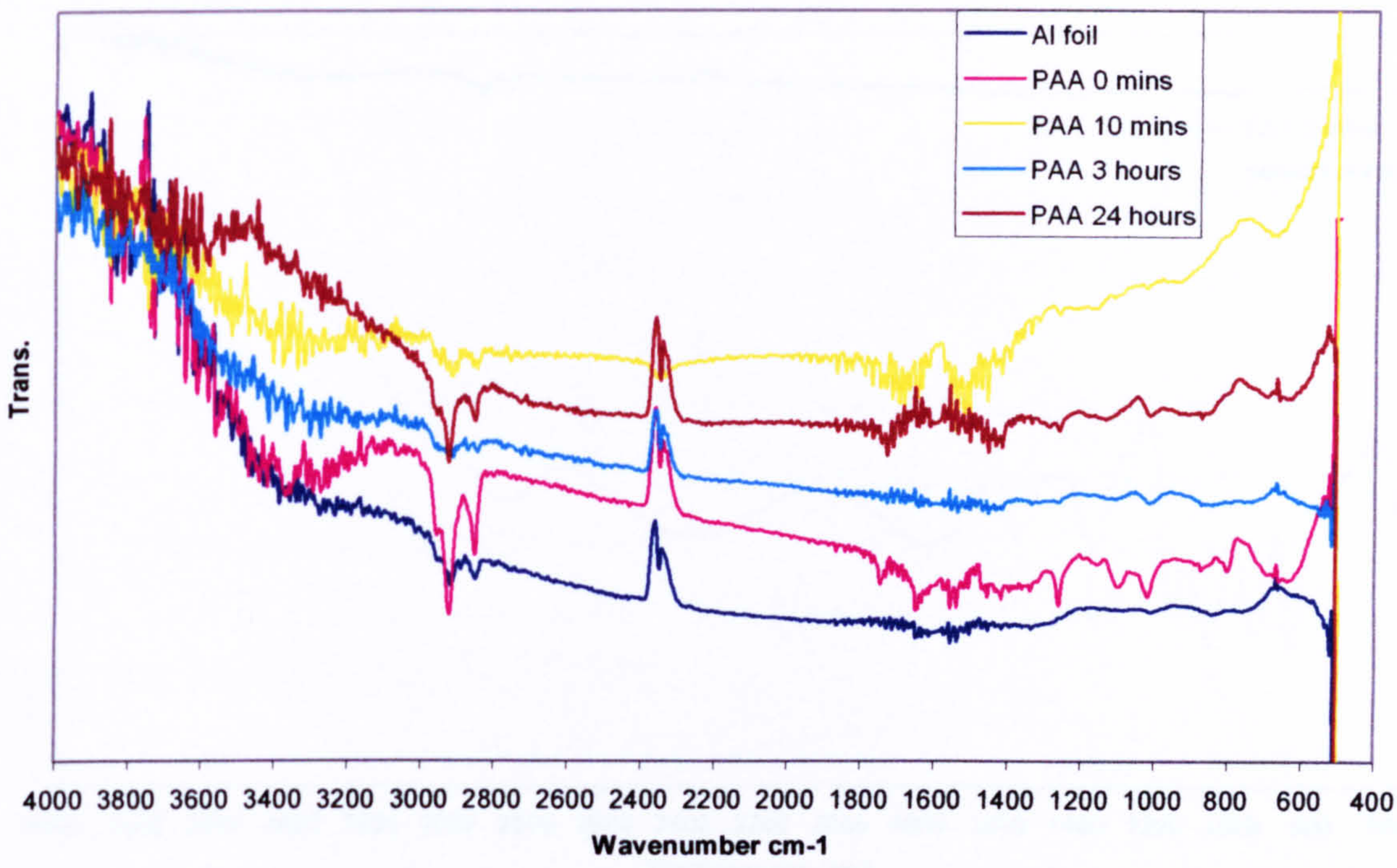


Figure 6.08. ATR spectra showing the effect of time on the surface of anodised aluminium

From the obtained spectra, it appears that the surface is more functionalised immediately after anodisation than that of either the bare aluminium foil or after leaving the sample. An indication of this loss in functionality can be seen by observing the O-H band at approximately 3300cm$^{-1}$. Immediately after anodisation

there is an intense band present, however, over time this decreases to show a very low hydroxyl group concentration. Although ATR spectra are not the most consistent for quantitative measurements it would make sense if deactivation of the surface was occurring with time.

There is also an increase in C-H activity (2800-2950cm$^{-1}$) probably caused by adsorption of organic species onto the reactive aluminium surface and also new peak formation between 1300-800cm$^{-1}$ immediately after anodisation. The new peaks that are present in this region are not due to the formation of phosphate species. As can be seen in figure 6.09, there are no corresponding bands in the DRIFT spectrum of sodium phosphate and therefore it is more likely that they are due to alumina species.

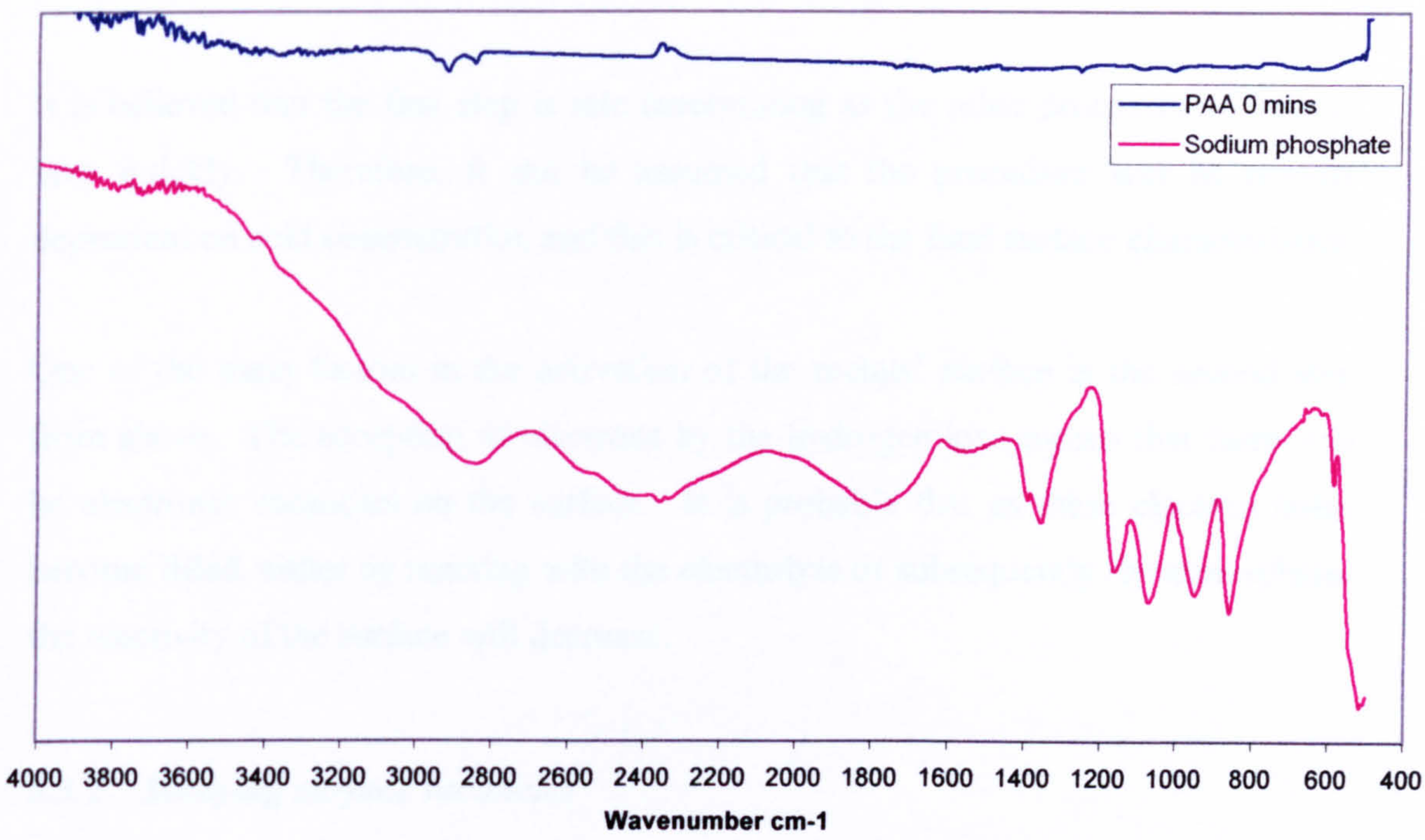


Figure 6.09. IR spectrum comparing a PAA aluminium surface against sodium phosphate

Al-O stretching occurs in the IR at approximately 1085cm$^{-1}$ [12] and this corresponds quite closely to the peak at 1078cm$^{-1}$ in figure 6.08. The other peaks in this region could be due to the complexation of the aluminium oxide layer with organic species

present in the atmosphere. All surfaces possess a large amount of carbonate species and these would account for some of the peaks in this region.

### *6.3.1 Metal surface activation*

Activation of the surface occurs because of a mechanism of attack of the metal by the acid. It is believed that this mechanism acts in the following manner, although there is at this time no conclusive proof. Hydrogen ions from the acidic electrolyte are attracted to the negative anode and therefore migrate to the metal surface. Here these ions accept electrons from the metals' surface and combine to be released as hydrogen gas molecules. The remaining metallic ions hydrate and diffuse away from the surface[14].

It is believed that the first step is rate determining as the other processes will occur very quickly. Therefore, it can be assumed that the procedure will be heavily dependent on acid concentration and this is critical to the final surface characteristics.

One of the main factors in the activation of the metals' surface is the second step from above. The accepting of electrons by the hydrogen ions means that there will be electronic vacancies on the surface. It is probable that as these electron holes become filled, either by reacting with the electrolyte or subsequently the atmosphere, the reactivity of the surface will decrease.

### *6.3.2 Studying surface vacancies*

A method developed to study the proposed theory of surface vacancies was to try and trap the electron holes using a suitable chemical agent. If there were electron holes, it is likely that a trapping agent would react with them and adsorb onto the surface of the substrate.

Initially cyclohexene oxide was used as the trapping agent. Aluminium samples were immersed in the epoxide as quickly as possible following anodisation. After

immersion, the surface was covered by a gel-like compound. Samples were then analysed using DRUV and ATR.

Figure 6.10 shows the DRUV spectra for the epoxide dipped anodised aluminium samples. It is clear that some form of organic species had adsorbed onto the aluminium surface, however, it is not purely residual cyclohexene oxide as the peak has shifted from 220nm for the pure epoxide to 259nm for the adsorbed compound.

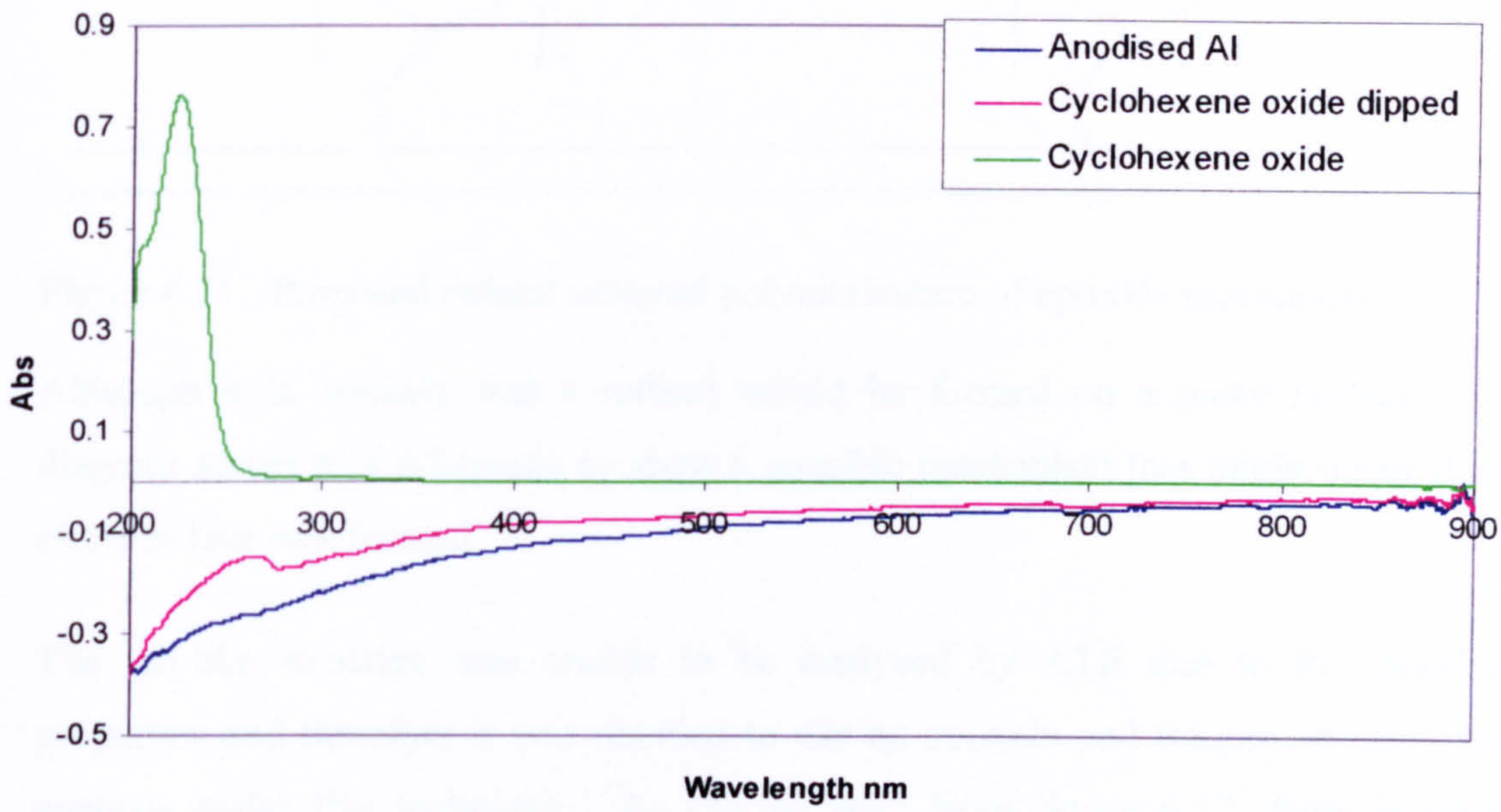


Figure 6.10. DRUV spectra showing the effect of dipping anodised aluminium in cyclohexene oxide

It is possible that this gel-like species is polymerised cyclohexene oxide, whereby the electron holes have acted as a catalyst for the polymerisation. Figure 6.11 shows a schematic diagram for a possible mechanism for this reaction, which proceeds via radical initiation.

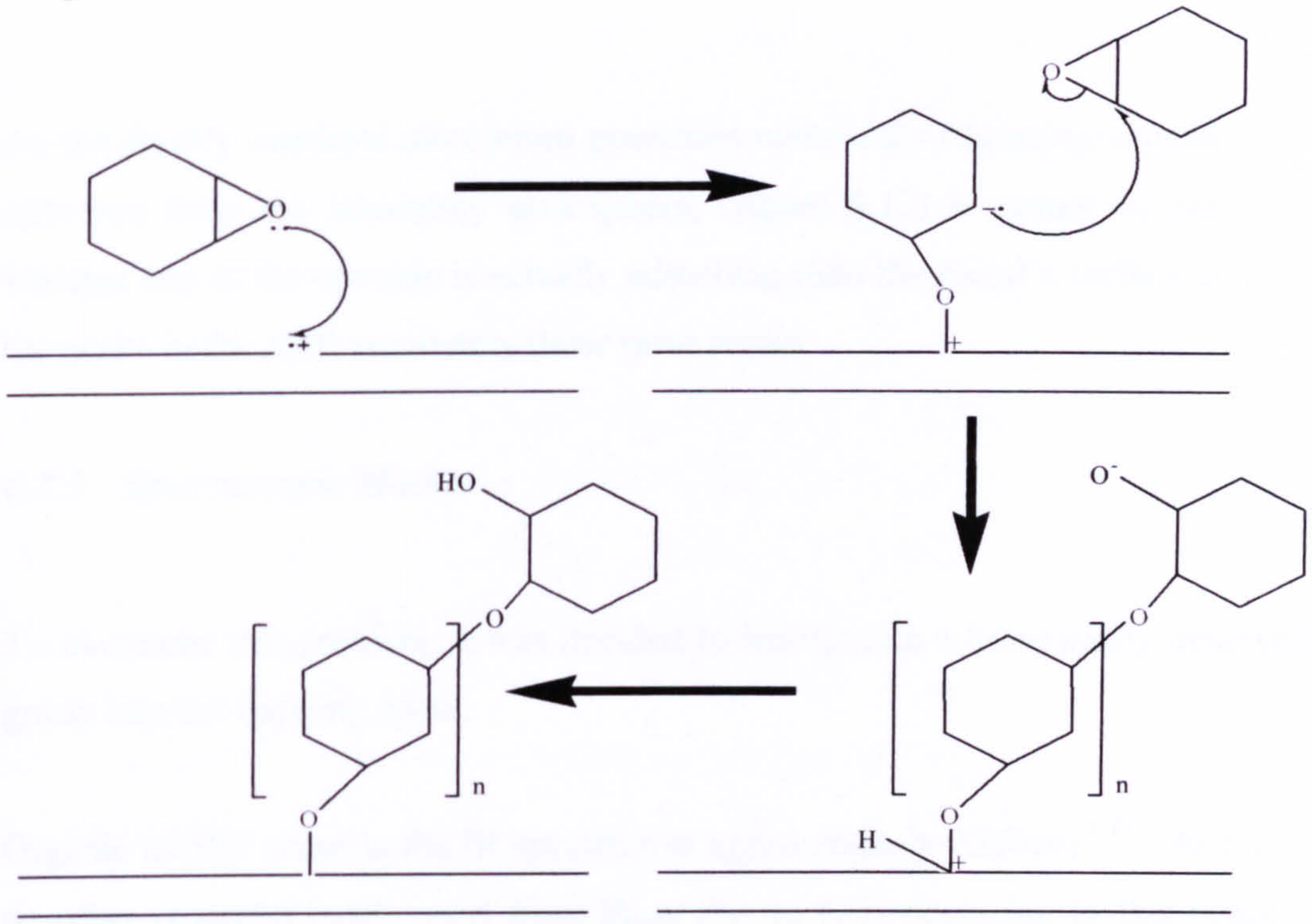


Figure 6.11. Proposed radical initiated polymerisation of epoxide mechanism

Although it is unlikely that a radical would be formed on a metal surface, this diagram serves as a schematic to show a possible mechanism that might occur if an electron hole was formed.

The gel-like structure was unable to be analysed by ATR due to its adhesive properties and therefore it was decided to use an epoxide and toluene solution for analysis under this technique. As can be seen from figure 6.12, there is little difference between the immersed sample and the spectrum obtained when analysing anodised aluminium.

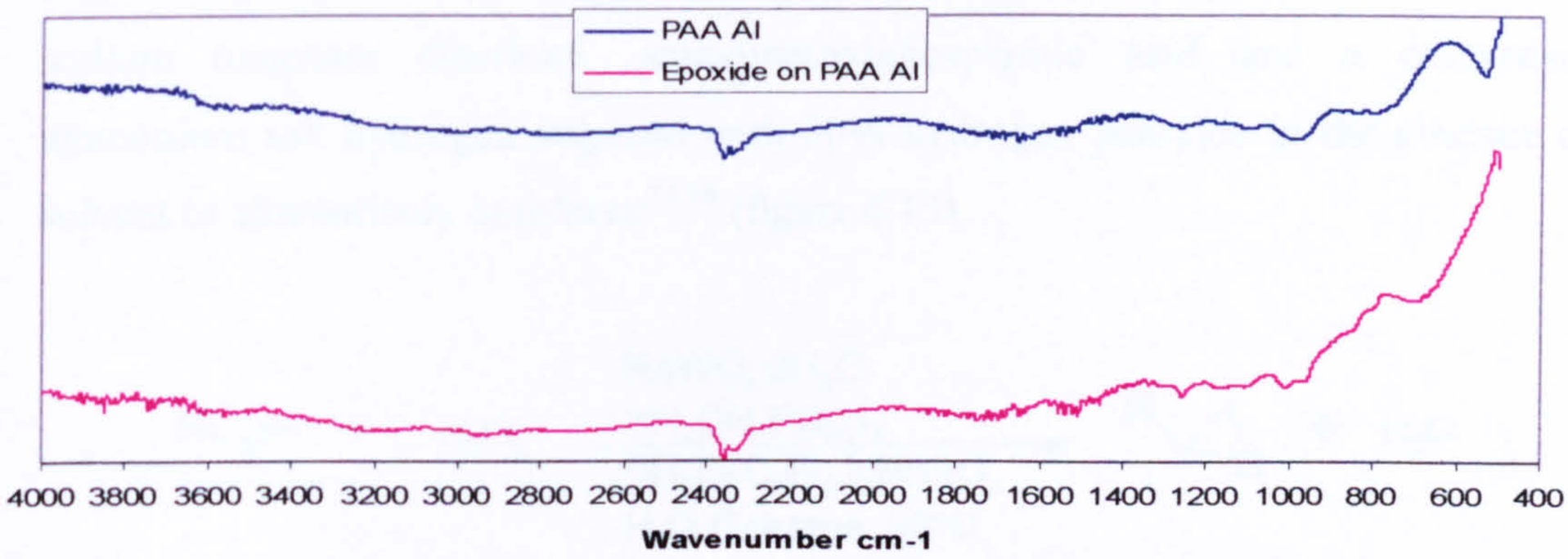


Figure 6.12. ATR spectra comparing anodised aluminium against cyclohexene oxide/toluene solution immersed aluminium

As the freshly anodised aluminium possesses commonly occurring organic species, adsorbed from the laboratory atmosphere, (figure 6.12) it cannot be stated as to whether any of the epoxide is actually adsorbing onto the metal's surface or whether the peaks in the ATR are merely these same peaks.

### *6.3.3 Spectroscopic Marker*

To overcome this problem, it was decided to incorporate a more easily observed IR group into the trapping agent.

Organic nitriles occur in the IR spectrum at approximately 2250cm$^{-1}$ [13]. As there are no other common bands apart from those due to $CO_2$ occurring in this range, this makes it an ideal group to study. However, compounds containing both epoxide and nitrile groups are not readily available. Therefore, it was necessary to synthesise one of these compounds, from the chosen starting material of pentenenitrile.

#### *6.3.3.1 Epoxynitrile background*

As there has been much research done into the area of green epoxidations[14,15], it was decided to use an optimised version of one of the published routes. Early work in this field conducted by Venturello concentrated on the epoxidation of terpenes such as α-pinene using transition metal substituted polyoxometalates[16]. Later work by Noyori improved on this original catalytic system, developing a cycle containing sodium tungstate dihydrate, aminomethylphosphonic acid and a quaternary ammonium salt hydrogen sulphate with 30% hydrogen peroxide in the absence of solvent or alternatively in toluene[17,18] (figure 6.13).

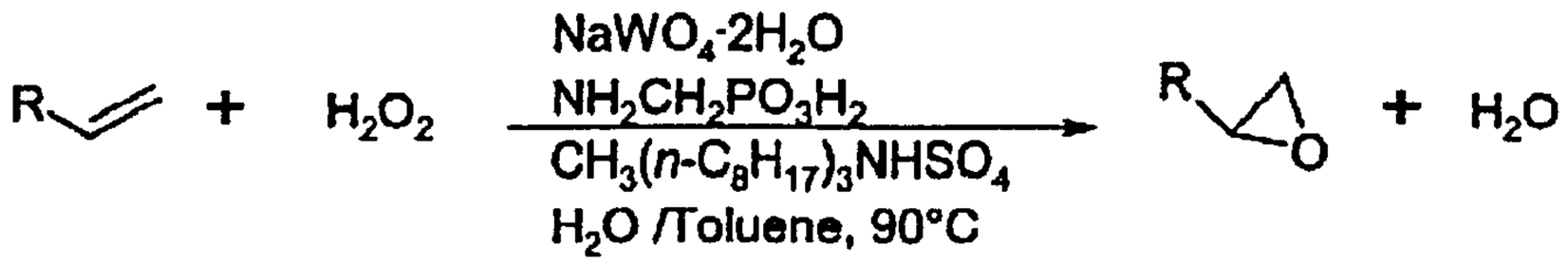


Figure 6.13 . Epoxidation of alkenes by phosphotungstate catalysts under PTC conditions

The addition of the lipophilic phase-transfer agent, quaternary ammonium hydrogensulphate, is necessary to enhance the yield of epoxide.

### *6.3.3.2 Phase transfer catalysts (PTCs)*

Phase transfer catalysis is a concept that was developed in the 1960s[19]. It relates to chemical reactions in which the reactants are in two different phases, such as; liquid-liquid[20], solid-liquid[21], or gas-liquid reactions. In cases such as these, rates and yields are very often limited by the slow transport of reactants from one phase to the other. PTCs were found to be instrumental in transporting the reactants, and therefore overcame these barriers allowing reactions that were otherwise not feasible or very difficult to carry out.

To transfer a reactive ion into the organic phase, the associated cation must be more organophilic than the standard cation. Quaternary ammonium (Quat) or phosphonium cations substituted with organophilic groups provide the necessary properties to facilitate the transfer[22]. The two phases are separated by an interfacial region. Most commonly, two liquid phases are involved and therefore the process is termed liquid-liquid phase transfer catalysis (ll-PTC) and since the quat is the vehicle for the transfer of anion between the two liquid phases the mechanistic scheme is termed the extraction mechanism.

In order for phase transfer catalysis to take place, the quat must effectively transport the reactant anion (nucleophile) from the aqueous phase through the interface into the organic phase. However, the successful transportation does not mean that PTC will take place. Once transferred, the anion must exist in a reactive state in the organic phase so that it can rapidly react with the electrophilic organic reagent. Finally, for the whole process to be successful, the quat must transport the product anion (leaving group) from the organic phase into the aqueous phase so that the catalytic cycle can begin again. If this final stage does not take place, the reaction will stop.

Generally for PTC processes involving relatively soft anionic reagents (cyanide, acetate, etc.) the most effective quats are those which contain organophilic alkyl or aryl substituents. This substantially separates the cationic centre (the positively charged nitrogen) from the anionic centre of the nucleophilic reagent. However, for PTC processes involving hard anions (i.e. hydroxide ion), quats having organophilic

character but at least one alkyl substituent which allows the anion (hydroxide ion) to approach close to the centre of positive charge are usually the most effective.

### *6.3.3.3 Epoxynitrile synthesis*

Noyori's methodology was further optimised and eliminated the need for inclusion of the aminomethylphophonic acid. This was achieved through the use of a $H_2O_2$/phosphate solution made from both $H_3PO_4$ and $NaH_2PO_4$ [23]. The formation of the epoxynitrile compound consisted of two different stages. The first of these involved the preparation of trioctylammonium hydrogensulphate.

The conversion of methyltrioctylammonium chloride to the hydrogensulphate ligand was necessary to make it much more lipophilic. As can be seen in figure 6.14, the IR spectrum shows that the chloride ligand compound contains a large concentration of hydroxyl groups (3100-3600$cm^{-1}$) meaning it has a high affinity for water. Alternatively, the IR spectrum for the hydrogensulphate species shows a low hydroxyl group concentration allowing it to be much more lipophilic.

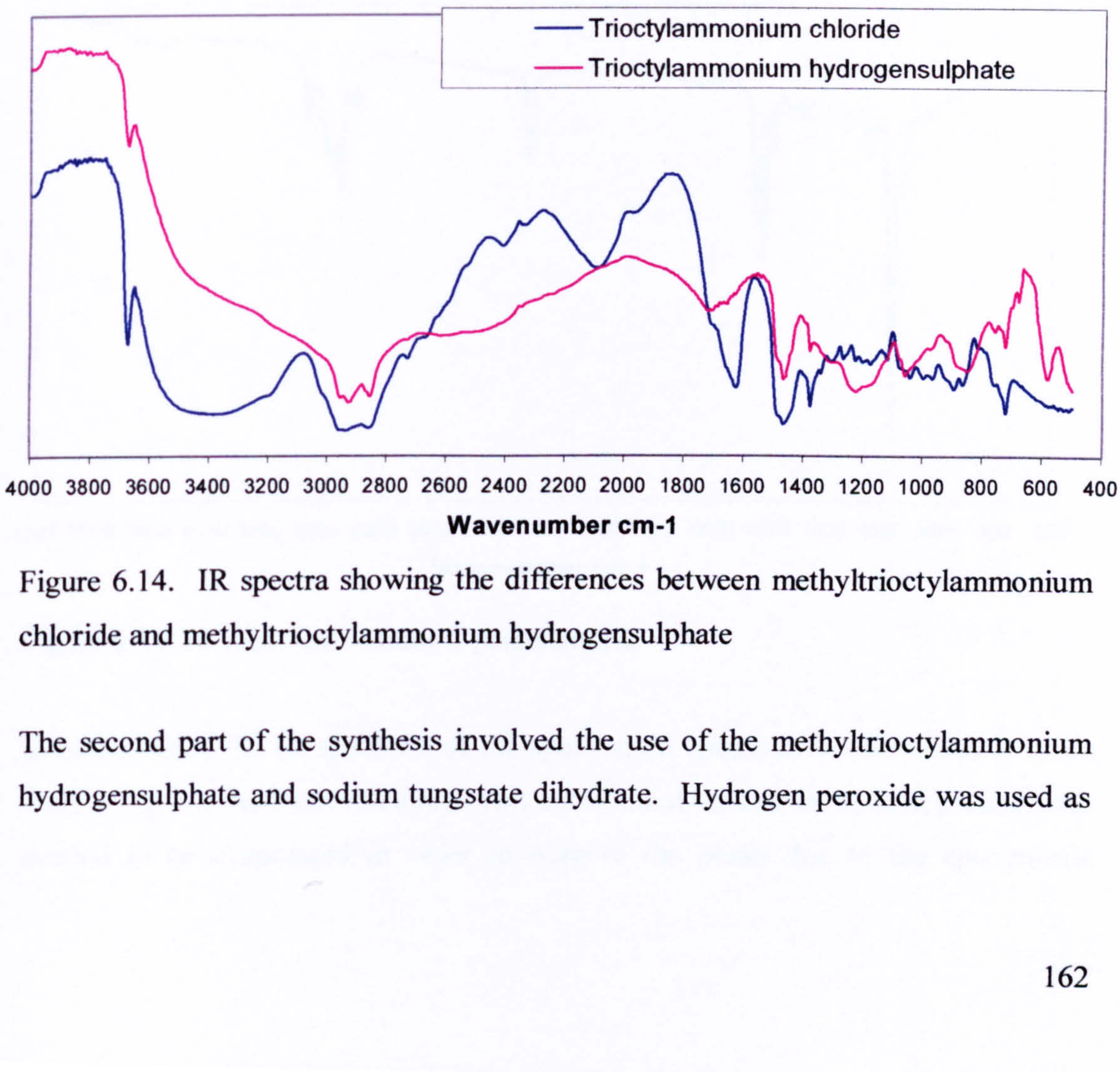


Figure 6.14. IR spectra showing the differences between methyltrioctylammonium chloride and methyltrioctylammonium hydrogensulphate

The second part of the synthesis involved the use of the methyltrioctylammonium hydrogensulphate and sodium tungstate dihydrate. Hydrogen peroxide was used as

the oxidant and the trans-3-pentenenitrile added later, with the whole process been carried out in toluene (figure 6.15).

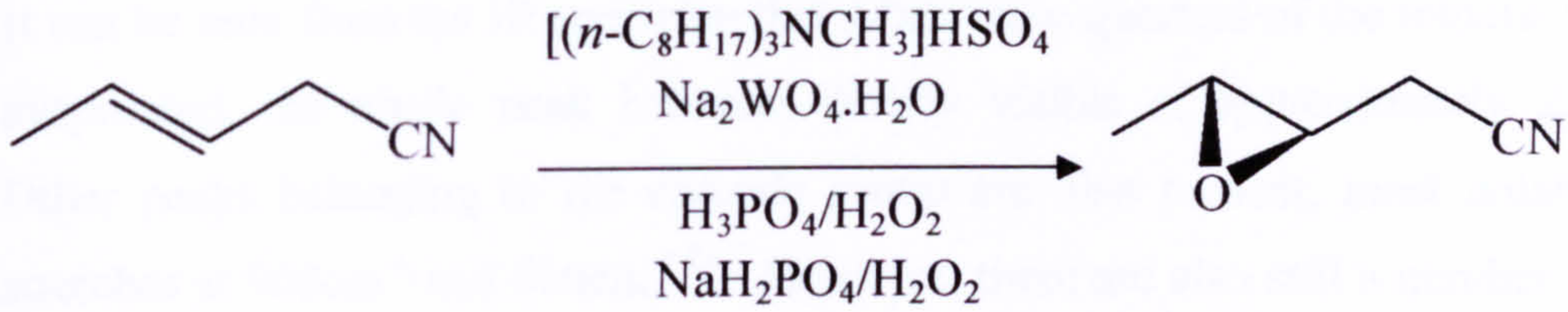


Figure 6.15. Synthesis of the epoxynitrile

### *6.3.3.4 Analysis*

As can be observed in the IR spectrum of trans-3-pentenenitrile (figure 6.16) it is clear that the nitrile band appears at around 2250cm$^{-1}$. The C-H stretching and bending modes are also present for both the alkyl (stretch 2850-2975cm$^{-1}$ and bend 1410-1460cm$^{-1}$) and alkene (stretch 3050cm$^{-1}$ and bend 970cm$^{-1}$) groups.

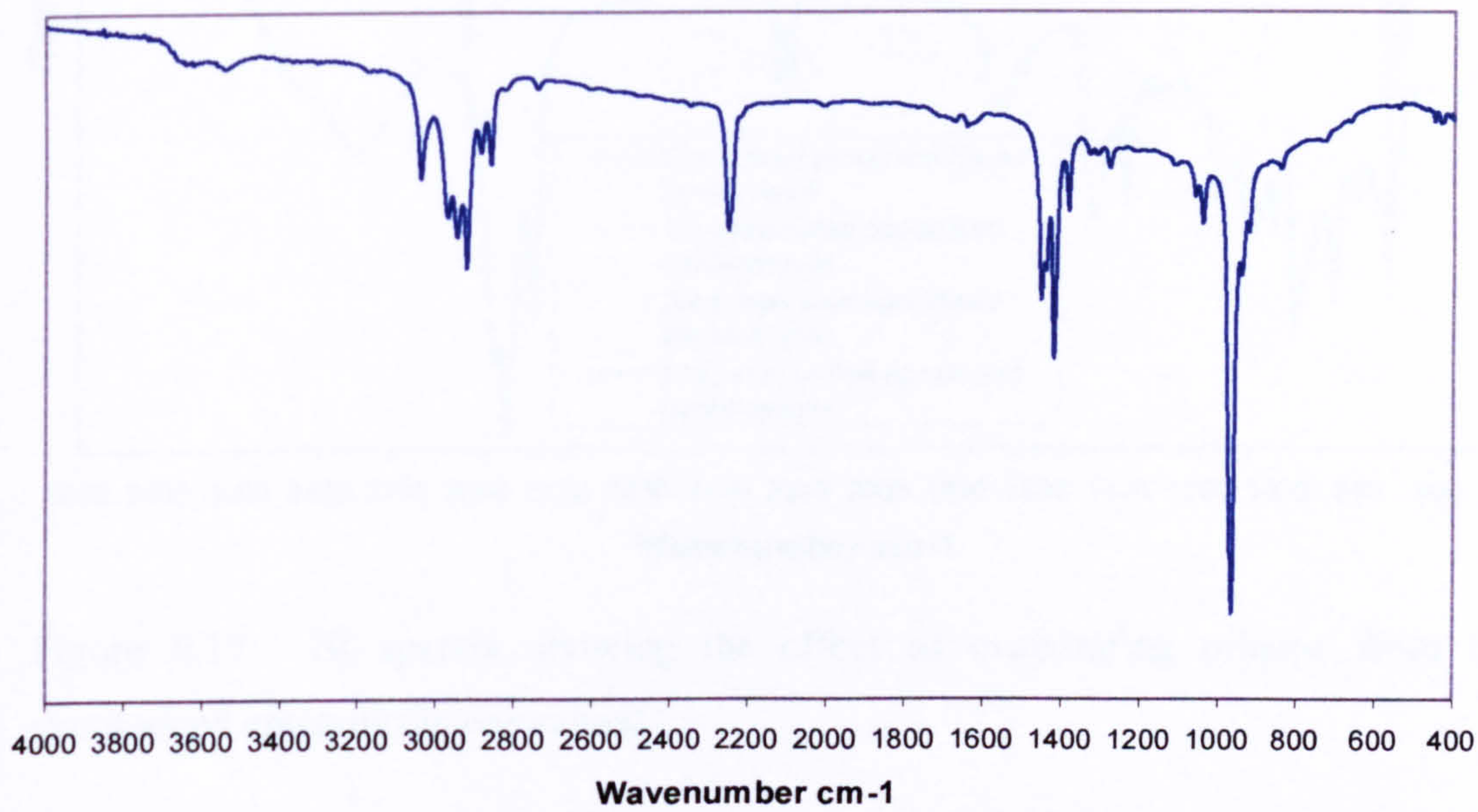


Figure 6.16. IR spectrum of trans 3-pentenenitrile

In comparison, the IR spectrum of the synthesised epoxynitrile compound is much more complex. As there was a high concentration of toluene in the final product, this needed to be evaporated in order to observe the peaks due to the epoxynitrile

compound. Figure 6.17 shows the effects of evaporating the toluene from the generated compound.

It can be seen from the IR spectrum that when three quarters of the toluene has been evaporated, the nitrile peak becomes clearly visible at approximately 2250cm$^{-1}$. Other peaks belonging to the epoxide group are also present, most notably; C-O stretches at 960cm$^{-1}$ and 860cm$^{-1}$ [24]. However, there are also still a number of peaks due to the presence of toluene. The most easily observed of these been the arene C-H bending modes at 730cm$^{-1}$ and 675cm$^{-1}$ [25].

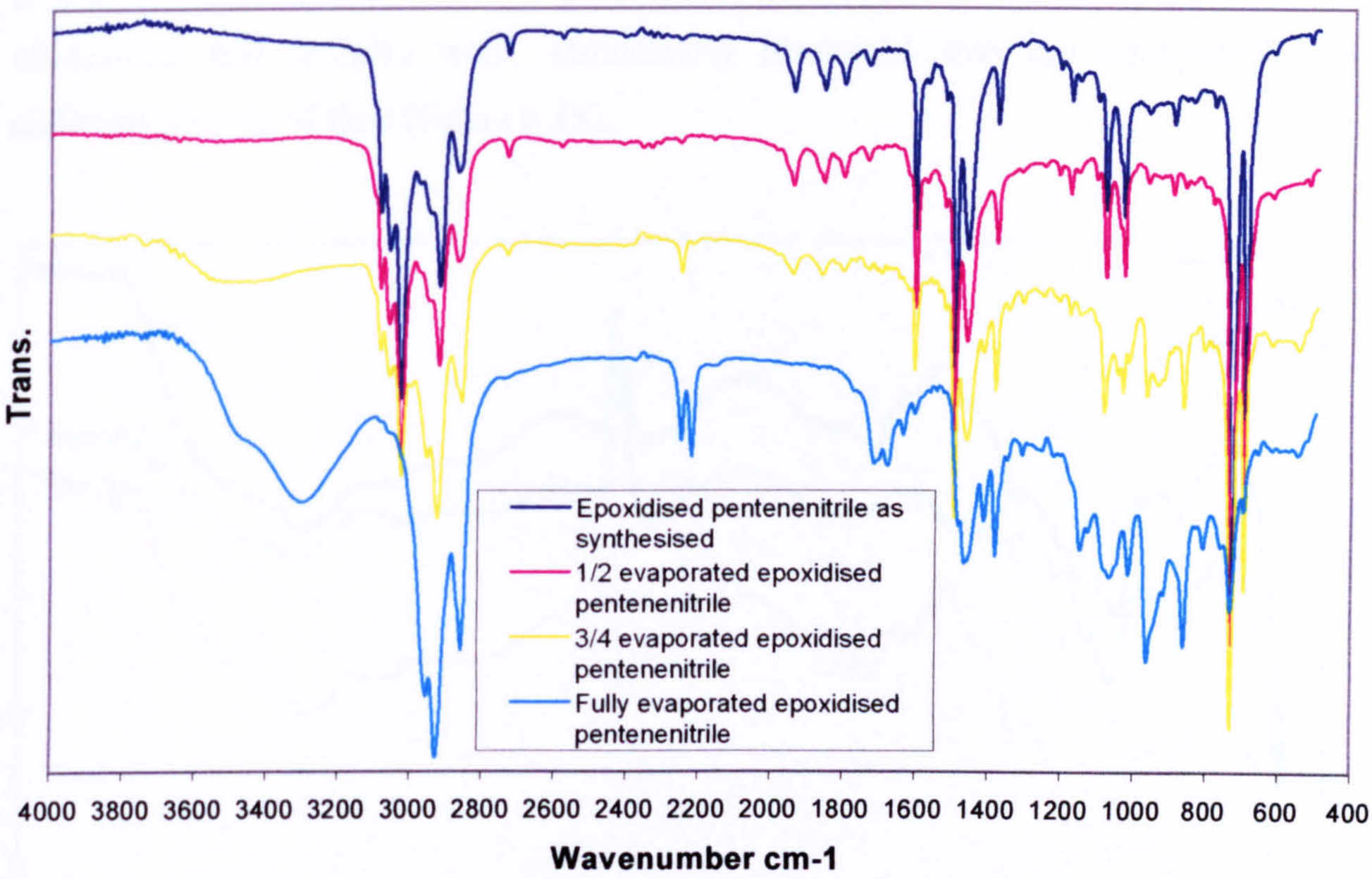


Figure 6.17. IR spectra showing the effect of evaporating toluene from the synthesised epoxynitrile compound

When fully evaporated, the epoxide C-O stretching peaks at 960cm$^{-1}$ and 860cm$^{-1}$ are much more intense. However, there is also the appearance of an additional nitrile peak at approximately 2220cm$^{-1}$ in this spectrum. This can be attributed to the fact that it was necessary to heat the sample in order to completely remove the toluene. This has led to some of the epoxide groups undergoing ring-opening reactions, thus

causing significant differences in the structure and interactions within the molecule. This can also be observed in the substantially more intense O-H stretching band. To limit these alterations to the compound, it was decided to carry out all further analysis using the epoxy nitrile when approximately three quarters of the toluene had been evaporated.

### *6.3.3.5 Use of the spectroscopic marker*

An initial investigation was conducted to observe under what conditions the nitrile group of the epoxynitrile would be visible in the ATR spectrum. Freshly anodised aluminium foil samples were immediately immersed into the epoxynitrile for different periods of time (figure 6.18).

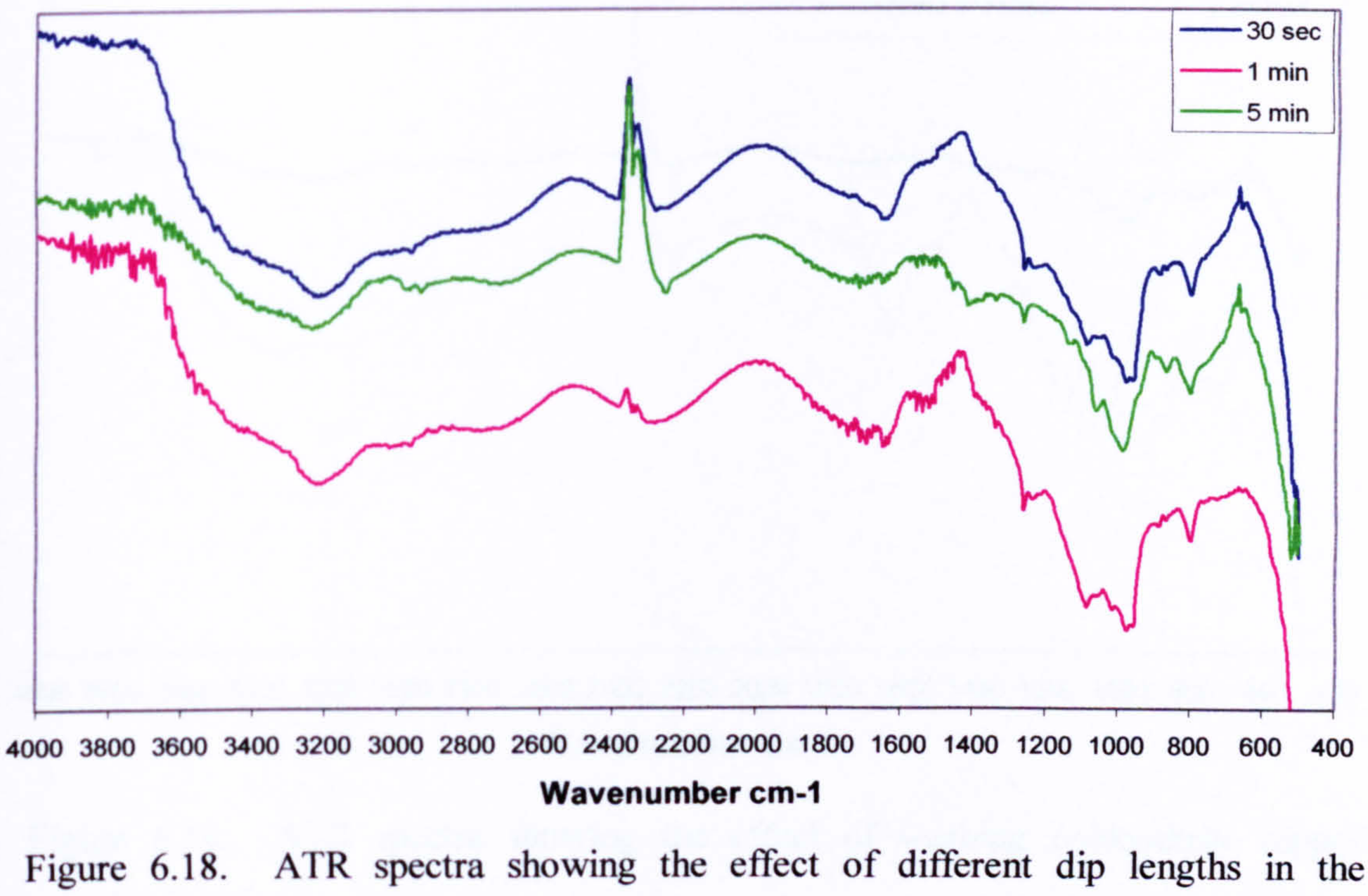


Figure 6.18. ATR spectra showing the effect of different dip lengths in the epoxynitrile

As can be seen from the ATR spectra after immersion times of both 30 seconds and 1 minute, the nitrile peak is not present. Also the presence of strong Al-O peaks at

1080cm$^{-1}$, signifies that there has been no reaction between the epoxynitrile and the anodised aluminium surface.

However, figure 6.18 illustrates that after 5 minutes of immersion, the nitrile peak is clearly present at 2247cm$^{-1}$. Additionally, there is a peak of moderate intensity at 860cm$^{-1}$ which is due to the C-O stretch of the epoxide. The presence of these two peaks, coupled to the fact that there is no observable Al-O peak at 1080cm$^{-1}$ suggests that there has been successful reaction between the anodised aluminium surface and the epoxynitrile.

To confirm that there was an actual reaction occurring between the surface and epoxynitrile, and that there was not merely a film of epoxynitrile physisorbed on the surface; samples were washed with toluene (figure 6.19).

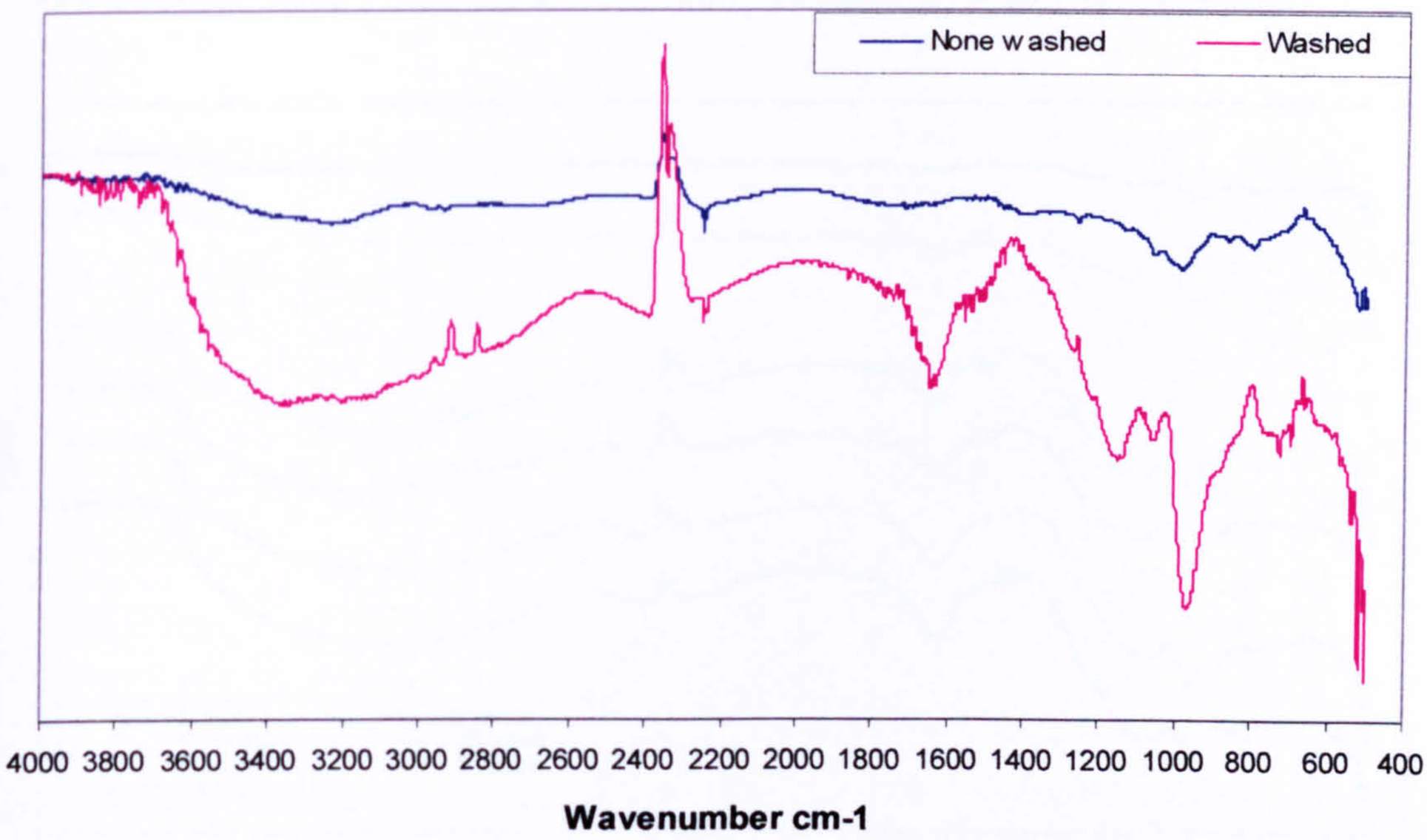


Figure 6.19. ATR spectra showing the effect of washing epoxynitrile dipped samples in toluene

As can be seen in figure 6.19, the toluene wash has little effect on the ATR spectrum of the sample. The C-N stretch at 2248cm$^{-1}$ is still present after the wash, as is the C-O peak at 960cm$^{-1}$. Some residual toluene can also be observed by the presence of

low intensity arene C-H stretches at 730cm$^{-1}$ and 695cm$^{-1}$. This suggests that there is indeed a chemical reaction occurring and that a polymeric film of epoxynitrile has not formed.

Additional tests were carried out using an immersion time of 10 minutes; however, after this period of time, a gel-like structure had once again formed, meaning that analysis was not possible. Therefore, for all further investigations the aluminium was immersed into the epoxynitrile for 5 minutes.

#### *6.3.3.6 Further analysis*

An investigation was conducted to observe the effects of aging anodised samples before been immersed in epoxynitrile. Samples were left under atmospheric conditions for differing periods of time over 24 hours before been dipped in epoxynitrile. They were then analysed by ATR spectroscopy (figure 6.20).

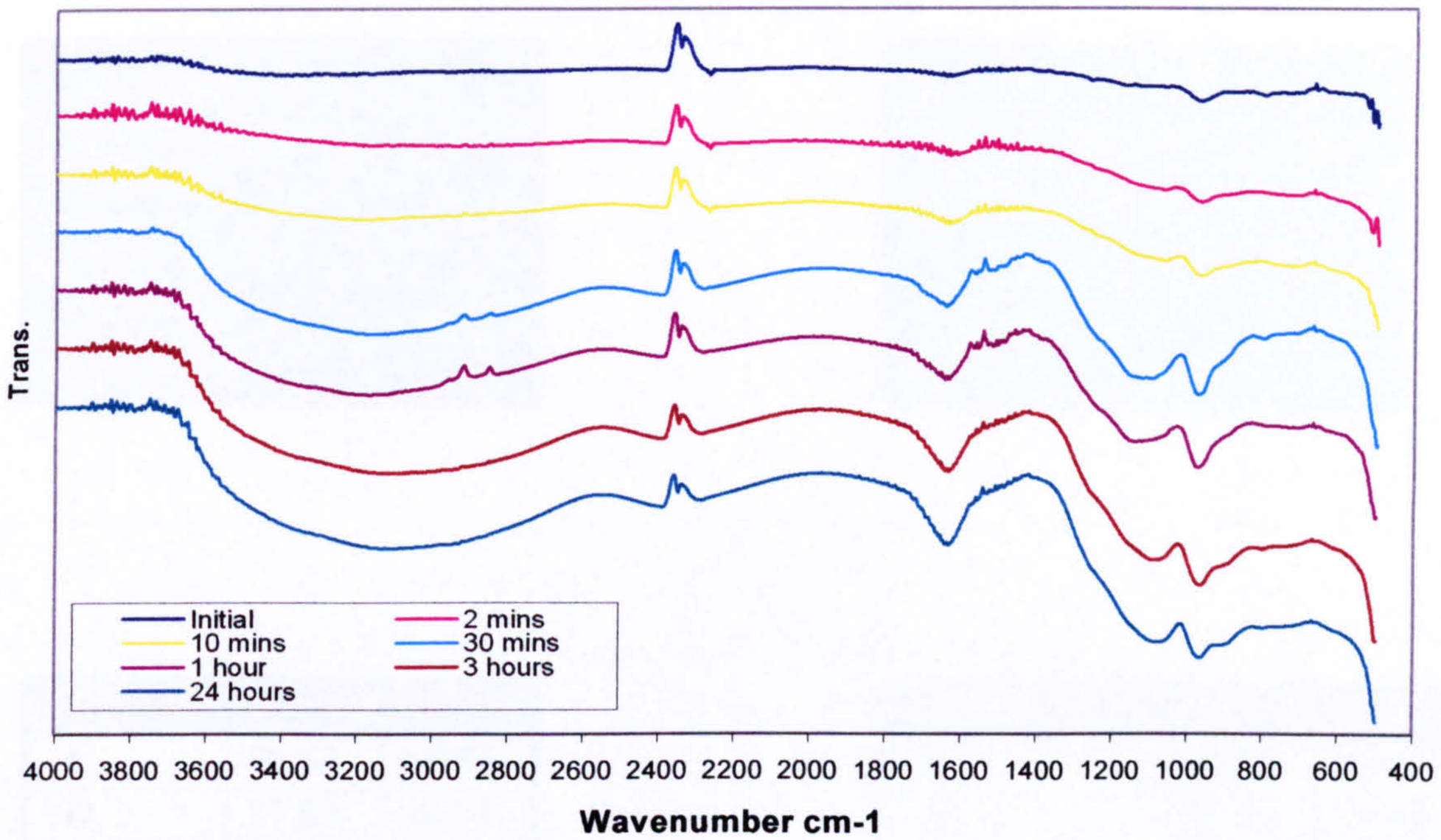


Figure 6.20. ATR spectra showing the effects of aging samples before immersing in epoxynitrile

From the ATR spectra it can be seen that the samples aged up to 10 minutes all exhibit strong C-N stretching peaks at approximately 2270cm$^{-1}$. However, after this

amount of time the intensity of this peak decreases and in the spectra after 3 hours and 24 hours, there is no observable C-N peak. This suggests that the reactivity of the surface is decreasing after approximately 10 minutes.

A reason for this could be due to the surfaces' reaction with the air and subsequent formation of an inert aluminium oxide layer on the surface. From figure 6.20, it can be seen that after aging for approximately 30 minutes, there is the emergence of a large peak at approximately 1080cm$^{-1}$ caused by the presence of Al-O. The intensity of this peak also increases up to the final sample after 24 hours. Another factor that supports this theory is the increase in intensity of the O-H band which becomes much more significant with the age of the sample.

### *6.3.3.7 SEM and EDX analysis*

SEM and EDX were also used to investigate the issue of sample aging, (figure 6.21a and b).

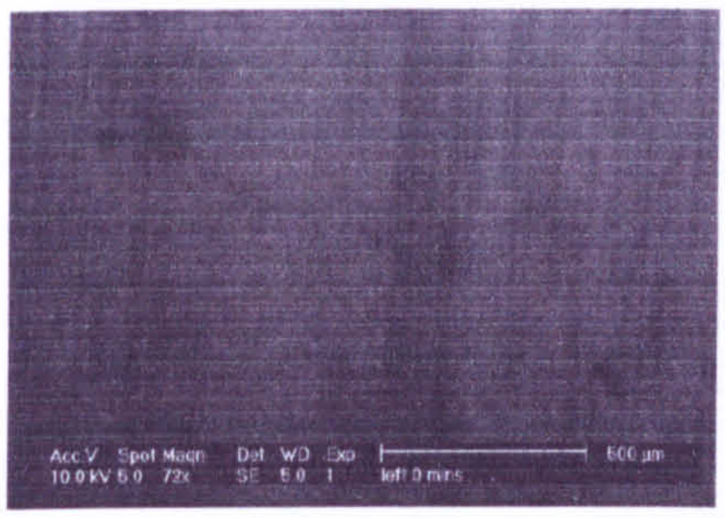


| *Element* | *Wt%* | *At%* |
|---|---|---|
| *C* | 02.62 | 04.84 |
| *O* | 27.89 | 38.74 |
| *Al* | 61.85 | 50.94 |
| *P* | 07.64 | 05.48 |

a

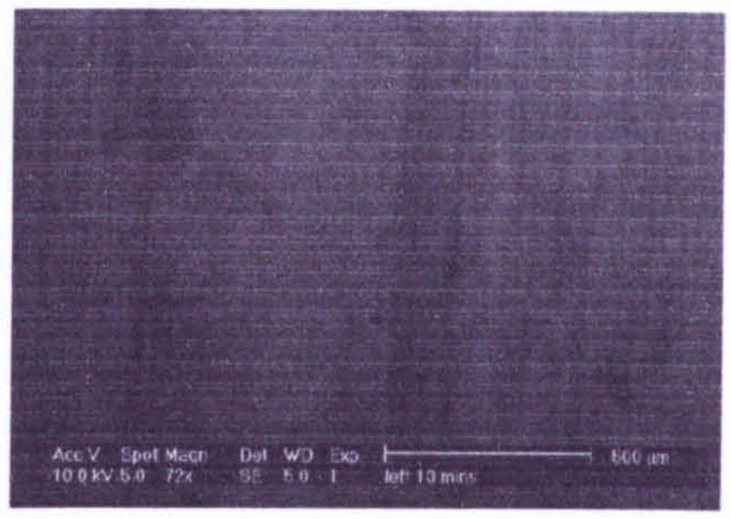


| *Element* | *Wt%* | *At%* |
|---|---|---|
| *C* | 02.51 | 04.69 |
| *O* | 26.85 | 37.58 |
| *Al* | 62.92 | 51.94 |
| *P* | 07.72 | 05.79 |

b

Figure 6.21. SEM images obtained at 15kV and 72x magnification of epoxynitrile dipped anodised aluminium after a. 0 mins and b. 10 mins and the relative EDX data

As can be seen from figures 6.21 a and b, the epoxynitrile dipped anodised aluminium surface appears as a dark coated metal surface. The EDX data for these two samples shows that there is approximately a 5% carbon concentration, 40% oxygen concentration and 50% aluminium concentration. However, when the samples have been aged for 30 minutes and longer, there is the emergence of a dense oxide layer in the SEM pictures (figure 6.22 a & b).


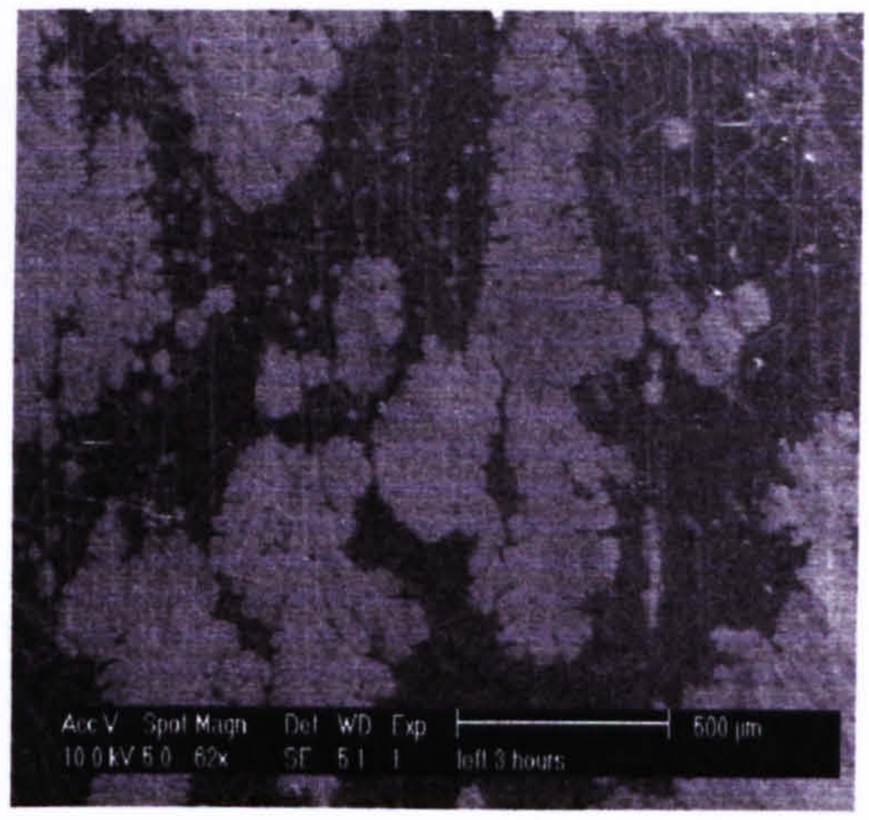


| *Element* | *Wt%* | *At%* |
|---|---|---|
| *C* | 01.54 | 2.53 |
| *O* | 53.92 | 66.56 |
| *Al* | 26.63 | 19.49 |
| *P* | 17.91 | 11.42 |

a

| *Element* | *Wt%* | *At%* |
|---|---|---|
| *C* | 01.31 | 02.14 |
| *O* | 55.71 | 68.30 |
| *Al* | 25.03 | 18.19 |
| *P* | 17.95 | 11.37 |

b

Figure 6.22. SEM images obtained at a. 10kV and 288x magnification and b. 10kV and 62x magnification showing the emergence of an oxide layer after aging the samples before dipping in epoxynitrile aged for a. 30 mins and b. 3 hours. EDX data corresponds to the white areas of the images

On aging the samples before immersion in the epoxynitrile, there is a huge change in the appearance of the samples (figure 6.22). The EDX data for these images illustrates that there is a substantial increase in oxygen concentration, from approximately 40% to approximately 70%, suggesting the formation of an oxide

layer. The high phosphate concentration in the white section suggests that the new substance formed is $AlPO_4$.

### *6.3.3.8 Vacuum*

In an attempt to limit the effects of atmospheric conditions, the same experiment was conducted; however, this time the samples were aged in a vacuum dessicator. ATR spectroscopy was once again employed to analyse these samples (figure 6.23).

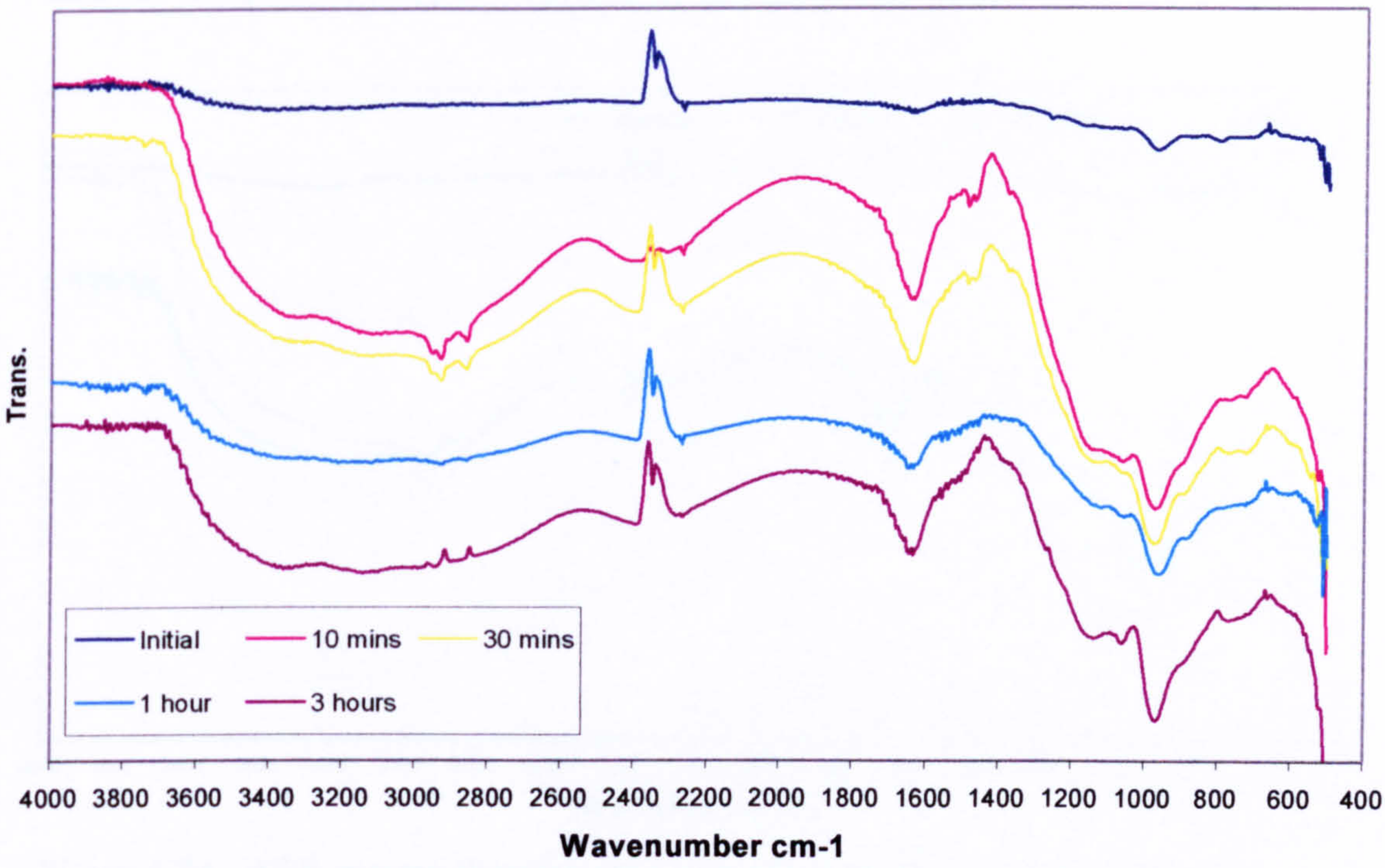


Figure 6.23. ATR spectra showing the effect of aging anodised samples under vacuum before immersion in epoxynitrile

The ATR spectra clearly illustrate that aging the samples in the vacuum has an effect on the ability of the anodised aluminium to react with the epoxynitrile. The C-N stretch is present as a strong peak at approximately 2270cm$^{-1}$ after 1 hour, and can still be partially observed after 3 hours. This obviously compares favourably against leaving the samples under atmospheric conditions, where the peak could not be seen after 30 minutes. Another factor that suggests a greater reaction with the epoxynitrile than formation of an oxide layer is the decrease in intensity of the Al-O peak at approximately 1080cm$^{-1}$.

### *6.3.3.9 Aging of epoxynitrile coated samples*

To investigate whether the reaction between the surface of the anodised aluminium and epoxynitrile occurred rapidly or over a longer period of time, it was decided to take one sample and analyse it by ATR over a period of time.

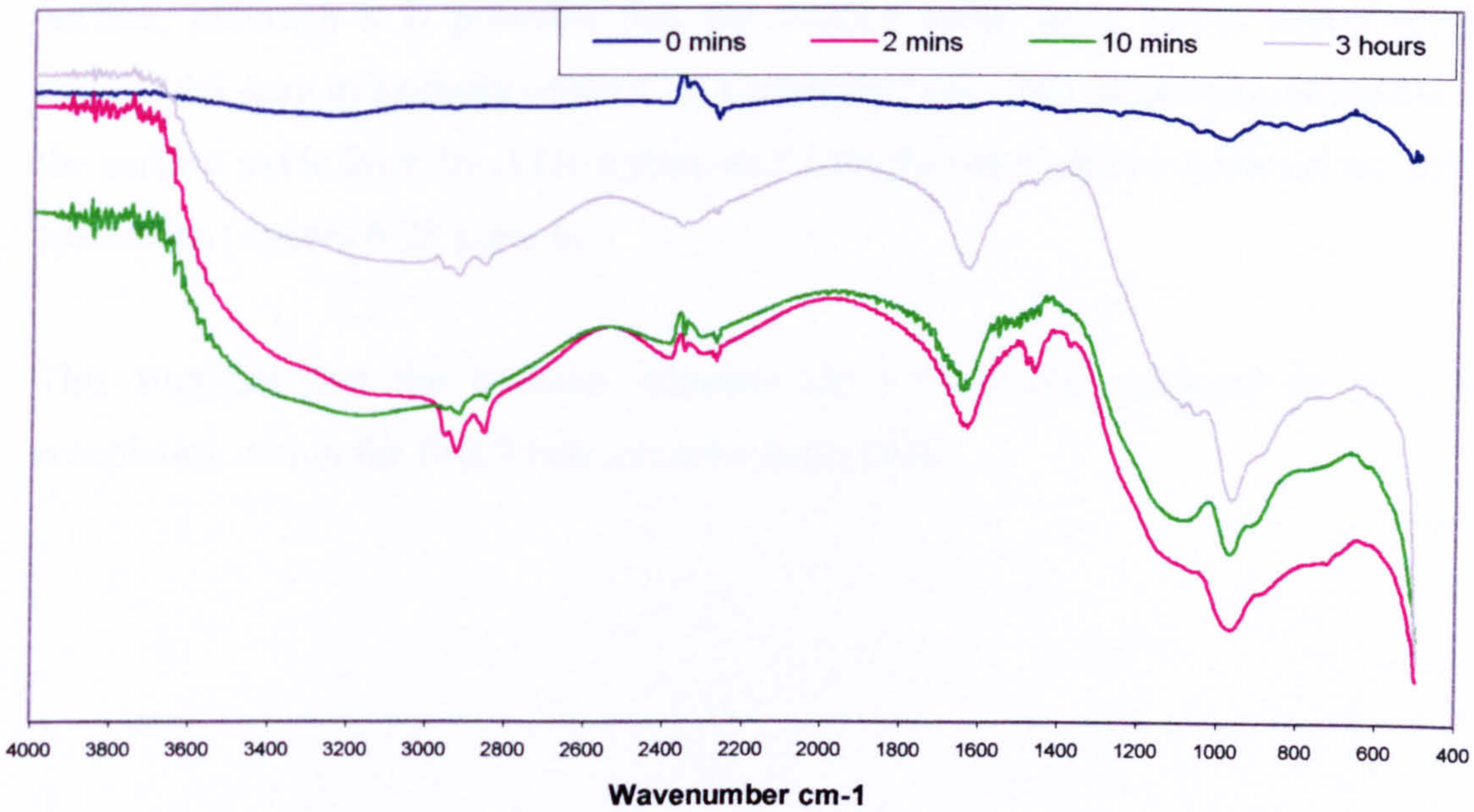


Figure 6.24. ATR spectra showing the aging effect on the epoxynitrile coating

A sample was anodised, immersed in the epoxynitrile and then immediately analysed by ATR. The sample was kept under normal atmospheric conditions and analysed after 2 minutes, 10 minutes and finally 3 hours (figure 6.24).

As can be seen in the ATR spectra, there is little variation in the nitrile region of the sample when it was analysed immediately after immersion in the epoxynitrile and then through to 10 minutes. However, the spectrum taken after 3 hours shows a slight drop in C-N stretch intensity with respect to the other peaks present in the spectrum.

It is possible that the reactive surface vacancies formed in the anodisation process react instantaneously with the epoxynitrile compound, hence the nitrile peak at 2270cm$^{-1}$ in the 0 minute spectrum. In the proceeding 2 minutes, there appears to be an oxidation of the remainder of the surface as there are large increases in the C-O stretch at 960cm$^{-1}$, O-H bending mode at 1623cm$^{-1}$ [26] and the O-H stretching mode at 3600-2600cm$^{-1}$. There then seems to be little change in the chemical structure of the surface, although it is probable that the surface oxide layer grows which would explain the drop in intensity of the C-N stretching peak. The suggestion of growth of the surface oxide layer by ATR agrees well with the observations made on the SEM specimens (figures 6.22 a and b).

This suggests that the reaction between the surface and epoxynitrile goes to completion within the first 2 minutes after immersion.

### *6.3.3.10 Further surface preparation*

To compare the effectiveness of anodisation against other surface pretreatments, the epoxynitrile compound was further employed. Samples were subjected to simple acid etching (phosphoric acid), alkali etching (sodium hydroxide) and fluoride treatment (potassium fluoride in methanol) and were subsequently immersed in epoxynitrile (figures 6.25 & 6.26).

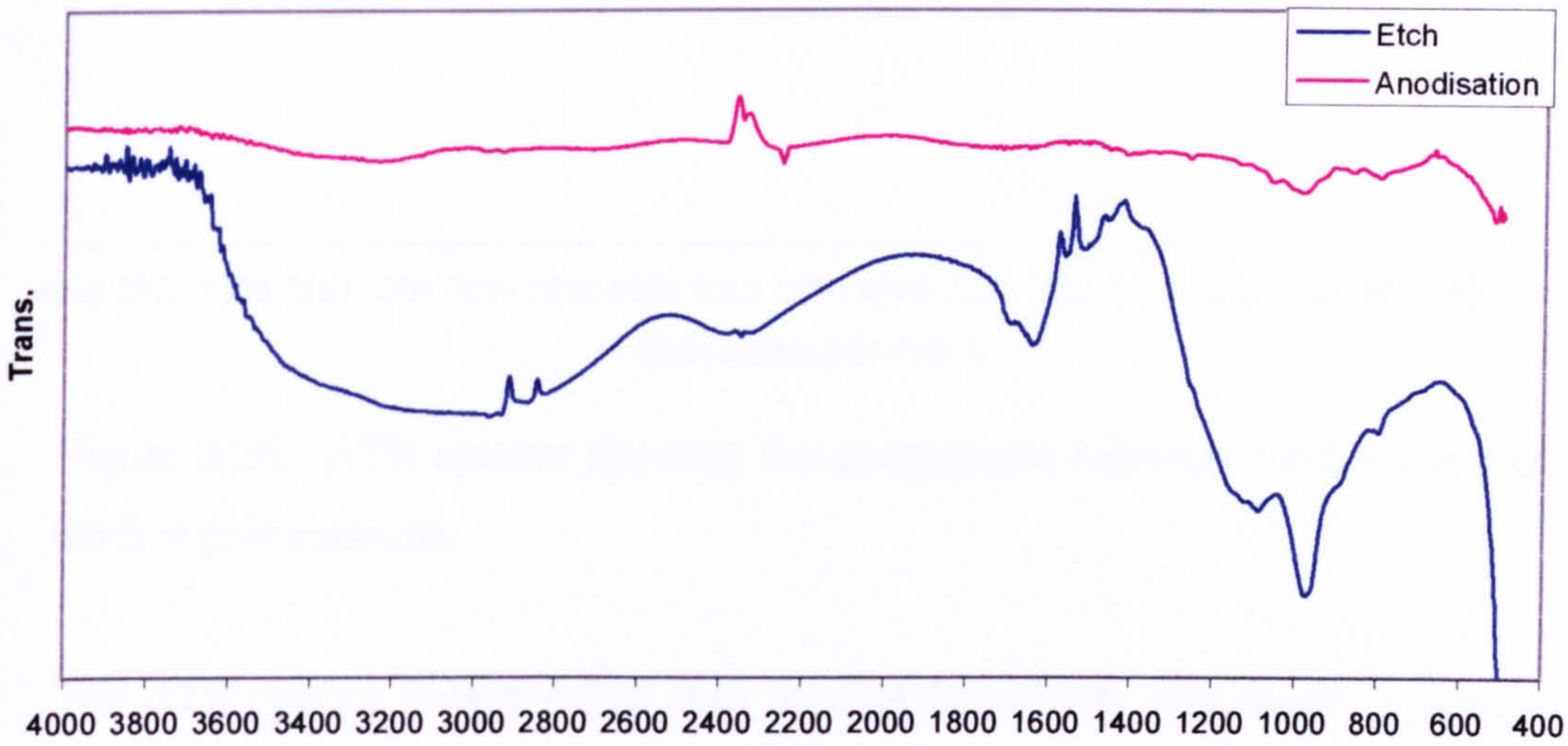


Figure 6.25. ATR spectra showing the differences between anodisation and etching after immersion in epoxynitrile

The presence of a C-O stretch at 960cm$^{-1}$ suggests that reaction between the etched surface and epoxynitrile has occurred. However, the appearance of both a large hydroxyl band and a strong Al-O peak at 1080cm$^{-1}$ coupled with the fact that there is no C-N stretch at 2248cm$^{-1}$ signify that no reaction has taken place. It is possible that the peak at 960cm$^{-1}$ could be due to surface carbonate group impurities.

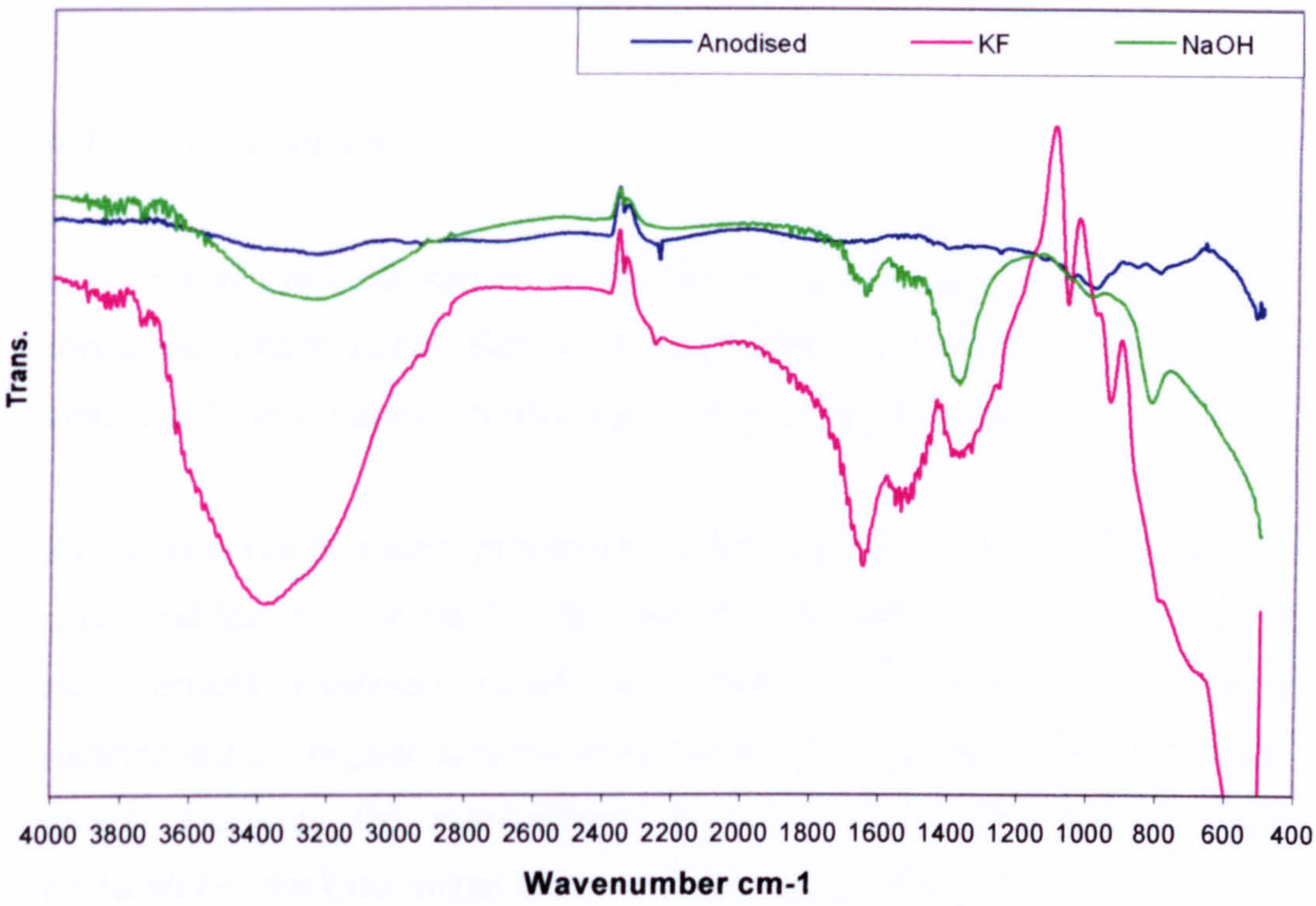


Figure 6.26. ATR spectra showing the comparison between anodisation and other surface pretreatments.

The ATR spectra illustrate that both the NaOH and KF react quite vigorously with the surface as there is a prominent O-H band present. However, the NaOH spectrum shows none of the key characteristic peaks (no C-N stretch, no C-O stretches) that would suggest reaction between the surface and epoxynitrile. Conversely, the spectrum for KF shows a fairly prominent peak due to the C-N stretch at 2248cm$^{-1}$, signifying a reaction.

The success of the fluoride pretreatment is not surprising as there is previously published literature based on other fluoride treatments which use a similar process[27,28,29]. However, most of these are combined with an anodisation procedure, which is costly and time consuming. The results obtained here suggest that a simple dip in a fluoride/methanol solution will give similar surface properties to those obtained via phosphoric acid anodisation.

### *6.3.3.11 KF-alumina*

It is probable that the success of the fluoride dip method can be attributed to the formation of basic surface sites on the aluminium. These basic sites would work in a similar fashion to the way in which KF-alumina was proven to work in the '80s[30].

KF-alumina can be simply prepared by adding neutral alumina to a solution of KF in water and leaving it to stir[31]. The basic species is then able to act as a catalyst for many organic reactions through the formation of hydrogen bonds between the fluorine and the organic species under reaction. The presence of this hydrogen bond greatly increases the susceptibility of the organic compound to subsequent nucleophilic attack due to the electron withdrawing impact of the fluorine.

The effect of KF-alumina as a catalyst has been illustrated in a large number of synthetic organic processes e.g. the Michael and Suzuki reactions[32]; however, at this time there appears to be no mention in the literature of its application with regard to epoxide chemistry.

### *6.3.3.12 Fluoride treatment mechanism*

The presence of fluoride ions on the surface of the treated aluminium would allow for the formation of hydrogen bonds between the fluorine and hydrogens bonded to the carbons of the epoxide ring[30]. This would increase the susceptibility of attack on the ring from surface hydroxyl groups and lead to bonding between the surface and epoxynitrile (figure 6.27).

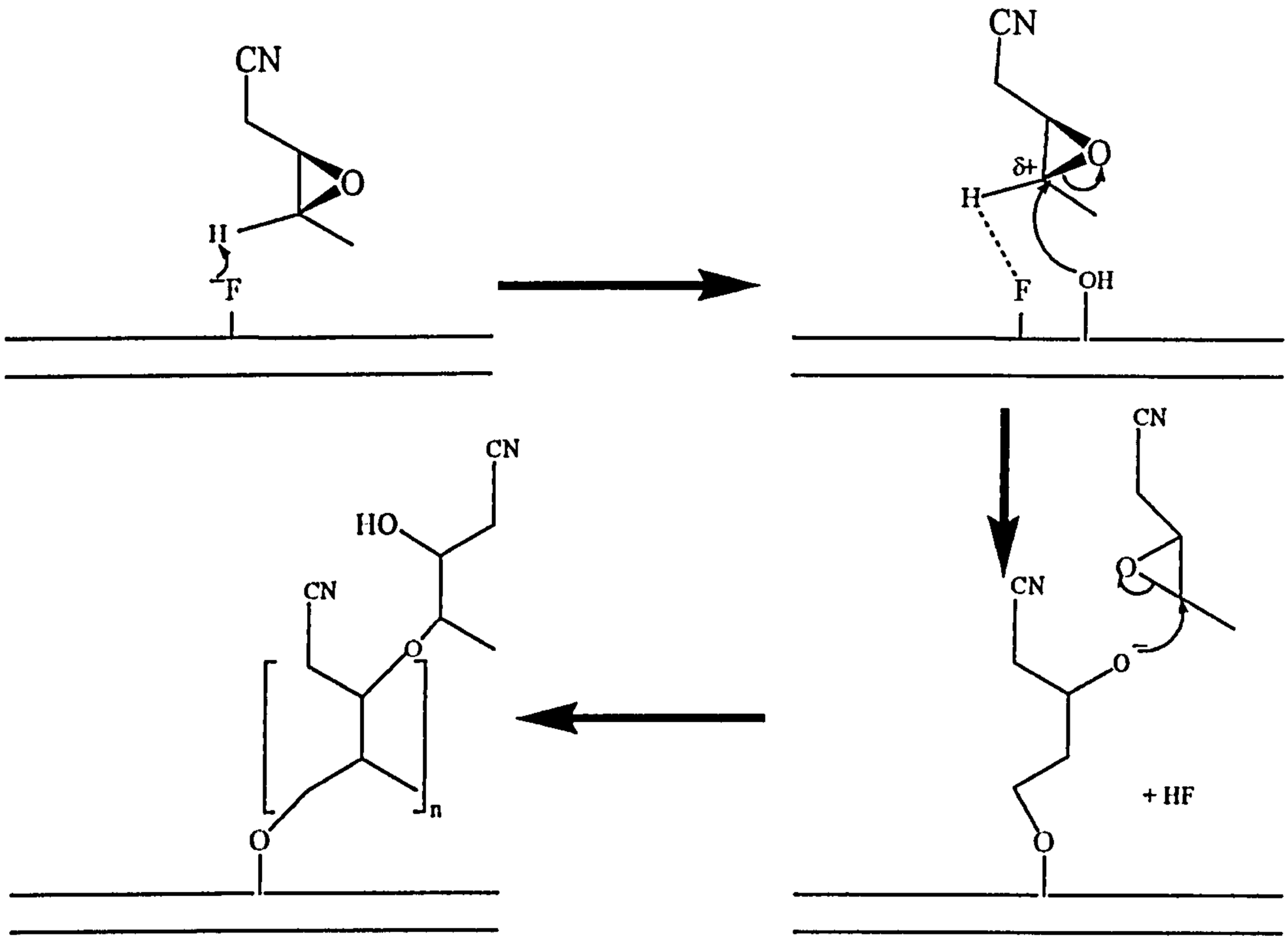


Figure 6.27. Diagram showing a possible mechanism for the reaction between a fluoride treated surface and the epoxynitrile.

## 6.4 Conclusions

This series of experiments has lead to several conclusions being drawn. Firstly, it is clear that from SEM work carried out that simple etching processes can give different effects depending on what acid is used as the etchant. In this investigation, chromic and nitric acids gave completely random morphologies whereas phosphoric acid gave a much more uniform surface morphology.

It has also been shown through SEM and EDX analysis that the thickness of the oxide layer achieved through anodisation can be varied by altering the time the material is anodised for. This has been shown by the large increase in oxygen content in the EDX values obtained.

ATR spectroscopy has clearly illustrated that anodisation significantly increases the level of surface functionality. This has been shown by large increases in the O-H stretching region in samples analysed immediately after anodisation. It is also clear that this initial increase in functionality begins to drop away after about 10 minutes. Subsequent analysis by ATR, SEM and EDX techniques has lead to the conclusion that this functionalised surface is becoming oxidised, thus leading to the formation of an inert oxide layer.

It has been shown by the use of ATR that the surface activation leading from anodisation is due to the formation of reactive surface electronic vacancies. In the investigated system these electron vacancies were trapped by an epoxynitrile spectroscopic marker for easy analysis. Aging studies under different atmospheric conditions lead to the conclusion that these surface electron vacancies were trapped immediately by the epoxynitrile which lead to the subsequent formation of the inert surface oxide layer.

An amalgamation of these results suggests that a direct combination of anodisation and priming in one bath could be considered as an alternative to the conventional system. If a suitable blend of acid and epoxide monomer could be found then they could combine to both form and subsequently trap surface electronic vacancies.

## 6.5 References

1. Pennisi, M.S., *The Powder Coater, Volume 1,* Coatings and Fabrication, New York, 2001.
2. Sulka, G.D., Parkoaa, K.G., *Thin Solid Films*, 515, 338, 2006.
3. Pennisi, M.S, Jones, D., *Anodising*, Coatings and Fabrication, New York, 2001.
4. Young, L., *Anodic Oxide Films*, Academic Press, London, 1961.
5. Thompson, G.E., *Thin Solid Films*, 297, 192, 1997.
6. BR127 Primer, Cytec Engineered Materials product data sheet.

7. Molitor, P., Barron, V., Young, T., *International Journal of Adhesion & Adhesives*, 21, 129, 2001.
8. Comyn, J., *Adhesion Science*, RSC, London, 1997.
9. Kinloch, A.J., *Adhesion and Adhesives: Science and Technology*, Chapman and Hall, Oxford, 1987.
10. Xie, L., Sohn, Y., Jordan, E.H., Gellet, M., *Surface and Coatings Technology*, 176, 57, 2003.
11. Technical notes, *Perkin Elmer Life and Analytical Sciences,* Perkin Elmer, 2005.
12. Shin, E.W., Jang, M., Park, J.K., Choi, S.I., *Environmental Science and Technology*, 38, 912, 2004.
13. Bicak, N., Atay, T., *Turkish Journal of Chemistry,* 22, 261, 1998.
14. Clark, J.H., Grigoropoulou, G., *Green Chemistry*, 5, 1,2003.
15. Venturello, C., *Journal of Organic Chemistry,* 48, *21, 1983.*
16. Venturello, C., D'Aloisio, R., *Journal of* Organic *Chemistry,* 53, 7, 1988.
17. Noyori, R., Ogawa, M., Hashimoto, T., *Journal of Organic Chemistry,* 61, 8310, 1996.
18. Noyori, R., Sato, K., Aoki, M., Ogawa, M., Hashimoto, T., Panyella, D., *Bulletin of the Chemical Society of Japan,* 70, 905, 1997.
19. Winstein, S., Savedoff, L.G., Smith, S.G., Stevens, I.D.R., Gall, J.S., *Tetrahedron Letters*, 9, 24, 1960.
20. Leska, B., *Tetrahedron Letters*, 47, 5673, 2006.
21. Makosza, M., *Pure and Applied Chemistry*, 43,439, 1975.
22. Griffith, K., *Phase Transfer Catalysis Review*, Sachem, 2001.
23. Clark, J.H., Grigoropoulou, G., Internal Publication for Quest PLC., 2003.
24. Royal Society of Chemistry, Infrared Spectroscopy, 2002.
25. Lin-Vien, D., Colthup, N. B., Fateley, W. G., Grasselli, J. G., *The Handbook of Infrared and Raman Characteristic Frequencies of Organic Molecules*, 1st Edition, Academic Press, London, 1991.
26. Burneau, A., Barres, O., Gallas, J.P., Lavalleyet, J.C., *Langmuir*, 6, 1364, 1990.

27. Verdier, S., et al, *Surface & Coatings Technology*, 200, 2955, 2006.

28. Tanaka, K., Kogoma, M., *International Journal of Adhesion and Adhesives*, 23 (6), 515, 2003.

29. *Surface treatments for Magnesium Alloys in Aerospace and Defence*, Magnesium Elektron.

30. Clark, J.H., *Chemical Reviews*, 80, 5, 1980.

31. Wang, X.-S., Shi, D.-Q., Wei X.-Y., Zong, Z.-M., *Journal of Chemical Research*, 10, 679, 2004.

32. Basu, B., Das P., Bhuiyan, M.M.H., Set, J., *TetrahedronLetters*, 44, 19, 2003.

# *Chapter 7*

# *Conclusions and further work*

## 7.1 Conclusions

There were three initial aims sets out in chapter one of this thesis. Firstly, to increase the understanding of the mechanism of chromium and its function in primer systems. Secondly, to find suitable environmentally benign alternatives that acted in a similar fashion to chromium. Thirdly, to create an overall increase in the corrosion resistance and adhesion promotion of primer systems.

As these aims were very wide reaching it was not proposed to carry out an in depth study into one specific area but to seek to open doors into a range of areas for further research to be carried out.

From this preliminary research, several conclusions have been generated which cover the manner in which chromium acts in primer systems, properties for a successful alternative and the possibility for a one step pretreatment and primer process.

### *7.1.1 Chromium as a Lewis acid catalyst*

The research has illustrated the fact that chromium acts as a Lewis acid catalyst for the oligomerisation of epoxides, independent of whether they are aliphatic or aromatic in structure. It also appears that this catalytic effect is due in part to the redox activity of chromium as it is reduced from its +6 state to a lower oxidation state, probably +3.

The ability of chromium to act as a catalyst is well published in the literature. However, the discovery that it is able to cause the oligomerisation of epoxides is of key interest to the whole primer area. Thought solely to affect the aluminium surface, it has been shown that chromium interacts favourably with the organic

species present in the formulation. Clearly, this factor is of great importance when it comes to hypothesising about possible 'green' alternatives to chromium.

### *7.1.2 Formation of an organochromate species*

The occurrence of simultaneous changes in the organic and inorganic phases suggests a new species is formed in the model system. It is likely that due to the catalytic effect of the chromium on the oligomerisation of the epoxide that a permanent bonding effect between the two occurs, leading to the formation of an organochromate.

Organochromates have been extensively reported in the literature. The fact that hexavalent chromium is a strong oxidising agent will allow it to react easily with the organic components in a primer compound, suggesting that there is likely to be some, if not a high concentration of, organochromate species present.

### *7.1.3 The position of chromium in a primed aluminium substrate*

This research has illustrated that chromium is not present at the surface of a primed aluminium substrate. It appears likely that the chromium is in fact strongly linked to the interfacial characteristics of the metal and primer layers.

The positioning of the chromium at this interface is reported in the literature as it has been said to pass into the pores of an anodised aluminium surface. However, it is also possible that a more simple reaction is occurring whereby chromium is reacting with the hydroxylated aluminium surface. This would create a strong Al-O-Cr bonding network which would give good adhesive properties.

The presence of the chromium at the metal-primer interface indicates that it is not involved in a reaction with any further adhesive layer that may be bonded. This suggests that successful bonding between the primer and adhesive is more likely achieved by standard curing chemistry at elevated temperatures.

As a result of the above conclusions, figure 6.01 shows a proposed structure which is probably similar to that which would be observed in a primed aluminium substrate.

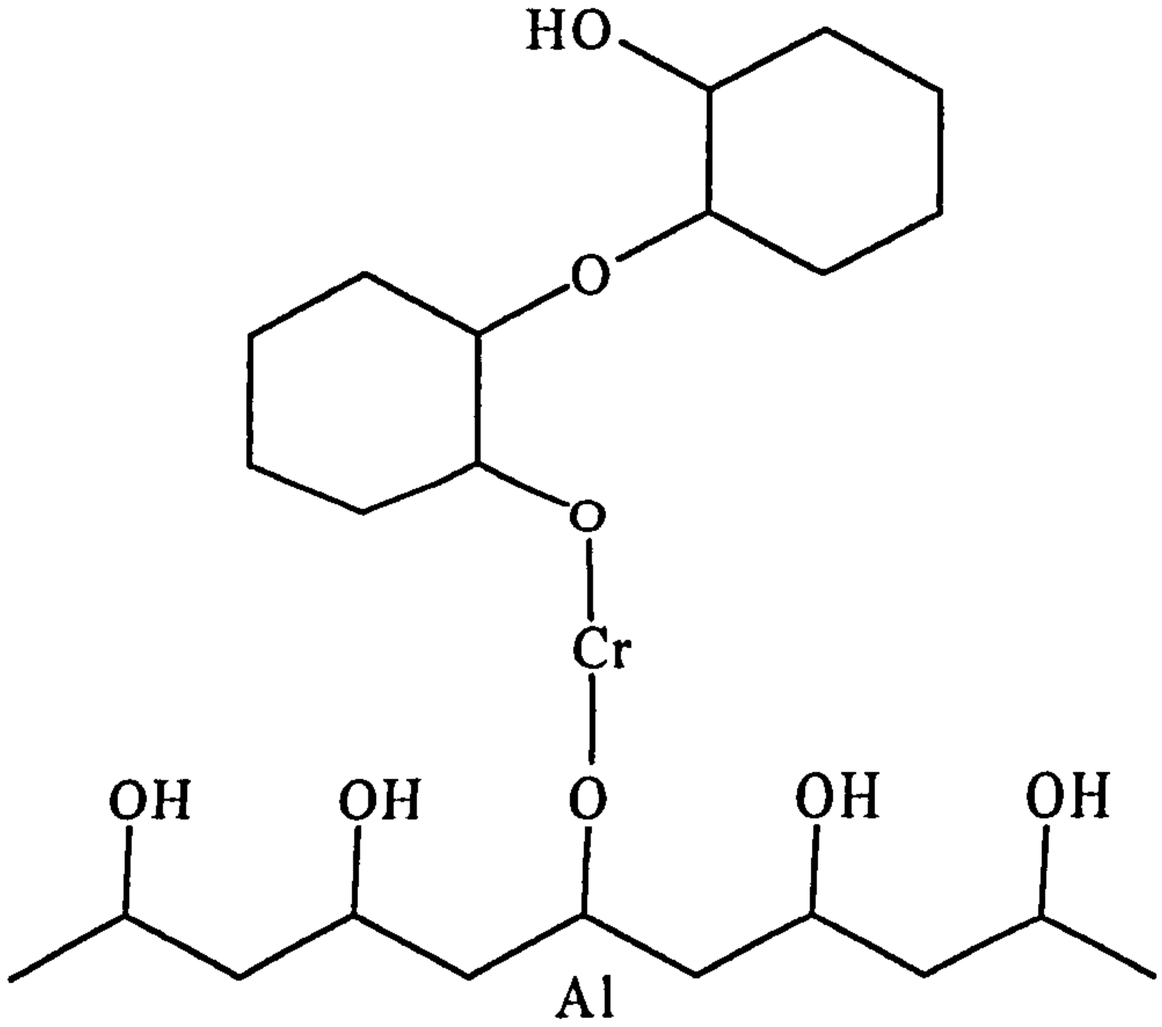


Figure 7.01. Proposed final structure of chromate model system

### *7.1.4 Suitable environmentally benign alternatives*

From the results obtained from the chromate model system, it was found that a successful 'green' replacement must exhibit three major chemical characteristics. It must be able to act as a Lewis acid catalyst to encourage the formation of epoxide oligomers. It must be able to form a strong Al-O-X bond, so that any replacement would be able to successfully form a similar compound to that shown in figure 6.01. Finally, although not integral to the compound, it would be beneficial to show a level of redox activity.

### *7.1.5 Zirconate was the most successful alternative*

Out of all the possible alternatives, the three that were selected (based on low cost, sustainability, low toxicity and promising properties); phosphate, tungstate and zirconate all exhibited some level of activity. However, it is clear that from those tested; zirconate was the most successful as a direct replacement for chromium.

From the results obtained it can be observed that zirconate has the ability to act in the same manner as chromium as a catalyst for the epoxide oligomerisation but at a greater kinetic level. Additionally, zirconate exhibits some redox activity, and although not on the same level as chromium, substantially more than the other two alternatives tested.

As zirconate is used in several coupling agents, its success is not that surprising. However, the level of its success demonstrated in this research will hopefully allow it to be studied further as a direct replacement in primer formulations.

### *7.1.6 One step treatment process*

The use of a spectroscopic marker in conjunction with anodisation has led to the development of a proposed mechanism whereby short-lived reactive surface electron vacancies are formed. These reactive vacancies can catalyse the opening of an epoxide ring and the oligomerisation that follows.

These findings suggest that a one step combination pretreatment and primer process could be established. The development of such a procedure would be hugely beneficial to the aerospace industry in particular but also to the automotive and marine industries as it would provide substantial economic benefits and also large decreases in the time required to prepare a bondable surface.

Current research is looking at the possibility of combining a vinyl monomer with an anodisation process; however, the results obtained in this investigation suggest that

the combination of a simple epoxide would give a successful outcome. This is important as it may lead to the possibility of keeping a similar formulation to the current generation of primers in combination with anodisation.

### *7.1.7 A simple fluoride treatment as an alternative to acid anodisation*

The research has also shown that a fluoride based treatment will give similar results to anodisation as a reaction between a fluoride treated aluminium substrate and epoxide based spectroscopic marker has been observed. It is possible that this reaction proceeds via a similar mechanism to anodisation with the formation of surface vacancies as has previously been reported for alumina supported fluoride materials. Alternatively, the formation of hydrogen bonds with the fluorinated surface may promote the desired reaction. As the area of fluoride-surface interactions is highly complex it is also possible that several other species generated during the process could be involved.

This work is of huge importance from an industrial perspective as the replacement of anodisation with a fluoride treatment provides several key advantages to the current procedure. Primarily, the fluoride treatment is a much more simple process than anodisation without the need for expensive electrical equipment. Additionally, there are economic benefits in waste disposal and further advantages in time and labour savings.

## 7.2 Further work

As the aim of this research was to open doors for future investigations to be carried out, there are many different directions where work could be conducted.

### *7.2.1 Adhesion and anticorrosive performance of a zirconate formulation*

The largest major area of further study would be the actual adhesive and corrosion resistive performance of some industrially formulated systems. An initial investigation would be based on chromate but then would lead into a comparison to investigate the effectiveness of a zirconate formulation.

The adhesion promotion of the industrial systems would be tested by combining the formulation with some aerospace aluminium and a commonly used aerospace adhesive. The systems would be cured and then subjected to one of the many different types of adhesion test such as the Boeing wedge test, the floating roller test or a simple t-peel test.

The drawback to corrosion testing is that to conduct a full study requires a large amount of time to get accurate results. One way to decrease the amount of time needed for corrosion testing would be to use a corrosion acceleration chamber. This is a device that can create the effects of atmospheric conditions but then by changing the temperature, humidity or pressure can cause a decrease in the rate constant, allowing for an overall decrease in the time taken to gain results.

### *7.2.2 Successful interactivity between a chromate and zirconate system*

It would also be interesting to investigate the level of interactivity between a chromate system and an alternative system based on zirconate. This would mean that if it was successful, current generation aircraft initially primed with a chromate compound could later be repaired using a zirconate or other alternative material.

Again, this would lead to large economic benefits and also would further lessen the environmental impact of any repairs to current generation aircraft.

### *7.2.3 One step pretreatment and primer process*

It is also necessary to investigate further into the possibility of a one step pretreatment and primer combination. This method is of great interest to aerospace companies as it would significantly reduce both their operating costs and time constraints. The initial findings reported suggest that this method is possible and it is now important to show it is feasible. It would be interesting to investigate an anodisation process coupled with an epoxide or vinyl monomer, initially on a laboratory scale but if successful then scaling up.

### *7.2.4 Fluoride as a replacement for anodisation*

Having illustrated that a simple fluoride treatment can give similar results to anodisation, it is now important to build on these initial findings. As the exact mechanism by which the fluoride is acting remains unknown it would be of interest to investigate further into this area. It would then be of interest to use the same monomers as for anodisation (epoxide and vinyl) to see whether the fluoride and primer stages can be merged into one.

# ***Chapter 8***

# ***Appendices***

## *8.1 Appendix 1. Basic temper designations*

| | |
|---|---|
| **F** | Denotes metal that has been fabricated to ordered dimensions. There are no mechanical property limits, and the strength levels may vary form lot to lot and from shipment to shipment. |
| **O** | Annealed. Applies to wrought products that have undergone a thermal treatment to reduce their mechanical property levels to their minimums. |
| **W** | Solution heat-treated. An unstable temper applying to certain of the (7XXX) heat-treatable alloys that, after heat treatment, spontaneously age harden at room temperature. |
| **H** | Strain-hardened. Applies to those wrought products which have had an increase in strength by reduction through strain-hardening or cold working operations. |
| **T** | Thermally treated to produce tempers other than F, O or H. Applies to those products which have had an increase in strength due to thermal treatments, with or without supplementary strain-hardening operations. |

## *8.2 Appendix 2. Subdivisions of "T" heat treatable alloys*

| | |
|---|---|
| T1 | Cooled from an elevated temperature and naturally aged. Usually associated with extruded products and limited to the 6XXX series alloys. |
| T2 | Cooled from an elevated temperature, cold worked, and naturally aged. Usually associated with cast products. |
| T3 | Solution heat-treated, cold worked, and naturally aged. (T4+cold work) |
| T4 | Solution heat-treated, and naturally aged. |
| T5 | Cooled from an elevated temperature and artificially aged. Usually associated with extruded products in the 6XXX series alloys. (T1+artificial age) |
| T6 | Solution heat-treated, and artificially aged. (T4+artificial age) |
| T7 | Solution heat-treated, and overaged/stabilized. |
| T8 | Solution heat-treated, cold worked, and artificially aged. (T3+artificial age) |
| T9 | Solution heat-treated, artificially aged and cold worked. (T6+artificial age) |
| T10 | Cooled from an elevated temperature, cold worked, and artificially aged. Usually associated with cast products.(T2+artificial age) |